

Study of a multiple kingpost truss bridge with framed joints

A case study of a cogging joint

*Master of Science Thesis in the Master's Programme Structural Engineering and
Building Technology*

ANNA TEIKE

Department of Civil and Environmental Engineering
Division of Structural Engineering
Steel and Timber Structures
CHALMERS UNIVERSITY OF TECHNOLOGY
Göteborg, Sweden 2013
Master's Thesis 2013:20

MASTER'S THESIS 2013:20

Study of a multiple kingpost truss bridge with framed joints

A case study of a cogging joint

Master of Science Thesis in the Master's Programme Structural Engineering and Building Technology

ANNA TEIKE

Department of Civil and Environmental Engineering
Division of *Structural Engineering*
Steel and Timber Structures

CHALMERS UNIVERSITY OF TECHNOLOGY

Göteborg, Sweden 2013

Study of a multiple kingpost truss bridge with framed joints

A case study of a cogging joint

Master of Science Thesis in the Master's Programme Structural Engineering and Building Technology

ANNA TEIKE

© ANNA TEIKE, 2013

Examensarbete / Institutionen för bygg- och miljöteknik,
Chalmers tekniska högskola 2013:20

Department of Civil and Environmental Engineering

Division of *Structural Engineering*

Steel and Timber Structures

Chalmers University of Technology

SE-412 96 Göteborg

Sweden

Telephone: + 46 (0)31-772 1000

Cover:

A 3D-computer-model of the timber truss bridge created by Anders Frøstrup.

Reproservice, Chalmers University of Technology, Göteborg, Sweden 2013

Study of a multiple kingpost truss bridge with framed joints

A case study of a cogging joint

Master of Science Thesis in the Master's Programme Structural Engineering and Building Technology

ANNA TEIKE

Department of Civil and Environmental Engineering

Division of *Structural Engineering*

Steel and Timber Structures

Chalmers University of Technology

ABSTRACT

The municipality of Mariestad is planning to build a multiple kingpost truss pedestrian bridge over the river Tidan in year 2014, with the mission name the *Bridge over Tidan*. The bridge is designed with three spans of 22 meters each and the loadbearing truss system is 3 meter high. The truss is located on each side of the bridge deck. The joints are designed according to a traditional carpentry method, so called timber framing, with very few steel parts in connections. A timber framed joint is a timber-to-timber joint which is manufactured by cutting the wood pieces to a locking configuration. Anders Frøstrup, at Timber AS, has conducted a preliminary design of the bridge and the timber framed joints. The details of the joints are presented in a 3D-computer-model. There are important requirements for structural design when timber framing are used in larger structures. The designs of the few structures with timber framing that exist today are often based on earlier design or design rules from older references. This can be noticed by the absence of a section related to timber framed joints in the current European design code, Eurocode 5. The principle objective of this Master's Thesis was to design the most critical timber framed joint in the *Bridge over Tidan* according to existing design rules. It was also important to achieve a greater understanding of the mechanical behaviour of a timber framed joint, as well as to investigate the applicability of the design rules in Eurocode 5. A literature study was conducted to understand the mechanical behaviour of the multiple kingpost truss bridge and the design of a timber framed joint. Furthermore, a global analysis was conducted to obtain the design load of the most critical joint. The analysis included three specific load cases which represented some of the worst load situations. The analysis was carried out with the finite element software Abaqus with the application Brigade/Plus. The literature study together with the global analysis showed that the cogging joint was the most critical joint in the timber truss since it had no redundancy. Failure of the cogging joint will lead to a mechanism resulting in a total collapse of the bridge. Three conventional designs of cogging joints have been found, one of which Anders Frøstrup has suggested for *Bridge over Tidan*. These designs resulted in different strength of the joint. The three key parameters which determine the maximum strength of a cogging joint were found to be compression perpendicular to grain, distribution of stresses and number of supporting contact surfaces. The sketched cogging joint in the global 3D-computer-model received from Anders Frøstrup has shown sufficient strength to carry the normal force by contact only when strength class D50 is used.

Key words: multiple kingpost, timber truss bridge, timber framed joint, cogging joint.

En studie av en träfackverksbro med träförbindningar
En fallstudie av en stöt och ansats träförbindning
Examensarbete inom Structural Engineering and Building Technology
ANNA TEIKE
Institutionen för bygg- och miljöteknik
Avdelningen för konstruktionsteknik
Stål- och träbyggnad
Chalmers tekniska högskola

SAMMANFATTNING

Mariestads kommun planerar att bygga en träfackverksbro över floden Tidan år 2014, med uppdragsnamn *Bron över Tidan*. Bron, som är en gång- och cykelbro består av tre 22 meters sektioner med en höjd av 3 meter. Träförbindningarna i fackverket är konstruerade enligt traditionell hantverksmetod, så kallad stolpverkskonstruktion, med mycket få ståldelar i anslutningarna. En träförbindning tillverkas genom att passa in träbalkar/pelare i en sammanfogad låsning. Anders Frøstrup vid Timber AS, har genomfört en preliminär utformning av bron och träförbindningarna. Detaljerna i träförbindningarna presenterades i en 3D-dator-modell. Utformningen av de stolpverkskonstruktioner som finns idag är ofta baserade på tidigare konstruktioner eller konstruktionsregler från äldre referenser. Detta märks genom frånvaron av ett avsnitt som rör träförbindningar såsom stolpverkskonstruktion i nuvarande europeiska konstruktionsregler, Eurokod 5. Huvudsyftet med detta examensarbete var att dimensionera den mest kritiska träförbindningen i *Bron över Tidan* enligt gällande konstruktionsregler. Det var också viktigt att få en större förståelse för det mekaniska beteendet hos träförbindningar i allmänhet, samt att undersöka tillämpligheten av konstruktionsregler i Eurokod 5. En litteraturstudie genomfördes för att förstå det mekaniska beteendet hos en fackverksbro och träförbindningar i allmänhet. Vidare har en global analys av träfackverksbron utförts för att erhålla dimensionerande last av den mest kritiska träförbindningen. I analysen ingick tre specifika lastfall som representerar några av de värsta lastsituationer som kan uppstå på bron. Analysen genomfördes med finita element programmet Abaqus med applikationen Brigade/Plus. Litteraturstudien tillsammans med den globala analysen visade att den mest kritiska träförbindningen kunde lokaliseras till den yttersta stöt och ansats träförbindningen eftersom den inte har någon redundans. Ett brott i den yttersta stöt och ansats träförbindningen kommer att leda till en mekanism som resulterar i en total kollaps av bron. Tre konventionella dimensioneringsmetoder anpassade för stöt och ansats träförbindning hittades. Anders Frøstrups preliminära design av stöt och ansats träförbindningen för *Bron över Tidan* kan härledas till en av dessa metoder. Dimensioneringsmetoderna resulterade i olika utformning. De tre nyckelparametrar som påverkar bärförmåga i en stöt och ansats träförbindning befanns vara tryck vinkelrätt fibrerna, spänningsdistribution över anliggningsytor och antal stödjande anliggningsytor. Stöt och ansats träförbindningen i den globala 3D-dator-modell som erhållits från Anders Frøstrup har visat tillräcklig bärförmåga för hållfasthetsklass D50 och kan därmed bära normalkraften genom anliggning.

Nyckelord: Fackverksbro av trä, äldre träförbindning, Stöt-och-ansats, FE-analys, mekaniskt verkningssätt, bärförmåga, stolpverkskonstruktion

Contents

ABSTRACT	I
SAMMANFATTNING	II
CONTENTS	III
PREFACE	VII
NOTATIONS	VIII
1 INTRODUCTION	1
1.1 Objectives and limitations	1
1.2 Method	2
1.3 Outline	2
2 <i>BRIDGE OVER TIDAN</i>	3
2.1 Terminology of trusses	3
2.2 Location	3
2.3 Construction process	4
2.4 Description of the structural system	4
3 HISTORICAL REVIEW OF THE TIMBER TRUSS BRIDGE	10
3.1 Part 1: The beginning and rise	10
3.1.1 China	11
3.1.2 Europe	12
3.1.3 USA	13
3.1.4 Sweden	14
3.1.5 Summary	16
3.2 Part 2: The declination	17
3.3 Part 3: The revival	18
4 THE MECHANICAL BEHAVIOUR OF TIMBER TRUSS BRIDGES	20
4.1 Strut frames	20
4.2 Parallel-chord truss	22
4.2.1 Long truss	22
4.2.2 Howe truss	23
4.2.3 Pratt truss	23
4.2.4 Multiple kingpost truss	24
4.3 Arch truss	25
5 TIMBER FRAMED JOINTS IN HISTORY	27
5.1 Earlier suggestions of timber framed joints	28
5.2 Cogging joints	31

5.3	Tension joint	34
5.4	Laminated beam	36
6	CURRENT DESIGN METHODS AND RESEARCH	39
6.1	Cogging joints	39
6.1.1	Design method 1	39
6.1.2	Design method 2	41
6.1.3	Numerical analysis of a cogging joints	42
6.2	Tension joint	44
6.3	Laminated beam	46
7	DESCRIPTION OF THE GLOBAL NUMERICAL MODEL	49
7.1	Simplifications of the structural system	49
7.2	Material properties	53
7.3	Element type, boundary conditions and mesh	55
7.4	Loads	57
8	RESULTS	64
8.1	Global analysis	64
8.2	Design methods	68
8.2.1	Comparison	68
8.2.2	Assumptions	69
8.3	Local joint design	69
9	DISCUSSION	75
9.1	Advantages and disadvantages of B, C and D joint design	75
9.2	Shear failure and compressive failure	76
9.3	Distribution of force	76
9.4	Shear strength	76
9.5	Joint slip	78
10	CONCLUSIONS	80
10.1	Further research	80
11	REFERENCES	83
	APPENDIX A – BRIDGES	1
	APPENDIX B – ORTHOTROPIC PLATE	1

APPENDIX C – POISSON’S RATIO	1
APPENDIX D – DESIGN LOAD	1
APPENDIX E – JOINT DESIGNS	1
JOINT AF	4
JOINT B	10
JOINT C	17
JOINT D	22
APPENDIX F – GLOBAL ANALYSIS	1

Preface

In this study, a design of a timber framed joint and a design evaluation of the multiple kingpost truss bridge *Bridge over Tidan* was conducted. The study was carried out from June 2012 to March 2013. The work was a part of a construction project of a bridge in Mariestad where the client is the municipality of Mariestad. The project was carried out at the Department of Structural Engineering, Steel and Timber Structures, Chalmers University of Technology, Sweden. The project was supervised by the company COWI. Professor Robert Kliger was the examiner of this Thesis.

This Master's Thesis was carried out by Anna Teike and supervisors were; Magnus Bäckström, Tomas Svensson and Robert Kliger. They are together with Nils-Eric Anderson highly appreciated for their passion and guidance. I would also like to thank Anders Frøstrup at Timber Frame AS for his co-operation and involvement.

Göteborg March 2013

Anna Teike

Notations

Roman upper case letters

EI_x	Bending stiffness in the x-direction
EI_y	Bending stiffness in the y-direction
E_x	Modified E-modulus in the x-direction for the converted bridge deck
E_y	Modified E-modulus in the y-direction for the converted bridge deck
$E1$	Elastic modulus in the local x-direction for the numerical model
$E2$	Elastic modulus in the local y-direction for the numerical model
$E3$	Elastic modulus in the local z-direction for the numerical model
$NU12$	Poisson's ration in the local xy-plane for the numerical model
$NU13$	Poisson's ration in the local xz-plane for the numerical model
$NU23$	Poisson's ration in the local yz-plane for the numerical model
$G12$	Shear modulus in the local xy-plane for the numerical model
$G13$	Shear modulus in the local xz-plane for the numerical model
$G23$	Shear modulus in the local yz-plane for the numerical model
$D40$	Strength class for hardwood species according to EN 338
$D30$	Strength class for softwood species according to EN 338
$Q_{serv.1}$	Distributed "concentrated" force for a front wheel of the service vehicle
$Q_{serv.2}$	Distributed "concentrated" force for a rear wheel of the service vehicle
AF	Cogging joint design by Anders Fröstrup
B	Cogging joint design according to design method 2
C	Cogging joint design according to design method 2
D	Cogging joint design according to design method 1

Roman lower case letters

$gr1$	Load group 1 according to EN 1991-2:2003 5.5 tab 5.1
$gr2$	Load group 2 according to EN 1991-2:2003 5.5 tab 5.1
a	Frontal contact surface of a cogging joint
b	Rear contact surface of a cogging joint
c	Frontal flatter contact surface of a cogging joint
d	Rear flatter contact surface of a cogging joint

e	Front notch of a cogging joint
f	Rear notch of a cogging joint
g	Front shear plane of a cogging joint
h	Rear shear plane of a cogging joint
i	End distance of a cogging joint

Greek letters

ψ_0	Partial factor for ULS according to SS-EN 1990 Tab A2.2
$\gamma_{F,i}$	Partial factor for variable load according to SS-EN 1990 6.3.2 (6.2b)
$\gamma_{f,i}$	Action partial factor according to according to SS-EN 1990 6.3.2 (6.2b)
γ_{sd}	Model partial factor according to SS-EN 1990 6.3.2 (6.2b)
γ_g	Action partial factor according to SS-EN 1990 6.3.2 (6.2b)
$\gamma_{G,j}$	Partial factor for permanent load in ULS according to SS-EN 1990 6.3.2 (6.2b)
$\gamma_{Q,1}$	Partial factor for variable load in ULS according to SS-EN 1990 6.3.2 (6.2b)
φ	Angle between the force and the grain at the front part in the a cogging joint
β	Angle between the force and the grain at the rear part in the a cogging joint
ϕ	Angle between the force and the grain at the rear part in the a cogging joint
$\sigma_{c.0.d}$	The load effect parallel to the grain
$\sigma_{c.20.d}$	The load effect in form of normal compression in 20° to the grain
$\sigma_{c.40.d}$	The load effect in form of normal compression in 40° to the grain
$\sigma_{c.70.d}$	The load effect in form of normal compression in 70° to the grain
τ	The load effect in form of shear parallel to the grain

1 Introduction

The municipality of Mariestad is planning to build a pedestrian timber truss bridge over the river Tidan in year 2014, with the mission name *Bridge over Tidan*. The bridge is of type; multiple kingpost bridge, which is described in more detail in Chapter 3. It is designed with three inclined spans of 22 meter and the loadbearing truss system is 3 meter high and is located above the bridge deck, see front page. The joints are constructed by a traditional carpentry method, timber framing, with very few steel parts in the joint. A timber framed joint is a timber-to-timber connection which is manufactured by cutting the wood pieces to a locking configuration; see more about timber framed joints in Chapter 4.

The timber truss bridge has been designed by Anders Frøstrup, at Timber AS. The author has received a 3D-computer-model of the timber truss bridge by Anders Frøstrup, see front page. The details of the connections are to some extent shown in the 3D model but no results from a stress analysis were received.

There are no easily accessible design rules for timber frame joints. The reason could be explained by the lack of experience in old timber techniques such as timber framing and few or no technical rules for timber framing in modern design rules, such as Eurocode.

There is a certain demand of structural design knowledge when timber framing are used in larger structures. The design of the few timber frame structures that are constructed in modern times are often based on earlier timber frame constructions or design rules from older references. This can be noticed by the absence of a section concerning timber frame joints in recently republished Eurocode 5.

The evolution of timber structures today is mostly focused on new timber products such as Engineered Wood Products (EWP). Little or no research is conducted in the area of civil engineering concerning timber frame techniques.

Bridges with influences of old carpentry techniques are often carrying a large architectural. A greater knowledge of the accessible design rules and mechanical behaviour of timber frame joints will facilitate an increasing number of constructed timber frame structures as well as slender and more efficient dimensions.

1.1 Objectives and limitations

The principle objective of this Master's Thesis was to design one critical timber framed joint in *Bridge over Tidan* according to existing design methods. It was also to evaluate the corresponding preliminary designed timber framed joint proposed by Anders Frøstrup with respect to load-bearing capacity. Furthermore, it was also to compare these design methods and highlight strength and weaknesses in each method. A sub objective was to achieve a greater understanding of the mechanical behaviour of timber framed joints as well as to investigate the applicability of the design rules in Eurocode 5.

One global bridge section with a span of 22 meters was studied. The finite element analysis (FEA) was based on a 3D-model with several simplifications of the real structure, see Chapter 5. Influences of climate conditions and dynamic response were not considered.

1.2 Method

A literature study was conducted to improve the understanding of the mechanical behaviour of the multiple kingpost truss bridge and timber framed joints in general. Anders Frøstrups preliminary design of the timber framed joints were studied and put into a perspective to other timber framed joints, with the literature study as a background. The joints in the *Bridge over Tidan* was studied and some design recommendations are presented.

The most critical timber framed joint in the *Bridge over Tidan* was designed according to existing design rules. The design load was calculated by a finite element analysis (FEA) of one timber truss section, based on reference loads from Eurocode 0, 1 and 2 and Swedish national codes. The analysis was carried out with the finite element software Abaqus with the application Brigade/Plus.

1.3 Outline

The content of this Master's Thesis is structured according to a basic to detail approach. Three major parts can be distinguished; a general informative part, a detailed design part and a concluding part.

The general informative part consists of Chapter 2-5. The first introduction of the study object, the *Bridge over Tidan*, will be given in Chapter 2. Thereafter in Chapter 3 the reader will be introduced to the historical development of structural systems in timber truss bridges with a focus on the type; multiple kingpost. Furthermore, the mechanical behaviour of the different truss systems is described in Chapter 4. Chapter 5 will provide the reader with a basic knowledge of different timber framed joint configurations and functionality in terms of historical design recommendations.

The detailed design part consists of Chapters 6 and 7 together with Appendices E and F. In Chapter 6 the timber framed joints are viewed from a current research perspective and several design recommendation based on numerical analysis are presented. In addition, two unconventional design methods for the most critical timber framed joint are presented, which was used in the local design. Chapter 7 describes the numerical model and the simplifications made to enable an efficient computational process. Moreover, the loads are also presented which will give the design load of which the critical timber framed joint was designed for. The explicit calculations and implementation values of the input load and the output load effect in form of characteristic stress and design stress can be viewed in Appendix E. The detailed design of the timber framed joint, according to unconventional design methods presented in Chapter 6 and the design strength based on Eurocode 5, are presented in Appendix F.

The concluding part consist of the final Chapters 8-10 which will summarize and discuss the results of the design process and finally present important conclusions of this Master's Thesis project. Suggestions of further research are also stated in the last Chapter 10.

2 Bridge over Tidán

The aim with this Chapter is to introduce the reader to the *Bridge over Tidán*. A thorough description will be presented in terms of the structural system and the material choice. A detailed description is chosen to facilitate the understanding of the mechanical behaviour as well as the simplifications made in the numerical model. The purpose of this Chapter is also to introduce the technical terms of trusses.

2.1 Terminology of trusses

The terminology is presented by an illustration to facilitate the understanding of this Master's Thesis report, see Figure 2.1.

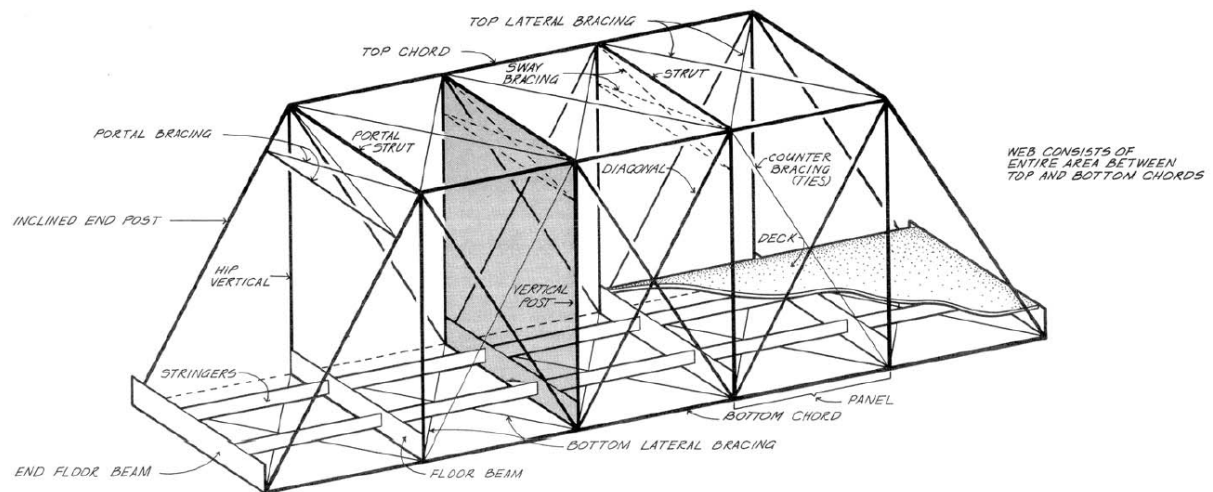


Figure 2.1 The terminology of trusses given in an illustration. (*History American Engineering Record*, 1976)

2.2 Location

The bridge will pass over the river Tidán, with EU-code SE650960-138526, which is an inflow to the largest lake in Sweden, Värnen. The bridge is planned to be located between Marieholmsbron and Gärdesbron in the centre of the town Mariestad, see Figure 2.2.



Figure 2.2 A photograph taken from Gärdesbron in the direction of the planned Bridge over Tidán (*Google*, 2009).

2.3 Construction process

The bridge will be constructed in two steps by two different carpentry teams. The first step is the construction of one bridge span which will be performed by the company Timber AS located in Tønsberg, Norway. The second step, the two latter bridge sections, will be constructed by two carpenters Mattias Hallgren and Mats Anderses, which are former students at the University of Da Capo. All sections will be manufactured in Timber AS workshop located in Tønsberg, Norway. The bridge section will then be transported to Mariestad where it will be assembled. The assembling process will be conducted by a group of carpenters with skills and knowledge about timber framing, the composition of the group is until this day yet unknown.

2.4 Description of the structural system

A multiple kingpost truss system is chosen for the *Bridge over Tidan*. The mechanical behaviour of the structural members is controlled by the truss type, see Figure 2.3.

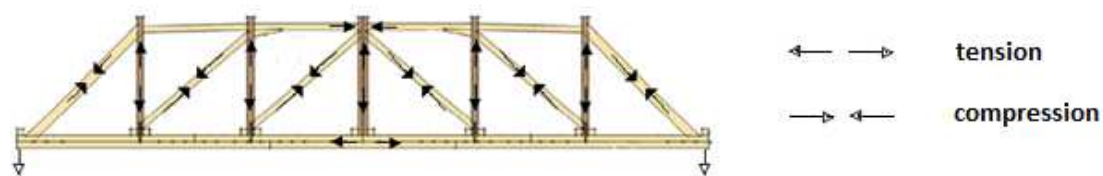


Figure 2.3 A multiple kingpost truss and the mechanical effect on each structural member (Frøstrup, 2012).

The structural system is basically two tall trusses carrying a bridge deck at the lower chord. The framework is illustrated in Figure 2.4. The truss consists of a compressed upper chord, a web and a tensioned lower chord. The chords are connected with struts in the top and floor beams in the bottom. The web consists of compressed diagonals and tensioned vertical posts.

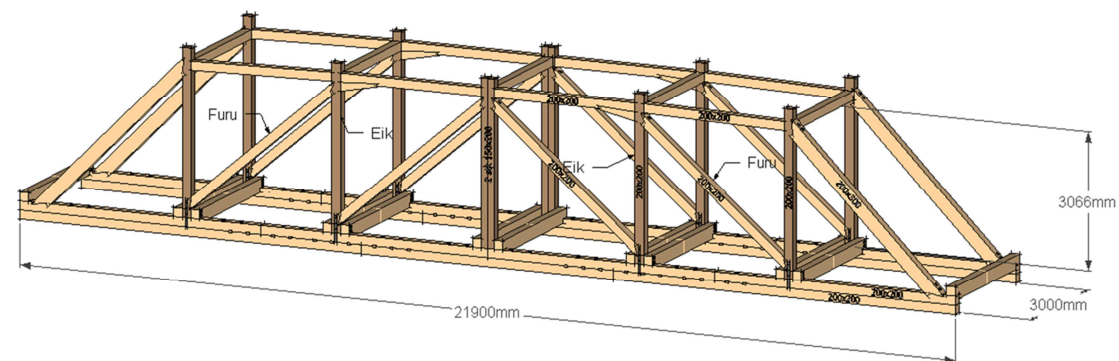


Figure 2.4 The 3D-model received from Anders Frøstrup in the beginning of the project (Frøstrup, 2012).

The bridge deck has a width of 3100 mm, length of 21 900 mm and a thickness of 250 mm. It is composed of floor beams and decking boards see Figure 2.5 and Figure 2.6. There are no stringers in the deck only closely positioned floor beams with a dimension of 100 mm x 200 mm which rest upon the lower chord. The floor beams support a decking of boards with a dimension of 120 mm x 50 mm. A total of 23 decking boards are placed along the width of the bridge deck, see Figure 2.5.



Figure 2.5 The decking of the bridge which together with the girders compose the bridge deck (Karlsson, 2012).

In Figure 2.4 only 12 floor beams are visible, but according to the tender documents, composed by Evy Karlsson at Martin & Co (2012), the floor beams should be positioned every 150 mm in the longitudinal direction, see Figure 2.6.

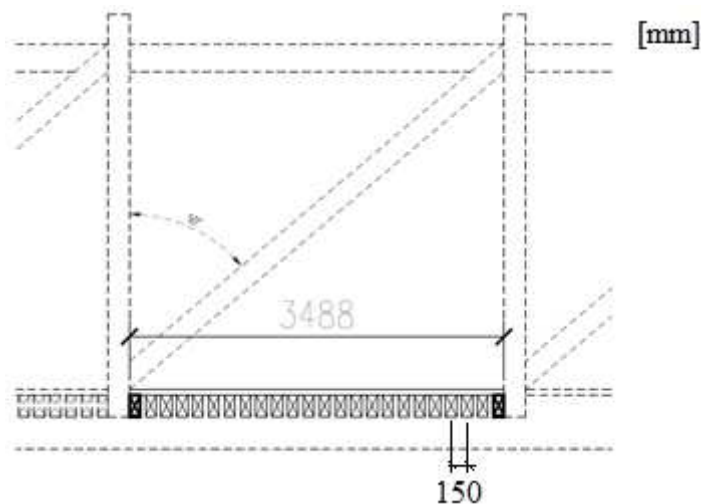


Figure 2.6 The floor beams are positioned every 150 mm (Teike, 2012).

The lateral stabilization is ensured by lateral bracings on the top and bottom of the bridge, see Figure 2.7. The end sections have no lateral bracing in the top, but could easily be added as a portal bracing to ensure the stability of the end sections. In this Master's Thesis it was assumed to be bracings of metal wires with an area of $201 \times 10^{-6} \text{ m}^2$. Hence, only tensile forces can be resisted by the bracings. Two vertical posts, one strut and one floor beam compose a timber frame which can function as a sway bracing provided that the timber framed joints connecting these part are firm. The large height of the truss facilitates an addition of sway bracings if certain strengthening is required.

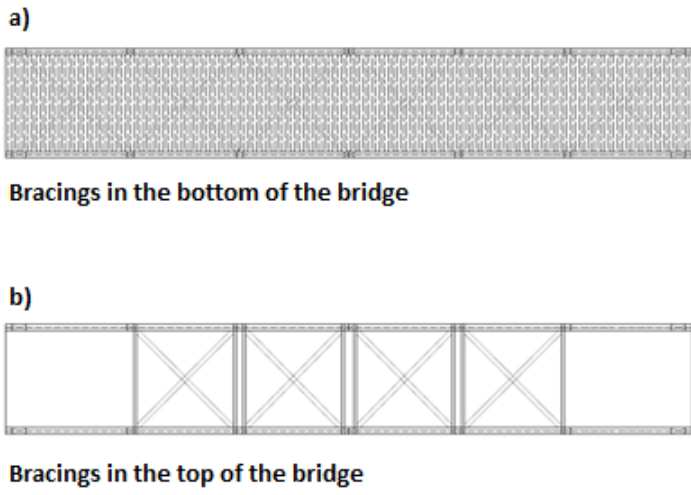


Figure 2.7 The bridge is stabilized by lateral bracings and frame action. In the top: lateral bracings in the bottom positioned under the bridge deck. In the bottom: Lateral bracings in the top are positioned in the four middle bridge sections (Karlsson, 2012).

There are six different configurations of timber framed joints in *Bridge over Tidan*. The primary load-bearing function of the joints are described in terms of T for tension and C for compression, to facilitate the understanding of the mechanical behaviour in each joint. The notations, T and C, are defined in accordance to loads applied in the primarily vertical direction such as the self-weight which generate a certain load effect in the joint.

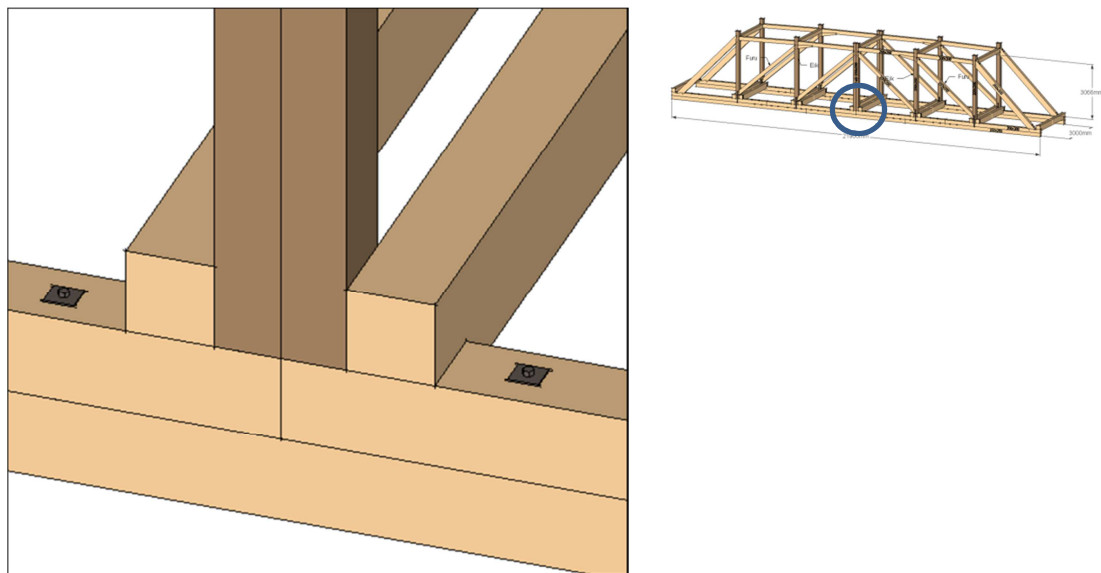


Figure 2.8 A timber framed joint loaded in tension, T-T-T-T. Tensile stresses are induced both from the lower chord, the vertical post and the floor beams, when loaded in the vertical direction (Frøstrup, 2012).

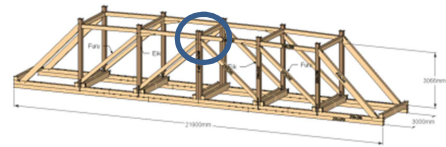
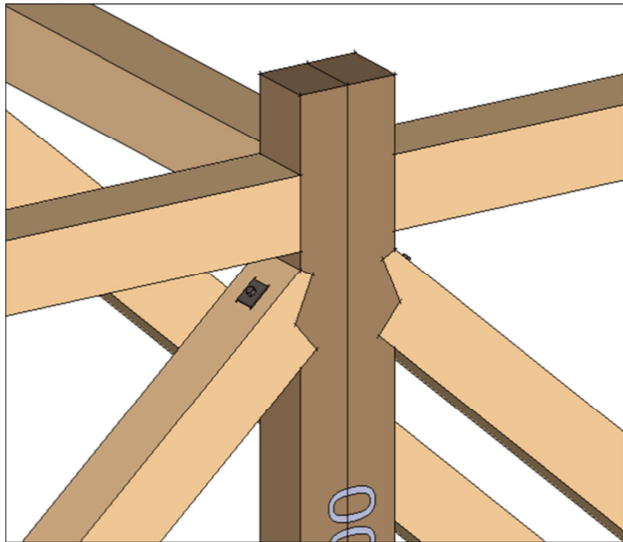


Figure 2.9 A timber framed joint loaded in compression and some tension, CCCCC-T. Tensile stresses are induced from the vertical post and compressive stresses are induced from the strut, the diagonals and the upper chord, when loaded in the vertical direction (Frøstrup, 2012).

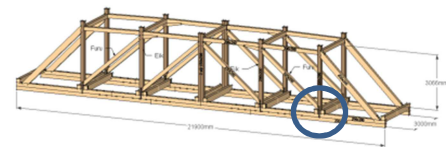
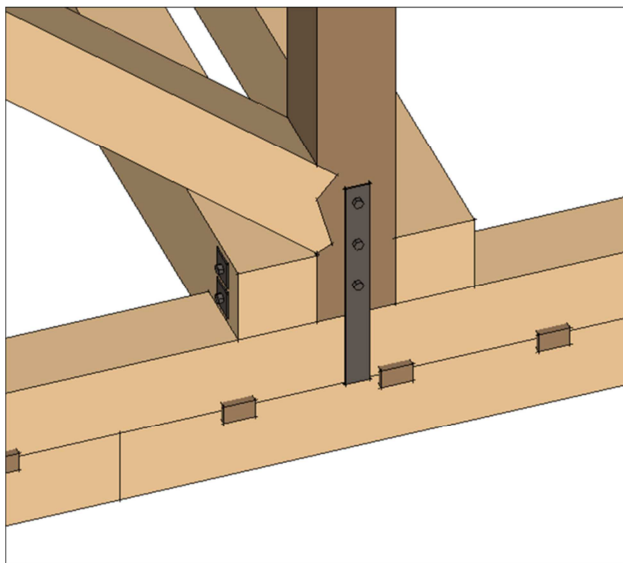


Figure 2.10 A timber framed joint loaded in tension and some compression, TTT-C. Tensile stresses are induced both from the lower chord, the vertical post and the floor beams, compressive stresses are induced from the diagonal, when loaded in the vertical direction (Frøstrup, 2012).

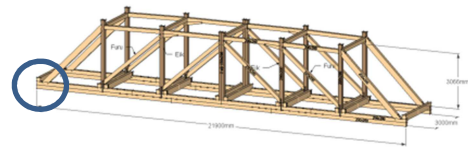
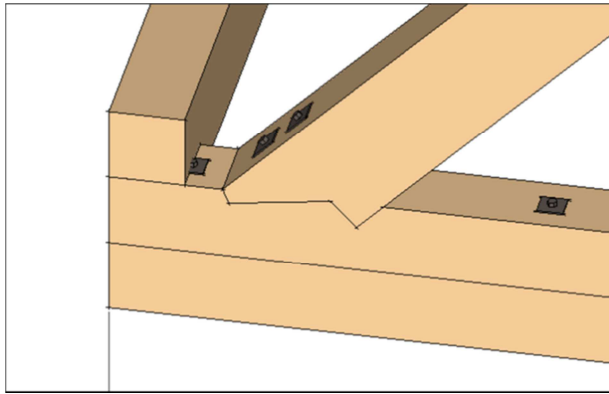


Figure 2.11 A timber framed joint loaded in tension and some compression, TT-C. Tensile stresses are induced both from the lower chord and the floor beams, compressive stresses are induced from the diagonal, when loaded in the vertical direction, (Frøstrup, 2012).

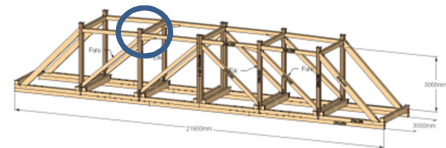
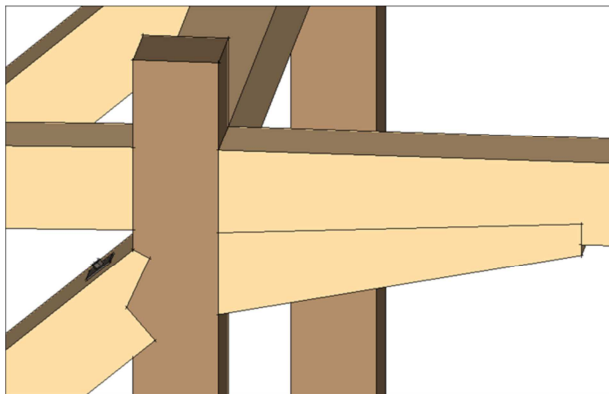


Figure 2.12 A timber framed joint loaded in compression and some tension, CCCC-T. Tensile stresses are induced from the vertical post and compressive stresses are induced from the strut, the diagonal and the upper chord, when loaded in the vertical direction, (Frøstrup, 2012).

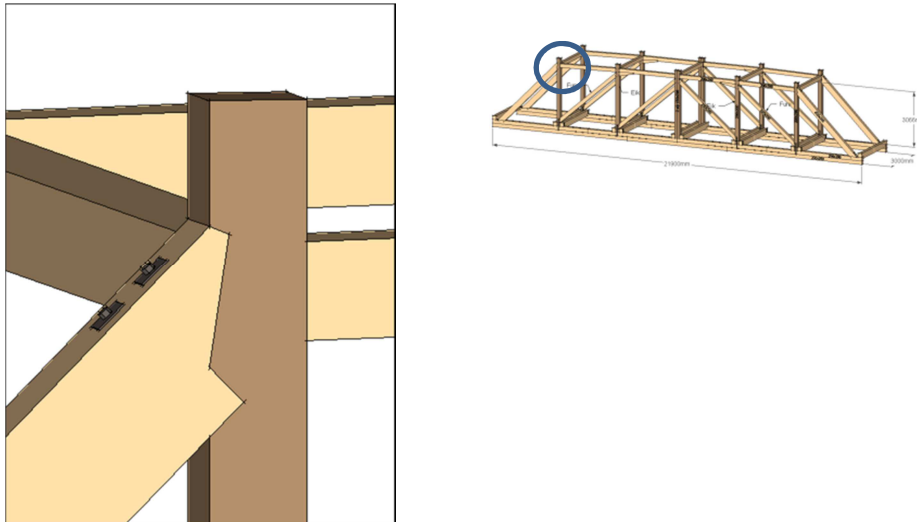


Figure 2.13 A timber framed joint loaded in compression and some tension, CCC-T. Tensile stresses are induced from the vertical post and compressive stresses are induced from the strut, the diagonal and the upper chord, when loaded in the vertical direction, (Frøstrup, 2012).

Small wedges are located at the top of the first and second vertical tie. This can be described as an elongation of the diagonal to transfer the compressive stress.

Two types of wood species are used in the bridge, pine and oak. Oak is in general stronger than pine and has particularly a higher compressive strength perpendicular to the grain. The vertical posts and part of the laminated beam are made of oak and the remaining parts consist of pine. The most outer upper part of the laminated beam is made of oak due to large compressive force from the inclined end post, see Figure 2.14. The multi-directed compression stress in the top of the vertical post makes oak a very good choice of material.

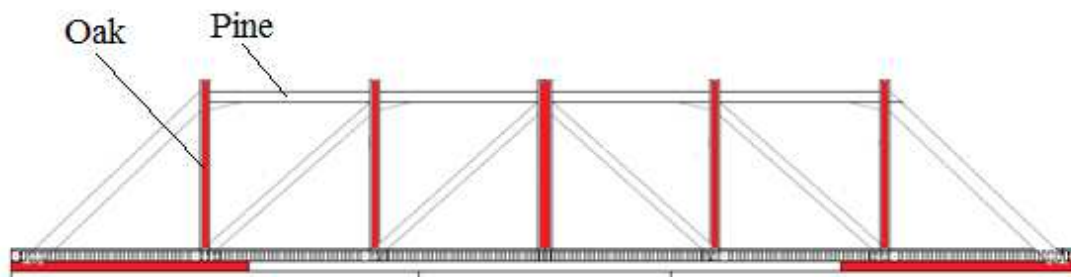


Figure 2.14 There are two different materials, oak and pine, in the bridge located in some part of the lower chord and in the vertical posts (Karlsson, 2012), (Revised: Teike, 2013).

3 Historical review of the timber truss bridge

This Chapter present timber truss bridges with specific touch-downs in time and place to emphasize historical contributions of a new truss type. The scope of the historical review is limited to cover the US and the European timber bridges, however it also include some examples of arch bridges from China. The leading countries in timber truss bridge construction and design throughout history are Switzerland, Germany and the United States of America (USA) (Yeomans, 1997). France and United Kingdom (UK) have to a large extent neglected timber as a structural material in bridges in a historical perspective and instead primarily used masonry and iron.

The historical review is divided into three parts structured both geographically and chronologically; *Part 1: The beginning and the rise*, *Part 2: The declination* and *Part 3: The revival*. The first part describes the earliest documented timber truss bridges until the peak during the 19th century, which resulted in various types of structural truss systems. Appendix A is recommended to be used actively while reading part 1 to support the understanding of the development of the structural system in each touch-down in history. Appendix A shows a compilation of illustrated timber truss bridges in the time range 16th mid-19th century geographically limited to Europe and the US. The appendix originates from the paper *The evolution of wooden bridge trusses to 1850* written by James (1982) which was limited to American and European timber truss bridges. The second part describes the declining number of built truss bridges during the late 19th century and reasons of the declination. The last part describes the comeback of the timber truss bridge in modern time.

3.1 Part 1: The beginning and rise

In the early years of mankind timber and vines were the obvious choice of material to build bridges. The materials were easy to handle and joints were conducted by use of various kinds of tools and handcraft. The structural system of a bridge was naturally explored by a pragmatic approach. The load-bearing structure was most certainly a large timber log from an adjacent tree acting as a simple beam or a woven string structure relying on string forces. However, as mankind slowly developed and gathered in small towns, a need of an infrastructure increased. Temporary dwellings were exchanged to permanent buildings with increasing volumes which in turn increased the use of roads and bridges to the emerging cities. This evolution required a more complex structural system due to increased use and loads.

In Roman times, 753 BC until 476 AD, the Roman Empire as well as adjacent kingdoms with great power built several bridges around Europe and in the Middle East (Ritter, 1990). Not only Romans but also Persians and other great rulers wanted to develop the infrastructure to facilitate the mobilization of their armies and to forge the people and land together as one unified empire. Unfortunately the documentation of timber bridges is very limited from this period. However during the 16th century the Venetian architect Palladio (1518-1580) documented several ancient bridges from the Roman time and also drew some bridges of his own. One military Roman bridge was described as fast assembled and constructed of beams and inclined struts, see Figure 3.1. Another Roman bridge described by Palladio was the circular timber arch bridge with a span of 50 meters, which is shown in Figure 3.2.

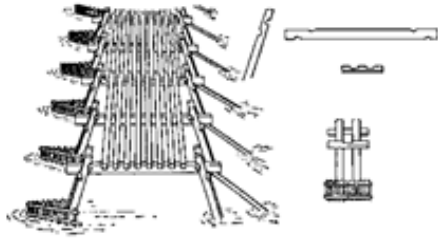


Figure 3.1 A military Roman bridge which was described as fast assembled and constructed of beams and inclined struts (Ritter, 1990).

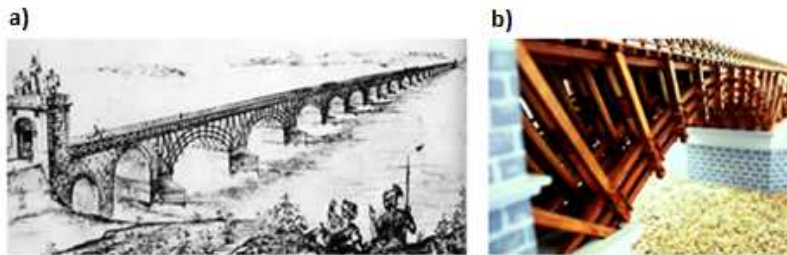


Figure 3.2 The Roman bridge, Trajan Bridge. To the left: a sketched reconstruction of the Trajan bridge in 1907 by the engineer E. Duperrex (Serban, 2009). To the right: A 3D-model of the Trajan bridge in a small scale (Freedman et al, 2002).

Palladio also designed and constructed his own timber bridges, for instance a multiple kingpost truss bridge which connected the cities Trent and Bassano with a span about 30 meters and an additional design of a multiple kingpost truss, see Figure 3.3 (Timoshenko, 1953). In the 17th century two other Italian architects, Scamozzi and Verantius, contributed with additional four bridge designs; an arch truss bridge, an arch bridge, a simple kingpost bridge and a lenticular bridge, see 1-4 and 42 in Appendix A.

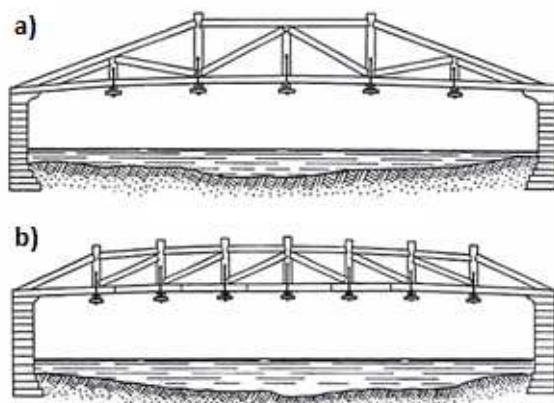


Figure 3.3 Multiple kingpost bridges. The upper bridge was constructed between Trent and Bassano and the lower bridge is one of Palladio's own designs but were never built. (Timoshenko, 1953)

3.1.1 China

It was not only the Europeans that possessed the skills for timber bridge construction. During the 12th century in China there were many arch bridges built called “rainbow bridges” (Yang, Chen and Gao, 2007). A rainbow bridge is a covered arch bridge that

has a structural system built up by two longitudinal arch systems and one transverse system made by horizontal members that carries the bridge deck. The system is very efficient since the three load-bearing systems lock each system into place by their location in a truss-like manner, see Figure 3.4.

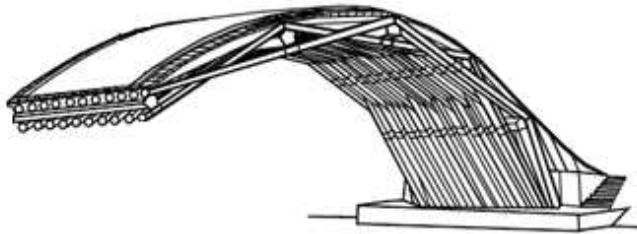


Figure 3.4 A Chinese rainbow bridge (Yang, Chen and Gao, 2007).

The Chinese artist Zhang Zeduan captured an ancient rainbow bridge in one of his paintings made around year 1120 (Yang, Chen and Gao, 2007). During this period in China many of these rainbow bridges were built around the nation with a span of up to 40 meters. Another type of arch bridge called “Extant Fujian-Zhejiang timber arch bridge” has also been found in China. The rise of the rainbow bridges is unknown but these different types started to be built at the same time. The youngest “Extant Fujian-Zhejiang timber arch bridge” was originally built in 1674 and one can still find old “bridge men” that knows the technique. Yang, Chen and Gao have continued to research Chinese arch bridge. In 2009 they presented another report which contained several pictures of the timber connections from ancient arch bridges, see Figure 3.5.

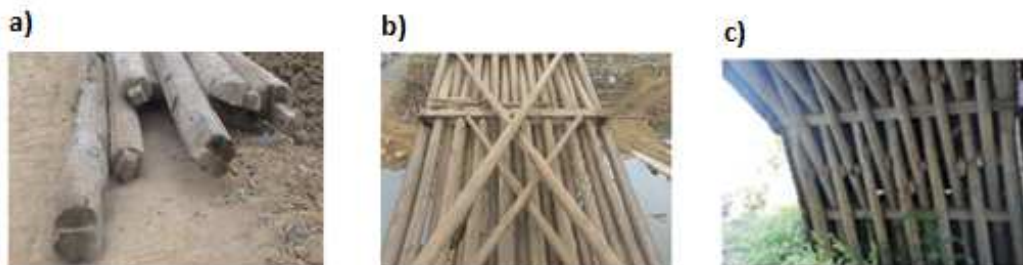


Figure 3.5 The timber frame joints of a Chinese rainbow bridge (Yang, Chen and Gao, 2009).

3.1.2 Europe

During the 16th and 17th century a few number of covered timber truss bridges where built in Switzerland, see 5-8 in Appendix A and Figure 3.6. It is argued whether or not the roof cover was an aesthetic choice or a conscious choice to protect the timber material from deterioration (Yeomans, 1997). Swiss and German carpenters continued to build and develop the covered bridges during the 18th century. The former simple kingpost and queen post was extended with struts under the lower chord to achieve longer spans and was later replaced by embedded struts between the upper and lower chord, see 9-16 in Appendix A. Finally the typical Swiss bridge emerged as a combination of an arch and a truss bridge, see Figure 3.7 and 17-28 in Appendix A.

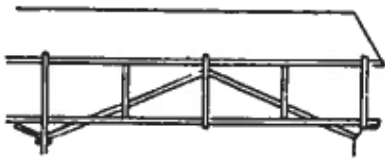


Figure 3.6 A covered timber truss bridge from the 16th century in Switzerland (Yeomans, 1999)

The Swiss family Grubenmann were very successful in building truss bridges strengthened with arch systems, see Figure 3.7 and 17-28 in Appendix A. After the breakthrough of Grubenmann several Swiss and German arch truss bridges were built in the 18th century see 29-35 in Appendix A. France and the UK where to a large extent neglecting timber as a structural material in bridges instead primarily used masonry and iron, however they contributed with a few timber truss bridges see 36-40 in Appendix A (Yeomans, 1999).

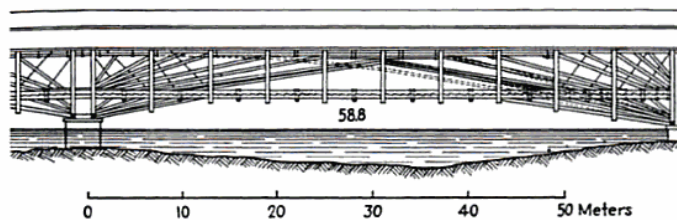


Figure 3.7 The two spans of the bridge over the Rhine at Schaffhausen built in 1757 by Grubenmann. The span lengths were 58 and 52 meter and could carry 25 ton with some safety marginal (Timoshenko, 1953).

In addition, during the 17th and 18th century arch bridges without the parallel-chord truss were built in Europe, see 41 and 43-48 in Appendix A. The arch itself was then constructed by a curved truss system or bow-shaped beams. Two additional timber truss bridges from Eastern Europe were built during the same time, see 49-50 in Appendix A.

3.1.3 USA

The emigration from Europe to USA gave rise to an intensification of the development of structural systems in timber truss bridges. The new land with large natural resources, the lack of infrastructure and the beginning of the industrialization were all contributing factors. The influential and famous American Timothy Palmer (1751-1821) built the first covered timber truss bridge in the USA, which is characteristic for bridges from the USA, see 51-55 in Appendix A.

Bridge builders in the USA dominated the bridge building during the 19th century, see 53-86 in Appendix A. About 10 000 bridges were built in the USA with spans up to 100 meters (Ritter, 1990). Several bridge types were built and patented but most of them were variations of truss bridges or a combination of an arch and a truss bridge. However, there were also innovative new structural systems such as the lattice bridges, several examples are shown in Appendix A see for example 68, 76 and 79. Some of the bridges failed before or after a short period of service which could be explained by the absence of structural analysis and stress control. The first mathematical calculations of a stress control, in the USA, were documented in the

mid-19th century. The design was often based only on empirical studies of other already existing bridges.

The American timber truss development that once was influenced by the European timber bridge construction was in the mid-19th century influencing European engineers and bridge builders. Several European timber truss bridges with obvious influences from the USA were built in the mid-19th century, see 88-101 in Appendix A.

3.1.4 Sweden

In Sweden, there are several old timber bridges still in operation. Lejonströmsbron is one of the oldest, see Figure 3.8. It is located in Skellefteå and was built in year 1737 but was almost entirely rebuilt in the early 19th century due to a total destruction by the Swedish army to prevent the Russian troops to pass over the Skellefteå River (Länssyrelsen, 1994). It has a free width of 5 meters and a total length of 207.5 meters. An iron rod transfers the load from the bridge deck up to the inclined struts, see Figure 3.9. The kingpost is here made as an iron rod. The high position of the bridge deck and uplifted by inclined struts with support under the bridge deck is typical characteristics of a strut frame. Therefore, the Lejonströmsbron can be seen as a combined kingpost-strut frame, because both systems can be seen in the bridge. A straining beam can be seen at both the intermediate strut frames and the outer kingpost-strut frames. It is an additional beam located under the main beams of the bridge deck in the free span which result in a strengthening of the main beams to decrease the risk of buckling.



Figure 3.8 The Lejonströmsbron (*Destination Skellefteå*, 2012).



Figure 3.9 The framework of Lejonströmsbron (Stenlund, 2010).

Another Swedish timber framed truss bridge with obvious similarities with the *Bridge over Tidan* is Vikbron, see Figure 3.10 and Figure 3.12. It was built in year 1888 with a length of 133 meter and a maximum span of 23 meters (Länsstyrelsen, 2005). The main span of the bridge consists of a truss system as can be seen in Figure 3.10. The truss part is divided in 4 sections with three vertical tension members. The chord is supported by a corbel to spread out the reaction force, see Figure 3.12.

Vikbron is of great interest since the bridge part for the main span has a length of 23 meters which is very similar to *Bridge over Tidan*, which has six vertical tension members and approximately the same span length. However, it is difficult to learn from the bridge, due to lack of information about the structural details of the bridge.



Figure 3.10 Vikbron is one of the longest timber bridges in Sweden (Milling, n.d.).

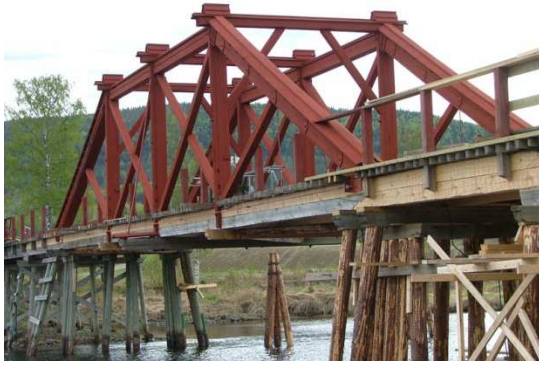


Figure 3.11 The main span of Vikbron (Kraftsamling Fränsta, 2013).



Figure 3.12 The lower chord and the main beams are connected with a timber framed joint called scarf joint (Kraftsamling Fränsta, 2013).

3.1.5 Summary

Part 1 is closely related to Appendix A which is directly taken from the paper generated by James J.G (1982). Hence, it seems reasonable to show a diagram based on the work done by James (1982) compiled by José Luis Fernández Cabo (2010). The peak of timber truss bridges is clearly illustrated in the diagram in *Figure 3.13* . According to Fernández, a dramatically increase of number of built bridges could be seen in the period 1800-1850. In addition, in a report by Kleppe and Aasheim (1996) it is claimed that the same rapid development of timber bridges could be seen in Norway in the latter part of the 19th century. However, a declination of built timber bridges can clearly be seen after 1850.

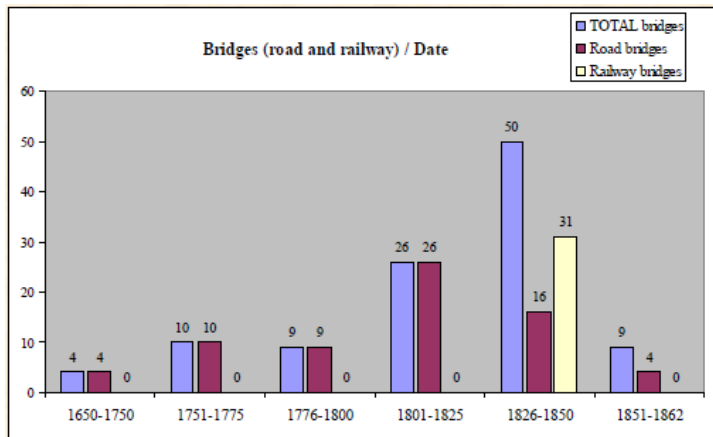


Figure 3.13 A diagram showing the peak of timber truss bridges based on the work done by James (1982) compiled by José Luis Fernández-Cabo. The vertical axis shows the number of built bridges and the horizontal axis the period of time for construction, (Fernández-Cabo, 2010).

3.2 Part 2: The declination

Timber trusses have almost constantly over time been supplemented with different iron products in form of nails, bolts and straps etc. Wrought iron, cast iron and steel are different materials but are produced from the same raw material, the iron ore. All types have been used to manufacture iron products for timber structures. The differences between these end-products had a major impact on the historical development of timber as a structural material, which in turn effected the development of the timber truss bridge.

The knowledge about wrought iron has been known in Europe since the Roman times and in China even longer. Wrought iron has a low carbon content and is therefore very ductile which is preferable for structural details loaded in tension. The raw material is hammered to form the end-product which is very time-consuming and it easily corrodes. As a building material in structures it was carefully managed because of the major economic impact, since it required a lot of work. This is an explanation to the obvious choice of timber as a building material. Therefore the main part of the constructed bridges was designed more or less only in timber.

During the medieval times cast iron made its first entry in Europe, but had long been used in China. Cast iron has a high carbon content and is therefore very strong but brittle when loaded in compression. The raw material is moulded to form the end-product which is a time-effective manufacturing process. It is also more resistant to corrosion than wrought iron. At the peak of timber bridge construction in Europe during the 19th century, illustrated in Figure 3.13, several of the bridges had components or full-sized members in cast iron often in tension. An example is the tie rods, a load-bearing component in the truss formation, introduced in the USA in the mid-19th century. In the late 19th century an increase of composite timber bridges could be seen such as a combination of structural members made of cast iron and timber (Ritter, 1990). In 1859, Howard Carroll was the first in the USA to build a railway bridge made only of iron.

After some years cast iron was replaced with steel which has lower carbon content than cast iron and therefore not as brittle but also not as ductile as wrought iron which

is suitable for structural components subjected to both tension and compression. It is easy and cheap to manufacture in relation to wrought iron and cast iron and it has a decreased ability to corrode. The introduction of steel resulted in a decreased interest of timber as a structural material. By the end of the century steel bridges became more economical to build than timber bridges. The same decline of timber bridges occurred in Norway in transition from the 19th to the 20th century (Kleppe and Aasheim, 1996). The abrupt end is explained by the reduction of the manufacturing and product costs of iron products.

3.3 Part 3: The revival

In Scandinavia, the construction of large timber structures started again during the 1960s but in a renewed shape (Kleppe and Aasheim, 1996). There are several new engineered-wood products which entered the timber industry market during the 20th century, such as glued laminated timber (Glulam), laminated veneer lumber (LVL), parallel strand lumber (Parallam), cross laminated timber (CLT), stressed-skin panels (SSP) and so on (Timberwork, 2000). The engineered wood products enabled larger dimensions, higher strength and less variability in terms of strength and stiffness. Glulam, CLT and LVL are used as structural members, in form of larger beams, columns and boards, while Parallam is often used for studs and beams and SSP is a composite material often used in floor structures.

Several different types of timber bridges have been built in the recent years but not near the number of steel or concrete bridges. Structural members of glulam, with the possibility of larger dimensions and more reliable material properties than structural timber in combination with steel connections, reversed the timber truss bridge into the modern time of the 20th century. Several timber bridges with glued laminated beams as primary load-carrying members were built in the late-20th century in Scandinavia (Kleppe and Aasheim, 1996).

In Sweden, several common timber bridge structures has appeared during the late 20th and in the beginning of the 21th century such as girder bridges, stress laminated bridges, composite bridges and kingpost truss bridges (Kliger, 2008). The literature study of this Thesis has a focus on timber truss bridges, therefore the kingpost truss will only be described. However, literature about the general modern timber bridge structures can easily be found in current research.

One example of a modern timber truss bridge is the Vihantasalmi Bridge in Finland, built in 1999, see Figure 3.14. It is a kingpost truss bridge with a span of 43 meters and the structural members is made of both glulam and steel. The vertical posts are designed as tie rods.

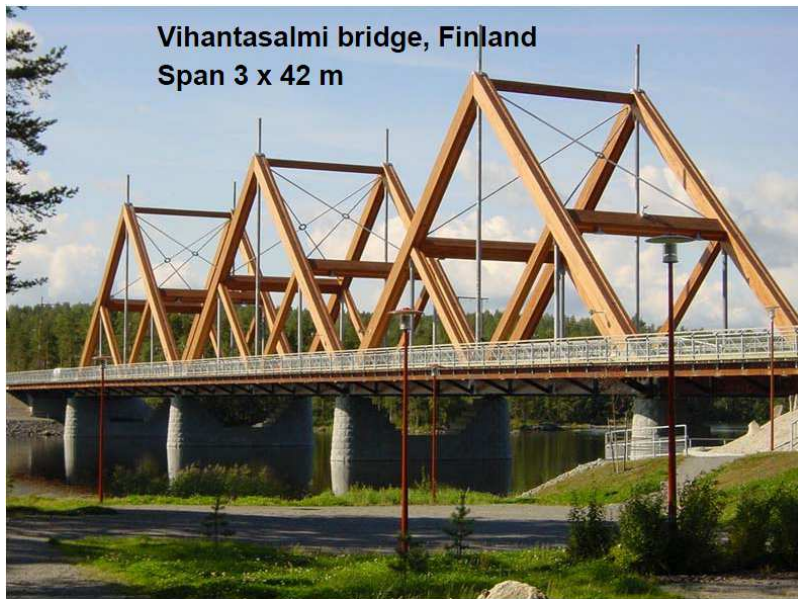


Figure 3.14 The modern kingpost bridge, Vihantasalmi bridge, built 1999 in Finland (Kliger, 2002).

4 The mechanical behaviour of timber truss bridges

The structural system of a timber truss bridge can have several designs, which will effect the mechanical behaviour. There is no conventional classification of different systems of timber truss bridges. The classifications found in reference literature of timber trusses have often a subjective or detailed subdivision which is inappropriate in this Master's Thesis since a general descriptive approach is chosen. The literature study has revealed that the structural systems of timber truss bridges are to a large extent influenced by the strut frame system, the parallel-chord truss system and the arch truss system. A timber truss bridge can be influenced of just one, two or all three types; several examples are illustrated in Appendix A. Therefore the mechanical behaviour of these three different structural systems will be described in more detail.

4.1 Strut frames

The simplest strut frame bridge is well suited for small bridge spans, around 5 meters (von Rothstein, 1890). The structural design of a strut frame truss is shown as number 279 in Figure 4.1. The load path can be traced down to a single point at the end of the struts often meeting a masonry foundation, see Figure 4.2. This often results in large wide masonry foundations as can be seen at the Lejonströmsbron in Figure 3.8.

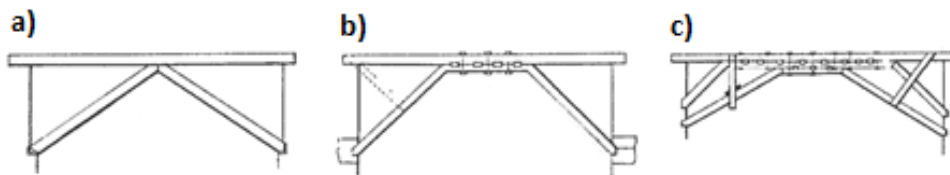


Figure 4.1 a) show strut frame (*spännverk [swe]*). b) and c) show the strut frame with longer spans (von Rothstein, 1890).

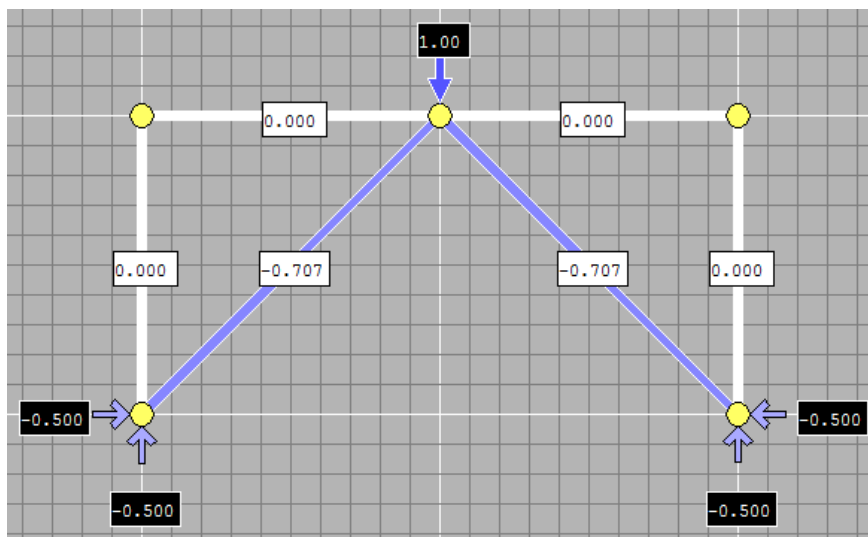


Figure 4.2 The simplest strut frame bridge as a theoretical model loaded with a concentrated unit load in the middle, generated by the simple software program *PointSketch2D*. The reaction forces in this system are concentrated at the end of the struts.

Longer bridge span require increased length of each member, which can lead to lateral buckling of the compression member. Secondary beams can be added to brace the struts and also a straining beam can be added to decrease the slenderness of the horizontal beam, see number 280 and 281 in Figure 4.1. A rule of thumb, according to von Rothstein, is that the length of each member should not exceed 4-5 meters to avoid lateral buckling and a straining beam should be added for spans over 9-10 meters.

The straining beam should be attached timber joints and iron bolts to the primary beam, to be able to act as a unified beam. The reason can be noted in the theoretical model in Figure 4.3. The edges of the horizontal beam are loaded in tension while the middle part is loaded in compression. The purpose of the straining beam is to transfer the compressive force between interior ends of the struts and act together as a compressed arch. The compressive stresses in the straining beam shall be transferred to the primary beam which will absorb the compression as internal stresses in the grains. The reaction forces at the corners of the frame seen in Figure 4.3 as tensile forces, almost disappear when a large beam is simulated by a truss formation in Figure 4.4.

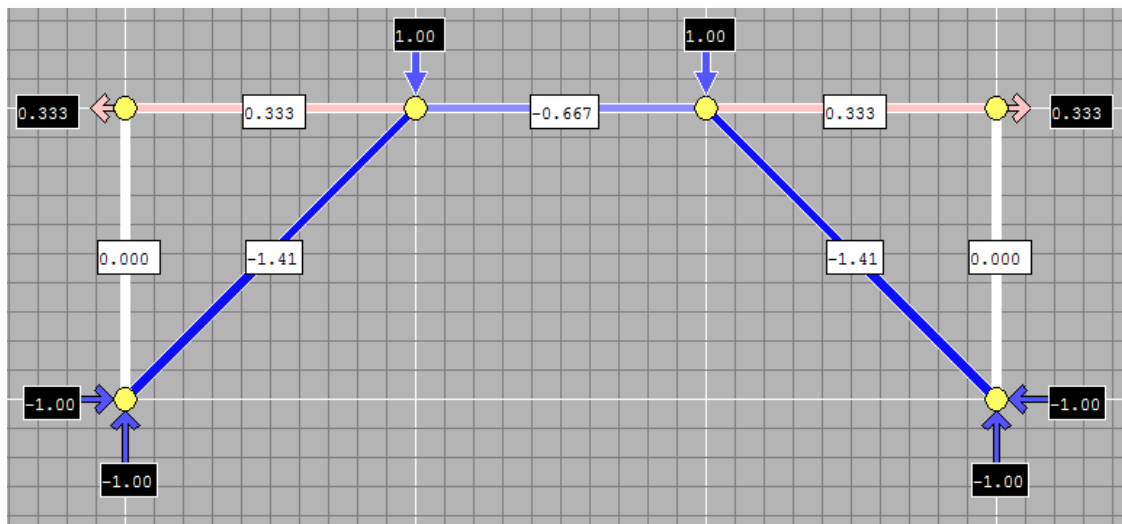


Figure 4.3 A strut frame example with a longer span loaded with two unit loads, generated by the simple software program PointSketch2D.

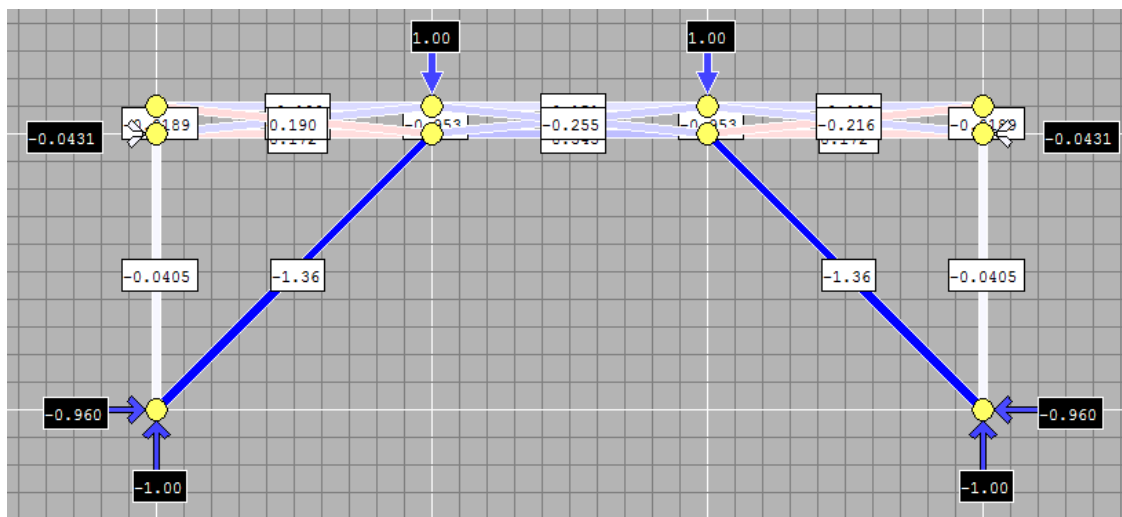


Figure 4.4 A strut frame bridge model with a longer span loaded with two unit loads, generated by the simple software program PointSketch2D.

4.2 Parallel-chord truss

A parallel-chord truss can be designed in accordance to several different types of configuration, see Figure 4.5. The mechanical behaviour differs between various configurations which influences the material choice and design. The upper chord transfer compression to the support and the lower chord transfer tension to the support, which is common for all parallel-chord trusses. It can be argued that both chords transfer bending stresses because it is hard to achieve a pure hinge when the chords are continuous. The differences in the mechanical behaviour are limited to the web of the truss. The type of stress (compression or tension) transferred in the structural members in the web is decided by the design of the structural system. The different configurations of parallel-chord trusses can be traced back to four simple types; Howe, Long, Pratt and the Multiple kingpost, see Figure 4.5.

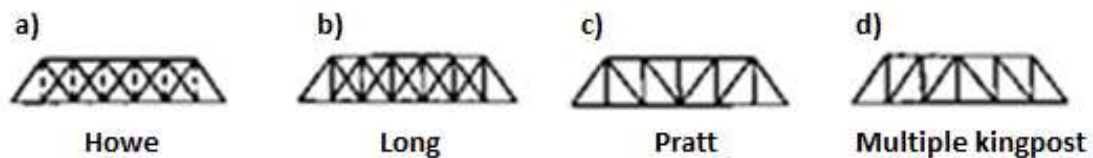


Figure 4.5 Four different types of parallel-chord trusses. a), b) and c) are named after the American bridge builders, who patented the design in the 19th century. The multiple kingpost bridge shown in d) is an old design first documented by the Venetian architect Palladio (Ritter, 1990).

4.2.1 Long truss

The Long truss consists only of timber members (Ritter, 1990). The timber framing technique is used together with wooden pegs and simple iron products to connect the members. It was patented by Stephen H. Long in 1830 and has a documented span of 45 meters. The vertical posts can transfer both tension and compression, thereby the mechanical behaviour will change according to current load positions, compare Figure 4.6 and Figure 4.7. The diagonals, with an inclination as the inclined end posts, will always transfer the compressive forces and the residual diagonals will carry the tensile forces.

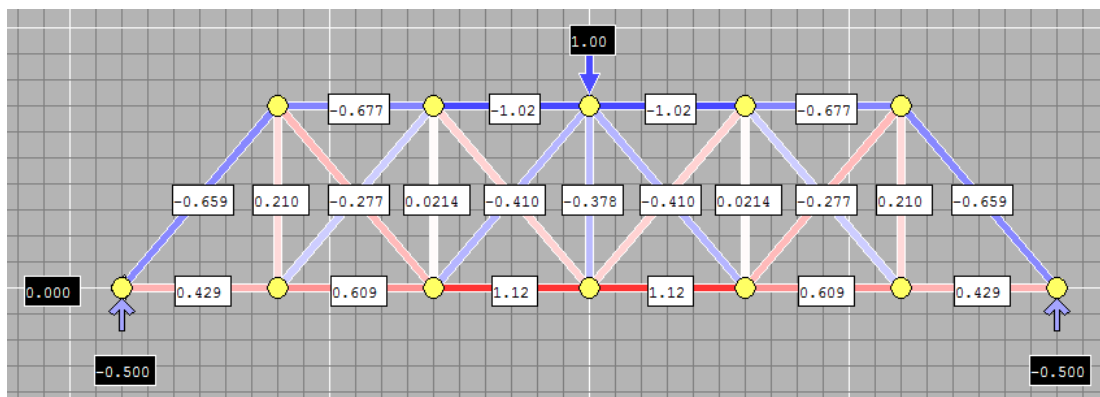


Figure 4.6 A theoretical model showing the mechanical behaviour of a Long truss applied with a concentrated unit force at the middle post, generated by the simple software program PointSketch2D.

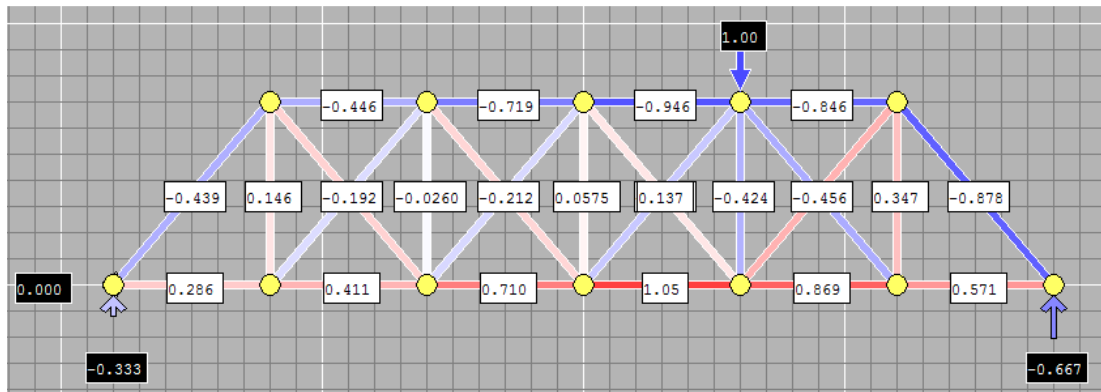


Figure 4.7 A theoretical model showing the mechanical behaviour of a Long truss applied with a concentrated unit force at the second post, generated by the simple software program PointSketch2D.

4.2.2 Howe truss

The Howe truss, which became very popular in the 19th century, was patented in the US by William Howe in 1840 (Ritter, 1990). It is a composite truss structured with both timber and iron members. The truss is structurally designed such that the vertical members are in tension as an iron rod and the diagonals are in compression and made of timber. Howe was the first to introduce iron as a general structural member in truss bridges. The Howe truss is often used in design of steel bridges. The theoretical model shown for the Long truss illustrates the natural behaviour when all members are capable of carrying compression. Howe manipulated the mechanical system by removing the compressive load-bearing capacity of the vertical members, by the choice of slender iron rods.

4.2.3 Pratt truss

The Pratt truss is a composite truss with both steel and timber members. The design was patented in US by Thomas W. Pratt in 1844 (Ritter, 1990). On the contrary to the Howe truss, it is characterized by having the vertical members in compression made of wood and the diagonals in tension made of iron rods. The compressive force in the upper chord is higher than the tensile force in the lower chord. The Pratt design was not used for timber truss bridges as much as the famous Howe design, but was often used in steel bridges.

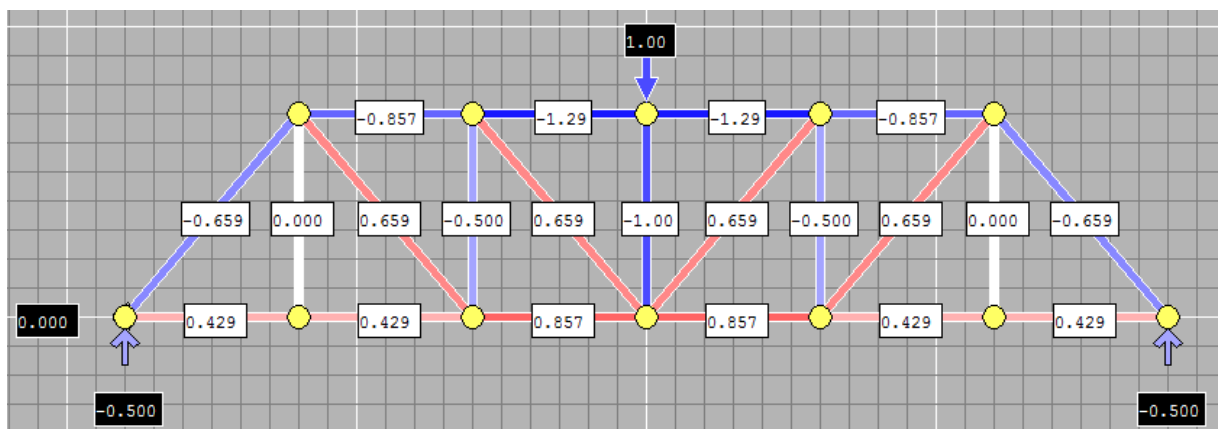


Figure 4.8 A theoretical model showing the mechanical behaviour of a Pratt truss applied with a concentrated unit force at the middle post, generated by the simple software program PointSketch2D.

4.2.4 Multiple kingpost truss

The kingpost and queen post are one of the oldest truss systems often used in roof structures, with an approximately maximal span of 18 meter (Yeomans, 1999). The Swedish architect Edvard von Rothstein (1890) gives a technical description and illustration of a king and queen post, see a) and b) in Figure 4.9. The kingpost truss is suggested by von Rothstein to be constructed with a span length not larger than 9-10 meters. Longer spans require two vertical posts to lift up the force, hence the queen post truss is suggested, a span about 13-15 meters can then be obtained. He further claims that an increased span of 20 meters can be obtained by the kingpost bridge types c) and d) and 30 meters by type e) in Figure 4.9. The combination of a queen post and a strut frame can have a span of approximately 22 meters, see f) in Figure 4.9. The longer spanned trusses were suggested by von Rothstein to have a more triangular shape than suggested by the American's Long, Howe and Pratt or the Swiss family Grubenmann. It could be argued that von Rothstein where mostly focused on buildings in various kinds.

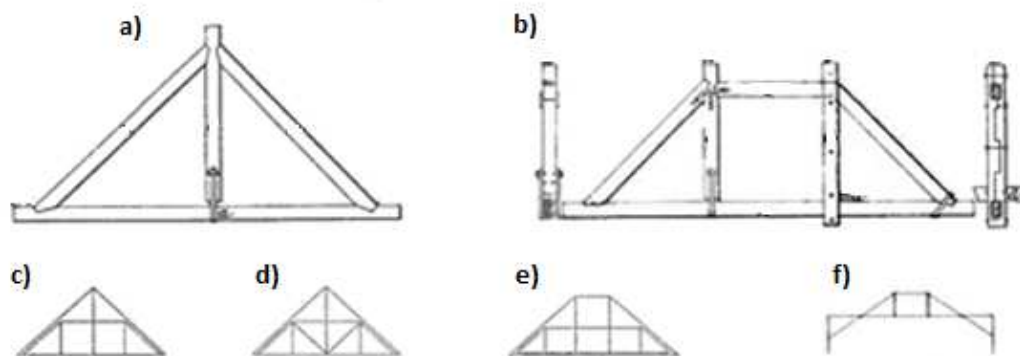


Figure 4.9 a) shows a kingpost truss and b) shows a queen post truss (hängverk [swe]). c), d) and e) show further suggestions from von Rothstein to increase the span length. f) shows a combination of a queen post and a strut frame. A queen post truss is a further development of the kingpost truss (von Rothstein, 1890).

A kingpost can be extended to a multiple kingpost which is the inverted counterpart of a Pratt truss, with respect to the diagonals. The mechanical behaviour is illustrated in Figure 4.10, with diagonals in compression and vertical posts in tension. The concentrated force is transferred by a vertical uplift in the posts and a horizontal movement towards the support in the inclined struts. Unlike the Pratt truss, the tensile force in the lower chord is higher than the compressive force in the upper chord. The infinitely low reaction force in the middle post shows that the critical tension joint is situated in the most outer vertical posts. It can be argued that the most critical joint in the total truss is the joint where the end diagonals meet the lower chord. If this joint fails, a mechanism will develop, which will result in a total collapse of the bridge.

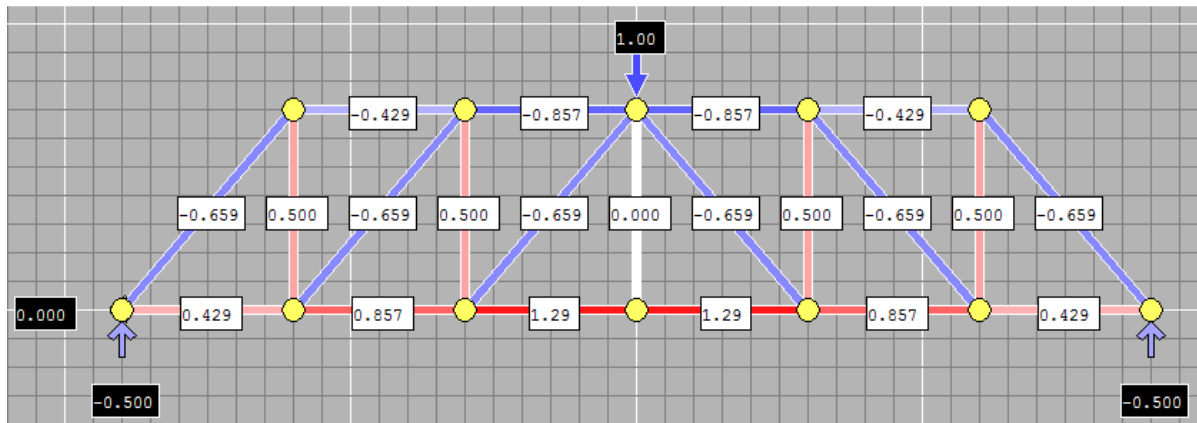


Figure 4.10 A theoretical model showing the mechanical behaviour of a multiple kingpost applied with a concentrated unit force at the middle post, generated by the simple software program PointSketch2D.

4.3 Arch truss

The arch appears in different forms in the structural system of the truss. The upper chord can have the shape of an arch or be parallel to the lower chord, see Figure 4.11. The arch action is the same for both types; the arch is compressed when loaded. Hence, it is sufficient to describe the mechanical behaviour of the parallel-chord truss with an embedded arch often referred to as the Burr Arch, see Figure 4.11. Theodore Burr patented the design in 1817 (US). The design can be described as an arch combined with a truss anchored below the lower chord in the foundation of the bridge. This type is frequently occurring in the history of timber truss bridges and was first used by the famous Swiss carpenters Grubenmann in 1739; see Appendix A number 17.

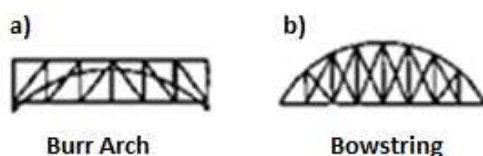


Figure 4.11 Two different truss system with an arch action, a) shows a Burr arch and b) shows a Bowstring (Ritter, 1990).

The arch action can be viewed in the theoretical models in Figure 4.12. The arch was often stretched down to the foundation under the lower chord, to obtain sufficient strength in the joint which connect the arch to the lower chord. Large horizontal reaction forces are induced both from the upper chord and the embedded arch. The

Burr Arch generated a smaller horizontal reaction force since the arch and the upper chord ended in two separate positions; resulting in approximately half the horizontal load in each joint, compare both models in Figure 4.12. The parallel chord truss, which embeds the arch, has the design of a multiple kingpost truss. An implementation of an arch in a multiple kingpost truss bridge will lower the forces in each member which will reduce the stresses in each joint and reduce the risk of buckling, compare Figure 4.10 and Figure 4.12.

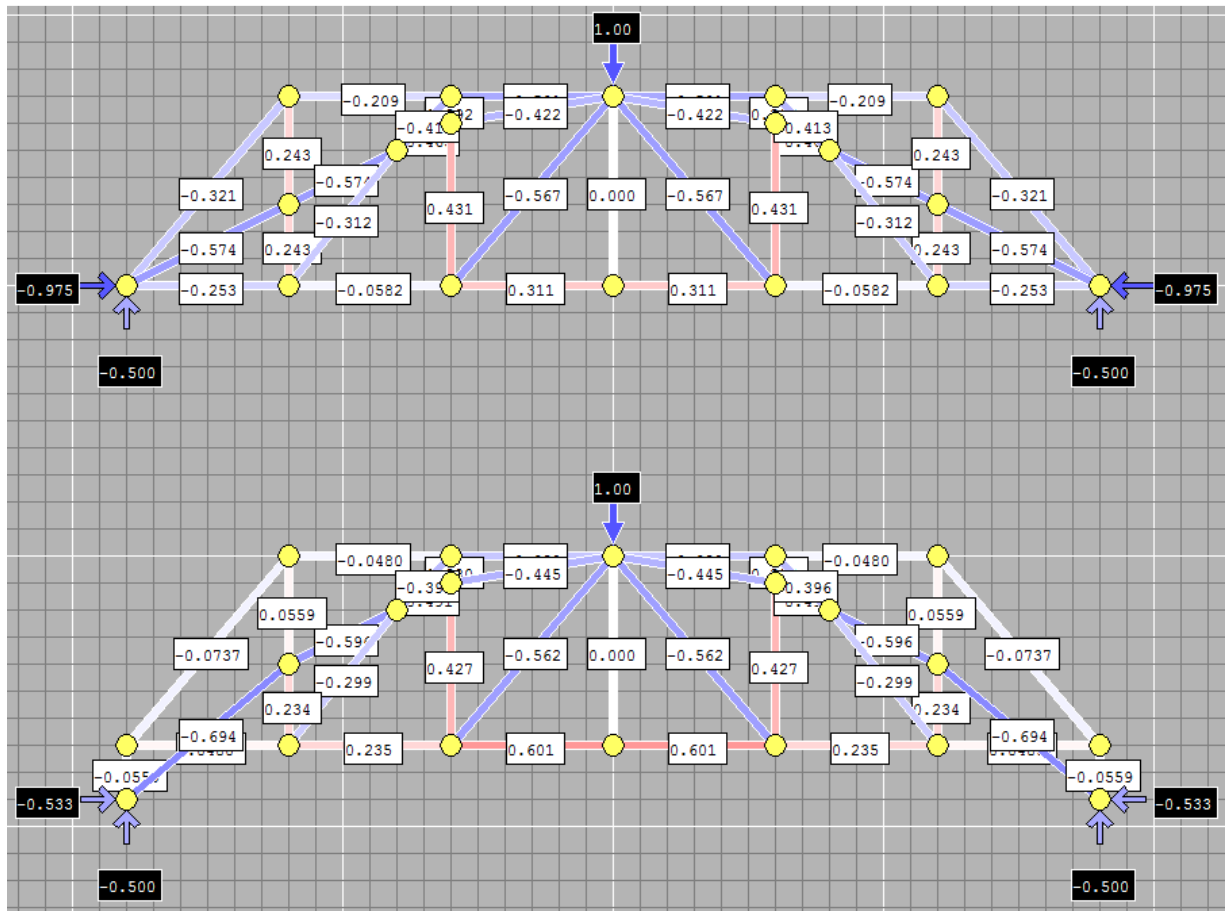


Figure 4.12 Two theoretical model of a parallel-chord truss combined with an arch loaded with one unit load. The lower truss is a Burr Arch, generated by the simple software program PointSketch2D.

5 Timber framed joints in history

The multiple kingpost bridge has been described as one of the oldest timber truss bridges, proven by the early design suggestions by the Venetian architect Palladio in the 16th century, see Chapter 2. Appendix A show a large number of timber truss bridges which have obvious influences from the multiple kingpost truss system. Furthermore, an introduction of the mechanical behaviour of the specific structural system was given in Chapter 3, and the function of each structural member with respect to tension and compression.

Anders Frøstrup has performed a general preliminary design of the multiple kingpost truss bridge *Bridge over Tidan* and thereby also sketched the timber framed joints. Illustrations of the joints together with the location in the bridge can be seen in Figure 5.1. Three different types of joints can be distinguished; the cogging joint see a), b), c) and d) in Figure 5.1, the tension joint see e) and f) in Figure 5.1 and the shear key connection of the laminated beam see e) and g) in Figure 5.1. These three types will be described in the following pages.

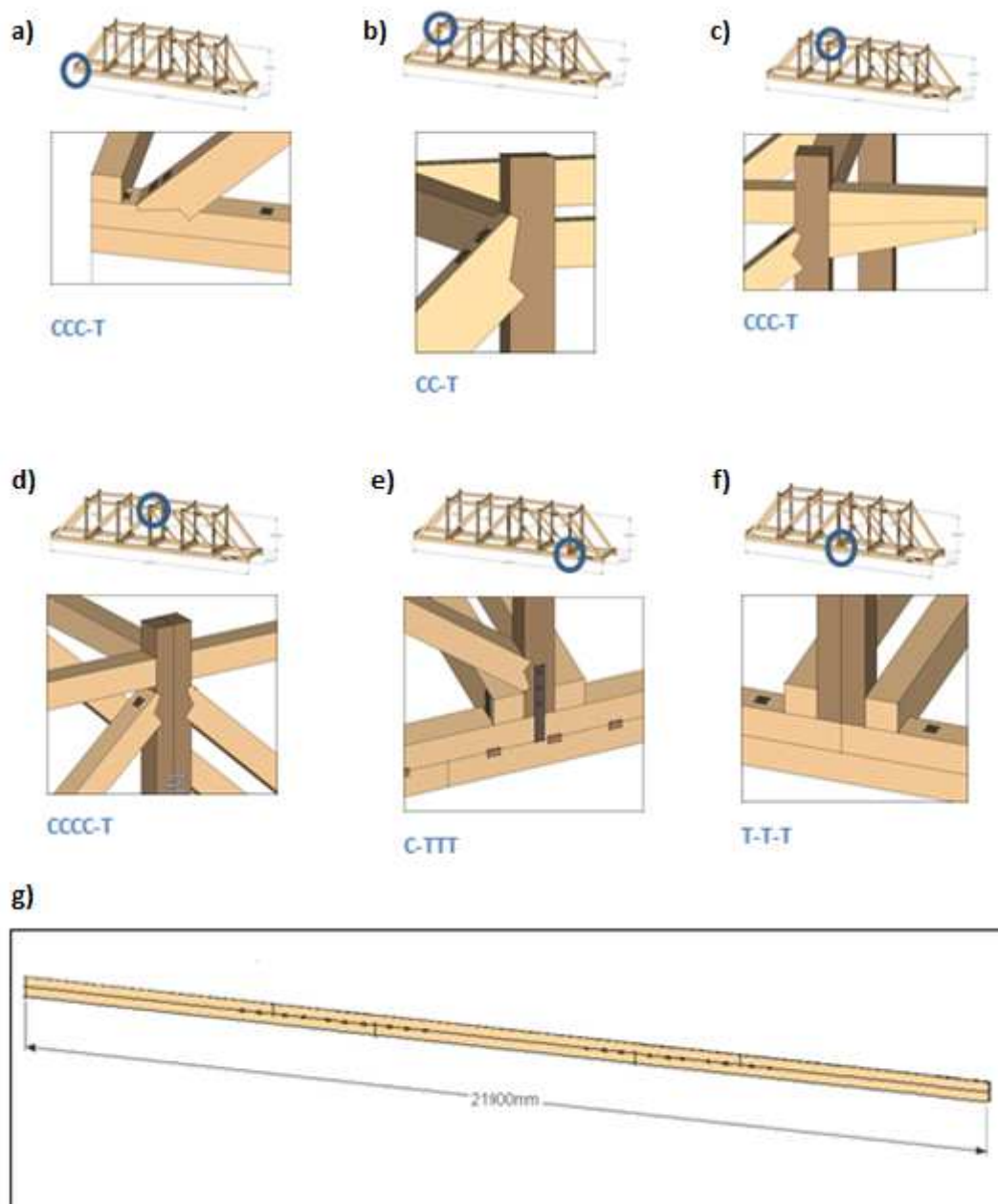


Figure 5.1 The seven joints from the Bridge over Tidan show three different types of joints; a cogging joint see a), b), c) and d), tension joint see e) and f) and finally the shear key connection of the laminated beam which can be seen e) and g) (Frøstrup, 2012).

5.1 Earlier suggestions of timber framed joints

An early design of timber framed joints particularly used in multiple kingpost trusses were found in Thomas Tredgold's *Elementary principles of carpentry* (1871), see Figure 5.2. He presented two different types of joints solutions; a framed joint and a notched-bolted joint. In the example with framed joint, he recommended a larger head of the vertical post to enable a more efficient cogging joint, see a) and c) in Figure 5.2. On the contrary, he claimed that the head should be as small as possible to not generate problems due to shrinkage cracks. The post should be made of hardwood,

which reduces the risk of failure due to compression perpendicular to grain, which is exactly the same recommendation as Anders Frøstrup has suggested in the preliminary design of *Bridge over Tidan*. However, Tredgold presented a second solution which he meant was better, were the framing is excluded, instead a notched and bolted joint is recommended, see b) and d) in Figure 5.2. The joint is bolted together and two notches on each side are added, through which the bolt is pierced.

Tredgold underpinned the time-spanning use of the notched and bolted joint in bridges and thereby emphasized that the solution illustrated in c) and d) is more suitable for bridges. He meant that an edge-to-edge contact between the diagonals together with supporting notches generated a stronger joint.

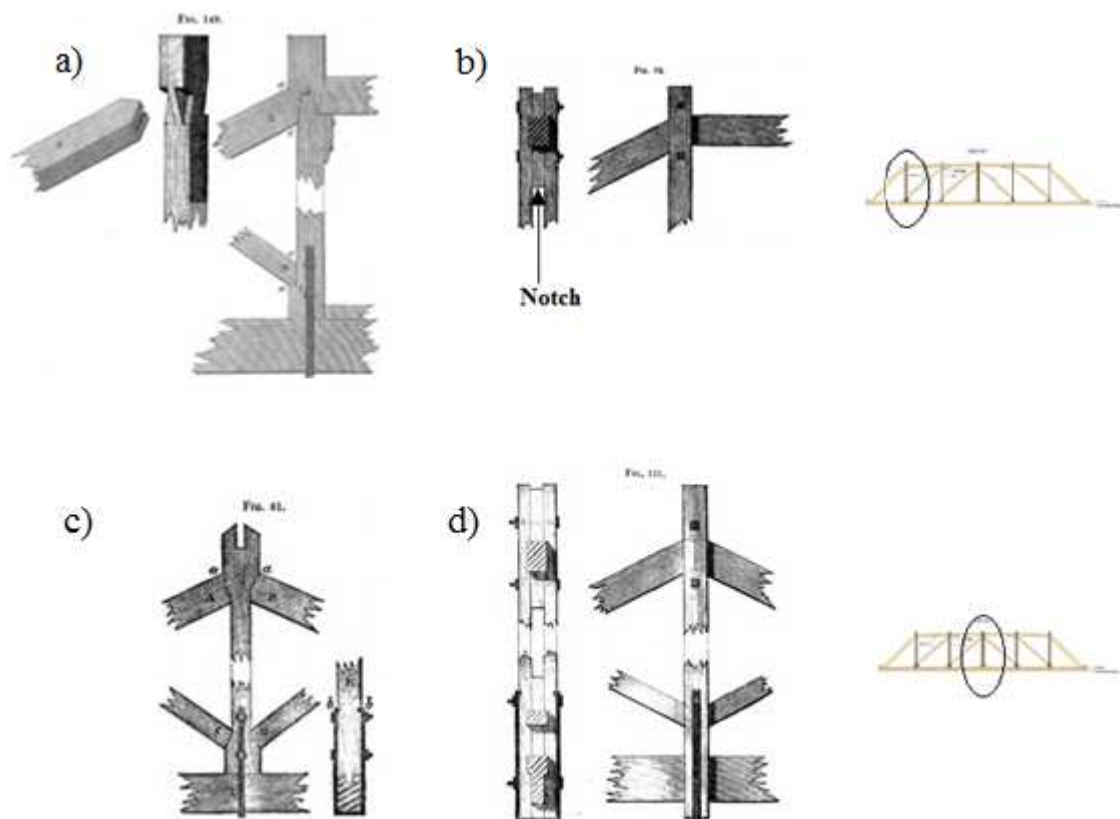


Figure 5.2 a) A timber framed joint solution for the most outer post in a multiple kingpost. b) A notched and bolted joint solution for the most outer post in a multiple kingpost. c) A kingpost with timber framed joints. d) A kingpost with which a notched and bolted joint (Tredgold, 1871).

His favouring of notched and bolted joints could also be motivated by a dreadful disaster in the late 19th century at the *Bridge of Neuilly*, due to shear failure parallel to the grain, which he described in his work. Seven timber members connected by timber framed joints split from end-to-end, which resulted in a total collapse of the bridge. He meant that the squared-edged timber framed joints induced concentrated stresses at the sharp corners of the joints due to uneven pressure between the contact surfaces in the connected members. In the light of the shear failure of the Bridge of Neuilly he proposed an additional joint type for bridges, namely a rounded framed joint. He meant that the rounded end allow a sliding of the joint which in turn will adapt to the new load direction due to movements in the bridge. He further informed that the

movements were induced by shrinkage or settlement of the structure. The rounded contact surfaces will spread the load uniformly, so the risk of concentrated pressure is seriously reduced. He also highlighted the decrease of induced moments due to induced restraints. These rounded framed joints were used at *the Bridge of Sainte Maxence* and *the Bridge de la Concorde (Paris)*. He did not comment the effect on the mechanical behaviour due to rounded framed joints in these bridges. It could be argued that large deflections occurred due to the large joint slip in each joint.



Figure 5.3 A rounded framed joint (Tredgold, 1871).

In contrary to Tredgold's recommendation of notched and bolted joints, von Rothstein (1890) suggested that the chords should not be pierced by bolts, but rather strapped. Notches are excluded in von Rothstein's design suggestions of timber truss joints. No further explanation is given from von Rothstein but it could be motivated by occurring failures near bolts in notched and bolted joints, see Figure 5.4, Figure 5.5 and Figure 5.6.

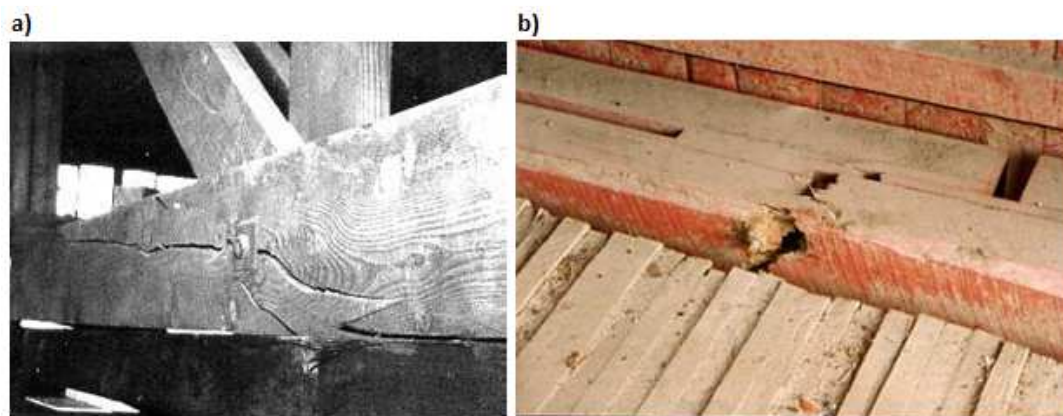


Figure 5.4 a) A bending failure in a lower chord in a warehouse truss due to bolt (Hall, 2009). b) A tension failure in a lower chord due to a bolt in a covered bridge (Hall, 2009).

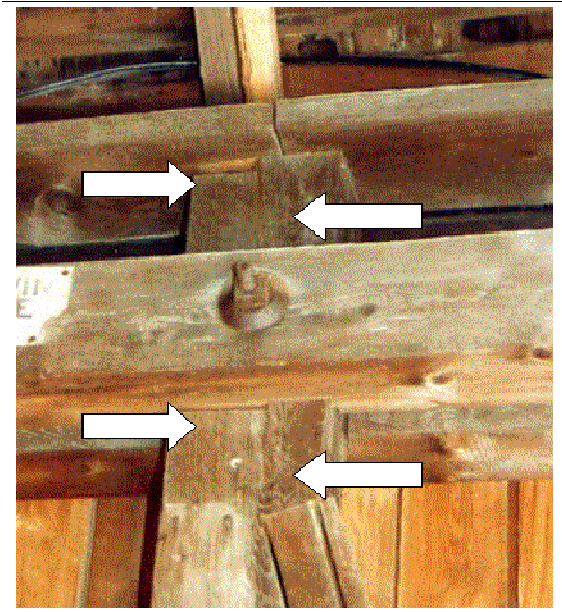


Figure 5.5 A shear failure parallel to the grain in a vertical post in a covered bridge due to a bolt (Hall, 2009)

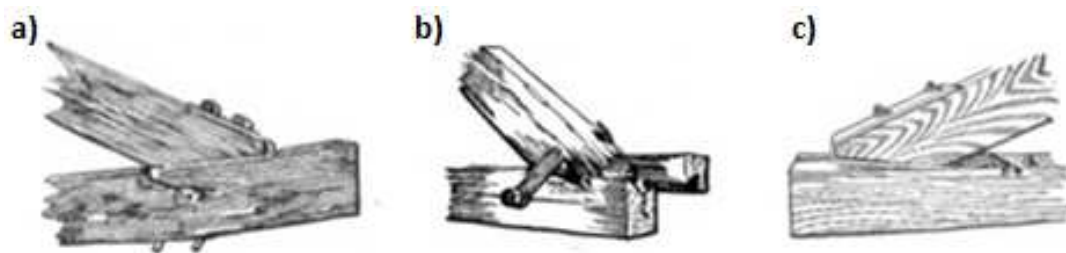


Figure 5.6 Different cogging joint failure. The joints illustrate; a) bending failure, b) shear failure and c) a weak iron shoe (Jacoby, 1909).

5.2 Cogging joints

There are several cogging joints in the *Bridge over Tidan*. Each diagonal ends with a cogging joint to the chord or a vertical post. There are several details in this type of joint and the technical terms are presented in Figure 5.7 together with an illustration.

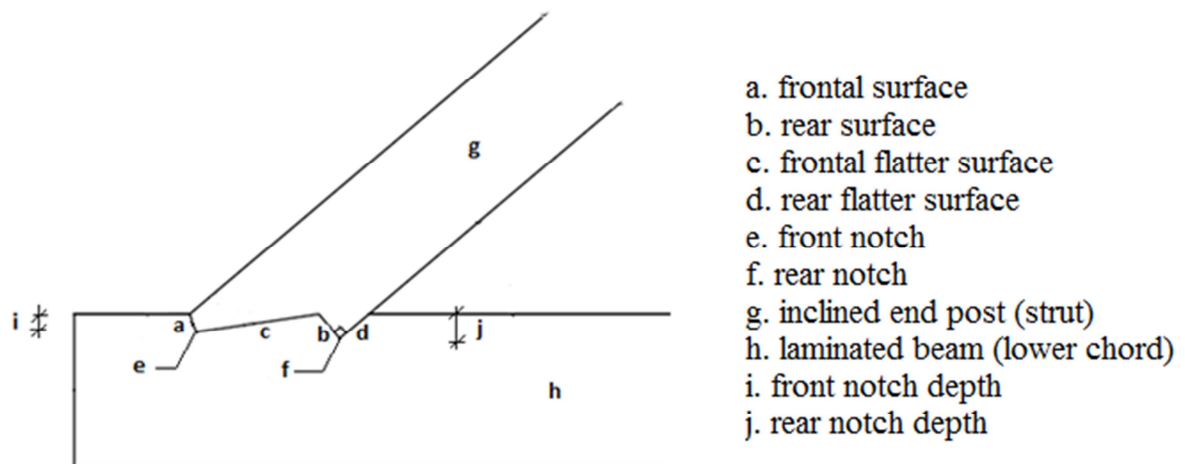


Figure 5.7 Terminology of a cogging joint.

Several design examples of cogging joints and design recommendations are presented in early engineering handbooks for instance by von Rothstein (1890), see Figure 5.8. He suggested that the compression should be applied parallel to the grain as far as possible; hence a joist hanger attached to the chord by nut and bolt was suggested which is illustrated in Figure 5.8 d). Cogging joints with iron supplements are always suggested in large spanned truss by von Rothstein.

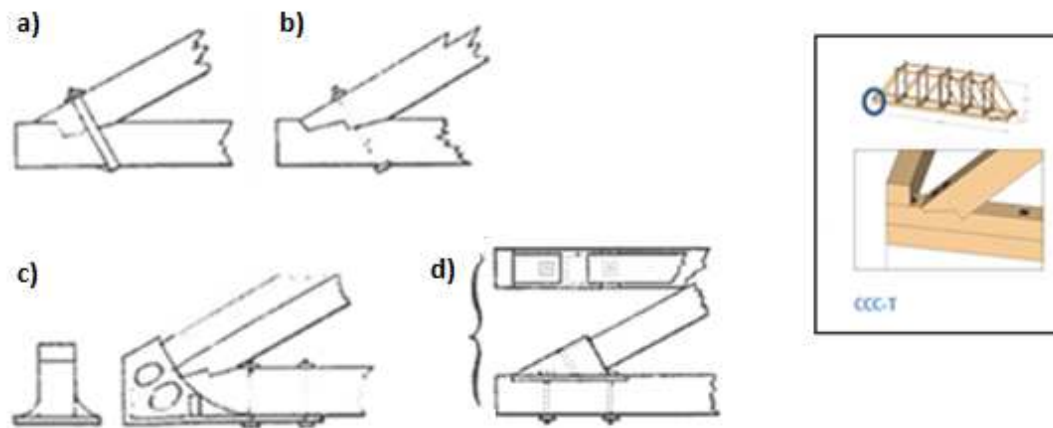


Figure 5.8 Cogging joints with iron supplements. a) A strapped cogging joint. b) A bolted cogging joint. c) A cogging joint with iron fittings. d) A cogging joint with a joist hanger made of iron to ensure parallel compression for the strut (von Rothstein, 1890).

A similar recommendation concerning the contact surfaces of the cogging joint were suggested by Tredgold. He meant that the frontal surface should be perpendicular to the flatter surface. He claimed that the components from the force then are efficiently applied at the contact surfaces. Furthermore, he suggested that an increase of the joint stability could be achieved by a mortise and tenon which is described later in the report, see Figure 5.11. However, he also highlighted the risk of a decreased load-bearing contact surface due to the risk of not fully-loaded tenon caused by shrinkage and/or limitations in craftsmanship. In general he discouraged a complex configuration such as double notched joints and cogging joints with mortise and tenon, since high demand of workmanship.

The importance of considering end grain penetration in the end of two timber members is emphasised by von Rothstein (1890). Steel plates should be mounted at the interface between two horizontally connected members. He meant that the grains from one member penetrated the other one to some extent when loaded in compression. The deformation of a bolted timber framed joint can cause an increased shear stress in the bolts, which can lead to shear failure of the bolt or exceeding of the embedding strength in the timber members. It could also be argued that the members will decrease in length which in turn can produce additional stresses in form of restraints in the global structure. The suggested steel plate between the contact surfaces by von Rothstein was probably an influence from the Germans according to Tredgold (1871). Tredgold further contradicted von Rothstein by explaining that the purpose of steel plates was to generate a more even spread of the load from member to member. Furthermore, Tredgold meant that this is unnecessary for timber members and only justified for masonry, since the effect of using steel plates are none or very small, when it comes to wood.

In a German engineering handbook from 1940 the importance of shear strength is highlighted. The cogging joint has to be designed so that the shear plane is sufficient otherwise there is a risk of shear failure parallel to the grain (Hoffman, 1940). Two design steps are highlighted to magnify the area.

- The beam end has to be located far enough from the notch, to avoid shear failure parallel to the grain see a) and b) in Figure 5.9.
- The notches in a doubled notch cogging joint should end at different depths in the timber beam which result in two shear planes; see c) and d) in Figure 5.9. This design will increase the shear strength.

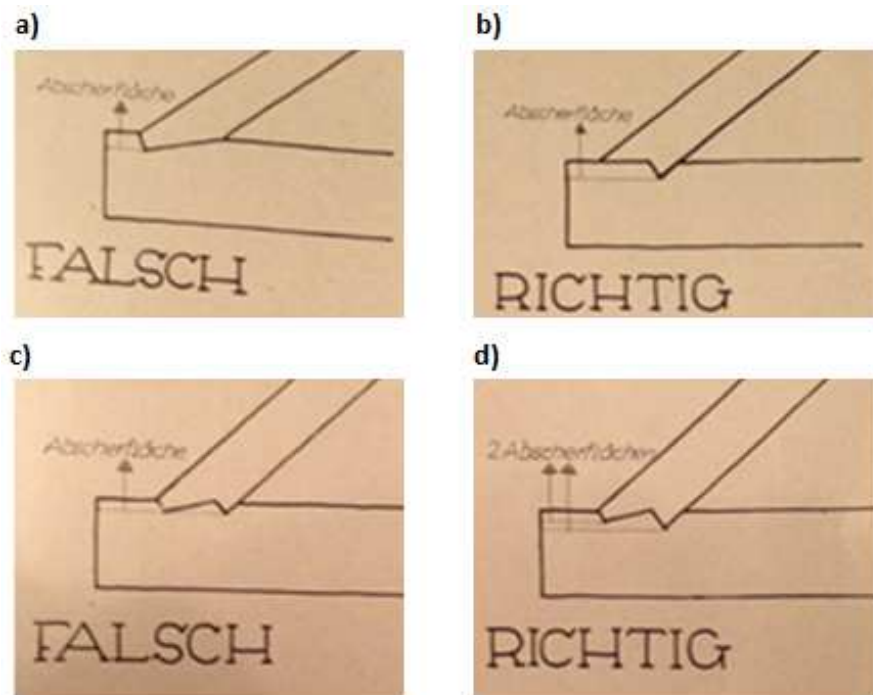


Figure 5.9 According to a German engineering handbook from 1940 joint b) and d) show the correct design of a cogging joint while a) and c) show the incorrect design which can lead to shear failure parallel to the grain (Hoffman, 1940).

Two coinciding cogging joints in a vertical post must behave limited notched depths to ensure sufficient tensile strength in the post. According to the German engineering handbook the cross-section of the post is too weak if only one third remains see a) in Figure 5.10. The correct design should be encountered by a limited notch depth, which is illustrated by b) in Figure 5.10.

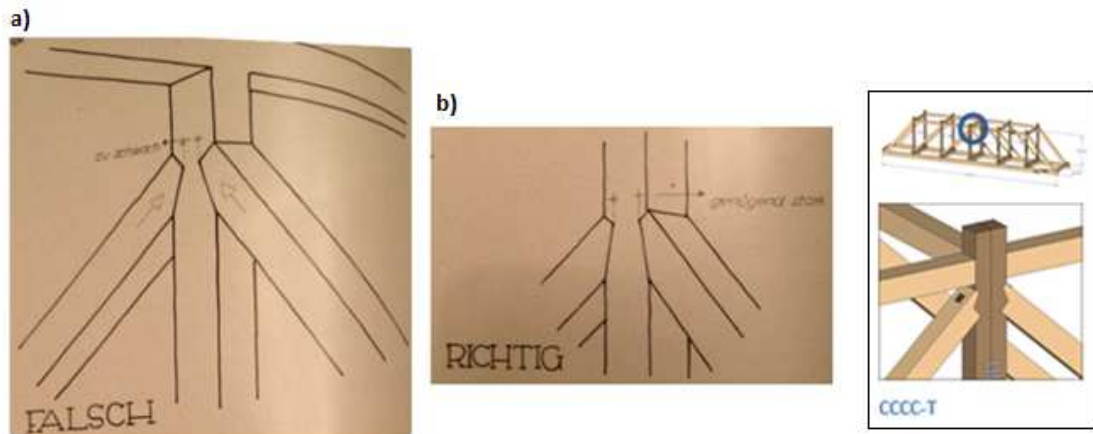


Figure 5.10 a) shows an incorrect design of two coinciding cogging joints while b) shows the correct design (Hoffman, 1940).

The use of timber framed joints is often seen as a stiffness challenge such as timber structures in general. Large deflections can be generated by joint slip. This aspect was addressed already by Tredgold in the late 19th century. He emphasized that the initial deflection could create a partially loaded contact surface in a cogging joint. Therefore the carpenters were urged to consider the initial deflection already in the manufacturing process. The deflection was prevented by an intentionally unbalance in the joint. The unbalance can be explained by a induced larger pressure on the frontal surface than on the flatter surface, which over time will be balanced by the expected initial deflection which generate a higher pressure on the flatter surface.

5.3 Tension joint

The design of tension joints in timber framed structures depend on the magnitude of the load. Heavy loaded tension joints are typically designed with some kind of steel such as straps, while the lightly loaded can be design as a pegged mortise and tenon joint.

A typical pegged mortise and tenon joint is shown in Figure 5.11. Tension is resisted by locking the tenon in the mortise by adding pegs. The joint is suitable when small tension stresses can be expected. Even though the connection is not subjected to tension in the service state, it may be subjected to tension during the assembling process. A further stabilisation of a mortise and tenon joint can be generated by an addition of a housing, which is a notched hole that will support the connecting member, see Figure 5.12.

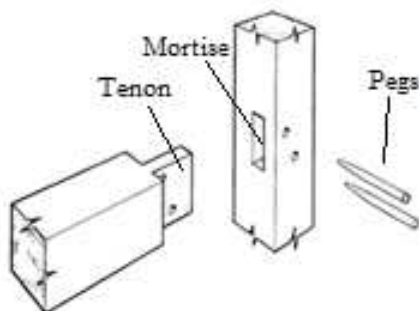


Figure 5.11 A mortise and tenon joint is referred to as a tying joint by Jack A. Sobon in *Timber framing fundamentals* (Sobon, 2011).

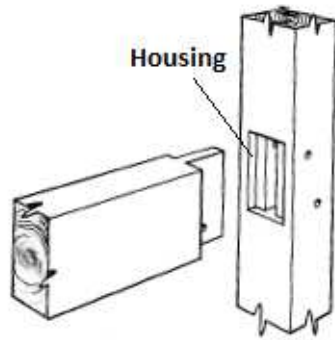


Figure 5.12 A housing of a mortise and tenon joint (Sobon, 2011).

The main purpose of the peg is to draw the contact surfaces tight together and to stabilize the joint (Ross, Mettem and Holloway, 2007). The required shear resistance to withstand tensile stresses in the joint is a secondary property. According to an interview with Associate Professor and carpenter Nils-Eric Anderson (2012), pegs are often made of oak and dried to a moisture content about 12%. The purpose of the strictly chosen moisture content is that the peg should be dryer than the timber members, so it swells when assembled, which results in a tightening of the connection. Pegs of pine and spruce are also possible to use, but to improve the mechanical bond an octagon-shape is used (Murphy, 2011). A peg of oak with an octagon-shape cannot be used since it will only destroy the hole, i.e. the oak is too hard.

The pegged timber members should be air-dried, which means in equilibrium with the environment. Air-dried timber has a moisture content in the range 15%-23% according to the Swedish industry association Skogsindustrierna (2004). According to the Swedish standard, SS 23 27 40, the highest moisture class deliverable to end user for direct mounting is 18, which corresponds to moisture content in the range 14-22% for a timber thickness greater than 25mm (AMA, 2013). The specified moisture content (12%) in the peg is thereby lower than the pegged timber, which is required.

In contrary to Ross, Mettem and Holloway (2007), Tredgold (1871) claimed that hardwood pegs had a considerable shear resistance. He referred to ship building, or more precisely referred to a certain Mr Parson who experimented with wooden pegs in the service of Her Majesty's dockyard around the shift of the 18th to 19th century. According to these experiments a peg of English oak had a shear capacity of 27.57 MPa perpendicular to the grain (the number recalculated from older units to modern units).

Furthermore, according to Tredgold the double tenon should be avoided, since in general, there is more load on one of them. He seems to prefer bolt and nut joints rather than timber framed joints, which he emphasizes continuously in the *Elementary principles of carpentry*. The British engineers and carpenters were not as experienced as the Swiss and Germans on large timber structures, which could be one of the reasons for preferring alternatives to timber framed joints.

A heavily loaded tension joint made only by timber was not found in the literature study. There are two heavily loaded tension joints with similar configuration in the *Bridge over Tidan*. The differences are highlighted in the following sections. Already in the late 19th century Tredgold (1871) recommended that certain iron complements should be added for joints loaded in tension. Several strapped tension joints of this type are found in von Rothstein's *Allmänna byggnadsläran*, see Figure 5.13. These

types of tension joints often referred to as kingpost joints are described in more detail by Ross, Mettem and Holloway (2007) which also illustrate the steel wedges for tightening of the tensile joint during service life to counteract the global deflection due to shrinkage, see Figure 5.14.

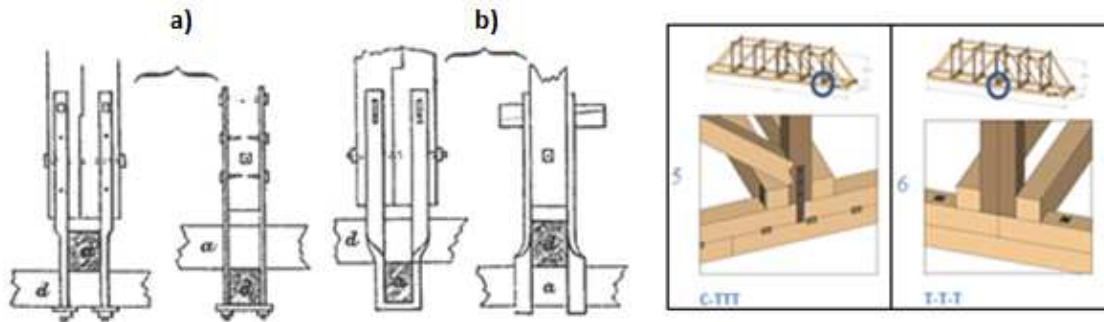


Figure 5.13 Heavily loaded tension joints suggested by von Rothstein (1890). a) An iron plates combined with bolts and nuts (von Rothstein, 1890). b) An iron strap (von Rothstein, 1890).

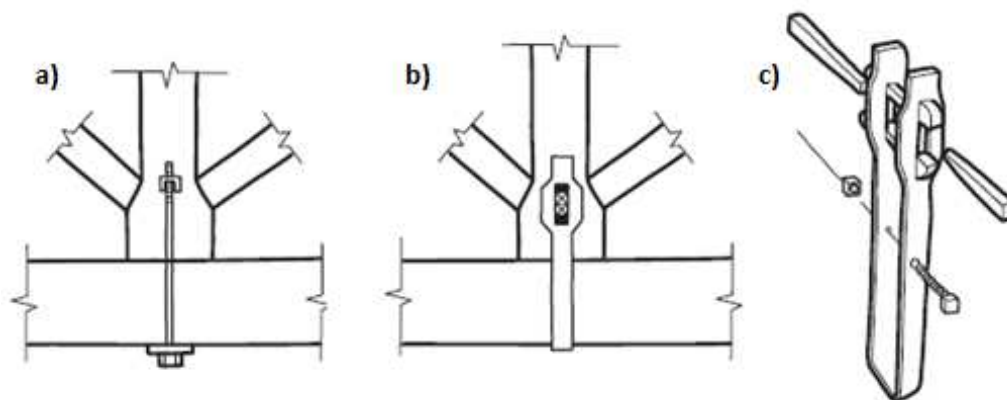


Figure 5.14 a) and b) show two different tension joints. c) show a detail of the steel strap revealing the possibility to tighten the tension joint during service life to counteract the global deflection due to shrinkage (Ross, Mettem and Holloway, 2007).

5.4 Laminated beam

Several references have been found concerning laminated beams. As early as the 15th century, references concerning laminated beams, are found, see the illustration by Leonardo da Vinci in Figure 5.15.

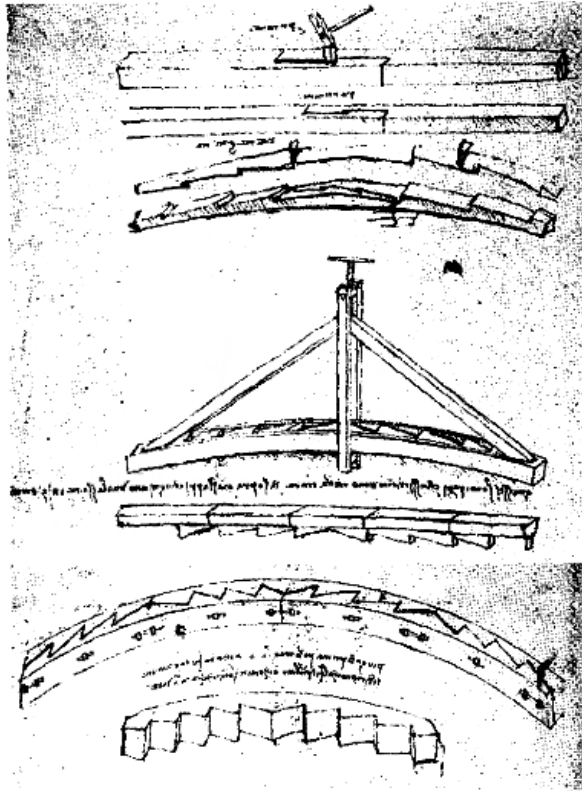


Figure 5.15 An illustration of a laminated beam done by the famous architect and artist Leonardo da Vinci (Ceraldi and Ermolli, 2003)

The laminated beam can be constructed in several configurations. Von Rothstein (1890) describes shortly the practice of the laminated beam. He argues that while the keys are inclined the wedging results in a type of prestressing which generate a ridge of the beam, see a) left-side and c) both sides in Figure 5.16. The ridge can be useful to reduce the deflection of the overall structure. Tredgold show similar beams in his work and underline the importance of having the hooks in the direction of the load.

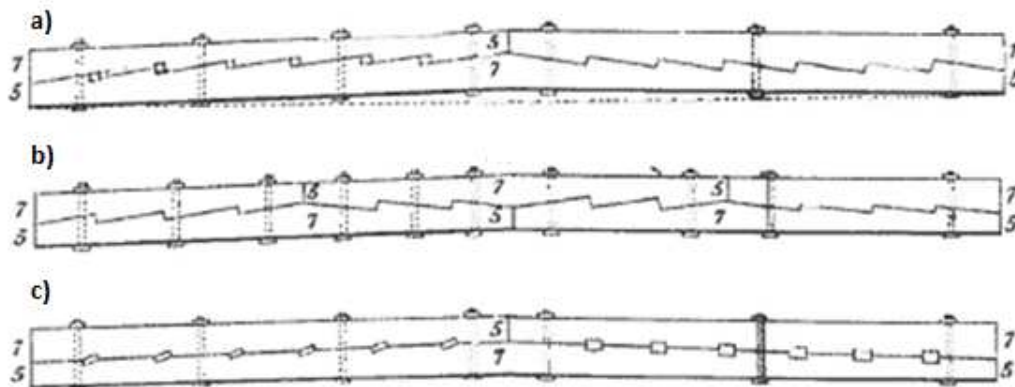


Figure 5.16 Six different types of laminated beams, illustrated both on the left and right side of a)-c) (von Rothstein, 1890).

Two examples of bridges in service with laminated beams are given by Brungraber (2009); a small bridge in Austria with a laminated beam as lower chord, see Figure 5.17 and a railway bridge with a girder made by a laminated beam with cast iron shear

keys, see Figure 5.18. Concrete and steel dominated the 20th century which rapidly ended the thriving development and utilization of the laminated beam.



Figure 5.17 A laminated beam in a bridge in Austria (Brungraber and Miller, 2009)



Figure 5.18 A girder in a railway bridge. The girder consists of a laminated beam using cast iron keys (Brungraber and Miller, 2009)

$$N_2 = N * \sin\left(\frac{\beta}{2}\right) \quad (6.2)$$

The frontal force component (N_1) is then uniformly distributed on the frontal surface, which has an area of $b * \frac{a}{\cos\frac{\beta}{2}}$.

$$\sigma_{c,\alpha,1} = \frac{N_1}{b * a} \cos\left(\frac{\beta}{2}\right) \leq f_{c,\alpha,1} \quad (6.3)$$

where $\alpha = \frac{\beta}{2}$ and for an orthogonal surface $a=h/2$

Further description of an orthogonal surface is not found in the handbook and here it is considered to be configured according to Figure 6.2.

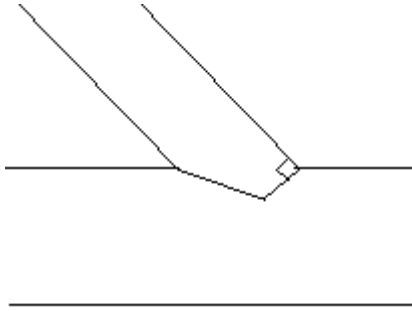


Figure 6.2 An orthogonal contact surface interpretation of design method 1 by the author.

The rear force component (N_2) is uniformly distributed over a weighted area of the flatter surface, which is decided by the strength of the material.

$$\sigma_{c,\alpha,2} = \frac{N_2}{b * d} = f_{c,\alpha,2} \quad (6.4)$$

where $\alpha = 90^\circ - \frac{\beta}{2}$ and d is decided by the expression.

According to this handbook, a secondary force component ($N_1 \cos(\frac{\beta}{2})$) from the frontal force component (N_1) is equal to the shear force component acting parallel to the grain. It is uniformly distributed of the total shear plane $b * s$.

$$\tau = \frac{N_1 \cos\left(\frac{\beta}{2}\right)}{b * s} \leq f_v \quad (6.5)$$

where $\min s=200\text{mm}$ and $\max s = 8 * a$

The width of the inclined end post shall fulfill following condition;

$$h \geq \left(a * \tan\left(\frac{\beta}{2}\right) + d * \cos\left(\frac{\beta}{2}\right) \right) * \sin \beta \quad (6.6)$$

One additional control need to be checked for β angles over 60° between the inclined end post and the laminated beam, then the distance $a \leq H/6$.

6.1.2 Design method 2

A second design approach was found in *Timber Engineering STEP 1*, a literature used in a PhD course in Timber engineering, in this Thesis it is called *Design method 2* (Ehlbeck and Kromer, 1995). According to this design only the frontal area of the contact surfaces in the joint can be accounted for as the load carrying contact surfaces, when the inclined end post and the laminated beam has an β angle between 30° and 60° . The angle of the frontal area is recommended to half the obtuse angle between the inclined end post and the laminated beam.

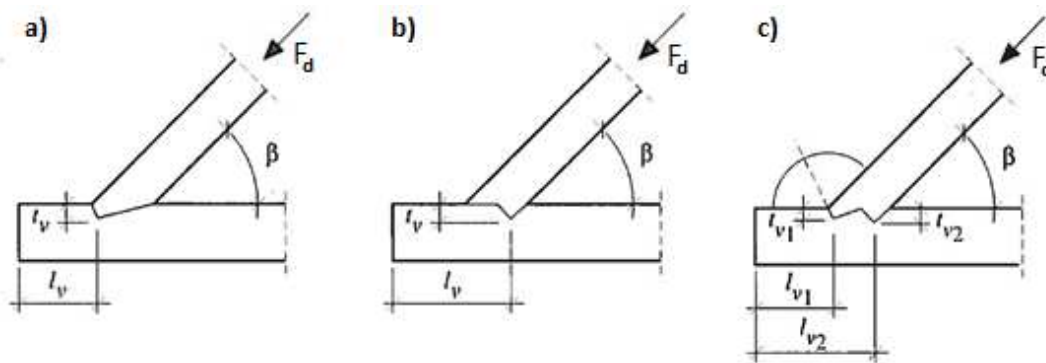


Figure 6.3 An illustration of design method 2. a) a single cogging joint with a frontal contact area. b) a single cogging joint with a rear contact area. c) a double cogging joint with a frontal and a rear area (Ehlbeck and Kromer, 1995).

The stress at an angle to the grain in the frontal area of a single cogging joint is calculated according to Eq. (6.7). This is exactly the same expression as in design method 1 Eq. (6.3).

$$\sigma_{c,\alpha,1} = \frac{F_d}{b_{ef} * t_v} \cos^2\left(\frac{\beta}{2}\right) \leq f_{c,\alpha,1} \quad (6.7)$$

For a single cogging joint with a rear area the compressive stress is expressed according to Eq. (6.8). The total force (F_d) is then uniformly distributed on the rear contact surface, which has an area of $b_{ef} * \frac{t_v}{\cos\beta}$.

$$\sigma_{c,\alpha,2} = \frac{F_d}{b_{ef} * t_v} \cos(\beta) \leq f_{c,\theta,d} \quad (6.8)$$

where $\theta = \beta$

The average shear stress in the laminated beam for a single cogging joint is calculated according to Eq. (6.9). A force component, $F_d \cos(\beta)$, from the total force component

(F_d) is equal to the shear force acting parallel to the grain. It is uniformly distributed of the total shear plane $b_{ef} * l_v$.

$$\tau_d = \frac{F_d \cos(\beta)}{b_{ef} * l_v} \leq f_{v,d} \quad (6.9)$$

where l_v is the horizontal shear plane length from the edge of the beam to the notch.

Furthermore, it is explained that in a double cogging joint, the horizontal component of the total compression force, should determine the length of the shear plane to the rear notch. The following expression should be used:

$$\tau_d = \frac{F_d \cos(\beta)}{b_{ef} * l_{v,2}} = f_{v,d} \quad (6.10)$$

A condition, concerning the double shear planes, must be fulfilled for a double cogging joint. The purpose of the condition is to assure that the two shear planes do not coincide.

$$t_{v,1} = \begin{cases} t_{v,2} - 10mm \\ 0.8 * t_{v,2} \end{cases} \quad (6.11)$$

The control of the tensile stress in the reduced cross-section of the laminated beam and bending stresses caused by eccentricities in the inclined end post are highlighted in the design recommendations according to design method 2.

6.1.3 Numerical analysis of a cogging joints

The assumptions in current simplified design approaches of cogging joints today are discussed in the recently published technical paper by Villar et al. (2006). A numerical analysis was conducted on a cogging joint designed according to the Spanish Technical Building code (CTE-SE-M (2006)), see Figure 6.4.

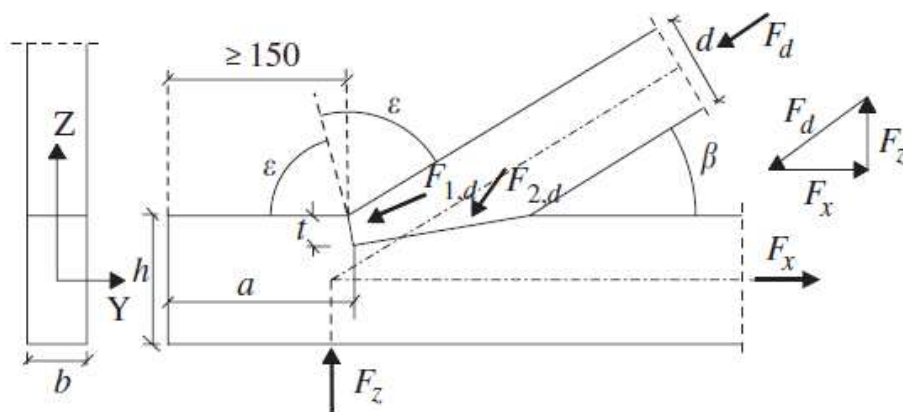


Figure 6.4 A cogging joint illustration from the Spanish Technical Building code, CTE-SE-M (2006), (Villar et al., 2006).

The stress distribution, the distribution of the applied normal force in the strut onto different contact surfaces and the neglect of the effect from friction was highlighted as unrealistic assumptions in current simplified cogging joint designs. It is concluded that a more realistic design of a cogging joint can be achieved by using a reduction factor developed from a numerical analysis of a cogging joint. The developed factor reduces the currently required notch depth (t) and the required length of shear plane (a), which result in a proportional increase of the predicted strength of the joint. Five different angles between the strut and the chord were studied; 25° , 30° , 35° , 40° and 45° . Several important conclusions were stated such as;

- Cogging joints with large angles (β =around 45°) between strut and chord have a larger distribution of the force onto the flatter area of the cogging joint than smaller angles (around 25°), which on the contrary carries most of the applied load at the frontal area, see Figure 6.5.
- The predicted shear plane length and notch depth can approximately be reduced by 15% for small angles and 30% for large angles. The following equation can be used to calculate the reduction factor y ;

$$y = 1.0245\beta - 14.363 \quad (10.12)$$

where β in $[\circ]$ is the angle between the strut and the chord and y is the reduction factor in $[\%]$. For example $\beta=40^\circ$ result in a reduction of 26.6%.

- Strength class of wood was found to have no effect on the reduction of the required notch depth and the required length of shear plane.
- The shear stress distribution was investigated by Villar et al., which concluded that the predicted shear stress was much higher than the modeled shear stress, sees Figure 6.6.
- The friction force was found to be totally neglected in current simplified design methods. It was concluded by the numerical analysis that the friction force gave a large contribution to the load-bearing capacity of a cogging joint.

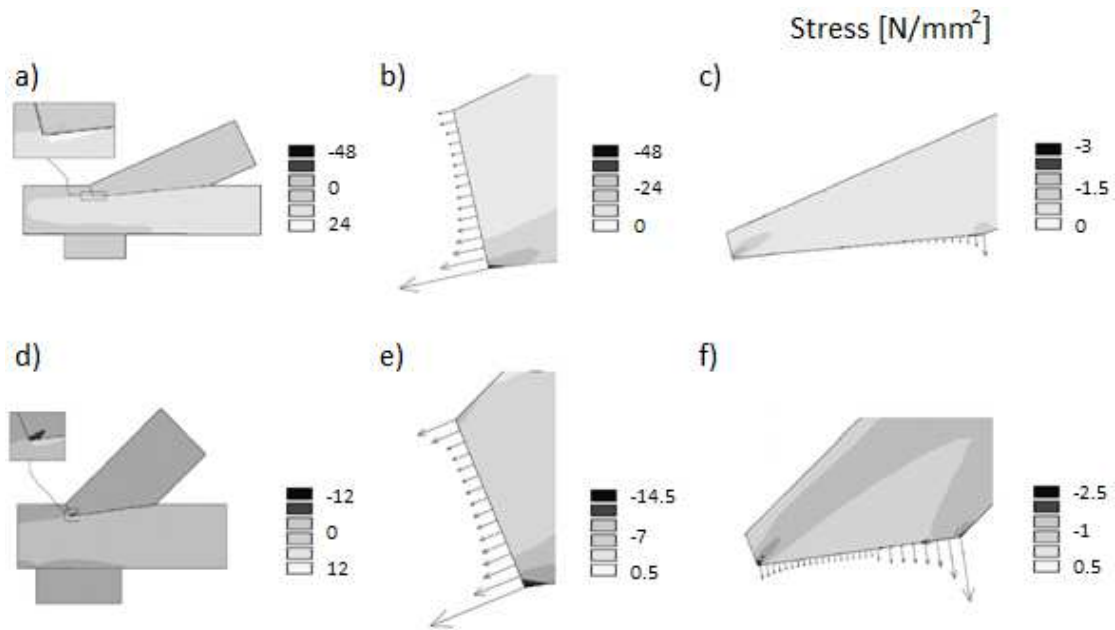


Figure 6.5 A numerical local analysis of a cogging joint with two different angles between the strut and the chord. a) shows a cogging joint with an angle of 25° and d) shows a cogging joint with an angle of 45° . b) and e) show the spread of the force component acting on the frontal contact surface while c) and f) show the spread of the force component at the flatter contact surface. The flatter contact surface contributes in a higher degree to the load-bearing capacity of a cogging joint when the angle between the strut and the chord is larger, due to friction (Villar et al, 2006).

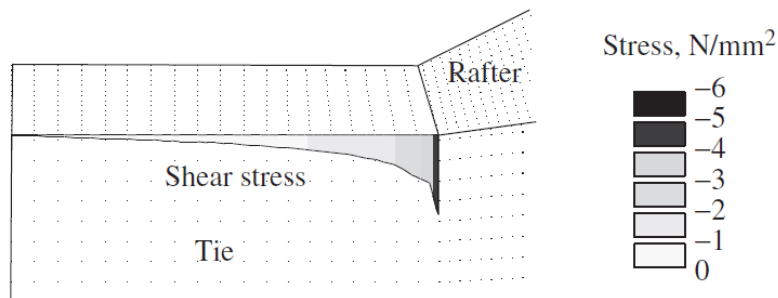


Figure 6.6 The shear stress distribution in a cogging joint according to a numerical analysis was lower than the predicted shear stress based on simplified design methods (Villar et al, 2006).

6.2 Tension joint

In the late 90s several research projects were conducted on mortise and tenon joints by both the Michigan Technological University and the University of Wyoming. A successive Master's Thesis project on the same subject was conducted in 2004 by Joseph Miller together with the supervisor Prof. Richard J. Schmidt (2004), a leading Civil engineer in the subject of timber framing both in testing and finite-element-modelling.

They proposed an empirical design equation, Eq. (6.13), for pegged mortise and tenon joints loaded in tension with the limitation of pegs with diameter of 25.4mm (1 inch) (Miller and Schmidt, 2004). Eq. (6.13) shows the allowable shear stress in the unit [psi] (multiply by 0.006894757 to obtain [MPa]) expressed in the specific gravity of the peg and base material. The limitations of Eq. (6.13) are $0.6 \leq G_{PEG} \leq 0.8$ and $0.35 \leq G_{BASE} \leq 0.75$.

$$F_v = 1365 G_{PEG}^{0.926} G_{BASE}^{0.778} \quad [psi] \quad (6.13)$$

The capacity of pegged mortise and tenon joints were investigated through several test in tension and shear and compared to results from non-linear FE-modelling based on input data from the National Design Specification for wood construction (NDS), which is an American design code for timber structures. 18 tests were performed for a pegged mortise and tenon joint loaded in tension. Five failure modes were found, such as:

- Mortise splitting caused by insufficient edge distance due to exceeding the tensile strength perpendicular to grain.
- Bending failure of the peg due to low embedding strength of base material, which was overrepresented in the test.
- Tenon splitting caused by insufficient end distance due to exceeding the tensile strength perpendicular to grain.
- Tenon row shear (block rupture) caused by insufficient end distance due to exceeding the shear strength parallel to grain.
- Shear failure of the peg due to high embedding strength of base material.

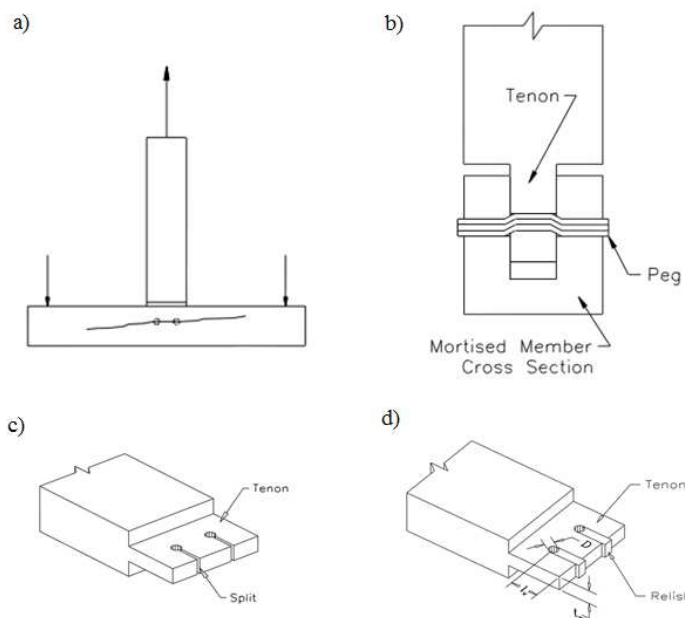


Figure 6.7 a) Mortise splitting failure. b) Bending failure of peg. c) Tenon splitting. d) Block rupture in tenon. (Miller and Schmidt, 2004)

The average yield stress of the joint was identified as 11.9 MPa with a standard deviation of 2.3 MPa, based on less than 18 tests since repaired and cyclically loaded specimen were excluded in the statistic calculations.

12 tests were performed for a pegged mortise and tenon joint loaded in shear. The joint had no housing and varying end-distance, edge-distance and spacing of the pegs. Three failure modes were found, such as:

- Tenon rolling shear which was described as a brittle failure.
- Tenon splitting below the lower peg hole, which was overrepresented in the tests.
- Bending failure of peg.

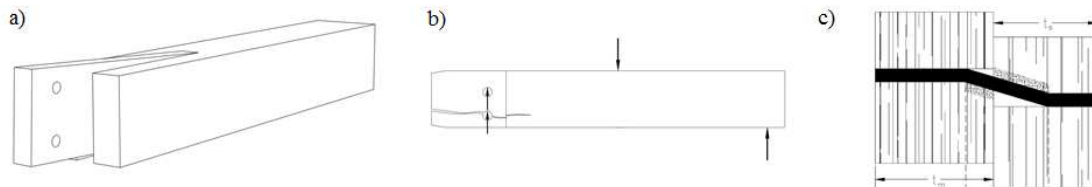


Figure 6.8 a) A tenon subjected to rolling shear. b) Tenon splitting below lower peg hole. c) A bending failure of peg (Miller and Schmidt, 2004).

The average yield stress was identified as 10 MPa with a standard deviation of 2.9 MPa, based on less than 12 tests since repaired and steel dowel specimen were excluded in the statistical calculations. According to Miller a pegged mortise and tenon joint is not a sufficient configuration of a joint loaded in shear, the housing must be added.

6.3 Laminated beam

Joseph Miller designed and analyzed the laminated beam using shear keys in his recently dissertated PhD (Miller, 2009). This composite beam is not as strong as the solid beam or the glulam beam but it has a high aesthetic value, see Figure 6.9 and Figure 6.10.



Figure 6.9 A modern laminated beam (Brungraber and Miller, 2009).



Figure 6.10 The framework of large building constructed by Hunter Timber Frame Structures. The roof structure is supported by a laminated beam, which clearly show that a structure of this size is possible to construct using laminated beams (Brungraber and Miller, 2009).

The design and analysis of mechanically-laminated beam using shear keys conducted by Joseph Miller (2009), can be summarized in some design steps which can be used in the *Bridge over Tidan*:

- The higher the stiffness of the shear key, the higher the stiffness of the beam. On the contrary, if the ratio between the stiffness values is too large the overall stiffness of the beam will decrease. This can occur if cast iron keys are used (Miller, 2009).
- Straps or bolts should be used to clamp the beam and prevent it to separate due to rotating keys. The amount of clamping components will not increase the capacity beyond the fact that the key is compressed instead of rotated (Miller, 2009).
- Inclined shear keys are preferred instead of squared keys. The inclined key will only be subjected to compression and require less dimension for the same result, while the squared key is subjected to both compression and shear and require more space. A positive aspect of the squared key is that the mechanical behaviour is not altered, if the load direction changes, which is the case for inclined shear keys (Miller, 2009).
- The height of the laminated beam should be limited to a maximum three layers (Miller, 2009).
- The keys should be kiln-dried and also the timber itself if possible, to avoid shrinkage of the keys. The performed study showed a clear result of decreasing load-carrying capacity of the beam when the stiffness of the keys decreased (Miller, 2009).
- The spacing of the keys has a certain minimum distance, which has to be fulfilled otherwise there is risk of shear failure in the intermediate part between the shear keys (Miller, 2009).

- The keys should be placed where the shear force is the largest i.e. near the supports. However, Miller suggests an even distribution of the key if the beam is subjected to concentrated loads (Miller, 2009).
- A cambered beam will minimize the deflections, which can be obtained by laminated beam using shear keys. The keys can be inserted in a prestressed beam to create a ridge. Hard driven key wedges in an unstressed beam will also create a ridge of the beam (Brungraber and Miller, 2009).
- A spring under the bolt that clamps the beam together can be inserted which will absorb the deflection due to shrinkage (Brungraber and Miller, 2009).
- A squared shear key can fail due to compression perpendicular to the grain or due to rolling shear (shear perpendicular to the grain), while the inclined shear key risk failure due to compression (Miller, 2009). According to current practice, hardwood keys are often used in softwood beams and iron-cast keys are used for hardwood beams. The proper function of the keys during construction are ensured by deliberately manufacturing a gap on the non-bearing surface, see Figure 6.11.

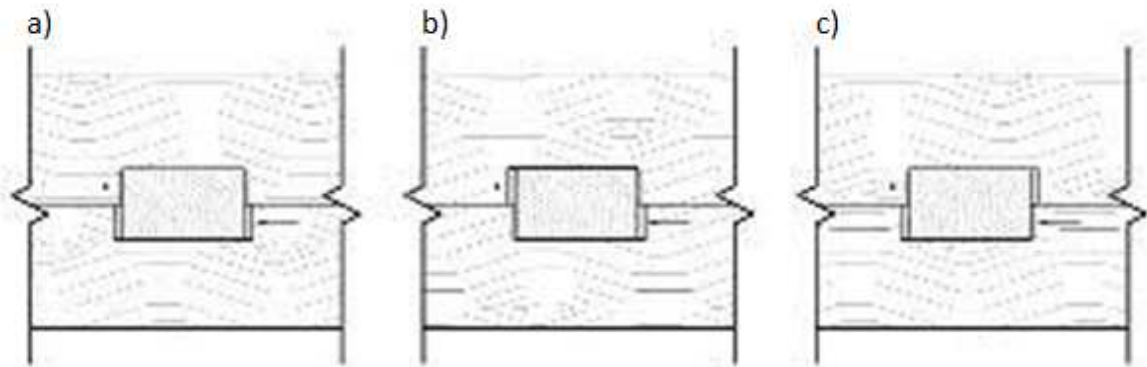


Figure 6.11 The proper function of the keys during construction are ensured by deliberately manufacturing a gap on the non-bearing surface. a) is incorrect. b) and c) are correct if the gap is manufactured on the non-bearing surface (Brungraber and Miller, 2009).

Miller declares that the design and manufacturing of a laminated beam still is a complex process because it is based on analytical studies of the beam. Only a very small part of the total design has been simplified and applied in Eurocode 5, which is not sufficient for a completely designed beam, see *Mechanically jointed beams* in EN 1995-1-1:2004 9.1.3 Annex B.

7 Description of the global numerical model

In this Chapter the global numerical model of the bridge will be presented, starting with a description of the structural model and the simplifications made. Additionally the Chapter continues with a description of the input data in form of material properties and loads.

7.1 Simplifications of the structural system

Several simplifications had to be introduced to be able to obtain a reasonable numerical model in both magnitude of the computational effort and the mechanical behaviour. All diagonals in *Bridge over Tidan* had an angle of 40° . The inclination was kept since the grain direction is of importance when studying an anisotropic material such as wood. The span of 21.9 m was also determined to be important and was implemented in the numerical model, see Figure 7.1.

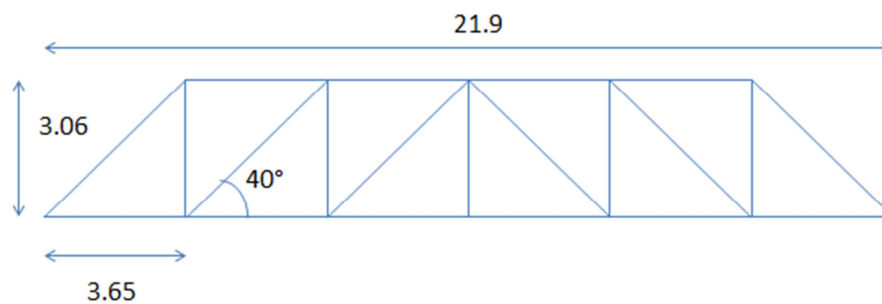


Figure 7.1 The dimensions of one truss which were modelled in Abaqus Brigade/Plus.

Every structural element was modelled with one intersection point to obtain a pure load path. The new intersection generates a lower height of the truss since the unchanged inclination of the strut requires a shortening of the vertical tie, see Figure 7.2. The tender document showed a straight upper chord in the truss, but the model received from Anders Frøstrup had a slight curve, see Figure 7.3. The bridge was modelled with a straight upper chord as Figure 7.1 shows.

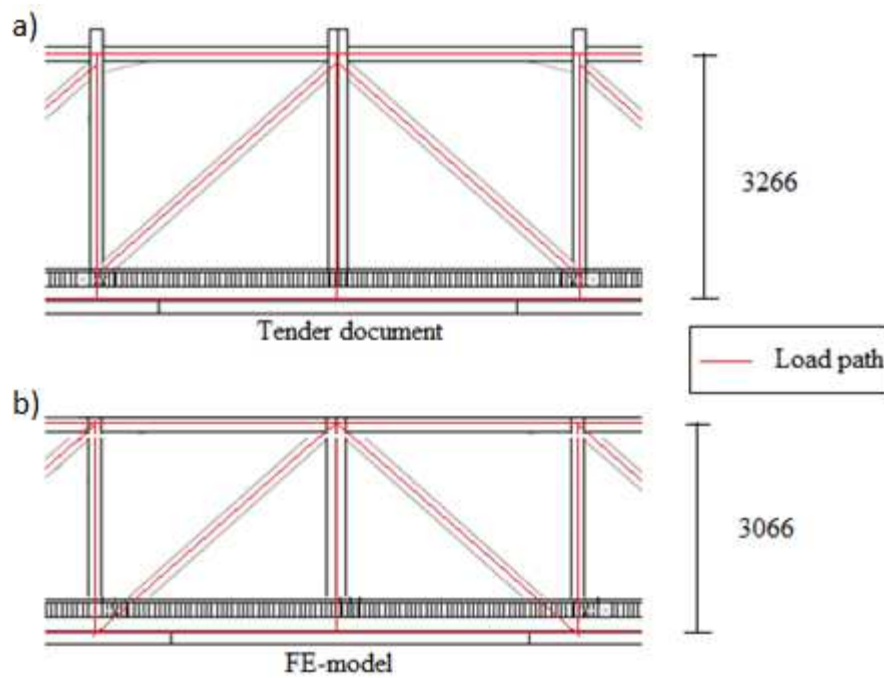


Figure 7.2 The new intersection points [mm]. a) shows the intersection points from the drawing in the tender documents, while b) shows the simplifications made in the FE-software (Karlsson, 2012) (Modified by Teike 2013).

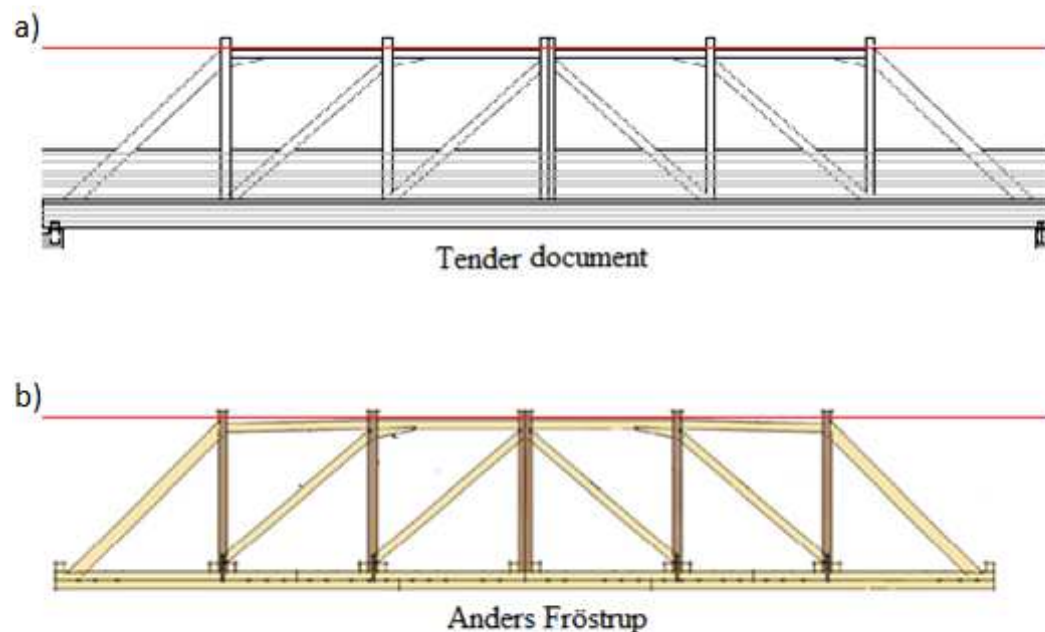


Figure 7.3 a) The upper chord of the truss are neglected in the tender document (Karlsson, 2012). b) The model received from Anders Frøstrup had a slight curve of the upper chord (Frøstrup, 2012). (Modified by Teike 2013)

The wedges in joint 3 in *Bridge over Tidán*, seen in Figure 5.1, are ignored in the global numerical model. Instead the beam elements are joined exactly in the centreline intersection of each beam, since there will be little or no second order effects on the

global behaviour. The protruding top of the tie was also ignored in the global analysis since it will not effect the distribution of forces through the global system. On the contrary, if the local system of a single connection was analysed, it would have had an impact on the total capacity of the upper connection and then it should be considered, but this was not the case in this Master's Thesis.

The laminated beam was modelled as a solid beam. The most outer floor beams were positioned where the last strut meet the bridge deck instead of being placed in the end of the dowelled-beam, see Figure 7.4. This simplification generated a clearly -defined load path.

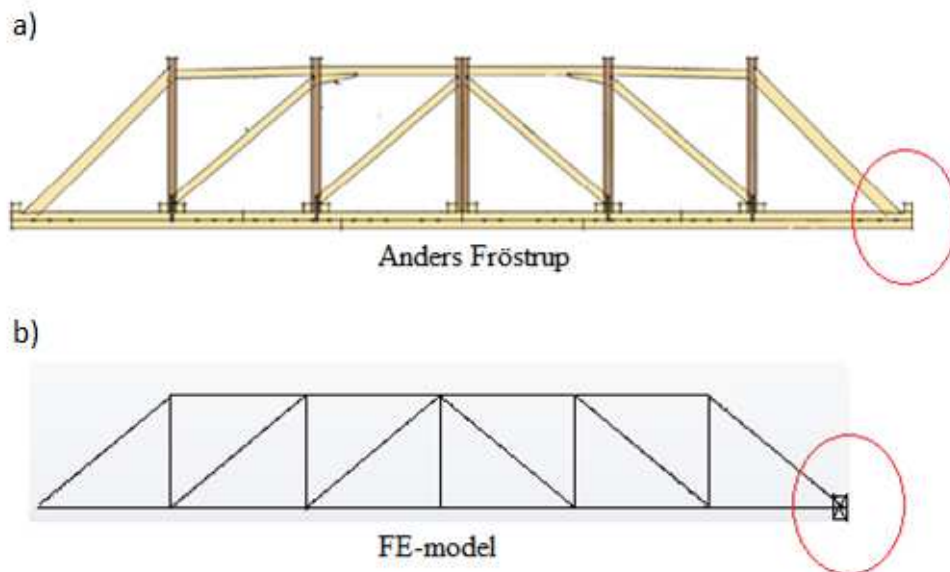


Figure 7.4 The most outer floor beam, seen in a), was moved to the intersection point of the strut and the dowelled-beam, seen in b), (Frøstrup, 2012). (Modified by Teike 2013)

The bridge deck was converted to a massive timber plate using the same density but modified bending stiffness values for each direction. According to the tender documents the floor beams and the decking were placed in different directions, which lead to the assumption of neglecting the bending stiffness in the weak direction for each type of member, Figure 7.5 and Figure 7.6 (Karlsson, 2012). The calculation of the bending stiffness in both x- and y-direction can be seen in appendix B. The result is shown in Table 7.1.

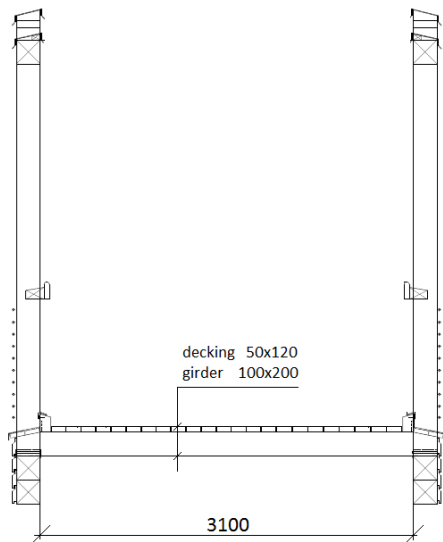


Figure 7.5 A section of the bridge showing the cross-section of the decking boards which determined the bending stiffness in the x-direction (Karlsson, 2012).

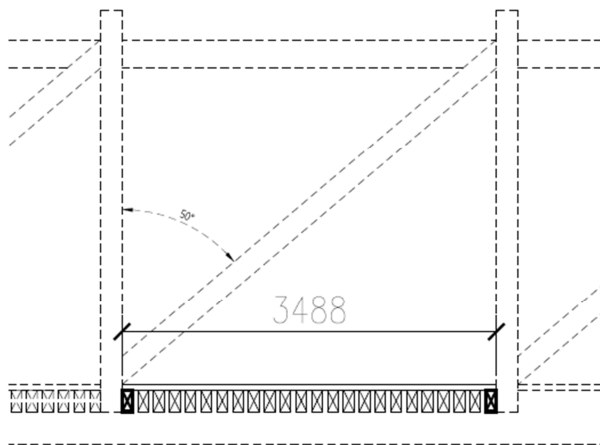


Figure 7.6 A section of the bridge showing the cross-section of the floor beams which determined the bending stiffness in the y-direction (Teike, 2012).

Table 7.1 The calculated bending stiffness of the shell element. The shell element is composed of decking boards and some of the girders.

Direction	Bending stiffness	Notation	Reference
X	0.345 MN/m ⁶	EI _x	Appendix B
Y	17.601 MN/m ⁶	EI _y	Appendix B

Thickness of the orthotropic plate was calculated to 0.193 m by evenly distributed the mass obtained from one square meter of the bridge deck. The calculation is shown in Appendix B. An elastic modulus for each direction was derived from the calculated bending stiffness in each direction by adapting the new modified thickness which resulted in a modified second moment of inertia. The same density and the modified second moment of inertia resulted in a converted elastic modulus linked to the orthotropic plate, see Table 7.2.

Table 7.2 The modified E-modulus of the bridge deck which were used as input data in Brigade/Plus.

Direction	Elastic modulus	Notation	Reference
X	0.197 GPa	E_x	Appendix B
Y	8.878 GPa	E_y	Appendix B

7.2 Material properties

Material properties were determined from SS-EN 338 and the Forest Products Laboratory (US). Timber is an anisotropic material but engineers often simplify the material to a transversely-isotropic material, which can be seen in SS-EN 338. Hence, a transversely-isotropic orientated coordinate system was chosen for the material, see Figure 7.7. The elastic modulus perpendicular and parallel to the grain and the shear modulus were determined according to SS-EN 338. The shear modulus in the weak direction (G_{23}), where determined to 0.1% of the shear modulus given in SS-EN 338.

The transversely-isotropic orientated coordinate system chosen in the finite-element-software required equivalent Poisson's ratios. A certain modification was done to convert the Poisson's ratios to fit the transversely-isotropic orientated coordinate system, since the tabulated values in the report by the Forest Products Laboratory where stated in principle axes of wood, see Appendix C for calculation and Figure 7.8. The Poisson's ratio was chosen to zero for the orthotropic plate which is on the safe side according to European design rules, SS-EN 1995-2:2004 5.1.1 NOTE.

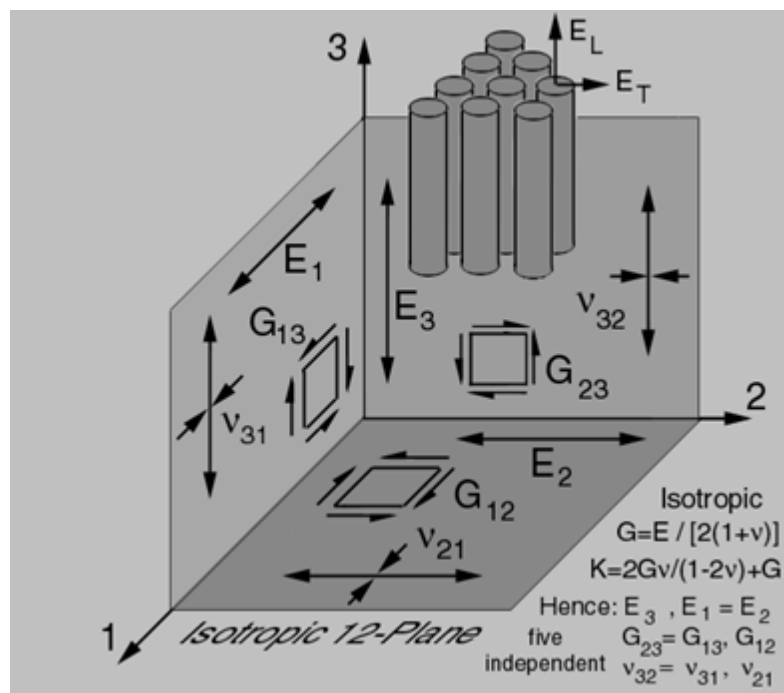


Figure 7.7 A transversely-orthotropic material (Kriz, 1997). (Modified by Teike 2013)

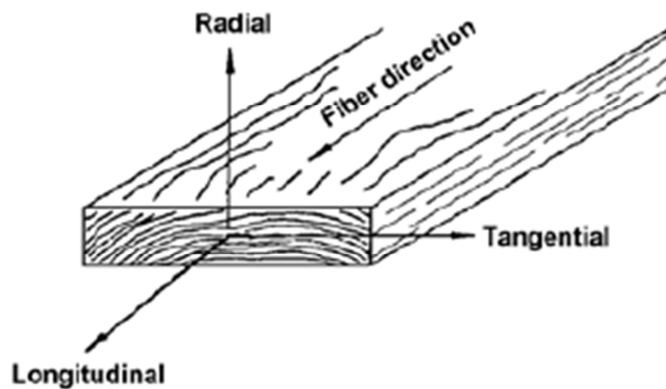


Figure 7.8 The principle coordinate system of timber. The principle axes are related to the grain direction and growth rings (Diaz, Nieto and Rabanal, 2008).

The implemented material properties are collected in Table 7.3. The values of the Poisson's ratio are called Nu12, Nu13 and Nu23 in Brigade/Plus. The shear modulus for the modified orthotropic plate was set to the same value as for Pine D30. The properties shown in Table 7.3 were implemented to each member in their local coordinate system.

Table 7.3 The material properties implemented in Brigade/Plus. Superscripted numbers are indices which show the reference of the values; 1: EN338, 2: Appendix B, 3: Forest laboratory and Appendix C, 4: Assumed value and 5: EN 1995-2 5.1.1 NOTE.

	Oak D40	Pine D30	Modified Plate
E1 [GPa]	13 ¹	12 ¹	10.02 ²
E2 [GPa]	0.86 ¹	0.4 ¹	0.22 ²
E3 [GPa]	0.86 ¹	0.4 ¹	0.22 ²
Nu12 [-]	0.448 ³	0.344 ³	0 ⁵
Nu13 [-]	0.455 ³	0.369 ³	0 ⁵
Nu23 [-]	0.455 ³	0.369 ³	0 ⁵
G12 [GPa]	0.81 ¹	0.75 ¹	0.75 ¹
G13 [GPa]	0.81 ¹	0.75 ¹	0.75 ¹
G23 [GPa]	0.00081 ⁴	0.00075 ⁴	0.00075 ⁴
Density [kg/m³]	660 ¹	460 ¹	460 ¹

7.3 Element type, boundary conditions and mesh

Three different element types were used in the numerical model; beam elements, truss elements and shell elements. The floor beams that support the bridge deck was modelled in two different aspects. Floor beams placed on each side of a vertical post and additionally one in the beginning and the end of the deck are modelled by beam elements. The residual girders together with the decking boards were modelled as a modified orthotropic plate using shell elements. Therefore all floor beams were not visible in the model, since the most part of them were hidden in the properties of the orthotropic plate i.e. transformed into an increased bending stiffness.

12 girders were modelled as beam elements the same amount that can be seen in the figure shown on the cover page, but only 7 beams can be seen in the numerical model, see Figure 7.9. The five beams in the middle consisted of two girders modelled as one but with larger dimensions. This does not effect the results of the global analysis since it was the forces transferred to the connection that was of interest.

The bracings were modelled by truss elements. The bracings had a diameter of 16 mm and were restrained to only have a load-bearing capacity in tension to simulate wires. The framework of the bridge was modelled with fixed connections with a simply supported bridge deck. The bridge deck were modelled separately and only used for analysing the load dividing lines of the bridge. The boundary conditions were set according to Figure 7.10. Three different types of bearings were used; fixed bearing, sliding bearing and sliding guided bearing.

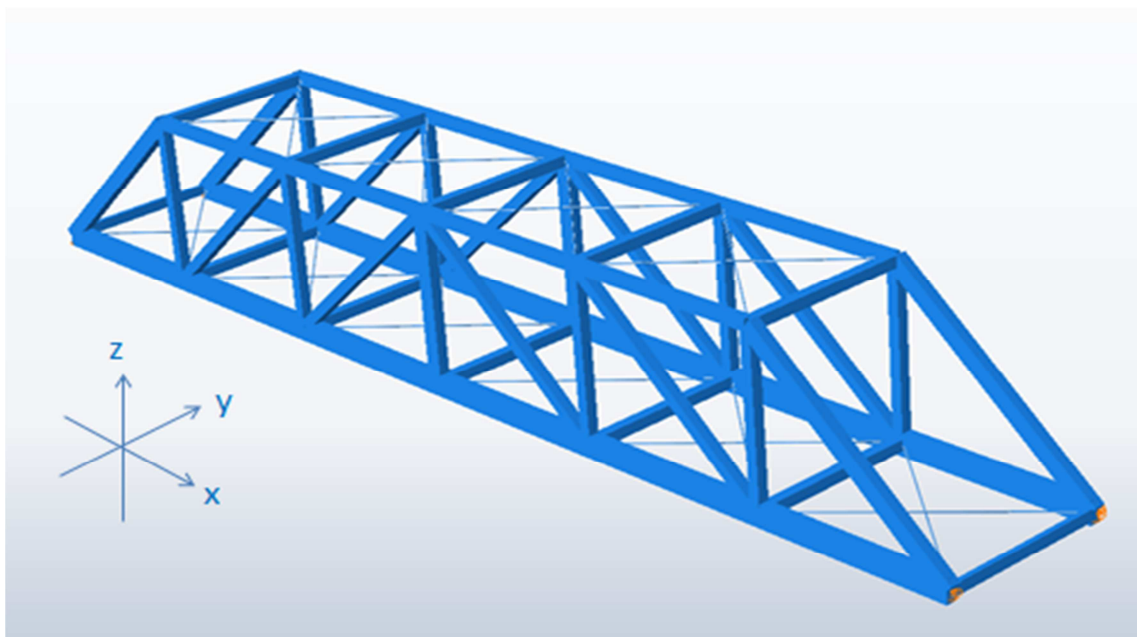


Figure 7.9 A numerical model of the Bridge over Tidán.

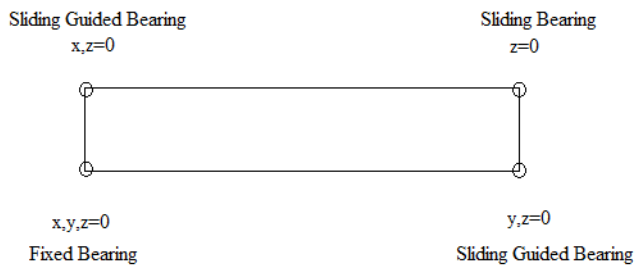


Figure 7.10 The boundary conditions of the numerical model, seen from above.

The mesh of the framework was composed by three-dimensional linear 2-noded beam elements and linear 2-noded truss elements, while the bridge deck was composed by quadrilateral 4-noded stress/displacement shell elements with reduced integration, see Figure 7.11. An algorithm that minimizes the mesh transition was used. The element size was chosen to 10cm, since a smaller element size showed approximately the same results but the computational time was markedly increased. The model consists of 2007 elements and 5931 nodes.

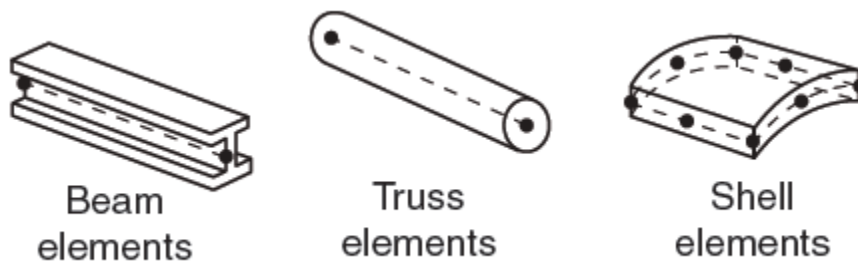


Figure 7.11 The mesh of the framework was composed by three-dimensional linear 2-node beam elements and linear 2-node truss elements, while the bridge deck was composed by quadrilateral 4-node stress/displacement shell element with reduced integration (Abaqus, 2013).

7.4 Loads

The loads on the numerical model are presented in Table 7.4.

Table 7.4 The applied loads.

Load type	Magnitude	Applied direction	Comments	Reference
Self-weight	660kg/m ³ (oak) 460kg/m ³ (pine) 9.81m/s ²	Vertical	Self-weight was calculated from the implemented density by the finite-element software	EN 338
Traffic load	5kN/m ²	Vertical	Surface load. Representing people walking on the bridge	EN 1991-2:2003 5.3.2.1 (2) NOTE.
Wind load	1.8kN/m ²	Transverse	An approximate value	The national bridge code of Sweden <i>Bro 2004</i>
Snow load	0	Vertical	The snow load was neglected	EN 1990 A2.2.3 (3)
Vehicle load	8.23kN/ 8.75kN	Vertical	Project specific service vehicle	EN 1991-2:2003 5.3.2.3 NOTE 1
Braking load	4.938kN/ 5.25kN	Longitudinal	60% of the vehicle loads	EN 1991-2:2003 5.4 (1) & (2)

The self-weight was calculated from the implemented mean densities of the timber and steel together with the volume and the gravitation of 9.81 m/s² by the FE-software *Brigade/Plus*. The self-weight of the bridge deck was implemented as a permanent load on the bridge framework.

A simplified wind load equal to 1.8kN/m² was chosen with reference to an older version of the national bridge code of Sweden *Bro 2004* (Vägverket, 2004). It was then an approved value to be used for bridges with a height up to 10 meters and a location not higher than 45 meters above surrounding environment. The wind load was applied uniformly on the projection plan XZ of the bridge at an angle of 90°. The residual part of the XZ-projected bridge surface and the area of the service vehicle were neglected.

There are three different widths on the tributary area of the wind load; 0.2m, 0.3m and 0.4m, see Figure 7.12. The projected XZ-surface of the inclined end posts had a width of 0.2m which resulted in a 360 N/m wind line load. The inclined end posts and the

central vertical post had a width of 0.3m which resulted in a 520 N/m wind line load. The laminated beam had a width of 0.4m which resulted in a 720 N/m wind line load.

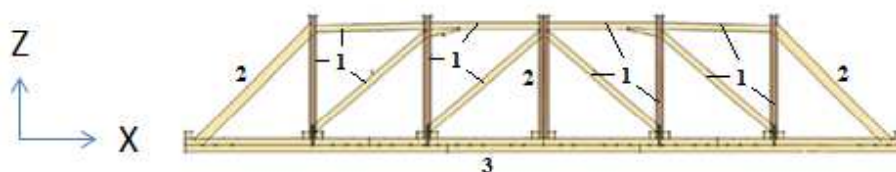


Figure 7.12 The tributary area of the wind load. Structural elements numbered 1 had a width of 0.2m. Structural elements numbered 2 had a width of 0.3m. Structural element numbered 3 had a width of 0.4m (Frøstrup, 2012, Revised by Teike).

The designer was allowed to neglect the snow load in the load combination when combined with traffic load for footbridges according to SS-EN 1990 A2.2.3 (3).

Two traffic loads were considered for *Bridge over Tidan*, a pedestrian load and a service vehicle load. A concentrated traffic load does not need to be considered if a service vehicle load is applied, according to EN 1991-2:2003 5.3.2.2 (3). The pedestrian load is stated as load group *gr1* and the service vehicle as load group *gr2* according to EN 1991-2:2003 5.5 tab 5.1. These denotations were used to find the related partial coefficient for each load in the load combination for the ultimate limit state.

A specific service vehicle is allowed according to EN 1991-2:2003 5.3.2.3 NOTE 1, see Figure 7.13. According to the previous referred NOTE 1 a dynamic contribution specified in the project could be used. The tender document for *Bridge over Tidan* specified a dynamical load factor equal to 1.4 (Karlsson, 2012). The service vehicle belonged to *gr2* according to Eurocode 1, which resulted in $\gamma_0 = \gamma_1 = 0$, see SS-EN 1990 Tab A2.2. The concentrated force for each wheel, see Figure 7.13, was recalculated to a “concentrated” distributed load acting on an area of 0.04 m² which resulted in $Q_{serv.1} = 218$ kN/m² and $Q_{serv.2} = 205$ kN/m², see Appendix D.

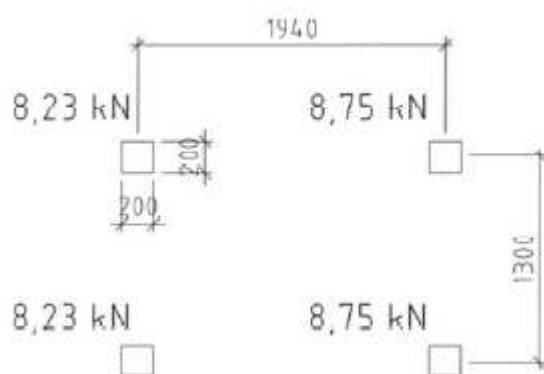


Figure 7.13 A schematic sketch of the service vehicle for which the bridge was design for. The vehicle was of the type, Wille 455B and the loads were multiplied with a dynamical factor 1.4 according to the tender documents (Karlsson, 2012).

The second traffic load simulated a crowd standing on the bridge, here called the pedestrian load. It was chosen as a uniform load of 5 kN/m² according to EN 1991-2:2003 5.3.2.1 (2) NOTE. The partial safety factors for gr1 are equal to $\gamma_0=0.4$ and $\gamma_1=0.4$ according to SS-EN 1990 Tab A2.2.

A horizontal load was chosen from the maximal value of 60% of the service vehicle load and 10% of the pedestrian load, see EN 1991-2:2003 5.4 (2). The load was then redirected to act horizontally in the bridge longitudinal axis in the plane of the bridge deck, see EN 1991-2:2003 5.4 (1). The horizontal load was decided to 60% of the service vehicle load. It was only active simultaneously with the service vehicle load in the load combinations. The horizontal load belongs to the service vehicle which results in partial coefficients equal to $\gamma_0=\gamma_1=0$.

Three different load cases were analysed see Figure 7.14. The variable load from the snow removing vehicle were simulated with four concentrated forces, which were repositioned manually in Brigade/Plus i.e a live load analysis was not executed. The load from the traffic loads were applied on the framework which is illustrated in Figure 7.14.

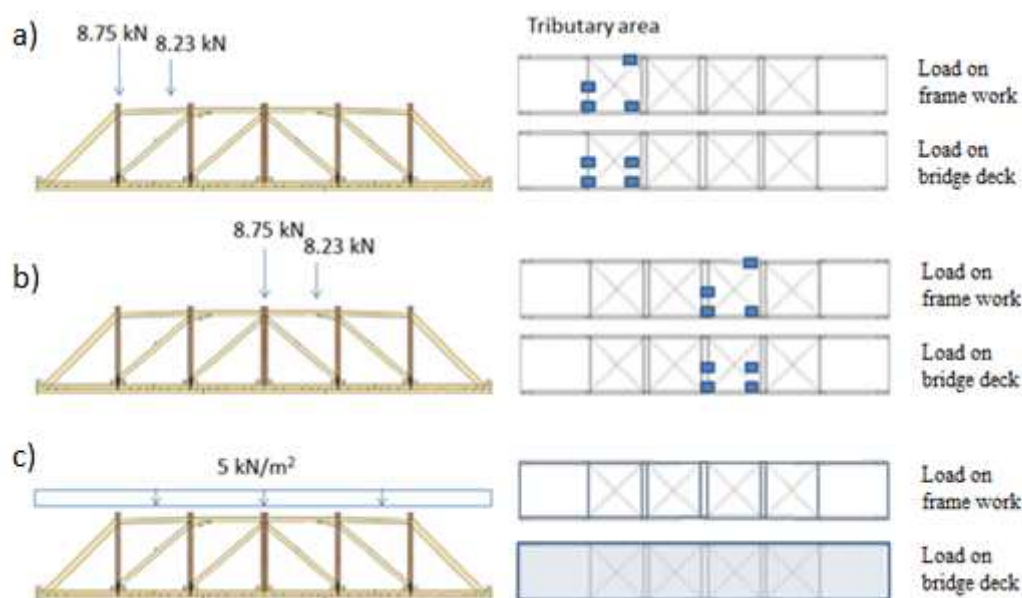


Figure 7.14 The three different traffic load cases which generate the maximum design loads. a) Load case 1 illustrates the service vehicle at the end of the bridge. b) Load case 2 illustrates the service vehicle in the middle of the bridge. c) Load case 3 illustrates the uniform load called pedestrian load, simulating a crowd standing on the bridge (Frøstrup, 2012, Revised by Teike).

The distribution of each load from the bridge deck onto the framework was determined by a separate analysis of the bridge deck. The distribution on the framework depends on the assumed connection between the bridge deck and the framework. The bridge deck was here assumed to be simply supported and will then have a related distribution to each side of the framework according to Figure 7.15.

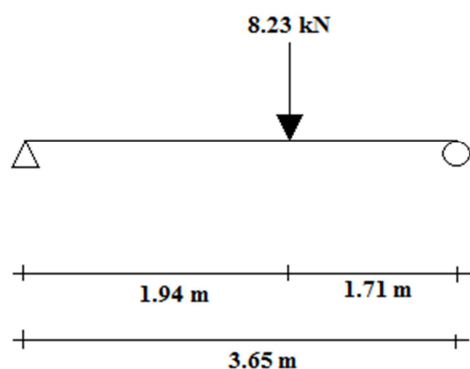


Figure 7.15 A simply supported beam loaded with a concentrated force, simulating the wheel pressure of the service vehicle in the transverse-direction of the bridge deck.

According to the separate analysis of the bridge deck the concentrated force from the service vehicle was transferred to the laminated beams in a stringent manner, see Figure 7.16, resulting in concentrated force on the laminated beams. The calculation of the resulting force on the laminated beams can be viewed in Appendix D.

The load dividing lines to distribute the self-weight of the bridge deck onto the framework were decided by studying the contour plots of a loaded bridge section, see Figure 7.17. A clear indication of the y-direction as the strong direction could be seen, which was consistent with given characteristics of the orthotropic plate. A more accurate load divider can be obtained by an “envelope” configuration, but the approximation with straight load divider lines was compensated by increasing the tributary area in the y-direction, see graph in Figure 7.18.

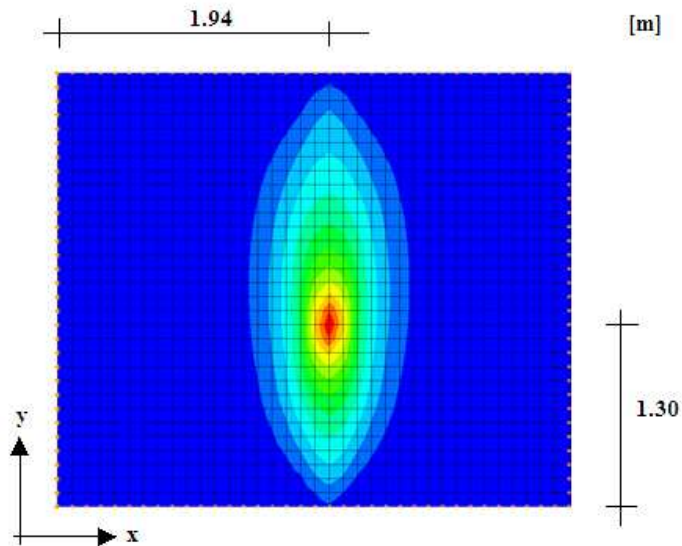


Figure 7.16 A contour plot of the bridge deck modelled as an orthotropic plate. The plot shows the stress distribution from a concentrated force caused by the pressure of a wheel from the service vehicle (8.23kN).

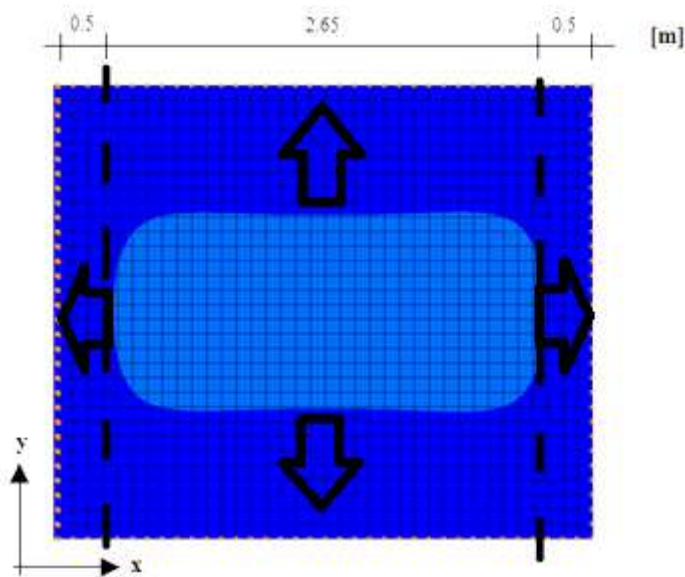


Figure 7.17 A contour plot of the moment around the x-axis on a uniformly loaded orthotropic plate (1kN/m^2). The x-direction is aligned with the longitudinal direction of the bridge deck. The dotted lines show the load dividers of how the load distributes to the floor beams at the right end left side of the figure and the laminated beams in the top and the bottom of the figure.

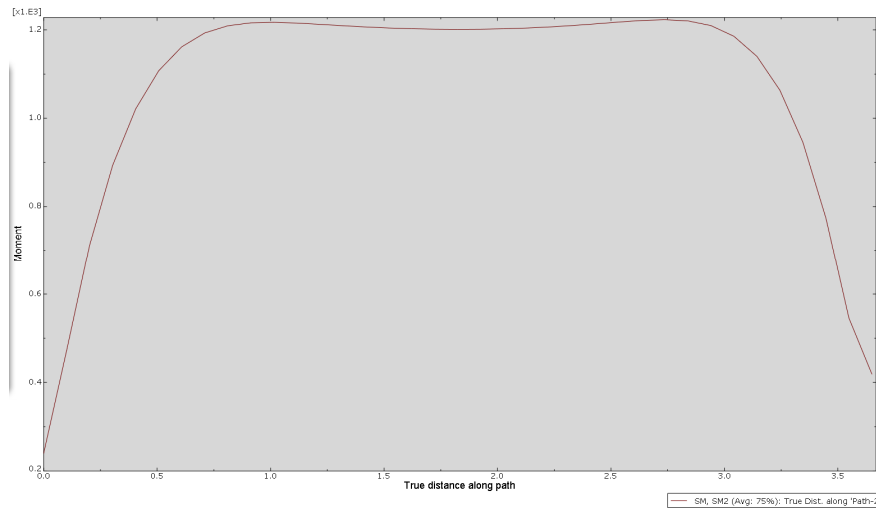


Figure 7.18 A graph of the variation of the moment around the x-axis in the x-direction in the middle of the section. A clear increase of the moment can be seen 50 cm from the edges, which indicates a load divider.

The ultimate limit state was considered according to EN 1990, see Equation (7.1).

ULS: STR

$$\sum_{j \geq 1} \gamma_{G,j} G_{k,j} + \gamma_p P + \gamma_{Q,1} Q_{k,1} + \sum_{i \geq 2} \gamma_{Q,i} \psi_{0,i} Q_{k,i} \quad (7.1)$$

according to SS-EN1990 6.4.3.2 (6.10)

The partial factors could be divided into different parts, to encounter the uncertainties in the numerical load model, see Equation (7.2). The first part, $\gamma_{f,i}$, accounts for deviations in actions. The second part, γ_{sd} , accounts for uncertainties in the action model/ action effect model. A maximum value of $\gamma_{sd} = 1.15$ could be chosen according to SS-EN1990 6.4.3.2 (6.10), which should be applied after the stresses are encountered from the FE-software, see Table 7.5. In this Master's Thesis the partial factors were applied after the results from the global analysis were obtained i.e. not divided in two separated parts.

$$\gamma_{F,i} = \gamma_{f,i} \times \gamma_{sd} \quad (7.2)$$

according to SS-EN 1990 6.3.2 (6.d)

Table 7.5 *The partial factors could be applied before and after stress analysis in Brigade/Plus, but in this Master's Thesis the partial factors were applied after the results from the global analysis were obtained i.e. not divided in two separate parts.*

Load type	Action factor	Model factor	Merged factor
Permanent	$\gamma_g = 1.174$	$\gamma_{sd} = 1.15$	$\gamma_{G,j} = 1.35$
Variable load, ULS	$\gamma_q = 1.304$	$\gamma_{sd} = 1.15$	$\gamma_{Q,1} = 1.5$
Variable load, SLS	$\gamma_{q,1} = 0.87$	$\gamma_{sd} = 1.15$	$\gamma_{1,1} = 1.0$

8 Results

8.1 Global analysis

The resulting output values, sectional forces, moments and transverse shear forces, from the global analysis are collected near the cogging joint in the inclined strut and the laminated beam. Results from the node that connect the beams in the numerical model have been avoided. Instead, all nodes in the total length of the structural member are studied to avoid singularities and numerical deviations in the results. Investigated nodes can be seen in figure below as path 1 and 2. The selection of a realistic value has been based on 54 nodes in the path 1 and 43 nodes in path 2. Six output values has been obtain from each node and load case, which were extracted by a python script.



Figure 8.1 Results from inclined end post are obtained from path 1. Results from the laminated beam are obtained from path 2.

The obtained sectional forces, moments and transverse shear forces from the global analysis are defined in Table 8.1 and presented for each type of load in Table 8.2. The critical load combinations for each type of stress are highlighted as grey boxes. The cogging joints were designed for the normal stress, σ_x , as a simplification.

The sectional forces, moments and transverse shear forces are expressed in stresses according to the equations in Table 8.3 and the resulting design stress values are calculated in Appendix D. The local directions in Abaqus are redefined into x-, y- and z-coordinates same as in EC 1995-1-1, see Figure 8.2. The geometric constants are presented in Table 8.4 and are used in each equations defined in Table 8.3

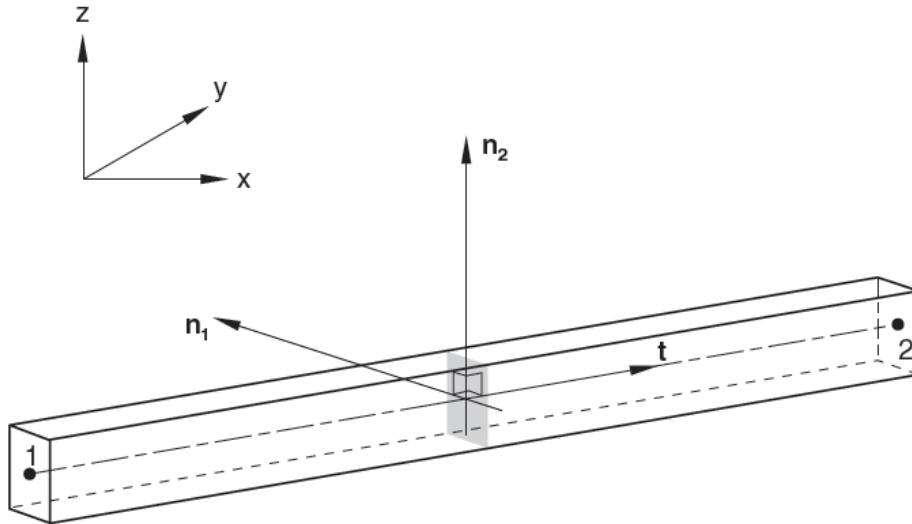


Figure 8.2 Local axis definition for beam-type elements (Abaqus, 2013).

Table 8.1 Definitions of sectional forces, moments and transvers shear forces (Abaqus, 2013)

Sectional forces, moments and transverse shear forces	Definition
SF1	Axial force
SF2	Transverse shear force in the local 2-direction
SF3	Transverse shear force in the local 1-direction
SM1	Bending moment about the local 1-axis
SM2	Bending moment about the local 2-axis
SM3	Twisting moment about the beam axis (tangent-axis)

Table 8.2 The obtained sectional forces, moments and transverse shear forces from the global analysis. The light grey cells in each column represent the most critical load combination, while the dark grey cells represent neglected loads in the critical load combinations. The reason to this was that the wind load was sometime favourable and thereby set to zero and the acceleration and retardation load are only active when LC1 belong to the most critical load combination otherwise it was set to zero.

Inclined end post												
	SF1 [N]	$\sigma_{x,k}$ [Pa]	SF2 [N]	$\tau_{z,k}$ [Pa]	SF3 [N]	$\tau_{y,k}$ [Pa]	SM1 [Nm]	$\sigma_{m,y,k}$ [Pa]	SM2 [Nm]	$\sigma_{m,z,k}$ [Pa]	SM3 [Nm]	$\tau_{tor,k}$ [Pa]
Self-weight	-35054	-584233	-322	-8050	-79	-1975	-327	-109000	-283	-141500	23	8297
Wind-load	-10837	-180617	-5	-125	-2025	-50625	-62	-20667	-1918	-959000	120	43290
LC1 Service vehicle Q	-32775	-546250	-87	-2175	-21	-525	81	27000	-177	-88500	34	12266
LC2 Service vehicle M	-22059	-367650	55	1375	116	2900	-196	-65333	249	124500	-16	-5772
LC3 Pedestrians	-111915	-1865250	544	13600	-350	-8750	-2254	-751333	-1375	-687500	130	46898
LC1 Acceleration load Q	-173	-2883	-3	-75	24	600	1	333	-59	-29500	8	2886
LC 1 Break load Q	-232	-3867	7	175	-31	-775	5	1667	61	30500	-8	-2886
Laminated beam												
	SF1 [N]	$\sigma_{x,k}$ [Pa]	SF2 [N]	$\tau_{z,k}$ [Pa]	SF3 [N]	$\tau_{y,k}$ [Pa]	SM1 [Nm]	$\sigma_{m,y,k}$ [Pa]	SM2 [Nm]	$\sigma_{m,z,k}$ [Pa]	SM3 [Nm]	$\tau_{tor,k}$ [Pa]
Self-weight	26165	327063	-1833	-34369	84	1575	-124	-23250	189	70875	16	4065
Wind-load	-8731	-109138	80	1500	-183	-3431	58	10875	1129	423375	54	13720
LC1 Service vehicle Q	24416	305200	-468	-8775	90	1688	-4	-750	-103	-38625	125	31758
LC2 Service vehicle M	10081	126013	-235	-4406	-38	-713	162	30375	-148	-55500	-20	-5081
LC3 Pedestrians	84505	1056313	-8359	-156731	402	7538	617	115688	866	324750	75	19055
LC1 Acceleration load Q	12934	161675	-23	-431	205	3844	0	0	25	9375	16	4065
LC 1 Break load Q	-14447	-180588	25	469	239	4481	13	2438	30	11250	-16	-4065

Table 8.3 The obtained sectional forces, moments and transverse shear forces from the global analysis are expressed in stresses according to basic mechanical equations.

Sectional forces, moments and transverse shear forces	Equation to obtain load effect
SF1	$\sigma_{x,k} = \frac{SF1}{A}$
SF2	$\tau_{z,k} = \frac{SF2}{A}$
SF3	$\tau_{y,k} = \frac{SF3}{A}$
SM1	$\sigma_{m,y,k} = \frac{SM1}{I_x} \times z_{max}$
SM2	$\sigma_{m,z,k} = \frac{SM2}{I_y} \times y_{max}$
SM3	$\tau_{tor,max,k} = \frac{SM3}{W_{tor}}$

Table 8.4 Geometric constants.

Geometry	Parameter/Equation	Inclined end post	Laminated beam
Height	h	300 mm	400 mm
Width	w	200 mm	200 mm
Area	$A = w \times h$	0.06 m ²	0.08 m ²
Second moment of inertia around x-direction	$I_x = \frac{w \times h^3}{12}$	450x10 ⁻⁶ m ⁴	1067x10 ⁻⁶ m ⁴
Second moment of inertia around z-direction	$I_z = \frac{h \times w^3}{12}$	200x10 ⁻⁶ m ⁴	267x10 ⁻⁶ m ⁴
Distance to most outer fibre in z-direction	$z_{max} = \frac{h}{2}$	150 mm	200 mm
Distance to most outer fibre in y-direction	$y_{max} = \frac{w}{2}$	100 mm	100 mm
Torsional resistance	$W_{tor} = c \times w^2 \times h$	2772 x 10 ⁻⁶ m ³	3936 x 10 ⁻⁶ m ³
Torsional constant	c	0.231	0.246

8.2 Design methods

In this section a comparison between design method 1 and 2 are presented together with an additional assumption which was required to perform the design according to method 2.

8.2.1 Comparison

A comparison of design methods 1 and 2 in Chapter 6 was conducted to highlight similarities and differences.

Similarities between the design methods;

- The compressive stresses at the frontal area are calculated by the same equation; see Eqs. (6.1), (6.3) and (6.7).
- The angle of the frontal surface in design method 1 was found to be the same as the recommended angle in design method 2.
- The force component acting on the frontal or rear surface which also determines the final shear stress had the same direction in both design methods; it was aligned with the chord.

Differences between the design methods;

- Double notched cogging joint
 - Only a single notched cogging joint was presented in design method 1.
 - Both single and double notched cogging joints were possible to design according to design method 2.
- Shear plane length
 - Only a certain interval of the shear plane length was allowed in design method 1, a maximum and minimum value was given in Eq. (6.5).
 - Design method 2 has no limiting value of the shear plane length i.e. an unlimited length can be accounted for to fulfill the shear strength condition.
- Notch depth
 - In design method 1 a certain notch depth was recommended for orthogonal contact surfaces, see Figure 6.2. In addition, when an angle of 60° between the strut and the chord was exceeded the notch depth was limited to a certain value.
 - In design method 2 notch depths of a double cogging joint had to fulfill a certain condition to ensure full utilization of both shear planes, see Eq. (6.11).
- Utilization of the flatter contact surfaces
 - In design method 1, the flatter surface was checked with a stress control, see Eq. (6.4).
 - In design method 2, the force component that acts at the flatter surface was not checked with a stress control when the strut and the chord had an angle between 30° and 60° . No further instructions were given for remaining angles.
- Width of strut
 - The width of the strut had to fulfill a certain condition in design method 1.
 - There are no design rules for the width of the strut in design method 2.
- Tensile and bending stresses

- A control of the tensile and bending stresses was highlighted in design method 2 and not in design method 1.

8.2.2 Assumptions

Additional assumptions necessary to permit a design of a cogging joint according to design method 2 was required. Equation (6.8) was assumed to account for the strength in the laminated beam while the strength of the inclined end post shall be determined by $f_{c,0,d}$.

It was explained in the design recommendations that the sum of the two stresses obtained for a single notched cogging joint with a frontal or a rear contact surface were allowed to be used for a double notched cogging joint. There were no further details stated on how the force should be divided between these double notches and contact surfaces. Thereby, the following weighted formulas were assumed in this study:

$$s_{dist} = \frac{\sigma_{c,\alpha,1}}{\sigma_{c,\alpha,1} + \sigma_{c,\alpha,2}} \quad (8.1)$$

$$\sigma_{c,\alpha,1} = \frac{F_d * s_{dist}}{b_{ef} * t_v} \cos^2\left(\frac{\beta}{2}\right) \leq f_{c,\alpha,1} \quad (8.2)$$

where index 1= frontal surface

$$\sigma_{c,\alpha,2} = \frac{F_d * (1 - s_{dist})}{b_{ef} * t_v} \cos(\beta) \leq f_{c,\theta,d} \quad (8.3)$$

where index 2 = rear surface

8.3 Local joint design

Four cogging joints were studied of which one was based on design method 1 and three were based on design method 2; joint AF, joint B, joint C and joint D, see Figure 8.3, Figure 8.4, Figure 8.5 and Figure 8.6. Joint AF is shown in figure below and is the originally sketched joint by Anders Fröstrup. Joint B and C were designed according to design method 2 and finally, joint D was designed according to design method 1. The calculated design normal stress, $\sigma_{x,d}$, from the global analysis was used as input data in the local design for all studied joints. The calculations for each joint can be viewed in Appendix E. Two different approaches were used when analysing the joints. Joint AF was evaluated, while joint B, C and D were designed with sufficient strength with respect to the design load obtained in the global analysis and the material strength C24.

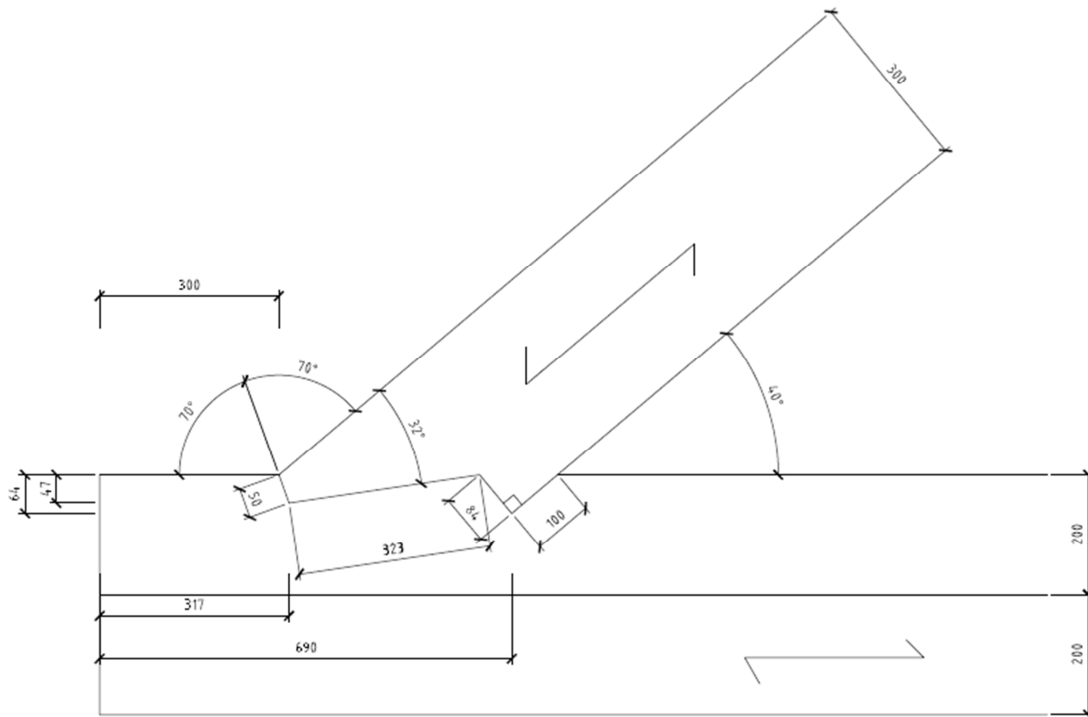


Figure 8.3 Joint AF designed according to design method 2 and obtained from the 3D-computer-model from Anders Fröstrup. It was found to have insufficient strength for a material strength equal to C24, but sufficient strength for a material strength equal to D50.

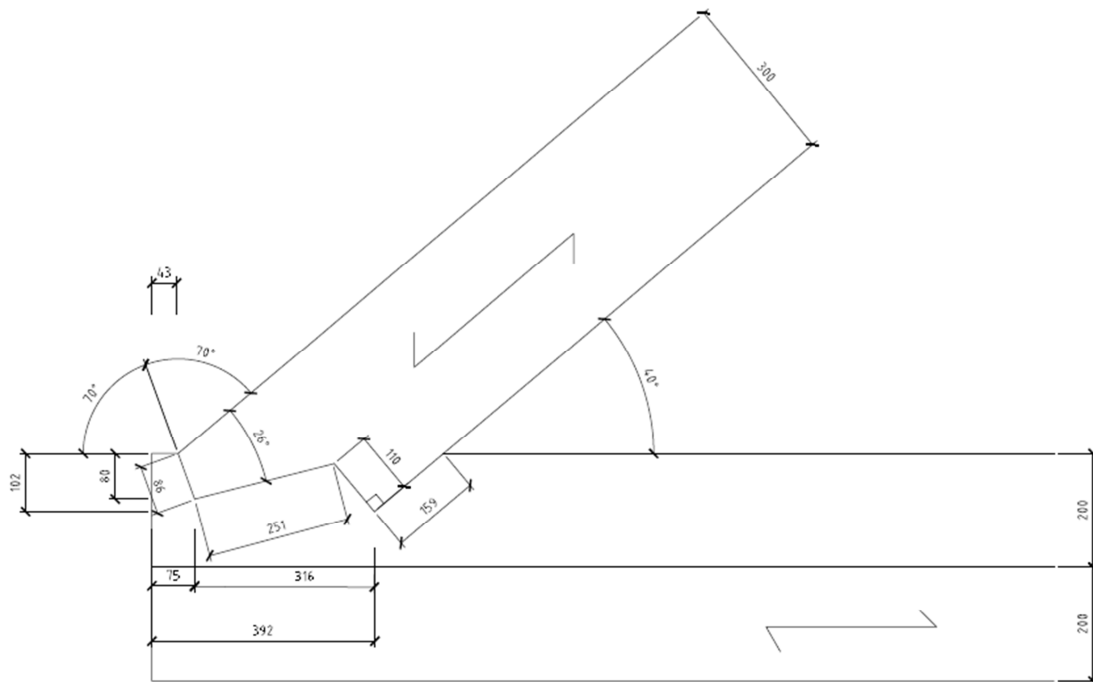


Figure 8.4 Joint B design with sufficient strength according to design method 2 and material strength C24.

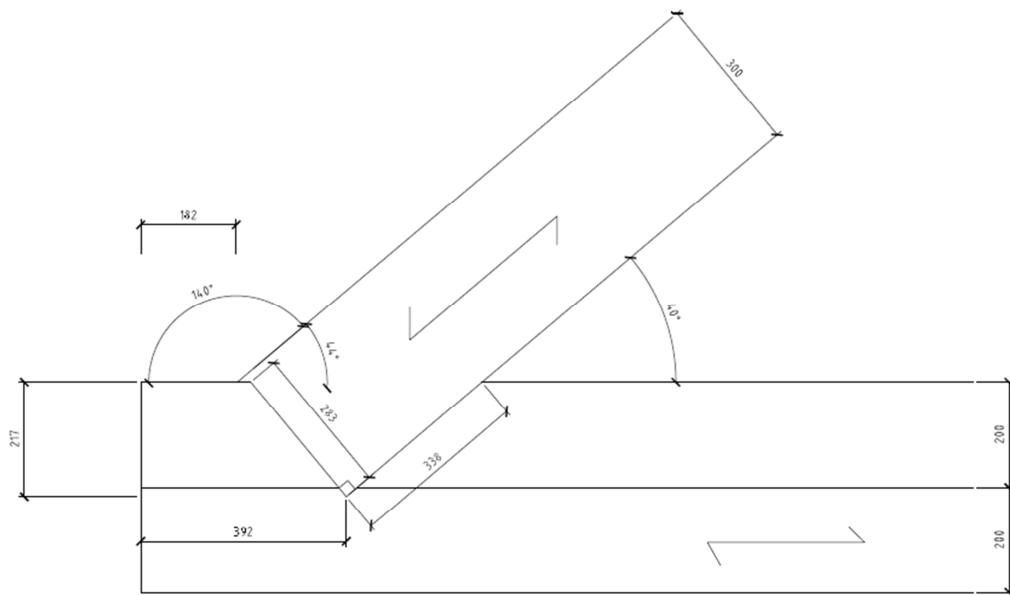


Figure 8.5 Joint C designed with sufficient strength according to design method 2 and material strength C24.

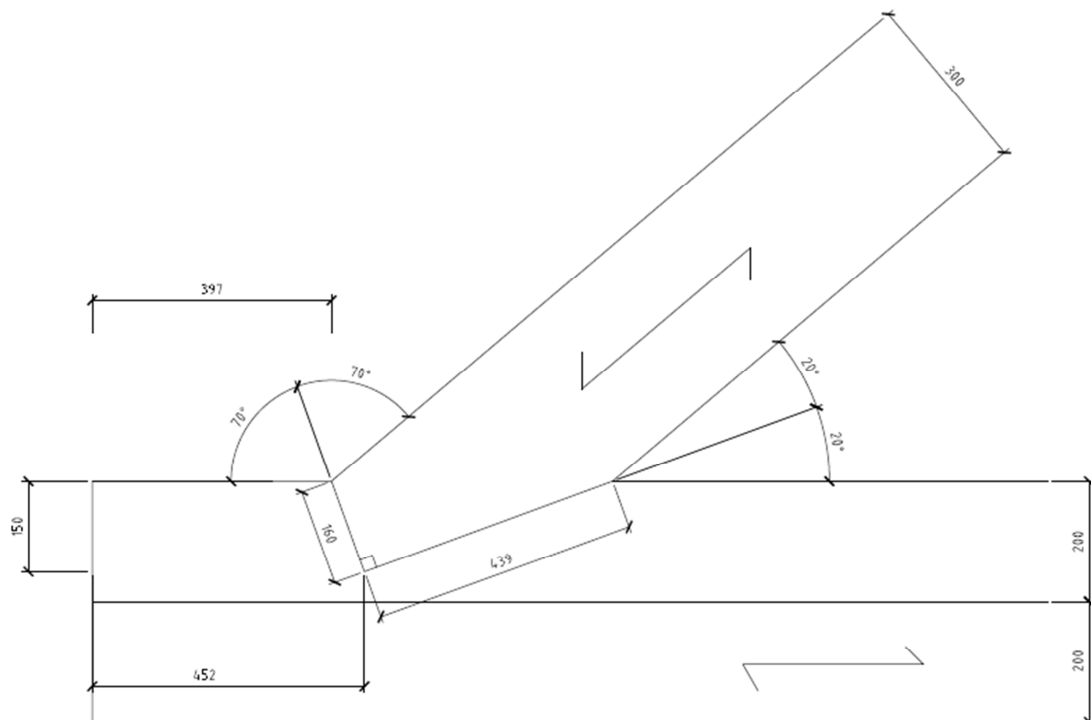


Figure 8.6 Joint D designed with sufficient strength according to design method 1 and material strength C24.

Joint B was designed with sufficient shear strength with a utilization rate of 100%, which resulted in a translation of 43 mm from the edge of the chord to ensure the shear strength. The design stress was obtained in the inclined end strut at the frontal surface and was designed with a utilization rate of 98%.

Joint C was designed with sufficient shear strength with a utilization rate of 100%, which resulted in a translation of 182 mm from the edge of the chord to ensure the shear strength. The design stress was obtained in the laminated beam at the rear surface with a utilization rate of 100%.

Joint D was designed with sufficient shear strength with a utilization rate of 100% which resulted in a significant translation of 397 mm from the edge of the chord to ensure the shear strength. A certain configuration had to be accepted due to the 90° angle between the frontal and flatter contact surfaces and the given inclination 20° for the frontal contact surface, which resulted in a utilization rate of 88% at the frontal contact surface and 100% of the flatter contact surface. The maximal width of the strut was exceeded according to the design recommendation in design method 1. No explanation of why this condition had to be fulfilled was found.

The investigated joints had a thickness of 200 mm. The 2D-geometry of joint B, C and D are presented in Table 8.5 together with an illustration in Figure 8.7, more detailed information of all joints can be seen in Appendix E.

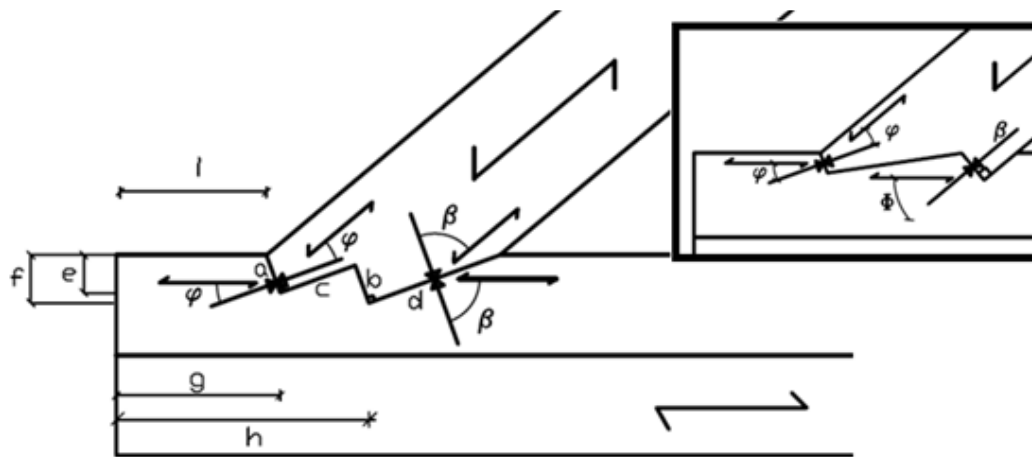


Figure 8.7 A principle sketch of a cogging joint to illustrate the different parameters of the 2D-geometry and also the angle between the force at the contact surface and the grain in each member.

Table 8.5 2D-geometry of the cogging joint. The parameters are illustrated in Figure 8.7.

	JOINT B	JOINT C	JOINT D
a	86	-	160
b	110	283	-
c	251	0	439
d	159	338	-
e	81	-	150
f	102	217	-
g	434	-	452
h	750	392	-
i	404	182	397
φ	20	-	20
β	0	0	70
Φ	40	40	-

The resulting load effects on each joint are shown in Table 8.6 and the utilization rates for the material strengths C24 and D50 for each joint are shown in Table 8.7 and Table 8.8. The presented load effects depend on the angle between the load and grain at the contact surfaces in each joint, the calculation of each load effect can be viewed in Appendix E. Design method 1 give compressive stresses at 20° and 70° angle to the grain, while design method 2 give compressive stresses at 20° and 40° angle to the grain and parallel to the grain.

The design strength of the strongest wood species in EN 338:2009 are presented for each type of stress, D40-D70, together with two example of a medium strong pine C24 and C30. A comparison between the design load effect obtained from each joint and the design strength can easily be made in Table 8.6.

Joint AF had insufficient strength with respect to a normal force equal to 220kN and a material strength equal to C24, due to high compressive stresses induced 20° to the grain at the frontal contact surface. On the contrary, it was found to have sufficient strength if a material strength equal to D50 was used, with a utilization rate of 91%. The utilization rate of the shear strength was found to be 57%.

Only three of four surfaces contributed to the load-bearing capacity in joint B and two of three in joint C, due to the straight surface at the rear flatter surface. A smaller decrease of the total cross-section of the laminated beam was achieved in joint B.

Table 8.6 The resulting load effects at the contact surfaces for each joint are presented together with design strength for several strength classes according to EN338.

	AF	B	C	D	C24	C30	D40	D50	D60	D70
$\sigma_{c,0.d}$	4.7	3.0	3.9	----	11.3	12.3	14.0	15.6	17.2	18.3
$\sigma_{c,20.d}$	12.6	7.2	-----	6.5	7.4	8.0	12.4	13.9	15.4	17.0
$\sigma_{c,40.d}$	4.7	3.0	3.9	----	3.9	4.2	9.7	10.8	12.1	14.3
$\sigma_{c,70.d}$	-----	-----	-----	0.9		2.4	7.1	8.0	9.0	11.4
τ	1.2	2.2	2.2	2.2	2.2	2.2	2.2	2.2	2.3	2.7
f	64	102	217	150	----	----	----	----	----	----
i	300	43	182	397	----	----	----	----	----	----

Table 8.7 The utilization rate for a material strength equal to C24.

	AF	B	C	D
$\sigma_{c,0.d}$	42	27	34	---
$\sigma_{c,20.d}$	171	98	---	88
$\sigma_{c,40.d}$	120	78	100	---
$\sigma_{c,70.d}$	---	---	---	38
τ	57	100	100	100

Table 8.8 The utilization rate for a material strength equal to D50.

	AF	B	C	D
$\sigma_{c,0.d}$	30	19	25	---
$\sigma_{c,20.d}$	91	52	---	47
$\sigma_{c,40.d}$	44	28	36	---
$\sigma_{c,70.d}$	---	---	---	12
τ	57	100	100	100

9 Discussion

In this Chapter the results from both the global and the local analysis are discussed. Interesting results from the literature study concerning timber framed joints in general are also discussed. Second order effects were not studied in this Master's Thesis project but some remarks will be done in relation to failure mechanisms.

9.1 Advantages and disadvantages of B, C and D joint design

Advantages and disadvantages for joint B, C and D were found. B, C and D represent the three different joint designs found in this Master's Thesis. Joint B only required a small end distance and the possibility of two shear planes increased the shear capacity. On the contrary, the shear stress at the frontal contact surface was never controlled, instead the shear stress capacity was checked by verifying that the total shear load can be carried by the rear contact surface.

Joint C allowed the cogging joint a closer position to the end of the laminated beam such as in joint B. However, the configuration was found to have a large risk. A crack can easily be initiated which could lead to a splitting of the strut, see Figure 9.1. The joint required a large notch depth, which cut through the upper part of the laminated beam. The mechanical connections that hold the laminated beam together at the end are thereby not functional. Hence, this joint cannot be used with these dimensions and loads of *Bridge over Tidán*. Even if the load was reduced, the notch is still deeper than the other joint designs, which could induce a shear or a tensile failure of the upper part of the laminated beam, see Figure 9.1. Furthermore friction forces can never contribute to the load-bearing capacity at the rear surface, since the surface is parallel to the load path.

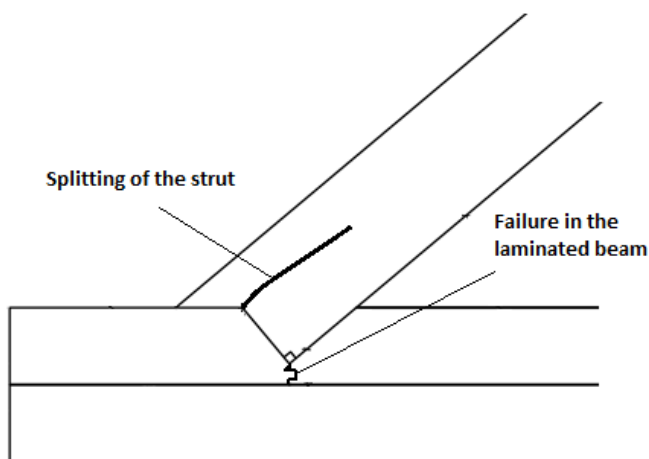


Figure 9.1 Failure in the laminated beam due to shear or tension parallel to the grain and splitting of the strut due to easily initiation of a crack at the top of the rear contact surface and a deep notch (Teike 2013).

In contrary to previous joint designs, a stress control was performed of the flatter contact surface in joint D. On the contrary, the cogging joint required a large end distance due to the single frontal contact surface that generated large shear stresses because of the shortening of the shear plane length. Furthermore, a deep notch in the beam was required.

9.2 Shear failure and compressive failure

A shear failure in a cogging joint is a rapid failure and lead to a total collapse of the bridge immediately, while a compression failure at an angle to the grain could be seen as less prone to contribute to a total collapse of the cogging joint, see Figure 9.2. On the contrary, the compression failure could lead to an unbalance in the contact pressure and thereby induce a second order moment in the inclined end post, see Figure 9.3. A reasonable conclusion was that the unbalances lead to increased stresses at specific locations in the joint, and thereby risk exceeding the design strength in the structural members, such as the shear strength.

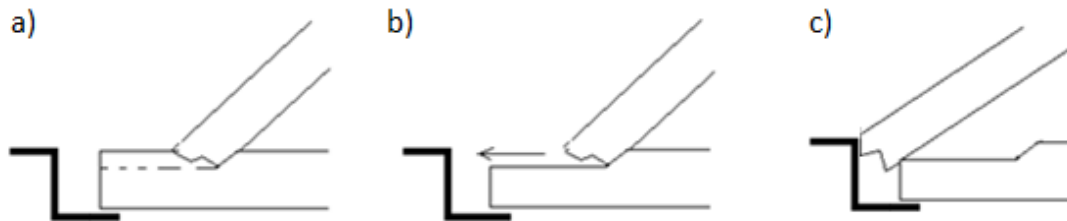


Figure 9.2 a)-c) illustrate the rapid shear failure of a cogging joint which result in a failure mechanism. The thicker line represents the concrete foundation and the gap between the foundation and the bridge is exaggerated (Teike, 2013).

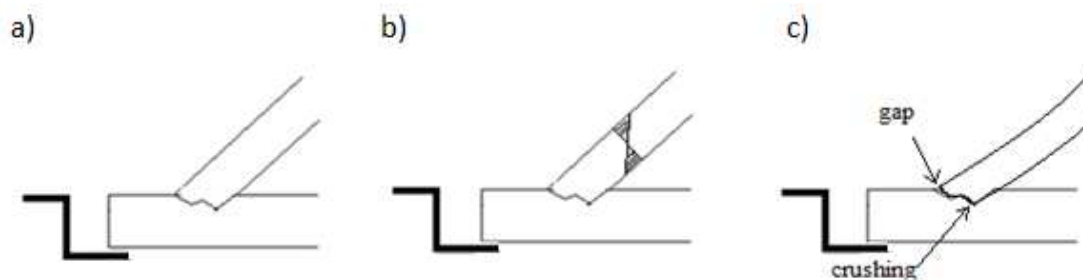


Figure 9.3 a)-c) illustrates the compression failure could lead to an unbalance in the contact pressure and thereby induce a second order moment in the inclined end post. The thicker line represents the concrete foundation and the gap between the foundation and the bridge is exaggerated (Teike 2013).

9.3 Distribution of force

The distribution of the normal force at a double notched cogging joint was assumed in this Master's Thesis, which effects the design result for joint B and the evaluation of joint AF. The distribution of the force for all joint types can be questioned since both design method 1 and 2 are simplified design methods. The numerical analysis conducted by Villar et al. (2004) showed that friction at larger angles between the strut and the chord generated a significant contribution to the load-bearing capacity of the cogging joint, which is disregarded in current simplified methods in this Master's Thesis.

9.4 Shear strength

The shear stress is induced parallel to the grain in the laminated beam for a cogging joint. The different shear stress criteria presented in design method 1 and 2 are not verified in Eurocode 5, and was thereby an uncertain parameter. In this Thesis, the

shear stress has been calculated according to the praxis for each design and then compared to the design strength value for shear stress, $f_{v,d}$ in EC 5, see a) in Figure 9.4. The same strength value is used for shear stresses induced by transversally loaded beams. This can strongly be questioned. It could be argued that a different shear strength should be used.

For example, the rolling shear is more suitable to use since it has a similar brittle failure, but this shear stress is perpendicular to the grains, which was not the case for the cogging joint, see b) in Figure 9.4. The shear stress induced by a cogging joint in the end of the beam can be illustrated as a local effect where parallel shear occurs locally between two grain layers in a limited part of the material, see Figure 9.5.

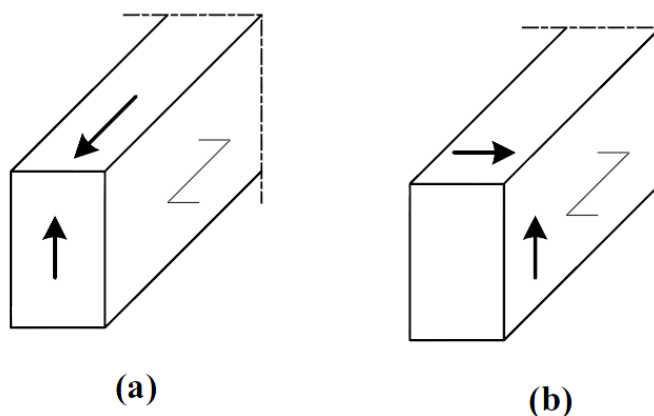


Figure 9.4 a) Shear strength parallel to the grain e.g. used for the shear stress generated from transversally loaded beam (EC5). b) Rolling shear, which is defined as the double tensile strength perpendicular to the grain (SS-EN 1995-1-1:2004 6.1.7) (EC5).

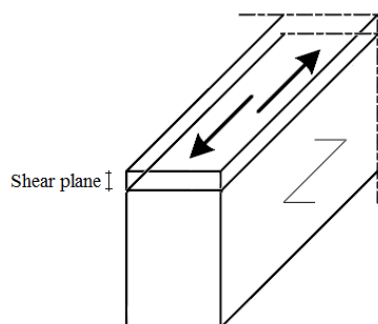


Figure 9.5 Shear stress parallel to grain when induced on local limited area (Teike 2013).

It could be argued that the shear stresses mentioned in European design rules are of different type than the shear induced in the cogging joint. For example, the shear stress induced from a transversally-loaded beam is induced over several shear planes. On the contrary, the shear stress induced at the notch of a cogging joint will only spread over a few shear planes with a high risk of only using one shear plane since there is a risk of concentrated stresses. The most similar approach found in EC 5 was that of block shear failure and plug shear failure of a multiple steel dowel connection,

see Figure 9.6 and Figure 9.7. This approach deals with shear stresses parallel to grain near edges of structural members, but is only valid for multiple steel dowel connections.

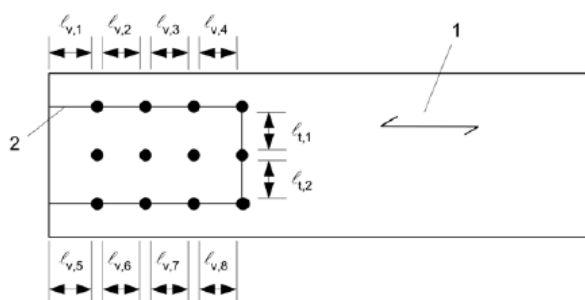


Figure 9.6 A multiple steel dowel connection (EC5).

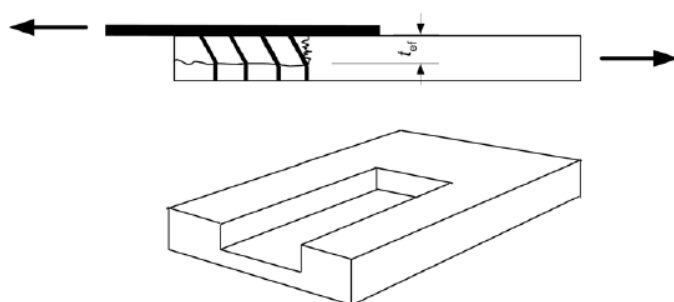


Figure 9.7 A block shear failure of a multiple steel dowel connection at the top and a plug shear failure at the bottom (EC5).

The literature study revealed that this has been an issue for a long time. The ancient designers even tried timber framed joints with rounded edges to avoid stress concentrations. This method reduced the risk of inducing large stresses at a limited surface, but increased the joint slip and thereby the total deflection of the structure, which was another important aspect of timber framed joints.

The sub objective of this Master's Thesis project was to find a tension joint designed only in timber adopted for heavy loaded structures. After a thorough investigation of both old and new literature and research, no such joint was found. It could be explained by insufficient shear strength parallel to the grain described as block rupture and insufficient tensile strength perpendicular to grain when pegs are used.

9.5 Joint slip

The use of timber framed joints is often seen as a stiffness challenge such as timber structures in general. Large deflections can be generated by joint slip and due to creep. The stiffness issue should be addressed in the design in all timber framed joints. Shrinkage and creep will relax timber framed joints which from the beginning have perfect contact.

Framing timber is a very heavy practice for the carpenter, which can effect the number of times a joint is tested for perfect fit before a satisfied result is achieve. In addition, timber is an anisotropic material both at macro and micro level with knots randomly located. Therefore, some imperfections must be accepted. These imperfections cause movements in the bridge structure when all members are

mounted and fully loaded due to joint slip, which in turn can generate a movement in the joint.

The literature study has shown that the deflection can be counteracted by preparing for future post tensioning of the bridge. This can be achieved by using longer shear keys in the laminated beam, which can be driven into the key holes and counteract the deflection. Strapped tension joints can be tightened with steel wedges to counteract the shrinkage. The stiffness issue of a cogging joint is not related to the shrinkage or creep deformations. It is rather related to second order effect and craftsmanship which was out of the scope of this Master's Thesis project.

10 Conclusions

The literature study together with the global analysis showed that the cogging joint was the most critical joint in the timber truss since it had no redundancy. Failure of the cogging joint located at the end of the lower chord will lead to a mechanism resulting in a total collapse of the bridge. The global numerical analysis of the bridge generated a design load of 220kN in ULS in the inclined end strut, which all joints were designed after. The numerical analysis was limited to only concern three different traffic load cases.

Two conventional design methods of cogging joints were found, in this Master's Thesis, called design method 1 and 2. Anders Frøstrup suggested a cogging joint according to design method 2 for *Bridge over Tidan*. The sketched cogging joint in the global 3D-computer-model received from Anders Frøstrup showed insufficient strength to carry the normal force, calculated for *Bridge over Tidan*, by contact only, if a material strength equal to C24 was used, but had sufficient strength for a material strength equal to D50.

All joint designs showed both advantages and disadvantages. Advantages can be summarized as:

- Small end distances were allowed for both joint B and C
- Increased shear capacity was generated in joint B due to the spread of the shear stress over two shear planes.
- Joint D could have had a much higher load-bearing capacity if the friction at the large flatter surface was accounted for.

Disadvantages can be summarized as:

- No shear strength verification at the frontal contact surface in joint B was conducted.
- Joint C and D had deep notches, which risk a shear failure or a tension failure in the laminated beam.
- The load-bearing contribution of friction was neglected in all joint designs.

The shear strength suggested in design method 1 and 2 were based on the shear strength $f_{v,d}$ in Eurocode 5, which is strongly questioned in this Master's Thesis. It could be argued that a different shear strength should be used, since the shear stresses induced in a cogging joint are more similar to block shear failure and plug shear failure of a multiple steel dowel connection described in Annex A in Eurocode 5.

10.1 Further research

The shear failure is a brittle failure and very dangerous in a cogging joint at the edge of a truss and should be investigated further. During this Master's Thesis project, Nils-Eric Anderson constructed two fully-scaled cogging joints, see Figure 10.1, which in the future should be tested at Chalmers University of Technology for shear failure at the end of the beam to learn more about cogging joints. The effect of shrinkage cracks near the shear plane should also be investigated, see Figure 10.2.



Figure 10.1 Fully-scaled cogging joint constructed by Nils-Eric Anderson at Da Capo University in Mariestad. Standing next to the cogging joint, Anna Teike (Teike, 2013).



Figure 10.2 A shrinkage crack is visible in the upper part of the laminated beam (Teike, 2013).

It would have been interesting to conduct laboratory testing and numerical analysis of design method 1 and 2 to investigate the shear behaviour in a cogging joint. Cracks due to shrinkage in the cogging joint with no redundancy are a huge risk and should thereby be investigated. Furthermore, a proposal of a cogging joint design applicable in Eurocode 5 should be prepared. A further knowledge of the joint slip in timber frame joints in general would be beneficial for the use of timber framed joints.

11 References

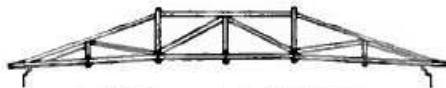
- AMA. (2013): *SS 23 27 40 Trävaror – Sågat och hyvlat virke av barrträ – Fuktkvot*.
And: 040422-Vikbron-004x.jpg etc.
- Anderson, N-E. (2012): *Interview on wooden pegs*. Interviewed by Anna Teike [mail],
September 2012, 10:20.
- Brungraber, B. and Miller J. (2009): *Mechanically laminated beams*. Journal of
Timber Framers Guild - Timber Framing. Vermont. US Available at:
<http://www.ftet.biz/index.php?action=resources.wp01>
- Carling, O (2001): *LIMTRÄ HANDBOK*. Sundsvall. Svenskt limträ.
- Ceraldi, C. and Ermolli, R. E. (2003): *The Swiss covered bridges of the eighteenth
century – A special case: The bridge of Schaffhausen*. Proceedings of the First
International Congress on Construction History, Madrid 20th-24th Jan 2003. [pdf]
Available at: <http://www.docstoc.com/docs/133338255/The-Swiss-covered-bridges-of-eighteenth-century-special-case>
- Cooper, L. J. (2010): *You Can't Judge a Bridge by its Cover*. Indiana. [pdf] Available
at: http://www.indianahistoricbridges.com/timber/ceylon_b.pdf
- Destination Skellefteå. (2012): *Lejonströmsbron i morgonljus*. [on-line] Available at:
<http://www.destinationsskelleftea.se/sv/Destination/Product/Lejonstromsbron/201604>
- Diaz, C.J.J., Nieto G. F. P. and Rabanal Á. C. (2008): *Finite element analysis of thin-
walled composite two-span wood-based loadbearing stressed skin roof panels and
experimental validation*. Thin-Walled Structures, Volume 46, Issue 3, March 2008,
Pages 276-289
- Ehlbeck, J. Kromer M. (1995); *Timber Engineering STEP 1-Carpentry joints*.
Netherlands. Salland De Lange.
- Faherty, K. F. and Williamson G. T. (1997): *Wood engineering and construction
handbook*. New York: McGraw-Hill. [on-line] Available at:
<http://lecture.civilengineeringx.com/bdac/wood-trusses/>
- Fernández-Cabo, J. L. (2012): *Remarkable ancient timber bridges up to the 1850's*.
International Conference on Timber Bridges 2010. Lillehammer, Norway.
Septemebr 12-15, 2010
- Freedman, G., et al. (2002): *Timber Bridges and Foundations*. Report [pdf] UK:
Forestry commission. Available at: [http://www.forestry.gov.uk/pdf/intectbfrep.pdf/\\$file/intectbfrep.pdf](http://www.forestry.gov.uk/pdf/intectbfrep.pdf/$file/intectbfrep.pdf)
- Hall, C. (2009): *The Carpentry way*. [blog] 14 Oct 2009. Available at:
<http://thecarpentryway.blogspot.se/2009/10/bracing-situation-iv-design-for.html>
- Heyden, S., Dahlblom O., Olsson, A. and Sandberg, G. (2005): *Introduktion till
strukturmekanik*. Studentlitteratur, Lund, Sweden (9789144051253)
- Historic American Engineering Record. (1976): *Trusses*. [Poster] Smithsonian
Institution, Washington, D.C. Available at:
<http://siahq.org/Images/haer/trusses3.pdf>

- Hoffman, J. (1940): *Baukunde für die praxis III: Bauschäden*. Stuttgart, Julius Hoffmann Verlag 1940
- Jameson, D. C. (1890): *The evolution of the modern railway bridge*. Popular Science Monthly, Vol 36, Feb. The state university of Iowa. US [on-line] Available at: http://en.wikisource.org/wiki/Popular_Science_Monthly/Volume_36/February_1890/The_Evolution_of_the_Modern_Railway_Bridge
- Karlsson, E. (2012): *Allmänna föreskrifter*. Förfrågningsunderlager för Bro över Tidån. Martin & Co.
- Kassimali, A. (1993): *Structural analysis*. PLUS Publishing Company, Boston.
- Kleppe, O. Aasheim, E. (1996): *Timber Bridges in Nordic Countries*. National conference on wood transportation structures. FPL-GTR-94. USDA, Forest Service, Forest Products Lab: Madison, WI [pdf] Available at: <http://www.woodcenter.org/docs/klepp96a.pdf>
- Kliger, R. (2012): Prof. Robert Kliger lectured in the course Timber Engineering in the spring of 2012 at Chalmers University of Technology.
- Kraftsamling Fränsta. (2013a): *040422-003x.jpg*, [online] (Last updated on 11th January 2013) Available at: <http://www.fransta.com/vikbron/Vikbrobilder%202004%20min.htm> [Accessed on 11th January 2013]
- Kraftsamling Fränsta. (2013b): *Gamla-spannetx.jpg*, [online] (Last updated on 11th January 2013) Available at: <http://www.fransta.com/vikbron/Vikbrobilder%202003%20min.htm> [Accessed on 11th January 2013]
- Kriz, R.D. (1997): *Microstructure Lectures*. Virginia Polytechnic Institute and State University. Blacksburg, Virginia. US [on-line] Available at: <http://www.jwave.vt.edu/crcd/kriz/lectures/ref.html>
- Kulicki, J. M. (2000): *Bridge Engineering Handbook. Section: Highway Truss Bridges*. Boca Raton: CRC Press [e-book] Available at: <http://freeit.free.fr/Bridge%20Engineering%20HandBook/ch16.pdf>
- Länsstyrelsen (2005): *Beslut om byggnadsminnesförklaring Dnr 432-4746-02*, Härnösand
- Länsstyrelsen (1994): *Beslut om byggnadsminnesförklaring 221-926/91*. Kulturmiljöenheten, Västerbottens län.
- Magee, M. (2010): *Testing Scarf joints in Bending*. Journal of Timber Framers Guild - Timber Framing. Vermont. US Available at: <http://www.ftet.biz/userimages/resources/other/TF98JointTesting.pdf>
- Mahan, D. H. (1877): *A treatise on civil engineering*. New York: Wiley p.pp 272.
- Middleton, D. W. (2001): *The Bridge at Québec*. Indiana University Press. Indiana, US. [e-book] Available at: http://books.google.se/books?id=JjdRuG7xmlwC&printsec=frontcover&hl=sv&source=gbs_ge_summary_r&cad=0#v=onepage&q&f=false
- Miller, J.F. (2009): *Design and analysis of mechanically laminated timber beams using shear keys*. [PhD]. Michigan Technological University Available at: <http://search.proquest.com.proxy.lib.chalmers.se/docview/304954294>

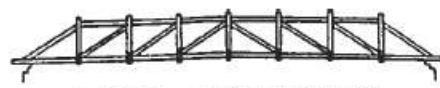
- Miller J.F. and Schmidt R.J. (2004): *Capacity of pegged mortise and tenon joinery*. [MSc]. Department of Civil and Architectural Engineering, University of Wyoming, Laramie, WY, US. [pdf] Available at: http://timberframeengineeringcouncil.org/images/pdf/miller_report.pdf
- Milling, L. n.d. *Vikbron*. [photograph] Available at: <http://www.ange.se/download/18.3f6678aa1165eefef988000675/th+18-1+H%C3%B6ga+kulturv%C3%A4rden.pdf> [Accessed 9 January 2013]
- Morrison, S. (2013): *Live-edge timber frame knee braces*. [on-line] Available at: <http://www.moresunwoodworking.com/Custom-Woodwork/Handcrafted.htm>
- Murphy, H. (2011): *Shop-made octagon pegs*. Scantlings – Newsletter of the timber framers guild number 160. TIMBER FRAMERS GUILD.
- Myers, P.V.N. (1901): *Rome, its rise and fall: a text-book for high schools and colleges*. Boston: Ginn & Company.
- Ritter, M.-A. (1990): *Timber Bridges: Design, Construction, Inspection, and Maintenance*. Washington, DC [e-book]
- Serban, M. (2009): *Trajan's Bridge over Danube*. International Journal of Nautical Archaeology, Vol 38, Issue 2, pp. 331-342, September 2009.
- SIS Förlag AB 1991. Available at: <http://ama.bygggtjanst.se/Default.aspx?articleId=153&Typ=AmaNytt>
- Skogsindustrierna. (2004): *Att välja trä*. Sörmlands grafiska Quebecor AB. Stockholm. [pdf] Available at: <http://www.martinsons.se/default.aspx?id=7035>
- Sobon, A. J. (2011): *Timber Framing Fundamentals – Traditional joinery*. Timber Framers Guild, New Hampshire
- Stenlund, C. (2010): *Farligt arbete på Lejonströmsbron*. Västerbottens Folkblad, [on-line] Available at: <http://www.folkbladet.nu/203166/broarbetet-ar-for-farligt>
- Sundsvalls tidning. (2000a). *Vikbron kämpar mot slutet*. Sundsvallstidning, [online] (Last updated 2000) Available at: http://www.fransta.com/vikbron/regnbro_artkl1.html [Accessed on 11th January 2013]
- Sundsvalls tidning. (2000b). *Vikbron kämpar mot slutet*. Sundsvallstidning, [online] (Last updated 2000) Available at: http://www.fransta.com/vikbron/regnbro_artkl4.html [Accessed on 11th January 2013]
- Sundsvalls tidning. (2005). *Återinvigning*. Sundsvallstidning, [online] (Last updated on 3rd Mars 2009) Available at: <http://st.nu/medelpad/ange/1.593430-aterinvigning> [Accessed on 11th January 2013]
- Svenskt Trä. (2013): *Träguiden- Träunderlagets egenskaper*. (Last updated 2000) Available at: <http://www.traguiden.se/TGtemplates/popup1spalt.aspx?id=6533> [Accessed on 6th February 2013]
- Timberwork (2000): *Timberwork – selected projects wood technology – the timber award 1961-1999*. Norway: Arkitekturforlaget
- Timoshenko, S. (1953): *History of Strength of Materials*. Courier Dover Publications
- Tredgold, T. and Hurst, J. T. (1871): *Elementary principles of carpentry*. London, E. & F.N. Spon. [E-book]

- Villar, J. R., Guaita M., Vidal P., Arriaga F. (2006): *Analysis of the Stress State at the Cogging Joint in Timber Structures*. Biosystems Engineering, [e-journal] (2007) 96 (1) available through: www.ScienceDirect.com
- VisitLjungdalen. (2012): *Upplev Ljungdalen*. [pdf] Available at: <http://np.netpublicator.com/netpublication/n26877615> [Accessed on 11th January 2013]
- von Rothstein, E. E. (1890): *Handledning I allmänna byggnadsläran med huvudsakligt afseende på husbyggnadskonsten*. Accent Förlag, Kristianstad, Sweden. (91-89622-12-X) p.p 419.
- Vägverket (2004): *Bro 2004-Vägverkets allmänna tekniska beskrivning för nybyggande och förbättring av broar*. Publ 2004:56. Printed 2004-06
- Yang, Y., Cheng, B. and Gao, J. (2007): *Timber arch bridges in China*. ARCH'07-5th International Conference on Arch Bridges. Fuzhou University. China. [pdf] Available at: http://www.pinehillpark.org/php/Arch_Bridge_files/Timber%20Arch%20Bridges%20in%20China.pdf
- Yang, Y., Cheng, B. and Gao, J. (2009): *Construction technology of the timber arch bridge in China*. Chinese-Croatian Joint Colloquium-Construction of arch bridges. Fuzhou, 05-09 October 2009. [pdf] Available at: <http://www.arch-bridges.cn/conf2009/pdf/341.pdf>
- Yeomans D. T. (1999): *The development of timber as a structural material*. Great Britain: Galliards

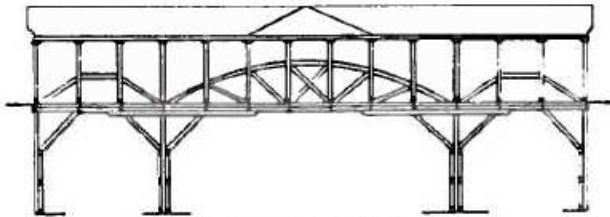
APPENDIX A – Bridges



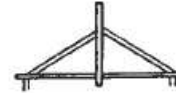
1. 1570 Cismone design (PALLADIO)



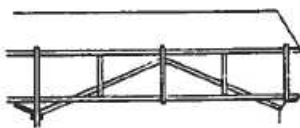
2. 1570 Suggested design (PALLADIO)



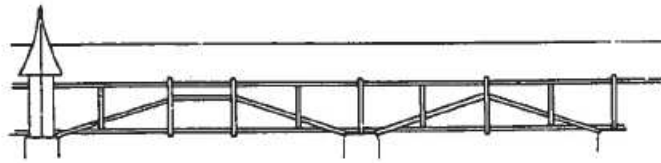
3. 1615 Pieve design (SCAMOZZI)



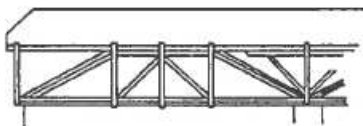
4. c1615 Design sketches (VERANTIUS)



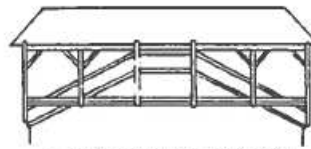
5. 1535 Neubrücke, Bern
c1550 Wangen (UNKNOWN)



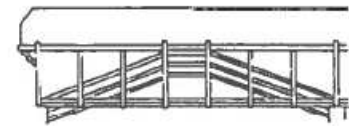
6. 1569 Spreuerbrücke, Luzern (UNKNOWN)



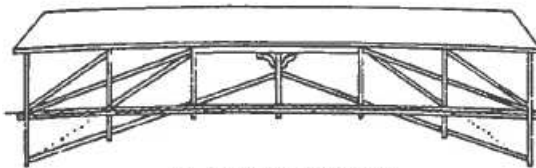
7. 1653 Pont de Berne, Fribourg (WINTER)



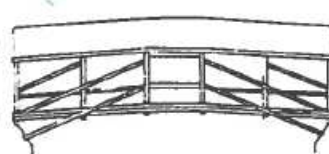
8. 1680 Steinbach (UNKNOWN)



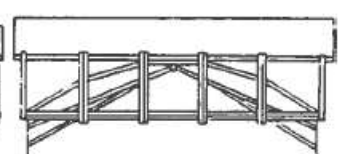
9. 1785 Emmenbaum (UNKNOWN)



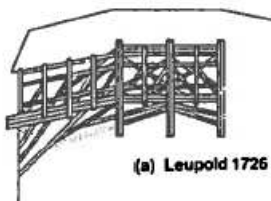
10. 1650 Baden (UNKNOWN)



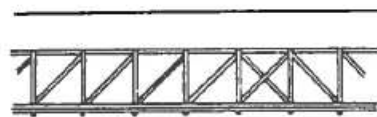
11. c1660 Design (WILHELM)



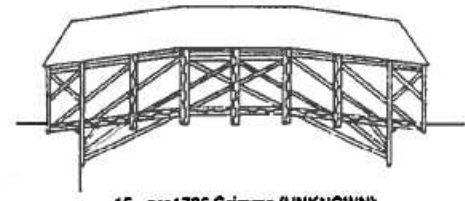
12. c1660 Design (WILHELM)



(a) Leupold 1726

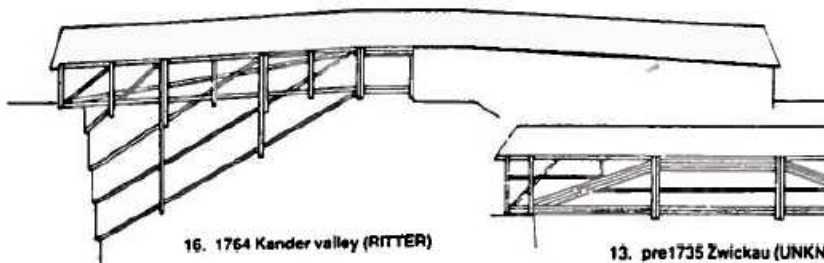


(b) Schramm 1735

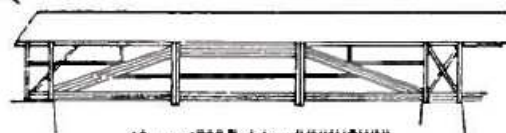


15. pre1726 Grimma (UNKNOWN)

14. 1657 Meissen (UNKNOWN)

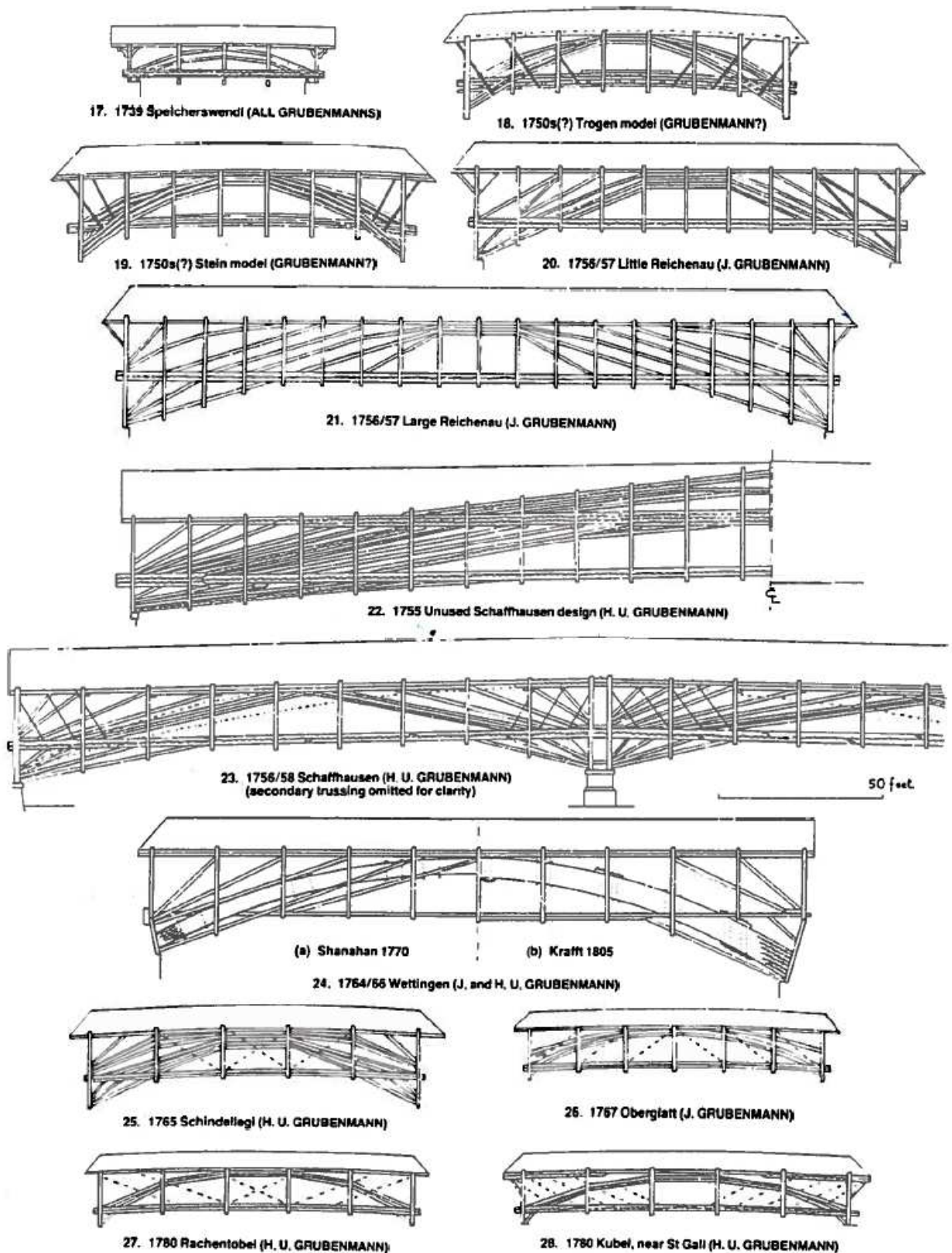


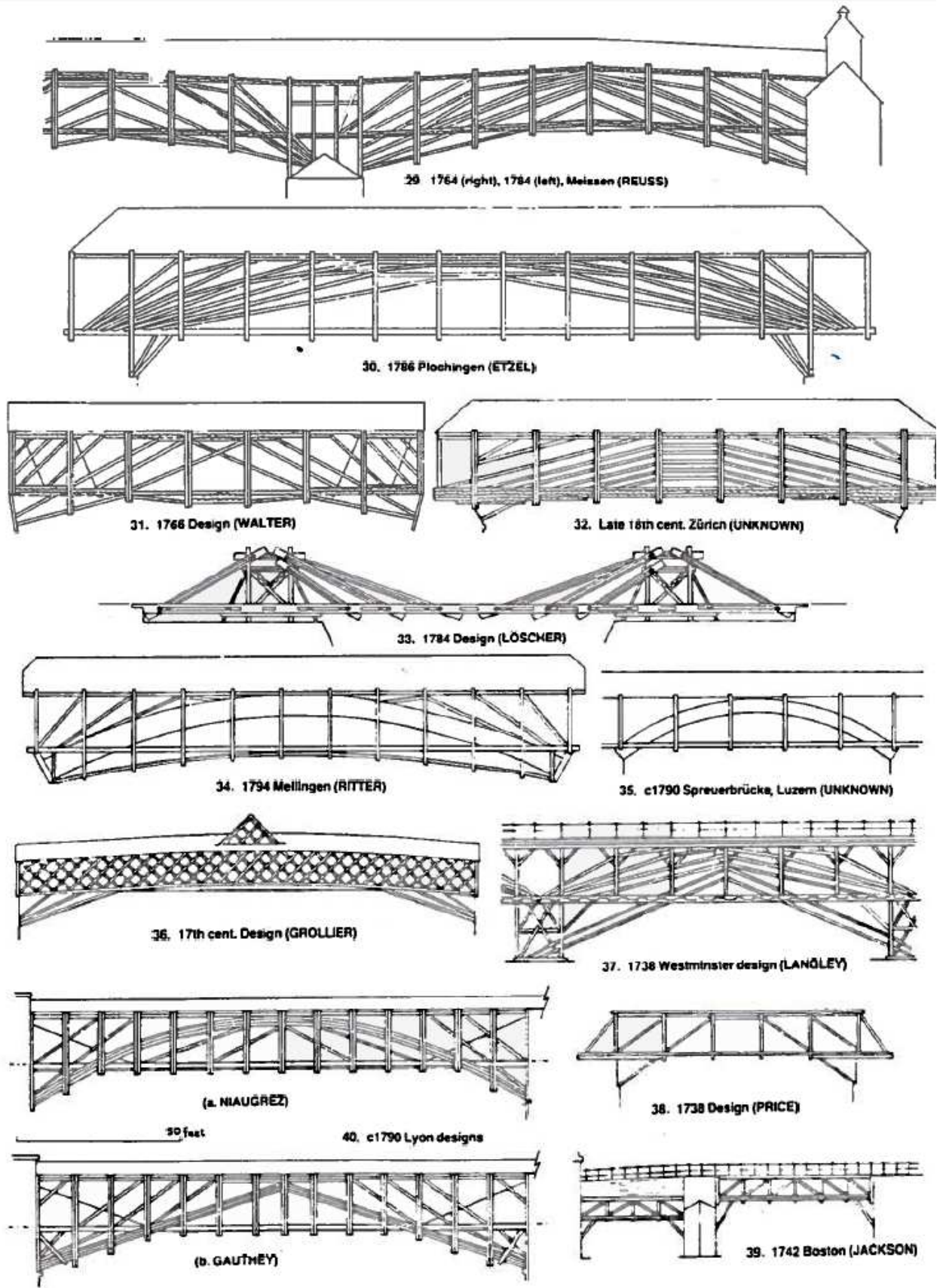
16. 1764 Kander valley (RITTER)

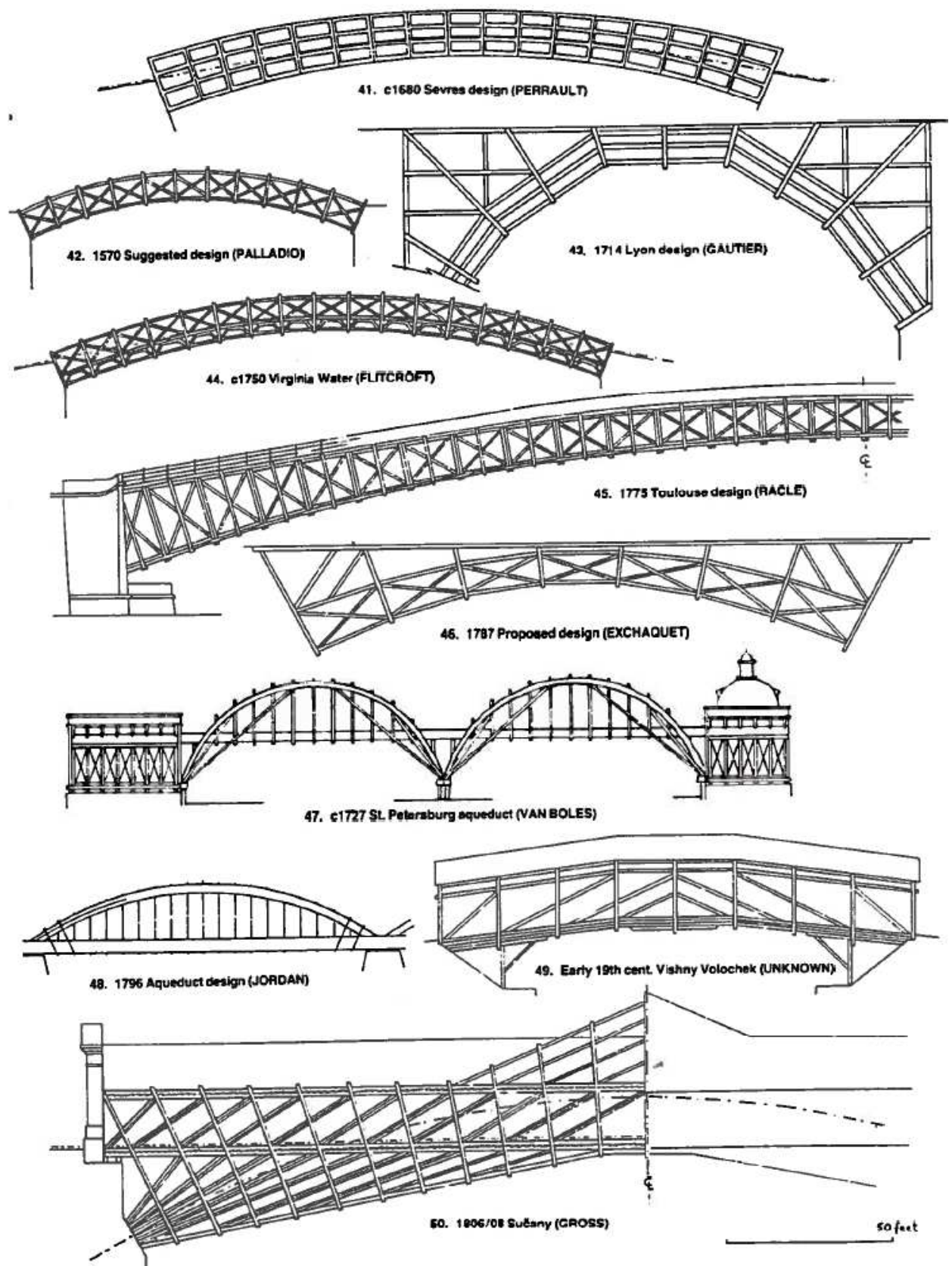


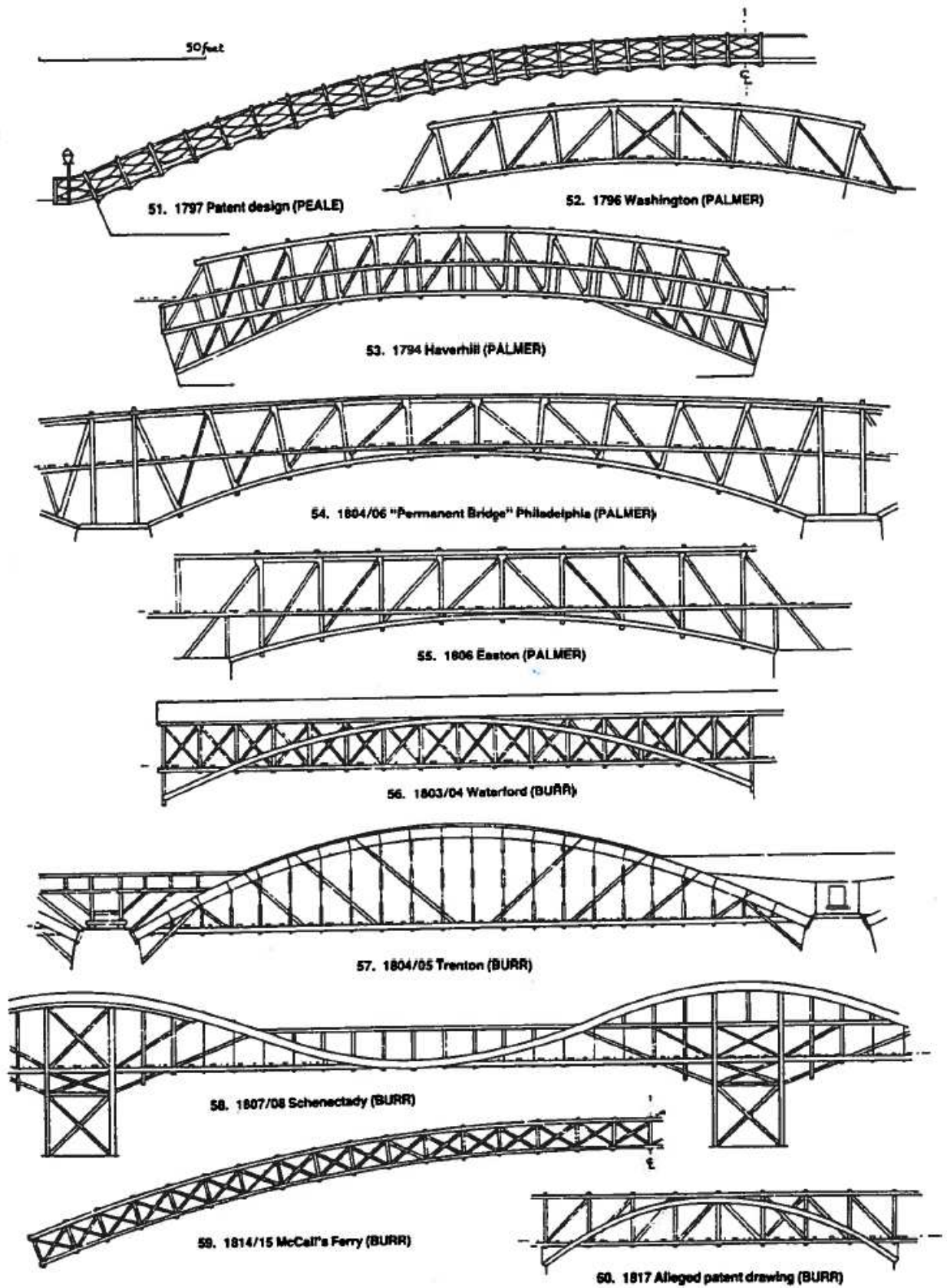
13. pre1735 Zwickau (UNKNOWN)

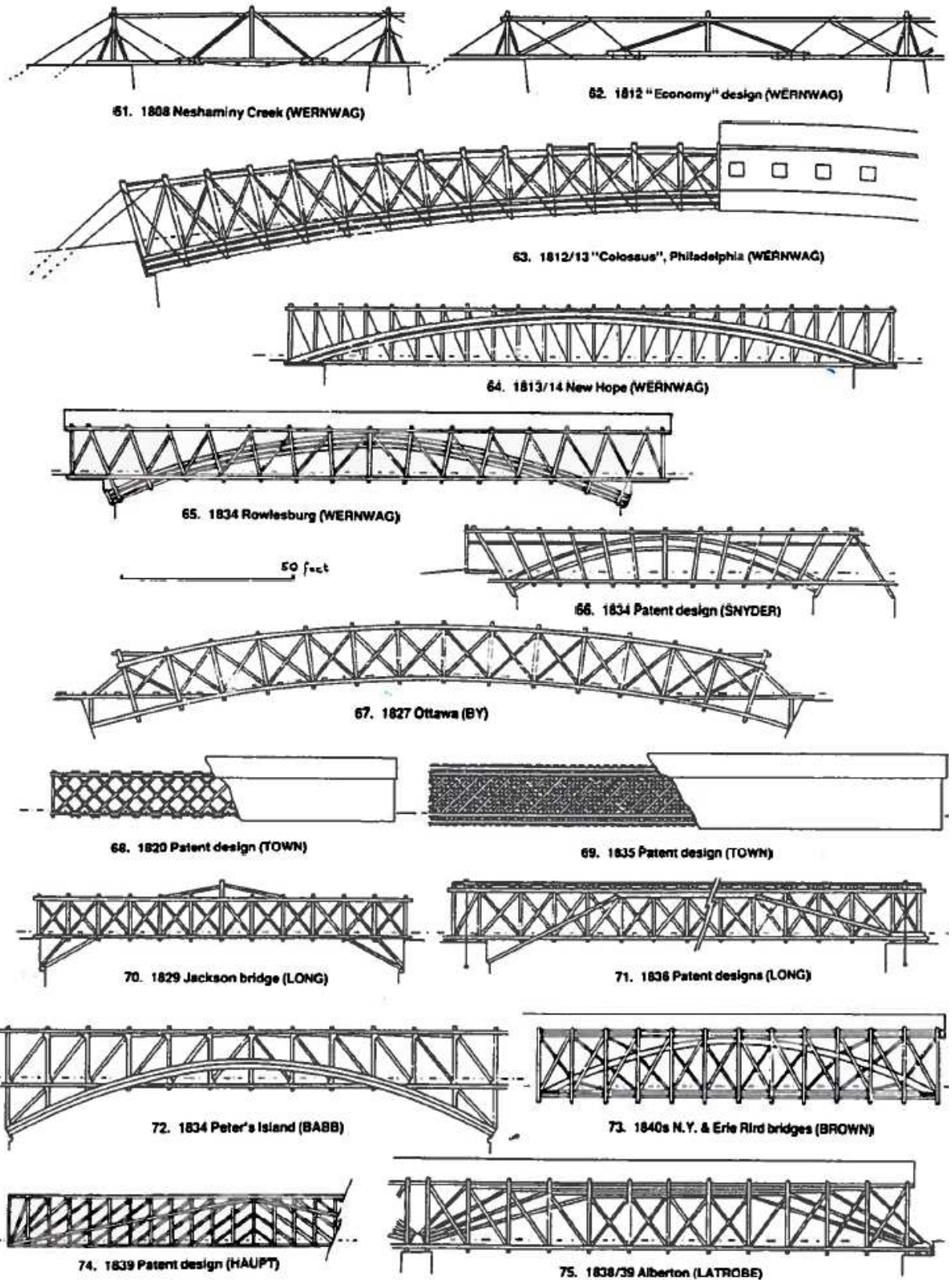
50 feet

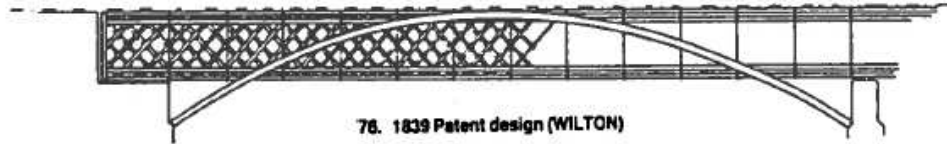




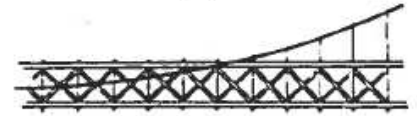
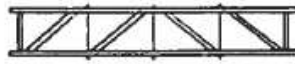
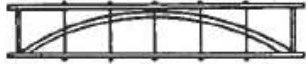






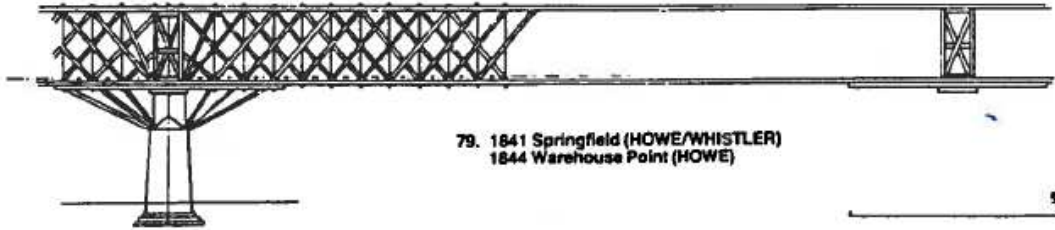


76. 1839 Patent design (WILTON)



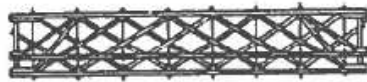
77. 1816 and 1835 designs (NICHOLSON)

78. 1823 Suspension bridge trussing (SEGUN).
(Scale increased for clarity)

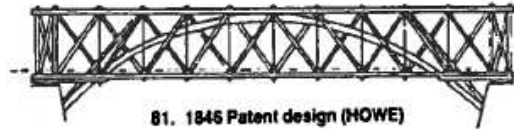


79. 1841 Springfield (HOWE/WHISTLER)
1844 Warehouse Point (HOWE)

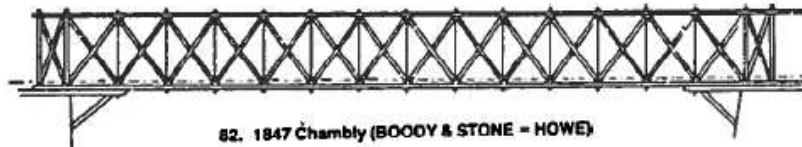
50 feet



80. 1840 2nd Patent design (HOWE)



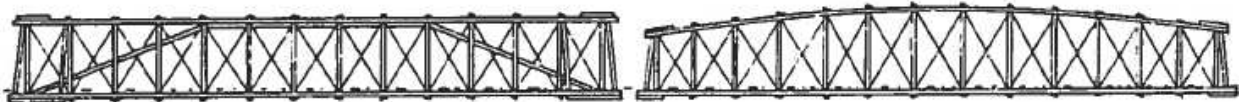
81. 1846 Patent design (HOWE)



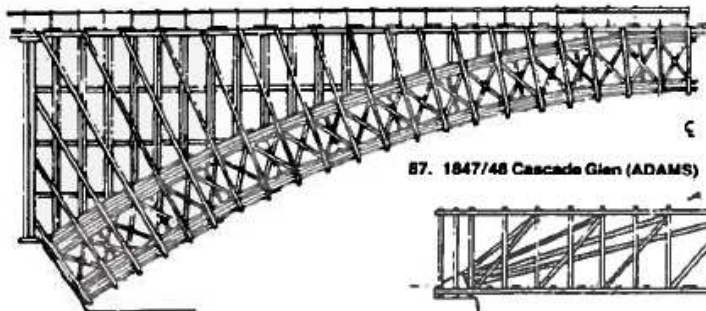
82. 1847 Chambly (BOODY & STONE - HOWE)



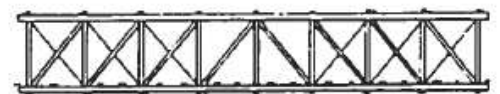
83. 1848/49 Rockville (STONE - HOWE)



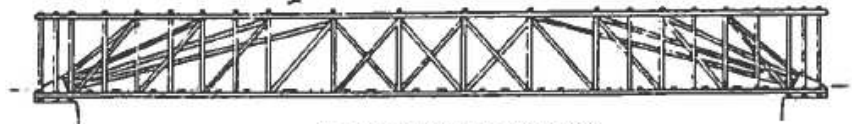
84. 1844 Patent designs (PRATT)



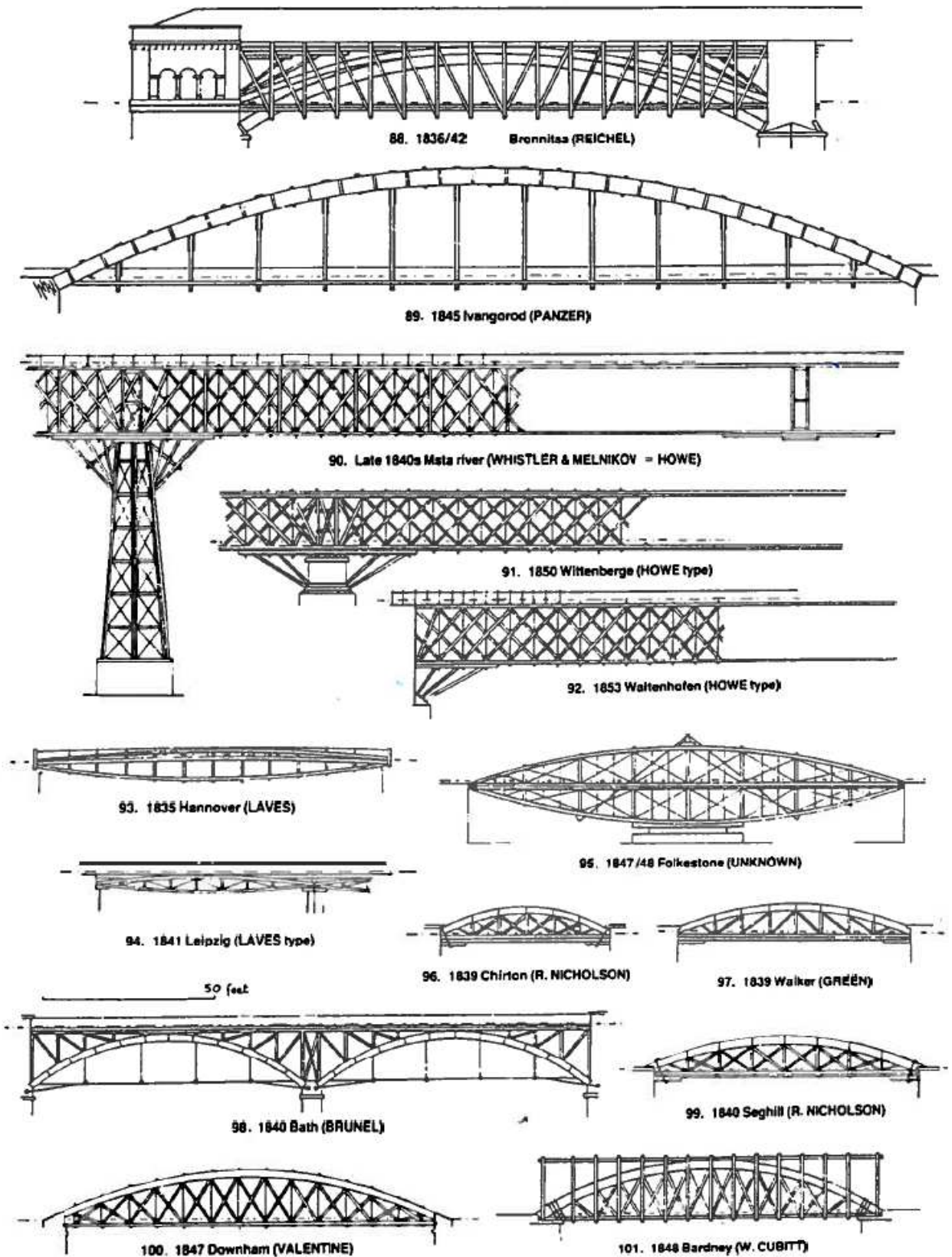
87. 1847/48 Cascade Glen (ADAMS)



85. 1846 Patent design (CHILDS)



86. 1846 Patent design (HASSARD)

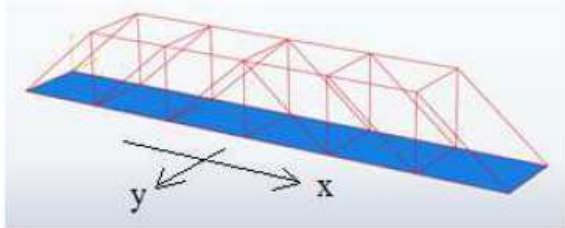


APPENDIX B – Orthotropic plate



To facilitate the FE-analysis the bridge deck needs to be converted into a uniform plate with corresponding bending stiffness in each direction.

Figure A1



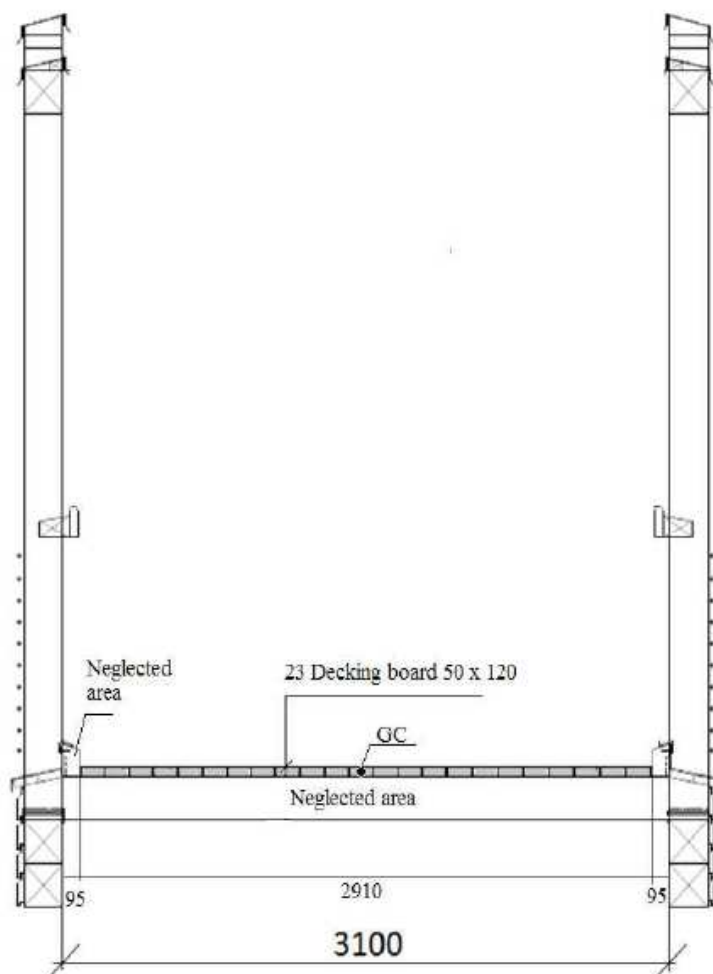
The principle axis of the bridge deck can be viewed in Figure A1.



1.1 Bridge deck in x-direction



The joists are neglected in the y-direction, since the bending stiffness perpendicular to the grains is low.



$$n_x := 23$$

$$E_{0,\text{mean}} := 12 \frac{\text{kN}}{\text{mm}^2} \quad \text{Pine C 30 SS-EN338} \quad \frac{\text{kN}}{\text{mm}^2} = 1 \cdot \text{GPa}$$

$$b_x := 0.12\text{m}$$

$$h_x := 0.05\text{m}$$



1.1.1 Second moment of inertia for rectangular cross-sections



$$I := \frac{b \cdot h^3}{12}$$

Assume gravity center in the middle.

$$I_x := \frac{b_x \cdot h_x^3}{12} = 1.25 \times 10^{-6} \text{ m}^4$$

$$I_{\text{tot},x} := I_x \cdot n_x = 2.875 \times 10^{-5} \text{ m}^4$$

or alternatively:

$$I_{\text{tot},x,\text{alt}} := \frac{n_x \cdot b_x \cdot h_x^3}{12} = 2.875 \times 10^{-5} \text{ m}^4$$

1.1.2 Bending stiffness in x-direction

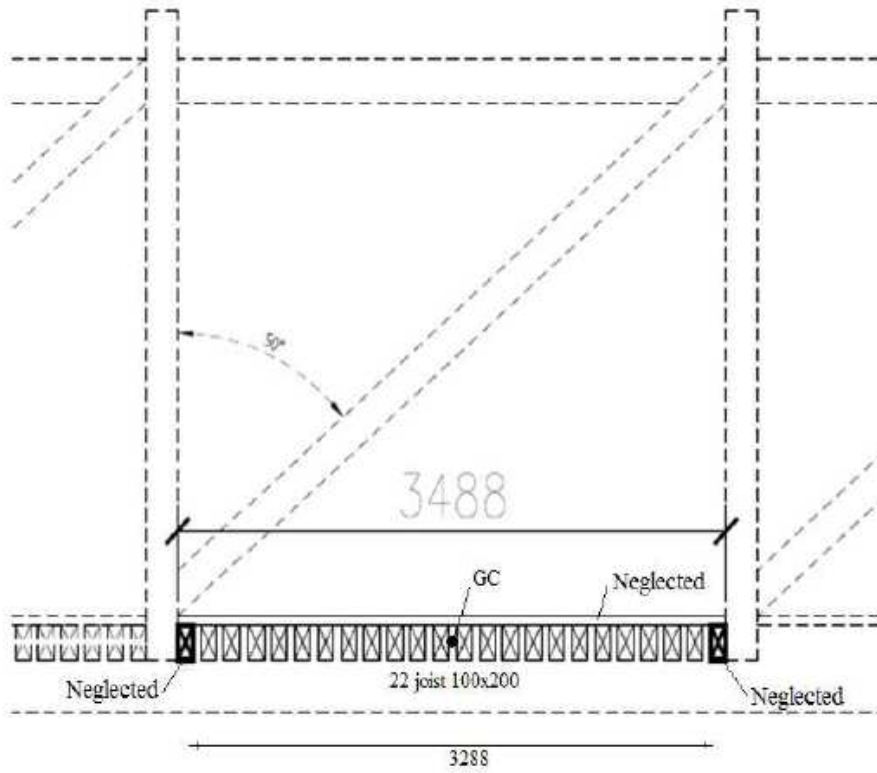
$$EI_x := E_{0,\text{mean}} \cdot I_{\text{tot},x} = 3.45 \times 10^5 \cdot \text{N} \cdot \text{m}^2$$



1.2 Bridge deck in y-direction



The decking board are neglected in y-direction since the the bending stiffness perpendicular to the grains are low. The most outer joist are also neglected because they support the vertical posts and stabilize the connection, hence they will be accounted for as beams and a part of the fframework.



$$n_y := 22$$

$$b_y := 0.1\text{m}$$

$$h_y := 0.2\text{m}$$



1.2.1 Second moment of inertia for rectangular cross-sections



Assume gravity center in the middle.

$$I_y := \frac{b_y \cdot h_y^3}{12} = 6.667 \times 10^{-5} \text{ m}^4$$

$$I_{\text{tot},y} := \frac{n_y \cdot b_y \cdot h_y^3}{12} = 1.467 \times 10^{-3} \text{ m}^4$$



1.2.2 Bending stiffness in x-direction



$$EI_y := E_{0,\text{mean}} \cdot I_{\text{tot},y} = 1.76 \times 10^7 \cdot \text{N} \cdot \text{m}^2$$



1.3 Modified thickness



The mass density [kg/m³] for Pine C30 according to SS-EN 338 is chosen for the bridge deck.

$$\rho_{\text{C30}} := 460 \frac{\text{kg}}{\text{m}^3} \quad (\text{Compare to Oak D40 } 660 \text{ kg/m}^3)$$

Calculation is based on one square meter.



1.3.1 Decking boards per square meter



$$b_{\text{bridge}} := 2.91 \text{ m}$$

$$D_{\text{B_per.meter}} := \frac{n_x}{b_{\text{bridge}}} = 7.904 \frac{1}{\text{m}}$$

$$A_{\text{D_B}} := b_x \cdot h_x = 6 \times 10^{-3} \text{ m}^2$$



1.3.2 Joists per square meter



$$b_{\text{section}} := 3.288\text{m}$$

$$\text{Joist}_{\text{per.meter}} := \frac{n_y + 2}{b_{\text{section}}} = 7.299 \frac{1}{\text{m}}$$

$$A_{\text{Joist}} := b_y \cdot h_y = 0.02 \text{ m}^2$$



1.3.3 Volume per square meter



$$V_{\text{square}} := A_{D_B} \cdot D_{B_per.meter} \cdot 1\text{m} \cdot 1\text{m} + A_{\text{Joist}} \cdot \text{Joist}_{\text{per.meter}} \cdot 1\text{m} \cdot 1\text{m} = 0.193 \cdot \text{m}^3$$



1.3.4 Mass per square meter



$$m_{\text{square}} := V_{\text{square}} \cdot \rho_{C30} = 88.968 \text{ kg}$$



1.3.5 Corresponding thickness



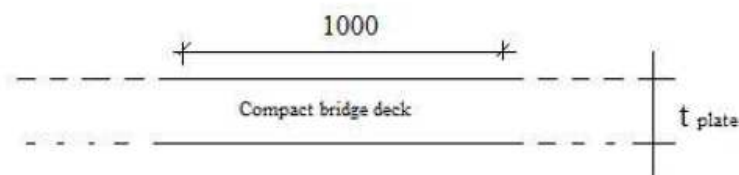
$$t_{\text{plate}} := \frac{m_{\text{square}}}{\rho_{C30} \cdot 1\text{m} \cdot 1\text{m}} = 0.193 \text{ m}$$



1.4 Modified E-modulus



The modified thickness generate a new second moment of inertia in each direction. The bending stiffness that was calculated in section 1.1 and 1.2 is preserved and a corresponding E-modulus are calculated in each direction, which can be implemented in the FE-software.



1.4.1 Second moment of inertia x-direction



$$I_{x.\text{mod}} := \frac{b_{\text{bridge}} \cdot t_{\text{plate}}^3}{12} = 1.754 \times 10^3 \cdot 10^{-6} \cdot \text{m}^4$$

compare to "real" bending stiffness: $I_{\text{tot.x}} = 2.875 \times 10^{-5} \text{ m}^4$



1.4.2 Second moment of inertia x-direction



$$I_{y,\text{mod}} := \frac{b_{\text{section}} \cdot t_{\text{plate}}^3}{12} = 1.982 \times 10^{-3} \cdot \text{m}^4$$

compare to "real" bending stiffness:

$$I_{\text{tot},y} = 1.467 \times 10^{-3} \cdot \text{m}^4$$



1.4.3 Modified E-modulus in x-direction



$$E_x := E_{0,\text{mean}} \cdot \frac{I_{\text{tot},x}}{I_{x,\text{mod}}} = 0.197 \cdot \text{GPa}$$



1.4.4 Modified E-modulus in y-direction



$$E_y := E_{0,\text{mean}} \cdot \frac{I_{\text{tot},y}}{I_{y,\text{mod}}} = 8.878 \cdot \text{GPa}$$



APPENDIX C – Poisson's ratio

Poissons ratio for Red Oak is used in the principle direction of wood according to the Forest Laboratory (USA).

Index explanation:

L = Longitudinal direction of log

R = Radial direction of a log

T = Tangential direction of a annular ring of the log

Red Oak is used for D40:

$$v_{D40.LR} := 0.350$$

$$v_{D40.LT} := 0.448$$

$$v_{D40.RT} := 0.560$$

$$v_{D40.TR} := 0.292 \quad \text{Neglected since these are only the inverted value of } v_{D40.RT}$$

$$v_{D40.RL} := 0.064 \quad \text{Neglected since these are only the inverted value of } v_{D40.LR}$$

$$v_{D40.TL} := 0.033 \quad \text{Neglected since these are only the inverted value of } v_{D40.LT}$$

Pine Western white is used for C30:

$$v_{C30.LR} := 0.329$$

$$v_{C30.LT} := 0.344$$

$$v_{C30.RT} := 0.410$$

$$v_{C30.TR} := 0.334 \quad \text{Neglected since these are only the inverted value of } v_{C30.RT}$$

No value given for the inverted value of $v_{C30.LR}$

No value given for the inverted value of $v_{C30.LT}$

The principle directions need to be converted to a material with transversely-orthotropic properties.

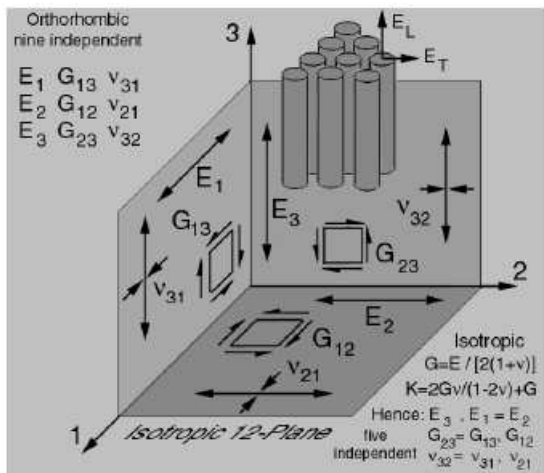
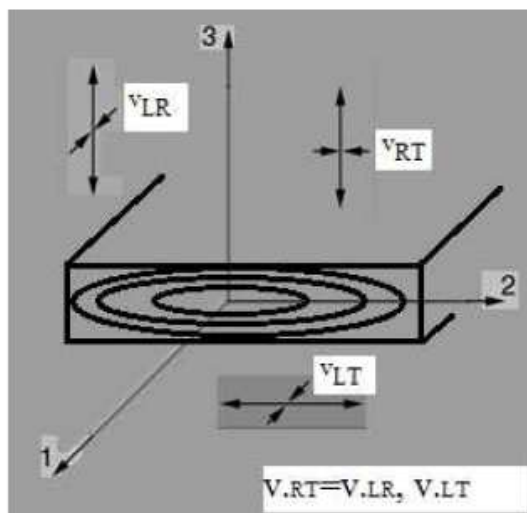


Figure shows a material with transversely-orthotropic properties, which is used in ABAQUS.

An assumption according to the figure below is applied into ABAQUS for each wood species.



Implemented in Abaqus Brigade Pluss for D40:

$$\text{Nu}_{D40.23} := \frac{v_{D40.LR} + v_{D40.RT}}{2} = 0.455$$

A mean value is calculated for the non-longitudinal direction.

$$\text{Nu}_{D40.13} := \text{Nu}_{D40.23} = 0.455$$

$$\text{Nu}_{D40.12} := v_{D40.LT} = 0.448$$

Implemented in Abaqus Brigade Pluss for C30:

$$\text{Nu}_{C30.23} := \frac{v_{C30.LR} + v_{C30.RT}}{2} = 0.369$$

A mean value is calculated for the non-longitudinal direction.

$$\text{Nu}_{C30.13} := \text{Nu}_{C30.23} = 0.369$$

$$\text{Nu}_{C30.12} := v_{C30.LT} = 0.344$$

APPENDIX D – Design load

GEOMETRY



$l_{\text{bridge}} := 21.9\text{m}$ Length of bridge span

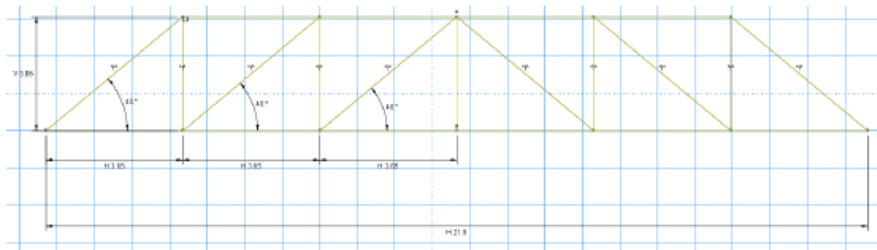
$w_{\text{bridge}} := 3.1\text{m}$ Width of bridge

$l_{\text{section}} := 3.65\text{m}$ Length of section

$h_{\text{bridge}} := 3.06\text{m}$ Height of bridge

$l_{\text{diag}} := 4.76\text{m}$ Length of diagonal

$\theta_{\text{bridge}} := 40\text{deg}$ Angle of the diagonal



Laminated beam

$h_{\text{LM}} := 400\text{mm}$ Height

$w_{\text{LM}} := 200\text{mm}$ Width

Inclined end post

$h_{\text{strut}} := 300\text{mm}$ Height

$w_{\text{strut}} := 200\text{mm}$ Width

Density

Mean density is chosen.

SS-EN 1995-2:2004 7.1 (1)

$\rho_{\text{D40}} := 660 \frac{\text{kg}}{\text{m}^3}$ Density of hardwood strength class D40

$\rho_{\text{C30}} := 460 \frac{\text{kg}}{\text{m}^3}$ Density of softwood strength class C30



LOADS

Self-weight



The self-weight of the bridge deck is applied as line-loads on the framework.

Geometry of the members in the bridge deck

Floor beam:

$l_{\text{fb}} := 3.1\text{m}$ Length

$h_{\text{fb}} := 0.2\text{m}$ Height

$w_{\text{fb}} := 0.1\text{m}$ Width

$s_{\text{fb}} := 0.15\text{m}$ Spacing

$n_{\text{fb}} := \frac{1\text{m}}{s_{\text{fb}}} = 6.667$ Number of floor beam per meter

Decking board:

$$h_{db} := 0.05\text{m} \quad \text{Height}$$

$$w_{db} := 0.12\text{m} \quad \text{Width}$$

$$n_{db} := \frac{1\text{m}}{w_{db}} = 8.333 \quad \text{Number of decking boards per meter}$$

Total volume/m²:

$$V_{BD} := (h_{fb} \cdot w_{fb} \cdot n_{fb} \cdot 1\text{m}) + (h_{db} \cdot w_{db} \cdot n_{db} \cdot 1\text{m}) = 0.183 \cdot \text{m}^3$$

Gravity:

$$g = 9.807 \frac{\text{m}}{\text{s}^2}$$

Total mass load/m²:

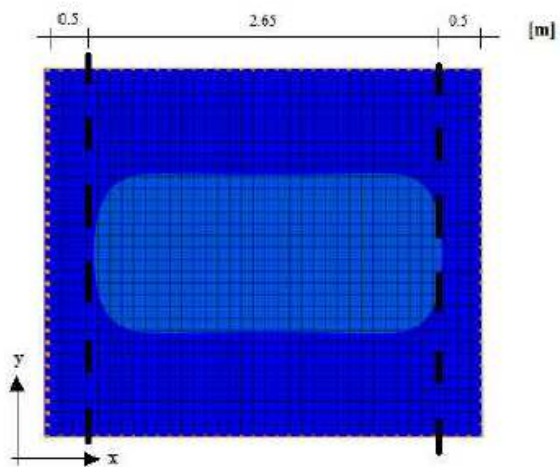
$$m_{BD} := \frac{V_{BD} \cdot \rho_{C30} \cdot g}{\text{m}^2} = 0.827 \cdot \frac{\text{kN}}{\text{m}^2}$$

Total load from bridge deck:

$$G_{BD} := m_{BD} \cdot l_{\text{bridge}} \cdot w_{\text{bridge}} = 56.147 \cdot \text{kN}$$

Tributary area to the framework

Load dividers in each bridge deck section:



Length of tributary area which transfer load to the floor beam:

$$l_x := 0.5\text{m}$$

Length of tributary area which transfer load to the lower chord (laminated beam):

$$l_y := 2.65\text{m}$$

Tributary areas for each frame member:

$$A_{\text{tr},1} := l_x \cdot w_{\text{bridge}} = 1.55 \text{ m}^2 \quad \text{Floor beam positioned at the end of bridge}$$

$$A_{\text{tr},2} := 2 \cdot l_x \cdot w_{\text{bridge}} = 3.1 \text{ m}^2 \quad \text{Floor beam}$$

$$A_{\text{tr},3} := l_y \cdot \frac{w_{\text{bridge}}}{2} \cdot 6 = 24.645 \text{ m}^2 \quad \text{Laminated beam}$$

Permanent line-loads:

$$g_{bd.1} := \frac{A_{tr.1} \cdot m_{BD}}{l_{fb}} = 0.414 \cdot \frac{kN}{m}$$

Floor beam positioned at the end of bridge

$$g_{bd.2} := \frac{A_{tr.2} \cdot m_{BD}}{l_{fb}} = 0.827 \cdot \frac{kN}{m}$$

Floor beam

$$g_{bd.3} := \frac{A_{tr.3} \cdot m_{BD}}{l_{bridge}} = 0.931 \cdot \frac{kN}{m}$$

Laminated beam

Input Brigade/Plus

Parameter:

Location:

$$\rho_{D40} = 660 \frac{kg}{m^3}$$

vertical posts

$$\rho_{C30} = 460 \frac{kg}{m^3}$$

residual framework

$$g_{bd.1} = 0.414 \cdot \frac{kN}{m}$$

end floor beam

$$g_{bd.2} = 0.827 \cdot \frac{kN}{m}$$

middle floor beam

$$g_{bd.3} = 0.931 \cdot \frac{kN}{m}$$

laminated beam



Wind load



Simplified wind load with reference to a older version of the national bridge code of Sweden.

Load

$$q_{k,\text{wind}} := 1.8 \frac{\text{kN}}{\text{m}^2}$$

Bro 2004 21.272 Publ 2004:56

The wind is applied as a line load in Abaqus. The wind load is then converted for each member with different dimensions. The framework has three different widths in ZX-plane;

$w_1 := 0.2\text{m}$ Width of members marked 1 in figure below.

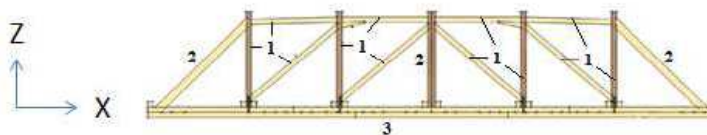
$w_2 := 0.3\text{m}$ Width of members marked 2 in figure below.

$w_3 := 0.4\text{m}$ Width of members marked 3 in figure below.

$q_{k,\text{wind},1} := q_{k,\text{wind}} \cdot w_1 = 0.36 \cdot \frac{\text{kN}}{\text{m}}$ Line load on members marked 1 in figure below.

$q_{k,\text{wind},2} := q_{k,\text{wind}} \cdot w_2 = 0.54 \cdot \frac{\text{kN}}{\text{m}}$ Line load on members marked 2 in figure below.

$q_{k,\text{wind},3} := q_{k,\text{wind}} \cdot w_3 = 0.72 \cdot \frac{\text{kN}}{\text{m}}$ Line load on members marked 3 in figure below.



Implemented in Brigade/Plus

$$q_{k,\text{wind},1} = 0.36 \cdot \frac{\text{kN}}{\text{m}}$$

$$q_{k,\text{wind},2} = 0.54 \cdot \frac{\text{kN}}{\text{m}}$$

$$q_{k,\text{wind},3} = 0.72 \cdot \frac{\text{kN}}{\text{m}}$$

Applied on the surfaces shown in figure above.



Snowload



The designer is allowed to neglect the snow load in the load combination when combined with traffic load for footbridges.

SS-EN 1990 A2.2.3 (3)



Traffic loads

Pedestrian load



Load

$$q_{fk} := 5 \frac{\text{kN}}{\text{m}^2}$$

EN 1991-2:2003 5.3.2.1 (2) NOTE

The pedestrian load is distributed on the framework in the same way as the self-weight of the bridge deck.

$$q_{fk.1} := \frac{A_{tr.1} \cdot q_{fk}}{l_{fb}} = 2.5 \cdot \frac{\text{kN}}{\text{m}} \quad \text{edge floor beam}$$

$$q_{fk.2} := \frac{A_{tr.2} \cdot q_{fk}}{l_{fb}} = 5 \cdot \frac{\text{kN}}{\text{m}} \quad \text{middle floor beam}$$

$$q_{fk.3} := \frac{A_{tr.3} \cdot q_{fk}}{l_{bridge}} = 5.627 \cdot \frac{\text{kN}}{\text{m}} \quad \text{laminated beam}$$

Implemented in Brigade/Plus

$$q_{fk.1} = 2.5 \cdot \frac{\text{kN}}{\text{m}} \quad \text{edge floor beam}$$

$$q_{fk.2} = 5 \cdot \frac{\text{kN}}{\text{m}} \quad \text{middle floor beam}$$

$$q_{fk.3} = 5.627 \cdot \frac{\text{kN}}{\text{m}} \quad \text{laminated beam}$$



Service vehicle load

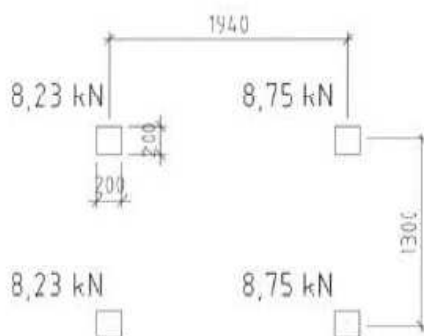


A specific service vehicle is chosen.

EN 1991-2:2003 5.3.2.3 NOTE 1

A concentrated traffic load does not need to be considered if a service vehicle load is applied.

EN 1991-2:2003 5.3.2.2 (3).



Specific service vehicle according to the tender document, (Karlsson, 2012).

Load

$P_{serv.1} := 8.75\text{kN}$ Concentrated force from vehicle wheel in the front.

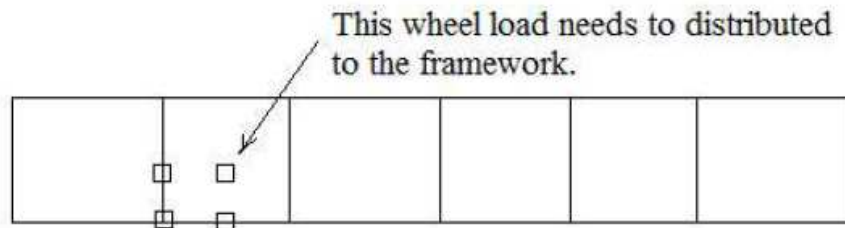
$P_{serv.2} := 8.23\text{kN}$ Concentrated force from vehicle wheel in the rear.

$A_{serv} := 0.2 \cdot 0.2\text{m}^2$ Distribution of the concentrated forces on an area.

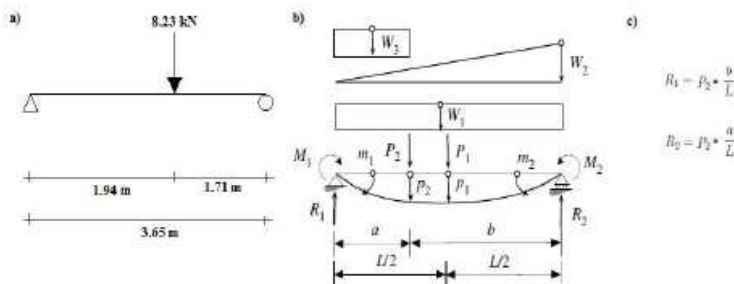
$Q_{serv.1} := \frac{P_{serv.1}}{A_{serv}} = 218.75 \cdot \frac{\text{kN}}{\text{m}^2}$ Distributed wheel force in the front.

$Q_{serv.2} := \frac{P_{serv.2}}{A_{serv}} = 205.75 \cdot \frac{\text{kN}}{\text{m}^2}$ Distributed wheel force in the rear.

Three of the wheels are positioned right above the framework, while one of the wheels are positioned in the middle of one bridge section. This force needs to be distributed onto the framework. It is assumed (based on contour plot FEA) that this load will only spread in the transverse direction to the lower chords on each side of the force.



The bridge deck is assumed to be simply supported on the framework. Hence; the elementary load case below can be used to obtain the force acting on the framework.



a) A point force is applied on the bridge deck. The boundary condition represent the laminated beam. Hence show a spread in the transverse direction of the bridge deck.

b) The elementary load case of a simply supported beam loaded with different loads.

c) Equations to calculate the resulting reaction force on the framework.

$l_{\text{axel.x}} := 1.94\text{m}$ Distance from applied wheel load to the framework.

$l_{\text{section}} = 3.65\text{ m}$ Length of bridge section

$w_{\text{LB}} := 0.2\text{m}$ Width of laminated beam

$w_{\text{bridge}} = 3.1\text{ m}$ Width of bridge

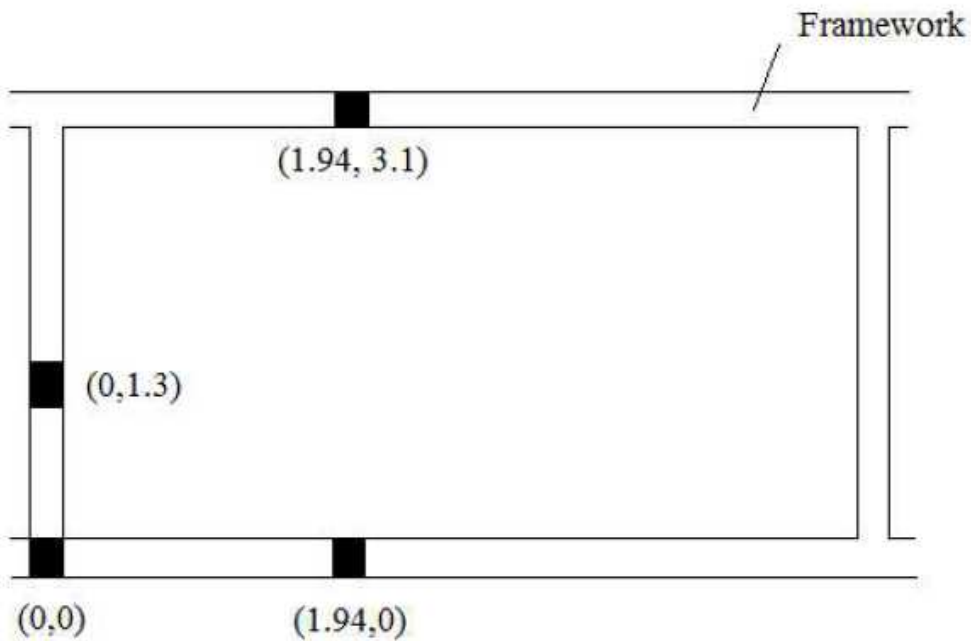
$$q_{\text{serv.2.1}} := Q_{\text{serv.2}} \cdot \frac{l_{\text{axel.x}}}{w_{\text{bridge}}} \cdot w_{\text{LB}} = 25.752 \cdot \frac{\text{kN}}{\text{m}}$$

Distributed force acting on one of the lower chords as line load.

$$q_{\text{serv.2.2}} := Q_{\text{serv.2}} \cdot \frac{(l_{\text{section}} - l_{\text{axel.x}})}{w_{\text{bridge}}} \cdot w_{\text{LB}} = 22.699 \cdot \frac{\text{kN}}{\text{m}}$$

Distributed force acting on the opposite lower chord as line load.

Four distributed forces of a length equal to 200mm is implemented in Brigade, see positions in figure below:



Distributed force onto framework: (0,0)

$$q_{s,1} := Q_{serv,1} \cdot w_{LB} = 43.75 \cdot \frac{\text{kN}}{\text{m}}$$

Distributed force onto framework: (0,1.3)

$$q_{s,2} := Q_{serv,1} \cdot w_{LB} = 43.75 \cdot \frac{\text{kN}}{\text{m}}$$

Distributed force onto framework: (1.94,0)

$$q_{s,3} := q_{serv,2.1} = 25.752 \cdot \frac{\text{kN}}{\text{m}}$$

Distributed force onto framework: (1.94,3.1)

$$q_{s,4} := q_{serv,2.2} = 22.699 \cdot \frac{\text{kN}}{\text{m}}$$

Implemented in Brigade/Plus

Coordinate 1 in the section: (0,0)

$$q_{s,1} = 43.75 \cdot \frac{\text{kN}}{\text{m}}$$

Coordinate 2 in the section: (0,1.3)

$$q_{s,2} = 43.75 \cdot \frac{\text{kN}}{\text{m}}$$

Coordinate 3 in the section: (1.94,0)

$$q_{s,3} = 25.752 \cdot \frac{\text{kN}}{\text{m}}$$

Coordinate 4 in the section: (1.94,3.1)

$$q_{s,4} = 22.699 \cdot \frac{\text{kN}}{\text{m}}$$



Horizontal load



Load

The horizontal load simulates a braking and acceleration load.

The maximal load of the traffic loads are chosen according to Eurocode 1.

$$Q_{flk.1} := \max(0.6 \cdot Q_{serv.1}, 0.1 \cdot q_{flk})$$

EN 1991-2:2003 5.4 (2)

$$Q_{flk.2} := \max(0.6 \cdot Q_{serv.2}, 0.1 \cdot q_{flk})$$

The horizontal load is equal to 60% of the vertical load of the Service vehicle:

Coordinate 1 in the section: (0,0)

$$q_{h.1} := q_{s.1} \cdot 0.6 = 26.25 \cdot \frac{\text{kN}}{\text{m}}$$

Coordinate 2 in the section: (0,1.3)

$$q_{h.2} := q_{s.2} \cdot 0.6 = 26.25 \cdot \frac{\text{kN}}{\text{m}}$$

Coordinate 3 in the section: (1.94,0)

$$q_{h.3} := q_{s.3} \cdot 0.6 = 15.451 \cdot \frac{\text{kN}}{\text{m}}$$

Coordinate 4 in the section: (1.94,3.1)

$$q_{h.4} := q_{s.4} \cdot 0.6 = 13.619 \cdot \frac{\text{kN}}{\text{m}}$$

Implemented in Brigade/Plus

Coordinate 1 in the section: (0,0)

$$q_{h,1} = 26.25 \cdot \frac{\text{kN}}{\text{m}}$$

Coordinate 2 in the section: (0,1.3)

$$q_{h,2} = 26.25 \cdot \frac{\text{kN}}{\text{m}}$$

Coordinate 3 in the section: (1.94,0)

$$q_{h,3} = 15.451 \cdot \frac{\text{kN}}{\text{m}}$$

Coordinate 4 in the section: (1.94,3.1)

$$q_{h,4} = 13.619 \cdot \frac{\text{kN}}{\text{m}}$$



Design load and load combination

Partial factors



SELF-WEIGHT

The permanent load is unfavourable, therefore the safety factor that ensembles the upper characteristic value is chosen.

SS-EN 1990.4.1.2 (2) P

SS-EN 1990 tab. A2.4 (B)

$$\gamma_{G,\text{sup}} := 1.35$$

WIND

$$\gamma_{Q,1,W} := 1.5$$

SS-EN 1990 tab A2.4(B) NOTE 2

$$\gamma_{1,1,W} := 1.0$$

SS-EN 1990 A2.4.1 (NOTE 1)

$$\psi_{0,W} := 0.3$$

$$\psi_{1,W} := 0.2$$

SS-EN 1990 Tab A2.2

PEDESTRIAN LOAD

$$\gamma_{Q,1,P} := 1.5$$

$$\gamma_{1,1,P} := 1.0$$

Service vehicle load is load group gr2.

EN 1991-2:2003 5.5 tab 5.1

$$\psi_{0,P} := 0.4$$

$$\psi_{1,P} := 0.4$$

SS-EN 1990 Tab A2.2

SERVICE VEHICLE

$$\gamma_{Q,1,S} := 1.5$$

$$\gamma_{1,1,S} := 1.0$$

Service vehicle load is load group gr1.

EN 1991-2:2003 5.5 tab 5.1

The partial safety factor ψ are zero both for ULS and SLS.

SS-EN 1990 Tab A2.2

Dynamical factor

Specific dynamic addition for specific project.

$$\alpha_{\text{dyn}} := 1.4$$

EN 1991-2:2003 5.3.2.3 NOTE 1

HORIZONTAL LOADS

The horizontal load belongs to the service vehicle load in load group gr1.

EN 1991-2:2003 5.5 tab 5.1

The partial safety factor ψ are zero both for ULS and SLS.

SS-EN 1990 Tab A2.2



Inclined end strut



Stresses obtain from the global analysis are collected and a design load combination is obtained.

Characteristic normal stress

Critical load case: Self-Weight, Wind, L3 - Pedestrian

$$\sigma_{x,k,g} := -0.584 \text{MPa}$$

$$\sigma_{x,k,w} := -0.180 \text{MPa}$$

$$\sigma_{x,k,LC3} := -1.865 \text{MPa}$$

Design normal stress:

$$\sigma_{c,d} := \gamma_{G,sup} \cdot \sigma_{x,k,g} + \gamma_{Q,1,P} \cdot \sigma_{x,k,LC3} + \gamma_{Q,1,W} \cdot \psi_{0,W} \cdot \sigma_{x,k,w} = -3.667 \text{MPa}$$

Characteristic bending stress in the strong direction (around y-axis)

Critical load case: Self-Weight, Wind, L3 - Pedestrian

$$\sigma_{m.y.k.g} := -0.109\text{MPa}$$

$$\sigma_{m.y.k.w} := -0.021\text{MPa}$$

$$\sigma_{m.y.k.LC3} := -0.751\text{MPa}$$

Design bending stress around y-axis:

$$\sigma_{m.y.d} := \gamma_{G,\text{sup}} \cdot \sigma_{m.y.k.g} + \gamma_{Q,1,P} \cdot \sigma_{m.y.k.LC3} + \gamma_{Q,1,W} \cdot \psi_{0,W} \cdot \sigma_{m.y.k.w} = -1.283 \cdot \text{MPa}$$

Characteristic bending stress in the weak direction (around z-axis)

Critical load case: Self-Weight, Wind, L3 - Pedestrian

$$\sigma_{m.z.k.g} := -0.142\text{MPa}$$

$$\sigma_{m.z.k.w} := -0.959\text{MPa}$$

$$\sigma_{m.z.k.LC3} := -0.688\text{MPa}$$

Design bending stress around z-axis:

$$\sigma_{m.z.d} := \gamma_{G,\text{sup}} \cdot \sigma_{m.z.k.g} + \gamma_{Q,1,P} \cdot \sigma_{m.z.k.LC3} + \gamma_{Q,1,W} \cdot \psi_{0,W} \cdot \sigma_{m.z.k.w} = -1.655 \cdot \text{MPa}$$

Characteristic shear stress

Critical load case: Self-Weight, Wind, L1 - service vehicle near the support,
Horizontal load

$$\tau_{z.k.g} := -0.008\text{MPa}$$

$$\tau_{z.k.w} := -0.0001\text{MPa}$$

$$\tau_{z.k.LC1} := -0.002\text{MPa}$$

Horizontal load is active but very small so it is neglected.

Design shear stress in z-dir:

$$\tau_{z.d} := \gamma_{G,\text{sup}} \cdot \tau_{z.k.g} + \gamma_{Q,1,S} \cdot \alpha_{\text{dyn}} \cdot \tau_{z.k.LC1} + \gamma_{Q,1,W} \cdot \psi_{0,W} \cdot \tau_{z.k.w} = -0.015 \cdot \text{MPa}$$

Critical load case: Self-Weight, Wind, L3 - Pedestrian

$$\tau_{y.k.g} := -0.002 \text{MPa}$$

$$\tau_{y.k.w} := -0.051 \text{MPa}$$

$$\tau_{y.k.LC3} := -0.0088 \text{MPa}$$

Design shear stress in y-dir:

$$\tau_{y.d} := \gamma_{G,\text{sup}} \cdot \tau_{y.k.g} + \gamma_{Q,1.P} \cdot \tau_{y.k.LC3} + \gamma_{Q,1.W} \cdot \psi_{0.W} \cdot \tau_{y.k.w} = -0.039 \text{MPa}$$

Characteristic torsion stress

Critical load case: Self-Weight, Wind, L3 - Pedestrian

$$\tau_{\text{tor.k.g}} := 0.008 \text{MPa}$$

$$\tau_{\text{tor.k.w}} := 0.043 \text{MPa}$$

$$\tau_{\text{tor.k.LC3}} := 0.047 \text{MPa}$$

Design torsional stress:

$$\tau_{\text{tor.d}} := \gamma_{G,\text{sup}} \cdot \tau_{\text{tor.k.g}} + \gamma_{Q,1.P} \cdot \tau_{\text{tor.k.LC3}} + \gamma_{Q,1.W} \cdot \psi_{0.W} \cdot \tau_{\text{tor.k.w}} = 0.101 \text{MPa}$$



Laminated beam



Stresses obtain from the global analysis

Characteristic normal stress

Critical load case: Self-Weight, Wind, L3 - Pedestrian, Horizontal load

$$\sigma_{2x.k.g} := 0.327 \text{MPa}$$

$$\sigma_{2x.k.w} := -0.109 \text{MPa} \quad \text{Favorable}$$

$$\sigma_{2x.k.LC3} := 1.056 \text{MPa}$$

$$\sigma_{2x.k.H} := 0.162 \text{MPa} \quad \text{Not active}$$

Design normal stress:

$$\sigma_{2t.0.d} := \gamma_{G,\text{sup}} \cdot \sigma_{2x.k.g} + \gamma_{Q,1.P} \cdot \sigma_{2x.k.LC3} + 0 \cdot \psi_{0.W} \cdot \sigma_{2x.k.w} = 2.025 \text{MPa}$$

Characteristic bending stress in the strong direction (around y-axis)

Critical load case: Self-Weight, Wind, L3 - Pedestrian, Horizontal load

$$\sigma_{2m.y.k.g} := -0.023\text{MPa} \quad \text{Favorable}$$

$$\sigma_{2m.y.k.w} := 0.011\text{MPa}$$

$$\sigma_{2m.y.k.LC3} := 0.116\text{MPa}$$

$$\sigma_{2m.y.k.H} := 0.003\text{MPa} \quad \text{Not active}$$

Design bending stress around y-axis:

$$\sigma_{2m.y.d} := \gamma_{G.sup} \cdot \sigma_{2m.y.k.g} + \gamma_{Q.1.P} \cdot \sigma_{2m.y.k.LC3} + \gamma_{Q.1.W} \cdot \psi_{0.W} \cdot \sigma_{2m.y.k.w} = 0.179\text{MPa}$$

Characteristic bending stress in the weak direction (around z-axis)

Critical load case: Self-Weight, Wind, L3 - Pedestrian, Horizontal load

$$\sigma_{2m.z.k.g} := 0.071\text{MPa}$$

$$\sigma_{2m.z.k.w} := 0.423\text{MPa}$$

$$\sigma_{2m.z.k.LC3} := 0.324\text{MPa}$$

$$\sigma_{2m.z.k.H} := 0.011\text{MPa} \quad \text{Not active}$$

Design bending stress around z-axis:

$$\sigma_{2m.z.d} := \gamma_{G.sup} \cdot \sigma_{2m.z.k.g} + \gamma_{Q.1.P} \cdot \sigma_{2m.z.k.LC3} + \gamma_{Q.1.W} \cdot \psi_{0.W} \cdot \sigma_{2m.z.k.w} = 0.772\text{MPa}$$

Characteristic shear stress

Critical load case: Self-Weight, Wind, L3 - Pedestrian, Horizontal load

$$\tau_{2z.k.g} := -0.034\text{MPa}$$

$$\tau_{2z.k.w} := 0.002\text{MPa} \quad \text{Favorable}$$

$$\tau_{2z.k.LC3} := -0.157\text{MPa}$$

$$\tau_{2z.k.H} := -0.00008\text{MPa} \quad \text{Not active}$$

Design shear stress in z-dir:

$$\tau_{2z.d} := \gamma_{G.sup} \cdot \tau_{2z.k.g} + \gamma_{Q.1.P} \cdot \tau_{2z.k.LC3} + \gamma_{Q.1.W} \cdot \psi_{0.W} \cdot \tau_{2z.k.w} = -0.281\text{MPa}$$

Critical load case: Self-Weight, Wind, L3 - Pedestrian, Horizontal load

$$\tau_{2y.k.g} := 0.0016 \text{MPa}$$

$$\tau_{2y.k.w} := -0.003 \text{MPa} \quad \text{Favorable}$$

$$\tau_{2y.k.LC3} := 0.008 \text{MPa}$$

$$\tau_{2y.k.H} := 0.00448 \text{MPa} \quad \text{Not active}$$

Design shear stress in y-dir:

$$\tau_{2y.d} := \gamma_{G.sup} \cdot \tau_{2y.k.g} + \gamma_{Q.1.P} \cdot \tau_{2y.k.LC3} + {}^0\gamma_{Q.1.W} \cdot \psi_{0.W} \cdot \tau_{2y.k.w} = 0.014 \text{MPa}$$

Characteristic torsion stress

Critical load case: Self-Weight, Wind, L3 - Pedestrian, Horizontal load

$$\tau_{2tor.k.g} := 0.0041 \text{MPa}$$

$$\tau_{2tor.k.w} := 0.013 \text{MPa}$$

$$\tau_{2tor.k.LC3} := 0.019 \text{MPa}$$

$$\tau_{2tor.k.H} := 0.0041 \text{MPa} \quad \text{Not active}$$

Design torsional stress:

$$\tau_{2tor.d} := \gamma_{G.sup} \cdot \tau_{2tor.k.g} + \gamma_{Q.1.P} \cdot \tau_{2tor.k.LC3} + \gamma_{Q.1.W} \cdot \psi_{0.W} \cdot \tau_{2tor.k.w} = 0.04 \text{MPa}$$



APPENDIX E – Joint designs



Design load



$$h_{\text{strut}} := 300\text{mm}$$

$$w_{\text{strut}} := 200\text{mm}$$

$$h_{\text{LM}} := 400\text{mm}$$

$$w_{\text{LM}} := 200\text{mm}$$

$$\theta_{\text{bridge}} := 40\text{deg}$$

$$N_{\text{Ed}} := \sigma_{\text{c.0.d}} \cdot h_{\text{strut}} \cdot w_{\text{strut}} = -220.014 \cdot \text{kN}$$



Resistance



Characteristic strength

$$\gamma_{\text{M}} := 1.3$$

Solid timber
SS - EN 1995-1-1:2004 Tab 2.3

$k_{\text{mod}} := 0.7$ Load-class = short-term for traffic load, medium-term for loads during construction and permanent for dead-weight, see report. Climate-class 2 if TRVR (F.1.2) and TRVK are fulfilled otherwise climate-class 3. Chosen: Short-term and class 3 (worst case). SS - EN 1995-1-1:2004 Tab 3.1

k.h is not possible to use as an increasing factor since it only applies to bending and tension. SS - EN 1995-1-1:2004 3.2 (3)

$k_m := 0.7$ SS - EN 1995-1-1:2004 6.1.6 (2)

$$k_{\text{shape}} := \min\left(1 + 0.15 \cdot \frac{h_{\text{strut}} w_{\text{strut}}}{m^2}, 2.0\right) = 1.009$$

$$k_{2\text{shape}} := \min\left(1 + 0.15 \cdot \frac{h_{\text{LM}} w_{\text{LM}}}{m^2}, 2.0\right) = 1.012$$

$k_{c,90} := 1.50$ Solid timber on discrete support which result in an increasing factor of the strength. SS - EN 1995-1-1:2004 6.1.5 (2)

Strength - Pine C24

$$f_{mk} := 24 \text{ MPa}$$

$$f_{t,0,k} := 14 \text{ MPa}$$

$$f_{c,0,k} := 21 \text{ MPa}$$

$$f_{c,90,k} := 2.5 \text{ MPa}$$

$$f_{m,k} := 4 \text{ MPa}$$



Design strength



Tension parallel to grain:

$$f_{t,0,d} := \frac{f_{t,0,k} \cdot k_{mod}}{\gamma_M} = 7.538 \text{ MPa}$$

Compression parallel to the grain

$$f_{c,0,d} := \frac{f_{c,0,k} \cdot k_{mod}}{\gamma_M} = 11.308 \text{ MPa}$$

Compression perpendicular to the grain

$$f_{c,90,d} := \frac{f_{c,90,k} \cdot k_{mod}}{\gamma_M} = 1.346 \text{ MPa}$$

Bending strength

$$f_{m,d} := \frac{f_{m,k} \cdot k_{mod}}{\gamma_M} = 12.923 \text{ MPa}$$

Shear strength

$$f_{v,d} := \frac{f_{v,k} \cdot k_{mod}}{\gamma_M} = 2.154 \text{ MPa}$$

Torsional strength

$$f_{tor,d} := k_{shape} \cdot f_{v,d} = 2.173 \text{ MPa}$$

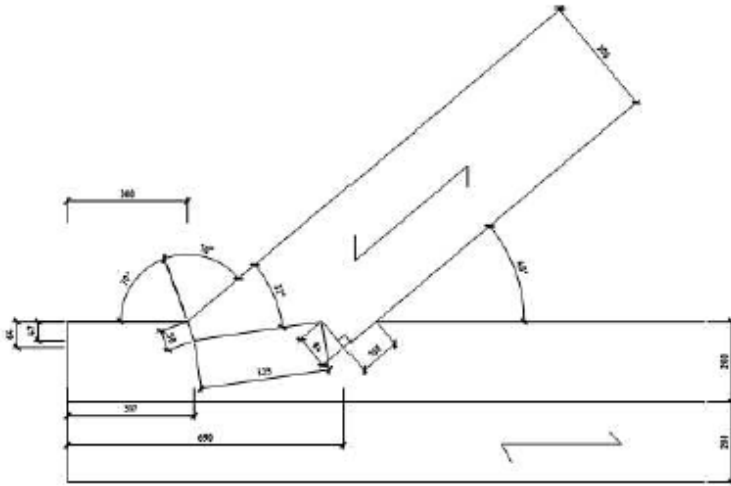


JOINT AF

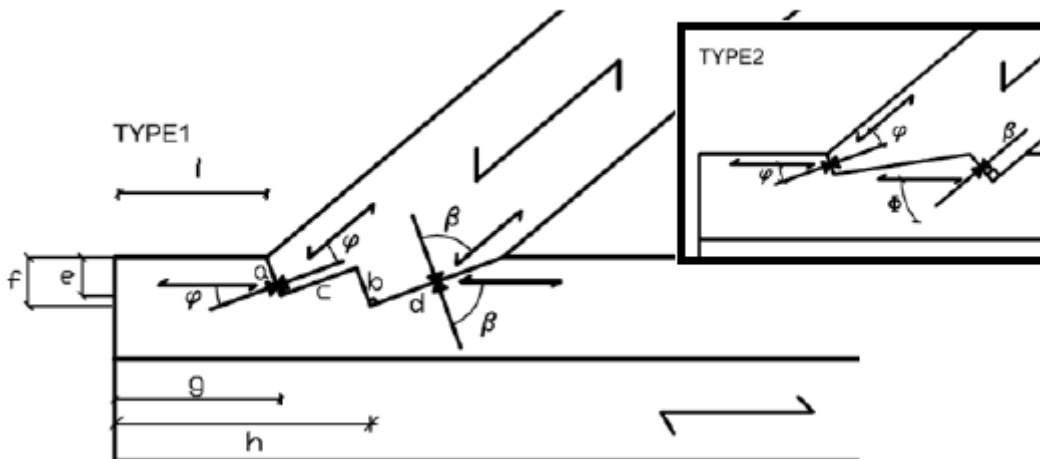
Geometry



Drawing of Joint AF:



Principle sketch showing notations:



Lengths of loaded surfaces:

$l_{2,a} := 50\text{mm}$ According to Timber engineering STEP 1:
Only the the frontal area shall be taken into account. Here frontal area is interpreted as both surface a and b.

$l_{2,b} := 84\text{mm}$

$l_{2,c} := 323\text{mm}$ The load-bearing capacity of surface c is neglected according to STEP 1.

$l_{2,d} := 100\text{mm}$ Surface d has no load-bearing capacity w.r.t. the design load.

$l_{2,e} := 47\text{mm}$

$l_{2,f} := 64\text{mm}$

$l_{2,g} := 317\text{mm}$

$l_{2,h} := 317\text{mm} + 373\text{mm} = 690\text{mm}$

$l_{2,i} := 300\text{mm}$ Distance from edge to frontal surface:

$l_{2,e} \leq \min(l_{2,f} - 10\text{mm}, 0.8 \cdot l_{2,f}) = 1$

The design criteria from STEP 1 is fulfilled, the shear planes do not coincide.

Angle between the stress and the grains in the inclined end post and the laminated beam at surface a:

$\varphi_2 := 20\text{deg}$

Angle between the stress and the grains in the inclined end post and the laminated beam at surface b:

$\beta_2 := 0\text{deg}$ inclined end post

$\phi_2 := 40\text{deg}$ laminated beam

Angles for surface c are neglected due to that the bearing-capacity of this surface is neglected.



Load effect



Load:

$N_{Ed} = -220.014\text{ kN}$

Design load for the strut

$$\sigma_{2f.0.d} = 2.025 \times 10^6 \text{ Pa}$$

Design stress for the laminated beam

Only the front areas of the cogging joint needs to be taken into account.

$$b_{ef} := w_{strut} = 0.2 \text{ m}$$

Stresses for a single cogging joint with a frontal area:

$$\sigma_{2.a.c.\alpha.d.s} := \frac{N_{Ed} \cdot \cos\left(\frac{\theta_{bridge}}{2}\right)^2}{b_{ef} \cdot l_{2,e}} = -20.668 \text{ MPa}$$

Uniform distribution of the stresses at surface a if one frontal surface is used.

Stresses for a single cogging joint with a rear notched area:

$$\sigma_{2.b.c.\alpha.d.s} := \frac{N_{Ed} \cdot \cos(\theta_{bridge})}{b_{ef} \cdot l_{2,f}} = -13.167 \text{ MPa}$$

Uniform distribution of the stresses at surface b if one rear surface is used.

Weighted expression to calculate the stresses for a double cogging joint:

$$s_{2dist} := \frac{\sigma_{2.a.c.\alpha.d.s}}{\sigma_{2.a.c.\alpha.d.s} + \sigma_{2.b.c.\alpha.d.s}} = 0.611$$

Stresses on the frontal area in the double cogging joint:

$$\sigma_{2.a.c.\alpha.d} := \frac{N_{Ed} \cdot s_{2dist} \cdot \cos\left(\frac{\theta_{bridge}}{2}\right)^2}{b_{ef} \cdot l_{2,e}} = -12.625 \text{ MPa}$$

Stresses on the rear area in the double cogging joint:

$$\sigma_{2.b.c.\alpha.d} := \frac{N_{Ed} (1 - s_{2dist}) \cdot (\theta_{bridge})}{b_{ef} \cdot l_{2,f}} = -4.67 \text{ MPa}$$

The required end distance to assure enough shear strength.

$$l_{2,h,eff} := \frac{|N_{Ed}| \cdot \cos(\theta_{bridge})}{b_{ef} \cdot f_{v,d}} = 391.255 \cdot \text{mm}$$

The required end distance generate a insufficient shear strength:

$$l_{2,h,eff} < l_{2,h} = 1$$

$$\tau_{2,Ed} := \frac{|N_{Ed}| \cdot \cos(\theta_{bridge})}{b_{ef} \cdot l_{2,h}} = 1.221 \cdot \text{MPa}$$

The tensile stresses in the laminated beam due to reduce cross-section:

$$\sigma_{2,t,0,d} := \frac{\sigma_{2,t,0,d} \cdot w_{LM} \cdot h_{LM}}{(h_{LM} - l_{2,f}) \cdot w_{LM}} = 2.411 \cdot \text{MPa} \quad \text{where:} \quad \begin{aligned} \sigma_{2,t,0,d} &= 2.025 \cdot \text{MPa} \\ w_{LM} &= 0.2 \text{ m} \\ h_{LM} &= 0.4 \text{ m} \end{aligned}$$

Compare to unreduced cross-section

$$\sigma_{2,t,0,d} = 2.025 \cdot \text{MPa}$$



Design strength depending on the joint design



Compression in an angle to the grain (20 deg) for both the laminated beam and the inclined end post:

$$f_{2,b,c,\phi,d} := \frac{f_{c,0,d}}{\frac{f_{c,0,d}}{k_{c,90} \cdot f_{c,90,d}} \cdot (\sin(\phi_2))^2 + (\cos(\phi_2))^2} = 3.898 \cdot \text{MPa}$$

$$l_{2,e.req} := \frac{|N_{Ed}| \cdot s_{2,dist} \cdot \cos\left(\frac{\theta_{bridge}}{2}\right)^2}{b_{ef} \cdot f_{2,a.c.\varphi,d}} = 0.081 \text{ m}$$

Calculate the required notch depth:

$$l_{2,e.req} \leq \min(l_{2,f} - 10\text{mm}, 0.8 \cdot l_{2,f}) = 0$$

The design criteria from STEP 1 is fulfilled, the shear planes do not coincide.

$$l_{2,f.req} := \max\left(l_{2,e.req} + 10\text{mm}, \frac{l_{2,e.req}}{0.8}\right) = 0.101 \text{ m}$$

$$l_{2,e.req} \leq \min(l_{2,f.req} - 10\text{mm}, 0.8 \cdot l_{2,f.req}) = 1$$

Ok sufficient notch depth.



RESULTS



Inclined end post

Compression in an angle ($\varphi=20\text{deg}$) to the grain:

Surface a:

$$\sigma_{2,a.c.\alpha,d} = -12.625 \text{ MPa}$$

$$f_{2,a.c.\varphi,d} = 7.352 \text{ MPa}$$

$$|\sigma_{2,a.c.\alpha,d}| \leq f_{2,a.c.\varphi,d} = 0$$

Utilization rate:

$$\frac{|\sigma_{2,a.c.\alpha,d}|}{f_{2,a.c.\varphi,d}} = 1.717$$

Compression parallell to the grain :

Surface b:

$$\sigma_{2,b,c,\alpha,d} = -4.67 \text{ MPa}$$

$$|\sigma_{2,b,c,\alpha,d}| \leq f_{c,0,d} = 1$$

$$f_{c,0,d} = 11.308 \text{ MPa}$$

$$\frac{|\sigma_{2,b,c,\alpha,d}|}{f_{c,0,d}} = 0.413$$

Utilization rate:

Laminated beam

Compression in an angle ($\varphi_2=20\text{deg}$) to the grain:

Surface a:

$$\sigma_{2,a,c,\alpha,d} = -12.625 \text{ MPa}$$

$$|\sigma_{2,a,c,\alpha,d}| \leq f_{2,a,c,\varphi,d} = 0$$

$$f_{2,a,c,\varphi,d} = 7.352 \text{ MPa}$$

$$\frac{|\sigma_{2,a,c,\alpha,d}|}{f_{2,a,c,\varphi,d}} = 1.717$$

Utilization rate:

Compression in an angle ($\varphi_2=40\text{deg}$) to the grain:

Surface b:

$$\sigma_{2,b,c,\alpha,d} = -4.67 \text{ MPa}$$

$$|\sigma_{2,b,c,\alpha,d}| \leq f_{2,b,c,\varphi,d} = 0$$

$$f_{2,b,c,\varphi,d} = 3.898 \text{ MPa}$$

$$\frac{|\sigma_{2,b,c,\alpha,d}|}{f_{2,b,c,\varphi,d}} = 1.198$$

Utilization rate:

Shear parallel to the grain in one shear plane (the rear):

$$\tau_{2,Ed} = 1.221 \text{ MPa}$$

$$|\tau_{2,Ed}| \leq f_{v,d} = 1$$

$$f_{v,d} = 2.154 \text{ MPa}$$

$$\frac{|\tau_{2,Ed}|}{f_{v,d}} = 0.567$$

Utilization rate:

Tension parallel to the grain:

$$\sigma_{2,t,0,d} = 2.411 \text{ MPa}$$

$$|\sigma_{2,t,0,d}| \leq f_{t,0,d} = 1$$

$$f_{t,0,d} = 7.538 \text{ MPa}$$

Utilization rate:

$$\frac{\sigma_{2,t,0,d}}{f_{t,0,d}} = 0.32$$

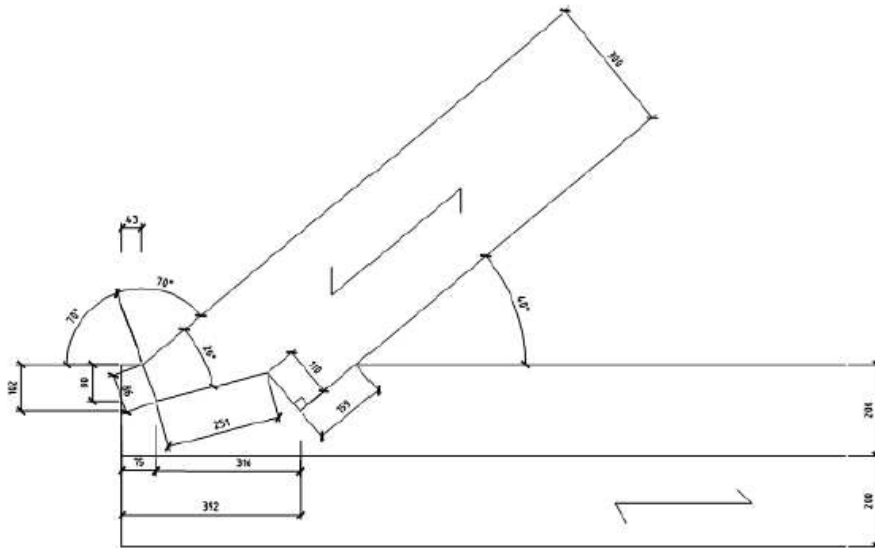


JOINT B

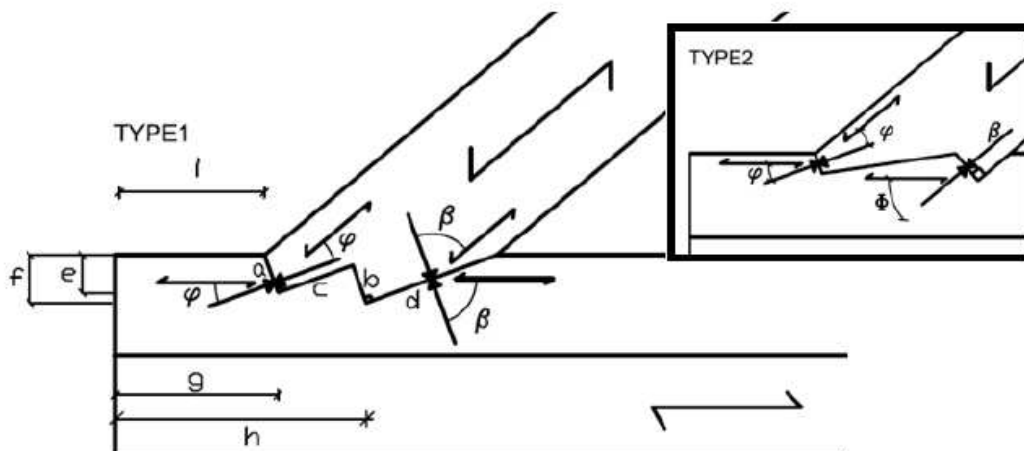
Geometry



Drawing of Joint B:



Principle sketch showing notations:



Lengths of loaded surfaces:

$$l_{2,a} := 86\text{mm}$$

$$l_{2,b} := 110\text{mm}$$

$$l_{2,c} := 251\text{mm}$$

The load-bearing capacity of surface c is neglected according to STEP 1.

$$l_{2,d} := 159\text{mm}$$

Surface d has no load-bearing capacity w.r.t. design load.

$$l_{2,e} := 80\text{mm}$$

$$l_{2,f} := 102\text{mm}$$

$$l_{2,g} := 75\text{mm}$$

$$l_{2,h} := 392\text{mm}$$

$$l_{2,i} := 43\text{mm}$$

$$l_{2,e} \leq \min(l_{2,f} - 10\text{mm}, 0.8 \cdot l_{2,f}) = 1$$

Distance from edge to frontal surface:

The design criteria from STEP 1 is fulfilled, the shear planes do not coincide.

Angle between the stress and the grains in the inclined end post and the laminated beam at surface a:

$$\varphi_2 := 20\text{deg}$$

Angle between the stress and the grains in the inclined end post and the laminated beam at surface b:

$$\beta_2 := 0\text{deg} \quad \text{inclined end post}$$

$$\phi_2 := 40\text{deg} \quad \text{laminated beam}$$

Angles for surface c are neglected due to that the bearing-capacity of this surface is neglected



Load effect



Load:

$$N_{Ed} = -220.014\text{ kN} \quad \text{Design load for the strut}$$

$$\sigma_{2t,0,d} = 2.025 \times 10^6 \text{ Pa} \quad \text{Design stress for the laminated beam}$$

Only the front surfaces of the cogging joint needs to be taken into account.

$$b_{ef} := w_{strut} = 0.2\text{m}$$

Stresses for a single cogging joint with a frontal area:

$$\sigma_{2.a.c.\alpha.d.s} := \frac{N_{Ed} \cdot \cos\left(\frac{\theta_{bridge}}{2}\right)^2}{b_{ef} \cdot l_{2.e}} = -12.142 \cdot \text{MPa}$$

Uniform distribution of the stresses at surface a if one abutment surface is used.

Stresses for a single cogging joint with a rear notched area:

$$\sigma_{2.b.c.\alpha.d.s} := \frac{N_{Ed} \cdot \cos(\theta_{bridge})}{b_{ef} \cdot l_{2.f}} = -8.262 \cdot \text{MPa}$$

Uniform distribution of the stresses at surface b if one contact surface is used.

Weighted expression to calculate the stresses for a double notched cogging joint:

$$s_{2dist} := \frac{\sigma_{2.a.c.\alpha.d.s}}{\sigma_{2.a.c.\alpha.d.s} + \sigma_{2.b.c.\alpha.d.s}} = 0.595$$

Stresses on the frontal area in the double notched cogging joint:

$$\sigma_{2.a.c.\alpha.d} := \frac{N_{Ed} \cdot s_{2dist} \cdot \cos\left(\frac{\theta_{bridge}}{2}\right)^2}{b_{ef} \cdot l_{2.e}} = -7.226 \cdot \text{MPa}$$

Stresses on the rear area in the double notched cogging joint:

$$\sigma_{2.b.c.\alpha.d} := \frac{N_{Ed} \cdot (1 - s_{2dist}) \cdot \cos(\theta_{bridge})}{b_{ef} \cdot l_{2.f}} = -3.049 \cdot \text{MPa}$$

The required end distance to assure enough shear strength.

$$l_{2,h,eff} := \frac{|N_{Ed}| \cdot \cos(\theta_{bridge})}{b_{ef} \cdot f_{v,d}} = 391.255 \cdot \text{mm}$$

$$\tau_{2,Ed} := \frac{N_{Ed} \cdot \cos(\theta_{bridge})}{b_{ef} \cdot l_{2,h}} = -2.15 \cdot \text{MPa}$$

The tensile stresses in the laminated beam due to reduce cross-section:

$$\sigma_{2,t,0,d} := \frac{\sigma_{2,t,0,d} \cdot w_{LM} \cdot h_{LM}}{(h_{LM} - l_{2,f}) \cdot w_{LM}} = 2.719 \cdot \text{MPa} \quad \text{where:} \quad \begin{aligned} \sigma_{2,t,0,d} &= 2.025 \cdot \text{MPa} \\ w_{LM} &= 0.2 \text{ m} \\ h_{LM} &= 0.4 \text{ m} \end{aligned}$$

Compare to unreduced cross-section

$$\sigma_{2,t,0,d} = 2.025 \cdot \text{MPa}$$



Design strength depending on the joint design



Compression in an angle to the grain (20 deg) for both the laminated beam and the inclined end post

$$f_{2,a.c,\varphi,d} := \frac{f_{c,0,d}}{\frac{f_{c,0,d}}{k_{c,90} \cdot f_{c,90,d}} \cdot (\sin(\varphi_2))^2 + (\cos(\varphi_2))^2} = 7.352 \cdot \text{MPa}$$

Compression in an angle to the grain (40 deg) for both the laminated beam and the inclined end post:

$$f_{2,b.c.\phi,d} := \frac{f_{c,0,d}}{\frac{f_{c,0,d}}{k_{c,90} \cdot f_{c,90,d}} \cdot (\sin(\phi_2))^2 + (\cos(\phi_2))^2} = 3.898 \cdot \text{MPa}$$

$$l_{2,e.req} := \frac{|N_{Ed}| \cdot s_{2dist} \cdot \cos\left(\frac{\theta_{bridge}}{2}\right)^2}{b_{ef} \cdot f_{2,a.c.\phi,d}} = 0.079 \text{ m}$$

Calculate the required notch depth from required:

$$l_{2,e.req} \leq \min(l_{2,f} - 10\text{mm}, 0.8 \cdot l_{2,f}) = 1$$

The design criteria from STEP 1 is fulfilled, the shear planes do not coincide.



RESULTS



Inclined end post

Compression in an angle ($\phi_2=20\text{deg}$) to the grain:

Surface a:

$$\sigma_{2,a.c.\alpha,d} = -7.226 \cdot \text{MPa}$$

$$f_{2,a.c.\phi,d} = 7.352 \cdot \text{MPa}$$

$$|\sigma_{2,a.c.\alpha,d}| \leq f_{2,a.c.\phi,d} = 1$$

Utilization rate:

$$\frac{|\sigma_{2.a.c.\alpha.d}|}{f_{2.a.c.\varphi.d}} = 0.983$$

Compression parallel to the grain :

Surface b:

$$\sigma_{2.b.c.\alpha.d} = -3.049 \cdot \text{MPa}$$

$$|\sigma_{2.b.c.\alpha.d}| \leq f_{c.0.d} = 1$$

$$f_{c.0.d} = 11.308 \cdot \text{MPa}$$

$$\frac{|\sigma_{2.b.c.\alpha.d}|}{f_{c.0.d}} = 0.27$$

Utilization rate:

Laminated beam

Compression in an angle ($\varphi=20\text{deg}$) to the grain:

Surface a:

$$\sigma_{2.a.c.\alpha.d} = -7.226 \cdot \text{MPa}$$

$$|\sigma_{2.a.c.\alpha.d}| \leq f_{2.a.c.\varphi.d} = 1$$

$$f_{2.a.c.\varphi.d} = 7.352 \cdot \text{MPa}$$

$$\frac{|\sigma_{2.a.c.\alpha.d}|}{f_{2.a.c.\varphi.d}} = 0.983$$

Utilization rate:

Compression in an angle ($\varphi=40\text{deg}$) to the grain:

Surface b:

$$\sigma_{2.b.c.\alpha.d} = -3.049 \cdot \text{MPa}$$

$$|\sigma_{2.b.c.\alpha.d}| \leq f_{2.b.c.\varphi.d} = 1$$

$$f_{2,b.c.\phi,d} = 3.898 \cdot \text{MPa}$$

Utilization rate:

$$\frac{|\sigma_{2,b.c.\alpha,d}|}{f_{2,b.c.\phi,d}} = 0.782$$

Shear parallel to the grain in one shear plane (the rear):

$$\tau_{2,Ed} = -2.15 \cdot \text{MPa}$$

$$f_{v,d} = 2.154 \cdot \text{MPa}$$

Utilization rate:

$$|\tau_{2,Ed}| \leq f_{v,d} = 1$$

$$\frac{|\tau_{2,Ed}|}{f_{v,d}} = 0.998$$

Tension parallel to the grain:

$$\sigma_{2,2t,0,d} = 2.719 \cdot \text{MPa}$$

$$f_{t,0,d} = 7.538 \cdot \text{MPa}$$

Utilization rate:

$$|\sigma_{2,2t,0,d}| \leq f_{t,0,d} = 1$$

$$\frac{\sigma_{2,2t,0,d}}{f_{t,0,d}} = 0.361$$

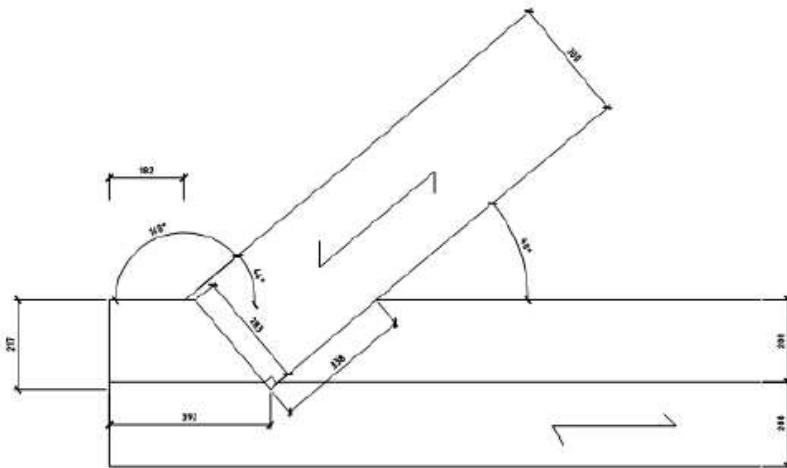


JOINT C

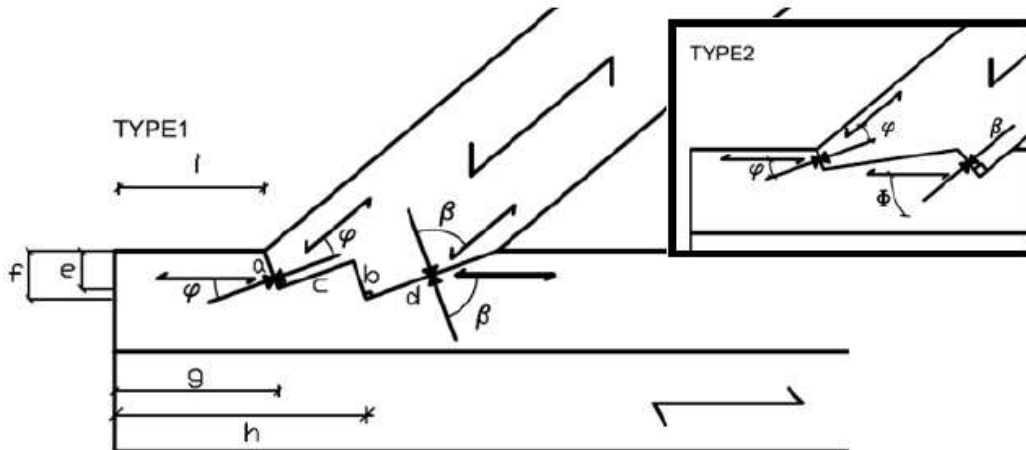
Geometry



Drawing of Joint C:



Principle sketch showing notations:



Lengths of loaded surfaces:

$$l_{2b} := 283\text{mm}$$

$$l_{2f} := 217\text{mm}$$

$$l_{2,h} := 392\text{mm}$$

$$l_{2,i} := 182\text{mm}$$

Distance from edge to abutment:

Angle between the stress and the grains in the inclined end post and the laminated beam at surface b:

$$\beta_2 := 0\text{deg} \quad \text{inclined end post}$$

$$\phi_2 := 40\text{deg} \quad \text{laminated beam}$$

Angles for surface c are neglected due to that the bearing-capacity of this surface is neglected



Load effect



Load:

$$N_{Ed} = -220.014 \text{ kN} \quad \text{Design load for the strut}$$

$$\sigma_{2t,0,d} = 2.025 \times 10^6 \text{ Pa} \quad \text{Design stress for the laminated beam}$$

Only the front areas of the cogging joint needs to be taken into account.

$$b_{ef} := w_{strut} = 0.2\text{m}$$

Stresses for a single notched cogging joint with a rear notched area:

$$\sigma_{2,b,c,\alpha,d} := \frac{N_{Ed} \cdot \cos(\theta_{bridge})}{b_{ef} \cdot l_{2,f}} = -3.883 \cdot \text{MPa}$$

$$f_{2,b,c,\phi,d} := \frac{f_{c,0,d}}{\frac{f_{c,0,d}}{k_{c,90} \cdot f_{c,90,d}} \cdot (\sin(\phi_2))^2 + (\cos(\phi_2))^2} = 3.898 \cdot \text{MPa}$$

$$l_{3.f.req} := \frac{|N_{Ed}| \cdot \cos(\theta_{bridge})}{b_{ef} \cdot f_{2.b.c.\phi.d}} = 216.167 \cdot \text{mm}$$

The required end distance to assure enough shear strength.

$$l_{2.h.eff} := \frac{|N_{Ed}| \cdot \cos(\theta_{bridge})}{b_{ef} \cdot f_{v.d}} = 391.255 \cdot \text{mm}$$

$$\tau_{2.Ed} := \frac{N_{Ed} \cdot \cos(\theta_{bridge})}{b_{ef} \cdot l_{2.h}} = -2.15 \cdot \text{MPa}$$

The tensile stresses in the laminated beam due to reduce cross-section:

$$\sigma_{2.t.0.d} := \frac{\sigma_{2t.0.d} \cdot w_{LM} \cdot h_{LM}}{(h_{LM} - l_{2.f}) \cdot w_{LM}} = 4.427 \cdot \text{MPa} \quad \text{where:} \quad \begin{aligned} \sigma_{2t.0.d} &= 2.025 \cdot \text{MPa} \\ w_{LM} &= 0.2 \text{ m} \\ h_{LM} &= 0.4 \text{ m} \end{aligned}$$

Compare to unreduced cross-section

$$\sigma_{2t.0.d} = 2.025 \cdot \text{MPa}$$



Design strength depending on the joint design



Compression in an angle to the grain (40 deg) for both the laminated beam and the inclined end post:

$$f_{2,b,c,\phi,d} := \frac{f_{c,0,d}}{\frac{f_{c,0,d}}{k_{c,90} \cdot f_{c,90,d}} \cdot (\sin(\phi_2))^2 + (\cos(\phi_2))^2} = 3.898 \cdot \text{MPa}$$



RESULTS



Inclined end post

Compression parallel to the grain :

Surface b:

$$\sigma_{2,b,c,\alpha,d} = -3.883 \cdot \text{MPa}$$

$$|\sigma_{2,b,c,\alpha,d}| \leq f_{c,0,d} = 1$$

$$f_{c,0,d} = 11.308 \cdot \text{MPa}$$

$$\frac{|\sigma_{2,b,c,\alpha,d}|}{f_{c,0,d}} = 0.343$$

Utilization rate:

Laminated beam

Compression in an angle ($\phi_2=40\text{deg}$) to the grain:

Surface b:

$$\sigma_{2,b,c,\alpha,d} = -3.883 \cdot \text{MPa}$$

$$|\sigma_{2,b,c,\alpha,d}| \leq f_{2,b,c,\phi,d} = 1$$

$$f_{2,b,c,\phi,d} = 3.898 \cdot \text{MPa}$$

$$\frac{|\sigma_{2,b,c,\alpha,d}|}{f_{2,b,c,\phi,d}} = 0.996$$

Utilization rate:

Shear parallel to the grain in one shear plane (the rear):

$$\tau_{2.Ed} = -2.15 \cdot \text{MPa}$$

$$f_{v,d} = 2.154 \cdot \text{MPa}$$

Utilization rate:

$$|\tau_{2.Ed}| \leq f_{v,d} = 1$$

$$\frac{|\tau_{2.Ed}|}{f_{v,d}} = 0.998$$

$$l_{2,i} = 0.182 \text{ m}$$

Tension parallell to the grain:

$$\sigma_{2.2t.0,d} = 4.427 \cdot \text{MPa}$$

$$f_{t.0,d} = 7.538 \cdot \text{MPa}$$

Utilization rate:

$$|\sigma_{2.2t.0,d}| \leq f_{t.0,d} = 1$$

$$\frac{\sigma_{2.2t.0,d}}{f_{t.0,d}} = 0.587$$

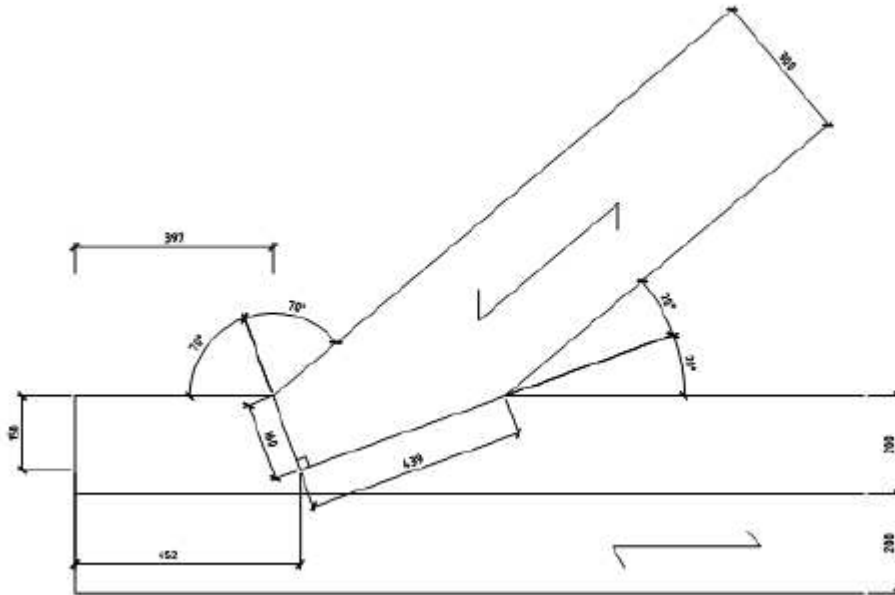


JOINT D

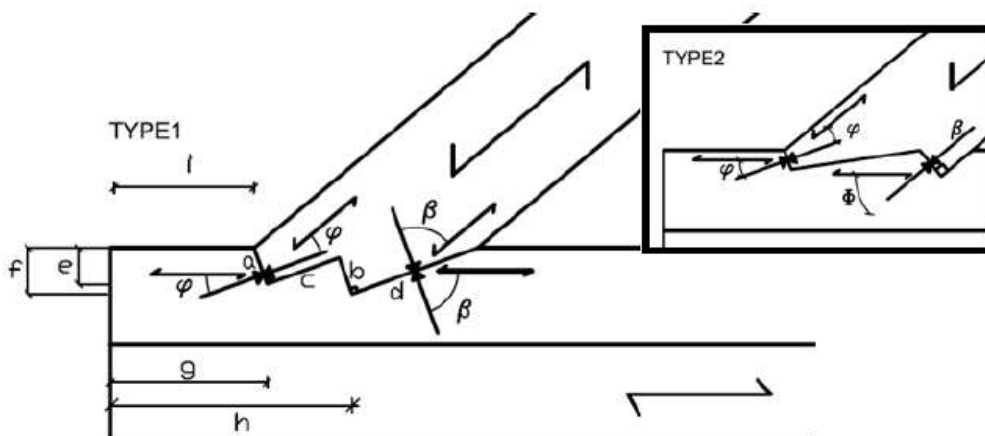
Geometry



Drawing of Joint D:



Principle sketch showing notations:



$$\theta_{\text{bridge}} \leq 60\text{deg} = 1$$

According to Limträhanboken there is no need for limitation in the depth of the strut.

Lengths of loaded surfaces:

$$l_{1,a} := 160\text{mm}$$

$$l_{1,c} := 439\text{mm}$$

$$l_{1,f} := 150\text{mm}$$

$$l_{1,h} := 452\text{mm}$$

$$l_{1,i} := 397\text{mm} \quad \text{Distance from edge to frontal surface:}$$

Controll of maximum utilization length of the shear plane:

$$s_1 := 8 \cdot l_{1,f} = 1.2 \times 10^3 \cdot \text{mm}$$

$$l_{1,h} \leq s_1 = 1 \quad \text{The length of the shear plane is lower than the maximum utilization length when calculating the shear stress. OK.}$$

Controll of the width of the strut:

$$h_{\text{strut}} \geq \left[l_{1,f} \cdot \tan\left(\frac{\theta_{\text{bridge}}}{2}\right) + (l_{1,c}) \right] \cdot \sin(\theta_{\text{bridge}}) = 0$$

$$\left[l_{1,f} \cdot \tan\left(\frac{\theta_{\text{bridge}}}{2}\right) + (l_{1,c}) \right] \cdot \sin(\theta_{\text{bridge}}) = 317.277 \cdot \text{mm}$$

$$h_{\text{strut}} = 300 \cdot \text{mm}$$

Comment : OK since very near the limit.

Angle between the stress and the grains in the inclined end post and the laminated beam:

$$\varphi_1 := 20\text{deg}$$

$$\beta_1 := 70\text{deg}$$



Load effect



Load:

$$N_{Ed} = -220.014 \cdot \text{kN}$$

Design load for the strut

$$\sigma_{2t.0.d} = 2.025 \times 10^6 \text{ Pa}$$

Design stress for the laminated beam

$$N_{1.a} := \cos\left(\frac{\theta_{\text{bridge}}}{2}\right) \cdot N_{Ed} = -206.746 \cdot \text{kN}$$

$$N_{1.c} := \sin\left(\frac{\theta_{\text{bridge}}}{2}\right) \cdot N_{Ed} = -75.249 \cdot \text{kN}$$

$$\sigma_{1.a.c.\alpha.d} := \frac{N_{1.a} \cdot \cos\left(\frac{\theta_{\text{bridge}}}{2}\right)}{w_{\text{strut}} \cdot l_{1.f}} = -6.476 \cdot \text{MPa}$$

Uniform distribution of the stresses at surface a.

The stresses at surface c are calculated in the section **Design strength depending on the joint design**.

Only $N_{1.a}$ will give rise to shear stress parallel to the grain in the end of the laminated beam. It will act at the tip of the notch.

$$\tau_{1.Ed} := \frac{N_{1.a} \cdot \cos\left(\frac{\theta_{\text{bridge}}}{2}\right)}{w_{\text{strut}} \cdot l_{1.h}} = -2.149 \cdot \text{MPa}$$

$$\sigma_{1.2t.0.d} := \frac{\sigma_{2t.0.d} \cdot w_{LM} \cdot h_{LM}}{(h_{LM} - l_{1.f}) \cdot w_{LM}} = 3.241 \cdot \text{MPa}$$

where:

$$\sigma_{2t.0.d} = 2.025 \cdot \text{MPa}$$

$$w_{LM} = 0.2 \text{ m}$$

$$h_{LM} = 0.4 \text{ m}$$

Compare to unreduced cross-section

$$\sigma_{2t.0.d} = 2.025 \cdot \text{MPa}$$



Design strength depending on the joint design



Compression in an angle to the grain (20 deg) for both the laminated beam and the inclined end post:

$$f_{1.a.c.\varphi.d} := \frac{f_{c.0.d}}{\frac{f_{c.0.d}}{k_{c.90} \cdot f_{c.90.d}} \cdot (\sin(\varphi_1))^2 + (\cos(\varphi_1))^2} = 7.352 \cdot \text{MPa}$$

$$\sigma_{1.a.c.\varphi.d} := \frac{N_{1.a} \cdot \cos\left(\frac{\theta_{\text{bridge}}}{2}\right)}{w_{\text{strut}} \cdot l_{1.f}} = -6.476 \cdot \text{MPa}$$

$$l_{1.f.req} := \frac{|N_{1.a}| \cdot \cos\left(\frac{\theta_{\text{bridge}}}{2}\right)}{w_{\text{strut}} \cdot f_{1.a.c.\varphi.d}} = 0.132 \text{ m}$$

Compression in an angle to the grain (70 deg) for both the laminated beam and the inclined end post:

$$f_{1.c.c.\beta.d} := \frac{f_{c.0.d}}{\frac{f_{c.0.d}}{k_{c.90} \cdot f_{c.90.d}} \cdot (\sin(\beta_1))^2 + (\cos(\beta_1))^2} = 2.234 \cdot \text{MPa}$$

$$l_{1.c.eff} := \frac{|N_{1.c}|}{w_{\text{strut}} \cdot f_{1.c.c.\beta.d}} = 168.427 \cdot \text{mm}$$

$$\sigma_{1.c.c.\alpha.d} := \frac{N_{1.c}}{w_{\text{strut}} \cdot (l_{1.c})} = -0.857 \cdot \text{MPa}$$

Uniform distribution of the stresses at surface c with an effective length.

$$l_{1.c.eff} \leq l_{1.c} = 1$$

Ok according to the design method. The strut has sufficient amount of area at the flatter surface to spread the load.

$$l_{1,h.req} := \frac{|N_{1,a}| \cdot \cos\left(\frac{\theta_{bridge}}{2}\right)}{w_{strut} \cdot f_{v,d}} = 0.451 \text{ m}$$

Required shear plane length!

$$l_{1,h} \geq l_{1,h.req} = 1$$



RESULTS



Inclined end

post

Compression in an angle ($\varphi_1=20\text{deg}$) to the grain:

Surface a and b:

$$\sigma_{1,a.c.\alpha.d} = -6.476 \text{ MPa}$$

$$f_{1,a.c.\varphi.d} = 7.352 \text{ MPa}$$

$$|\sigma_{1,a.c.\alpha.d}| \leq f_{1,a.c.\varphi.d} = 1$$

Utilization rate:

$$\frac{|\sigma_{1,a.c.\alpha.d}|}{f_{1,a.c.\varphi.d}} = 0.881$$

Compression in an angle ($\beta_1=70\text{deg}$) to the grain:

Surface c and d:

$$\sigma_{1,c.c.\alpha.d} = -0.857 \text{ MPa}$$

$$f_{1,c.c.\beta.d} = 2.234 \text{ MPa}$$

$$|\sigma_{1,c.c.\alpha.d}| \leq f_{1,c.c.\beta.d} = 1$$

Utilization rate:

$$\frac{|\sigma_{1,c.c.\alpha.d}|}{f_{1,c.c.\beta.d}} = 0.384$$

Laminated beam

Compression in an angle ($\varphi_1=20\text{deg}$) to the grain:

Surface a and b:

$$\sigma_{1.a.c.\alpha.d} = -6.476 \cdot \text{MPa}$$

$$f_{1.a.c.\varphi.d} = 7.352 \cdot \text{MPa}$$

$$|\sigma_{1.a.c.\alpha.d}| \leq f_{1.a.c.\varphi.d} = 1$$

Utilization rate:

$$\frac{|\sigma_{1.a.c.\alpha.d}|}{f_{1.a.c.\varphi.d}} = 0.881$$

Compression in an angle ($\beta_1=70\text{deg}$) to the grain:

Surface c and d:

$$\sigma_{1.c.c.\alpha.d} = -0.857 \cdot \text{MPa}$$

$$f_{1.c.c.\beta.d} = 2.234 \cdot \text{MPa}$$

$$|\sigma_{1.c.c.\alpha.d}| \leq f_{1.c.c.\beta.d} = 1$$

Utilization rate:

$$\frac{|\sigma_{1.c.c.\alpha.d}|}{f_{1.c.c.\beta.d}} = 0.384$$

Shear parallel to the grain in one shear plane:

$$\tau_{1.Ed} = -2.149 \cdot \text{MPa}$$

$$f_{v.d} = 2.154 \cdot \text{MPa}$$

$$|\tau_{1.Ed}| \leq f_{v.d} = 1$$

Utilization rate:

$$\frac{|\tau_{1.Ed}|}{f_{v.d}} = 0.998$$

Tension parallel to the grain:

$$\sigma_{1.2t.0.d} = 3.241 \cdot \text{MPa}$$

$$f_{t.0.d} = 7.538 \cdot \text{MPa}$$

$$|\sigma_{1.2t.0.d}| \leq f_{t.0.d} = 1$$

Utilization rate:

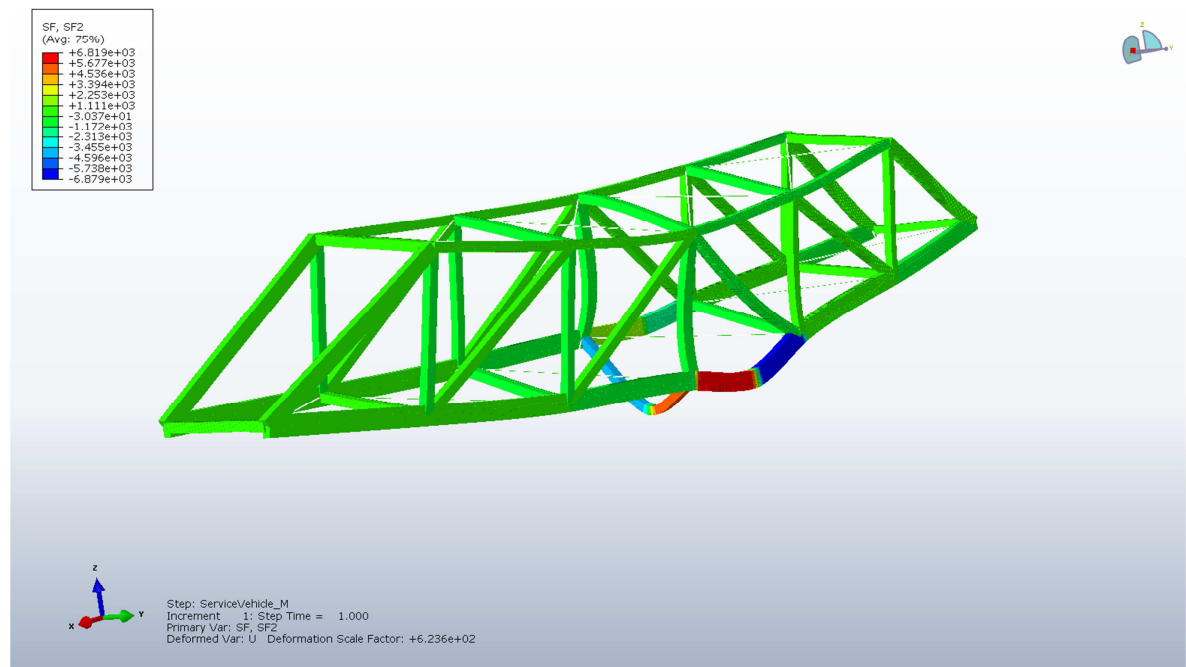
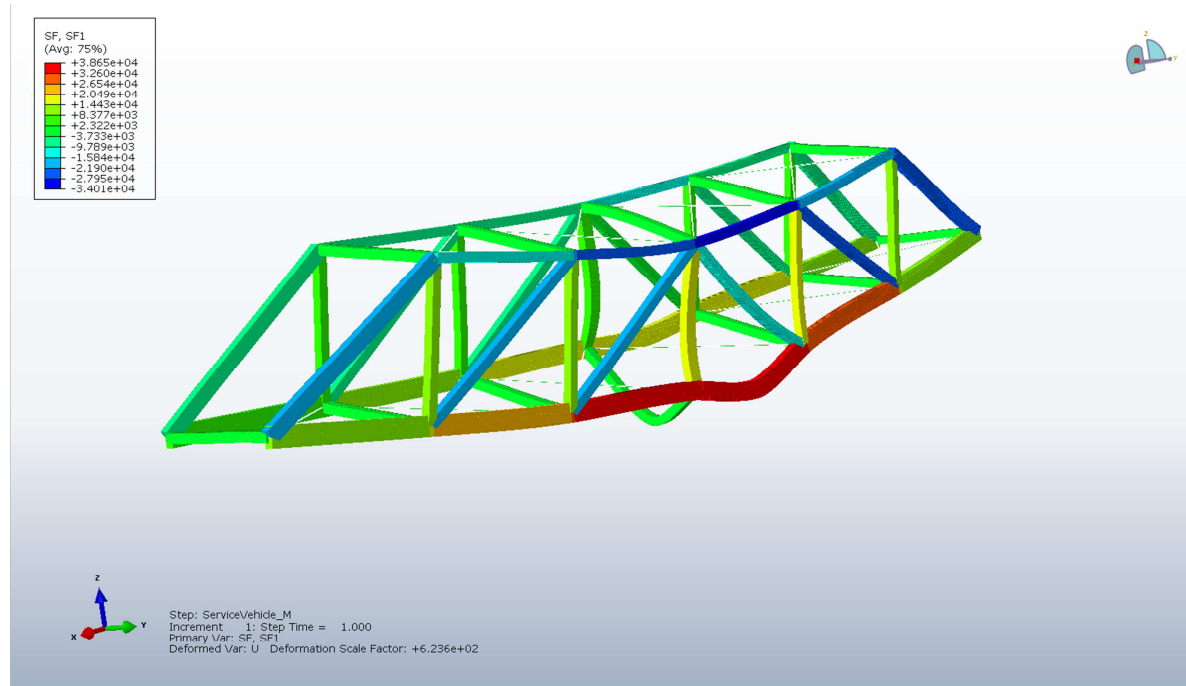
$$\frac{\sigma_{1.2t.0.d}}{f_{t.0.d}} = 0.43$$

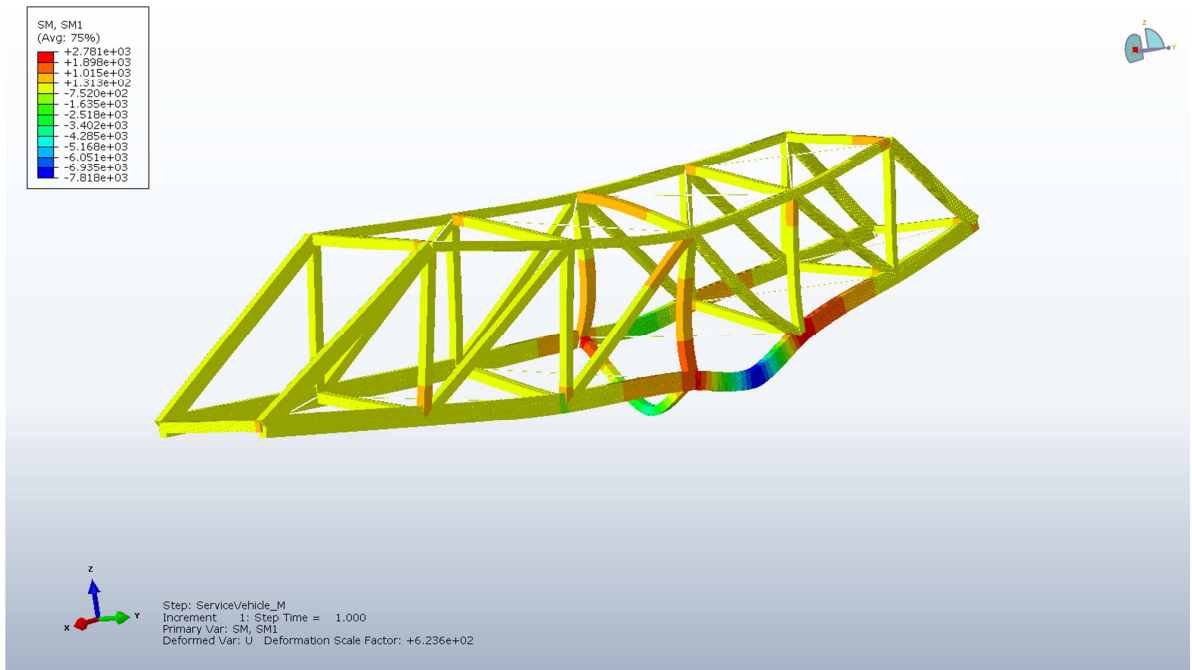
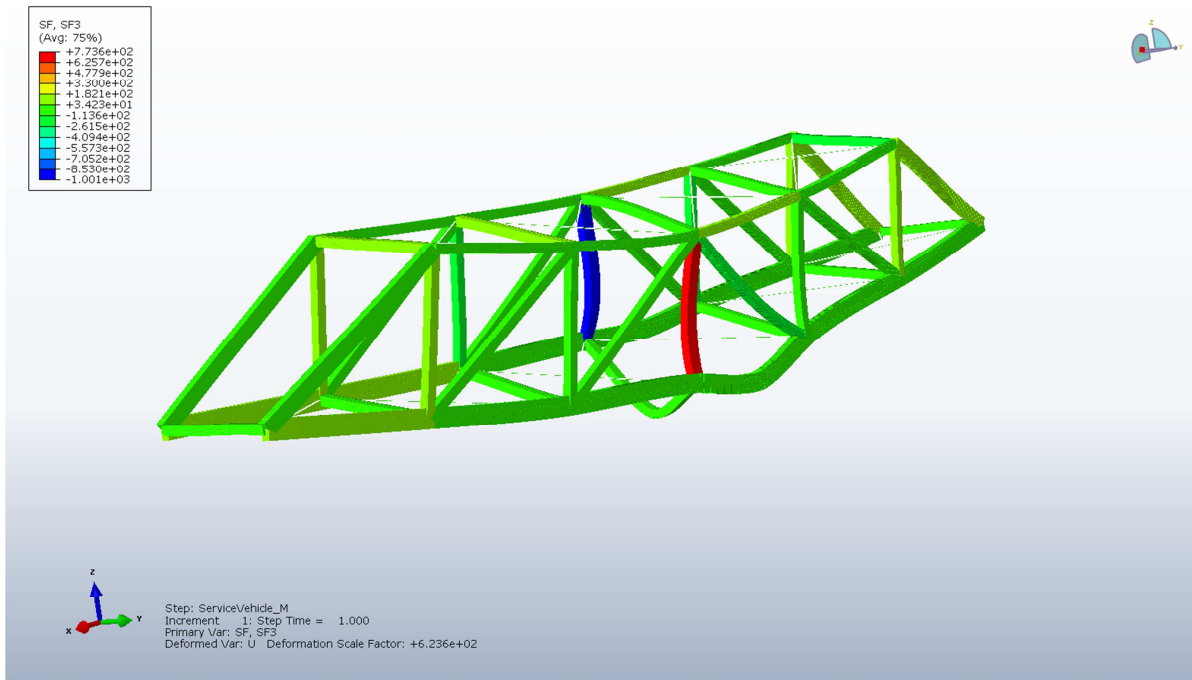


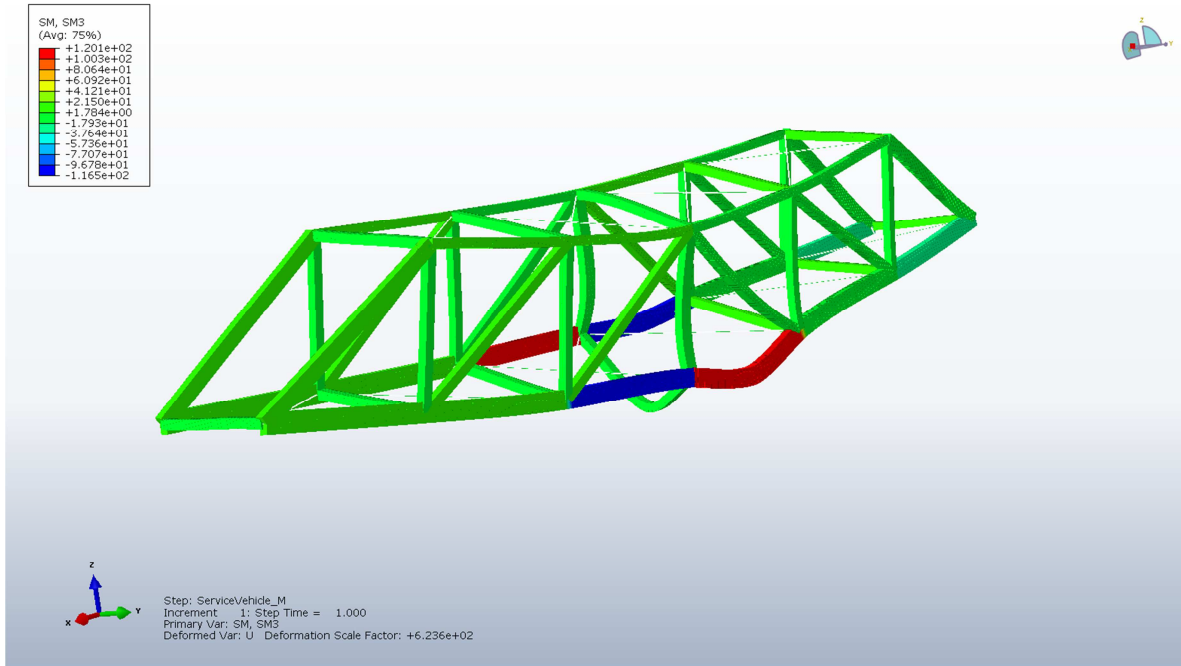
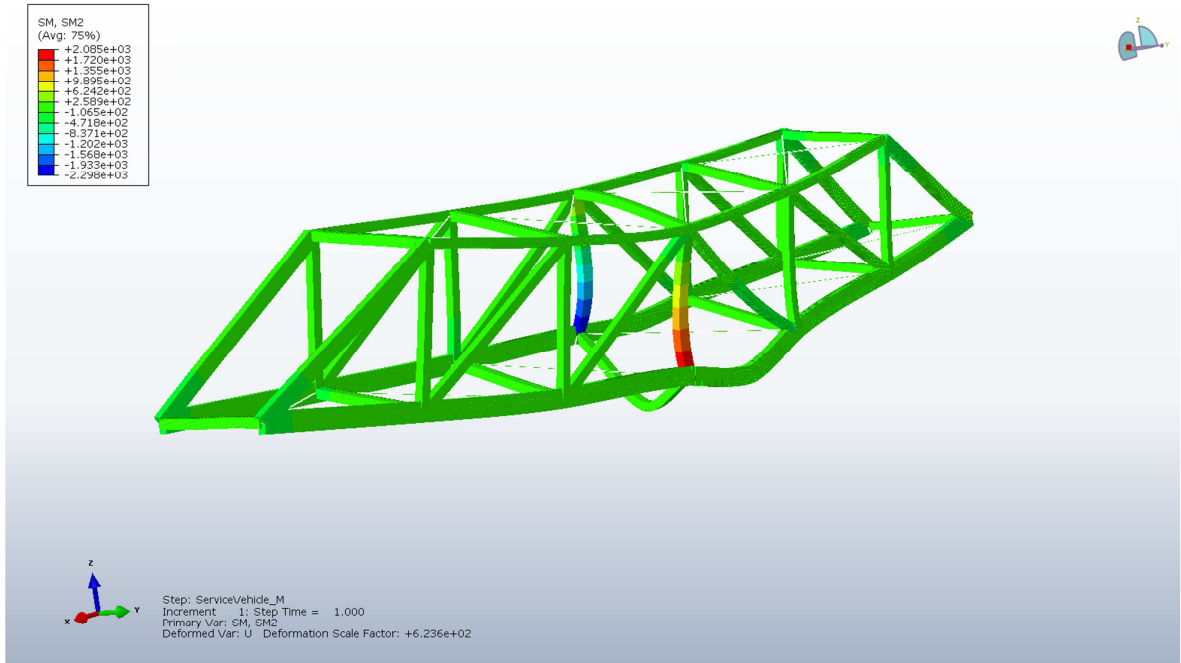
APPENDIX F – Global analysis

Obtained results from Brigade+:

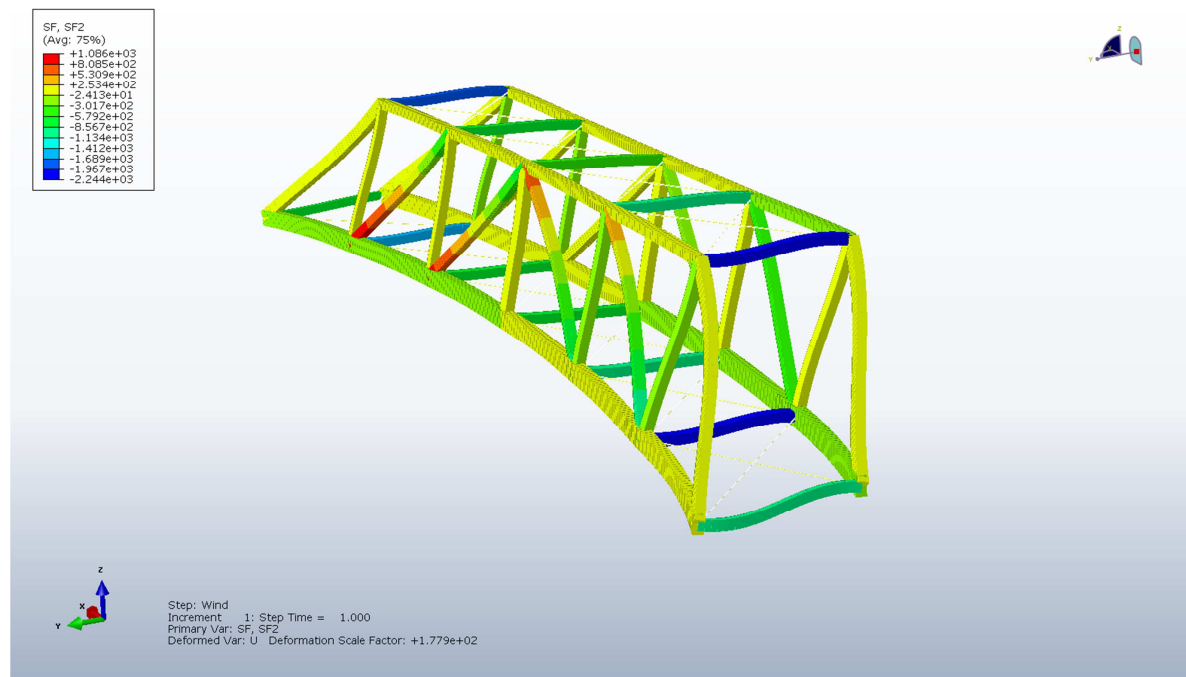
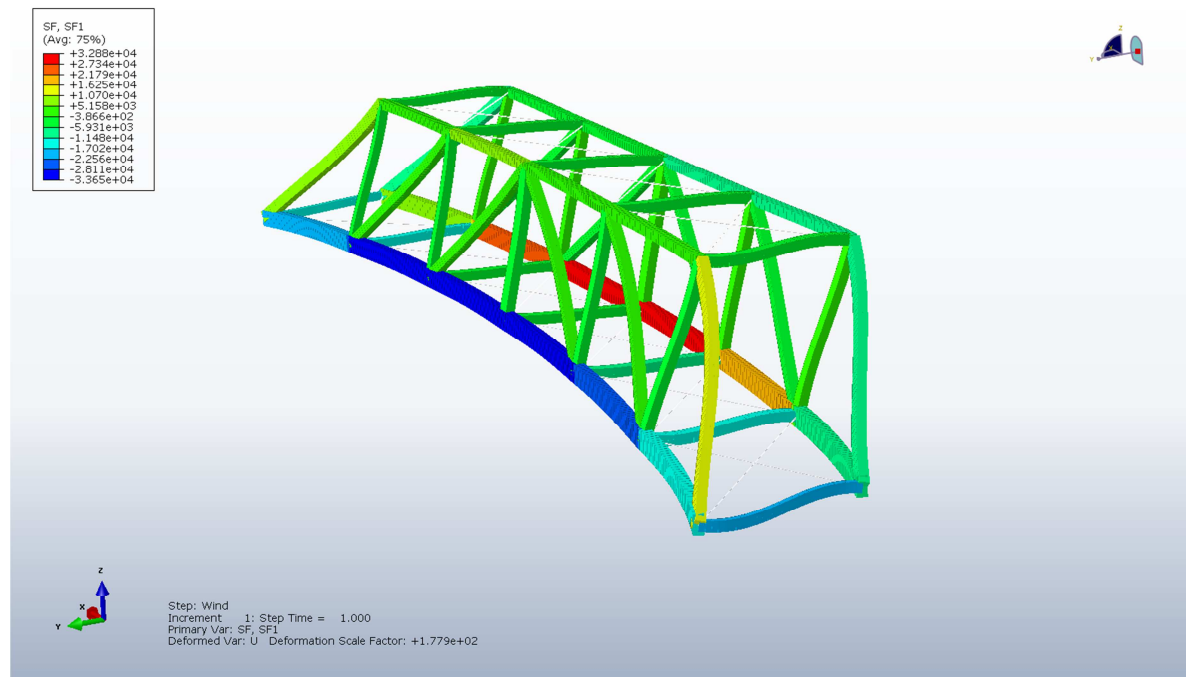
Self-weight

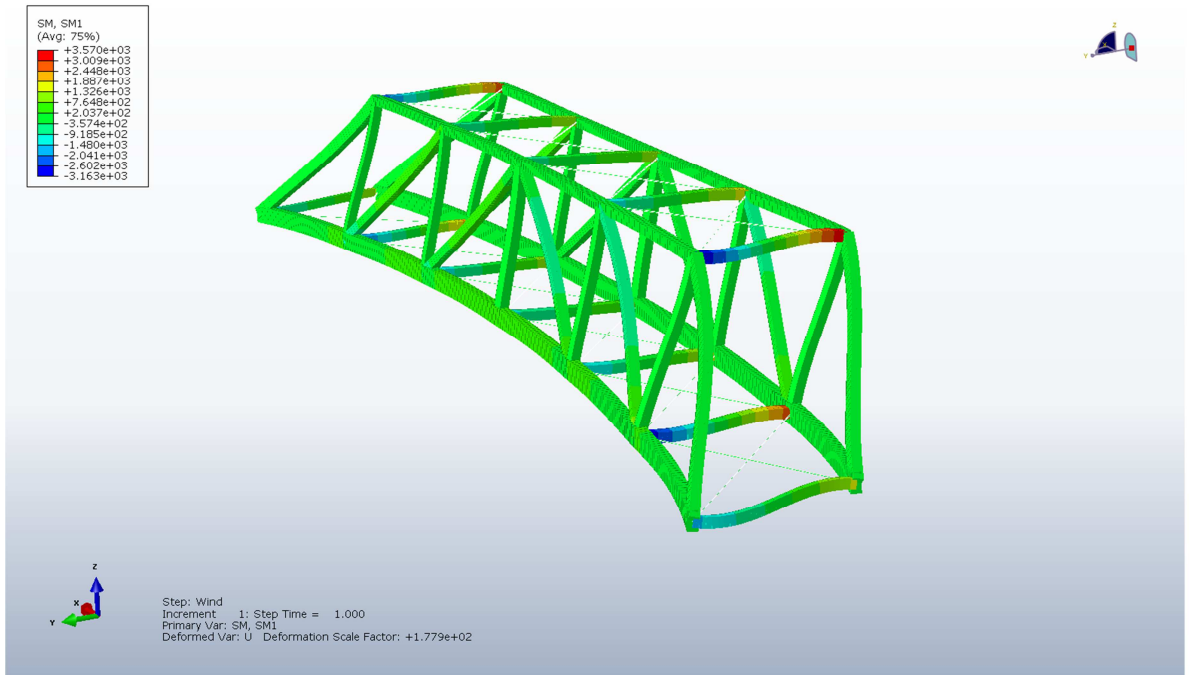
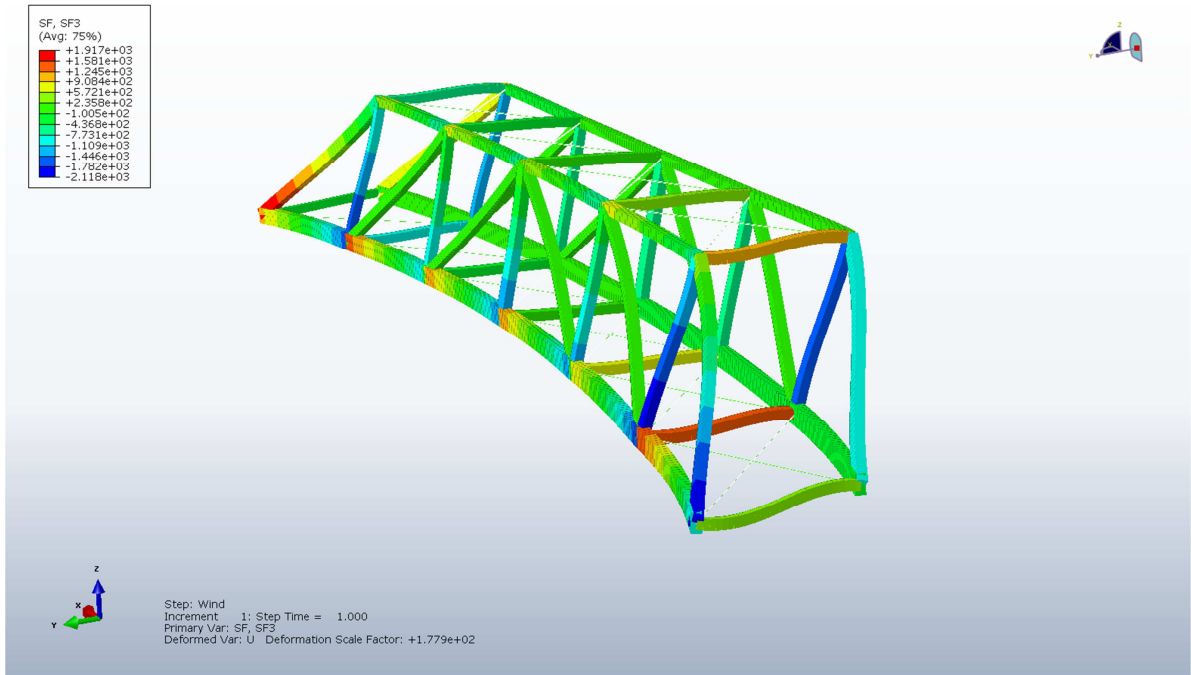


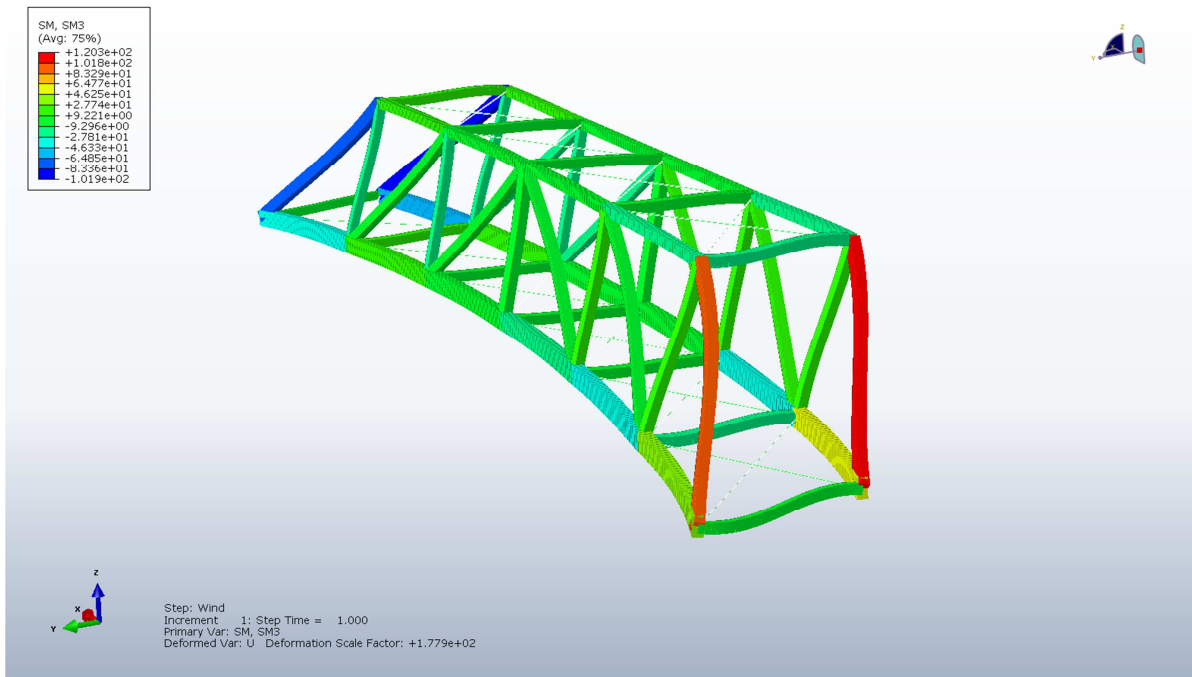
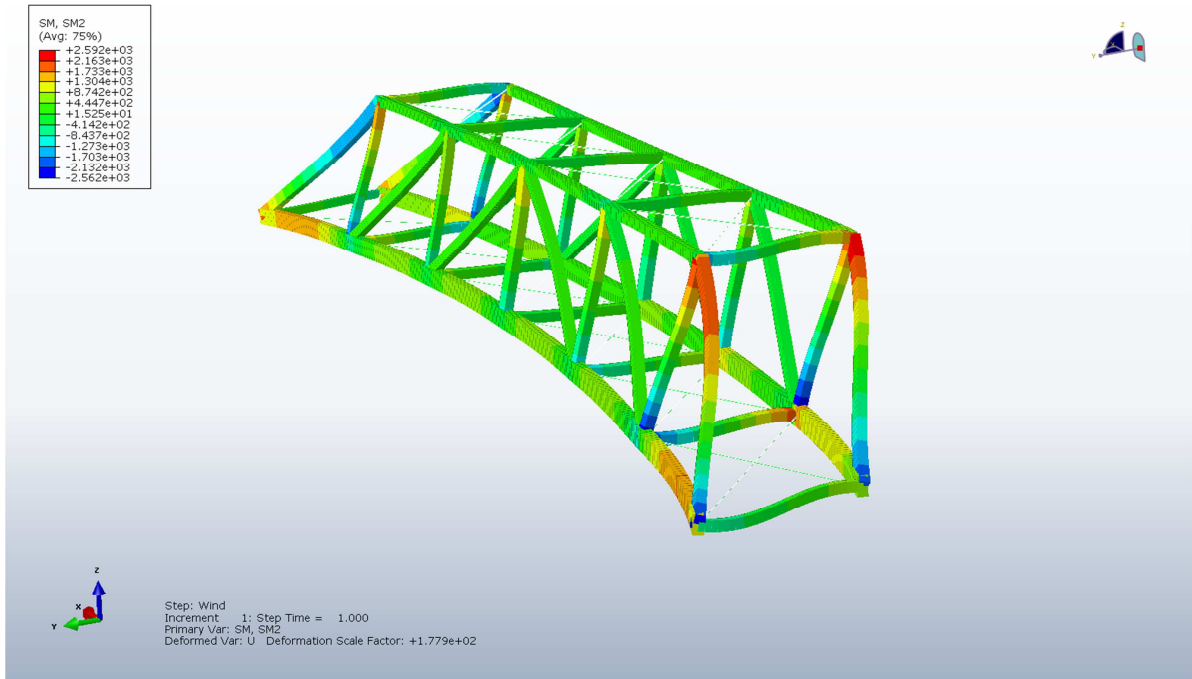




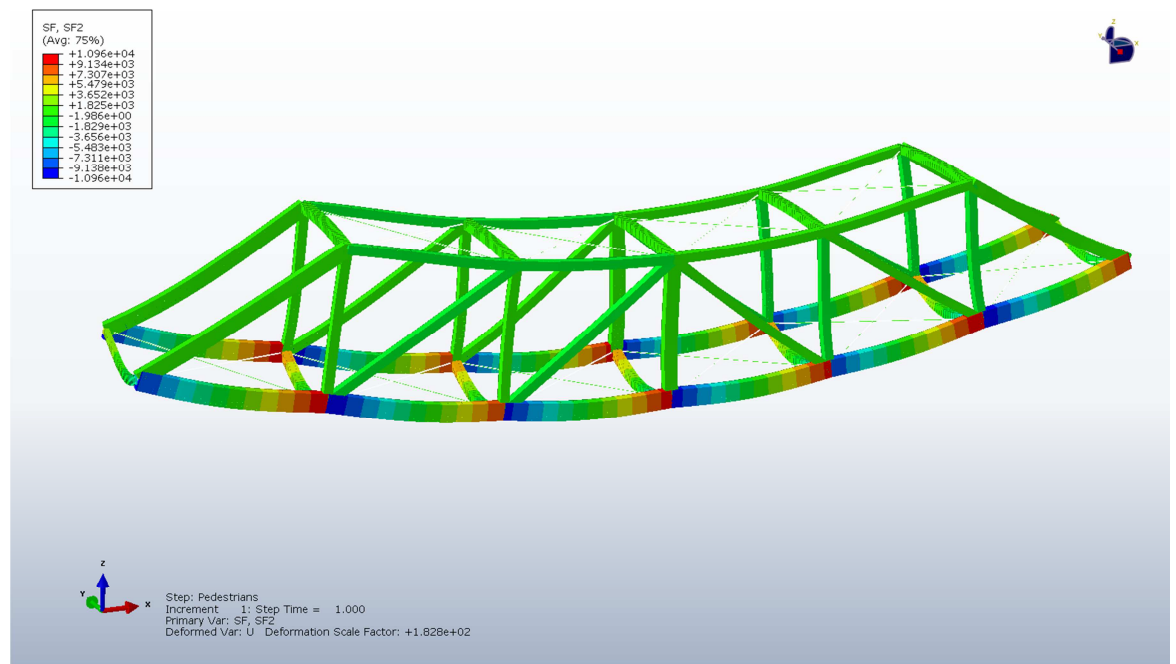
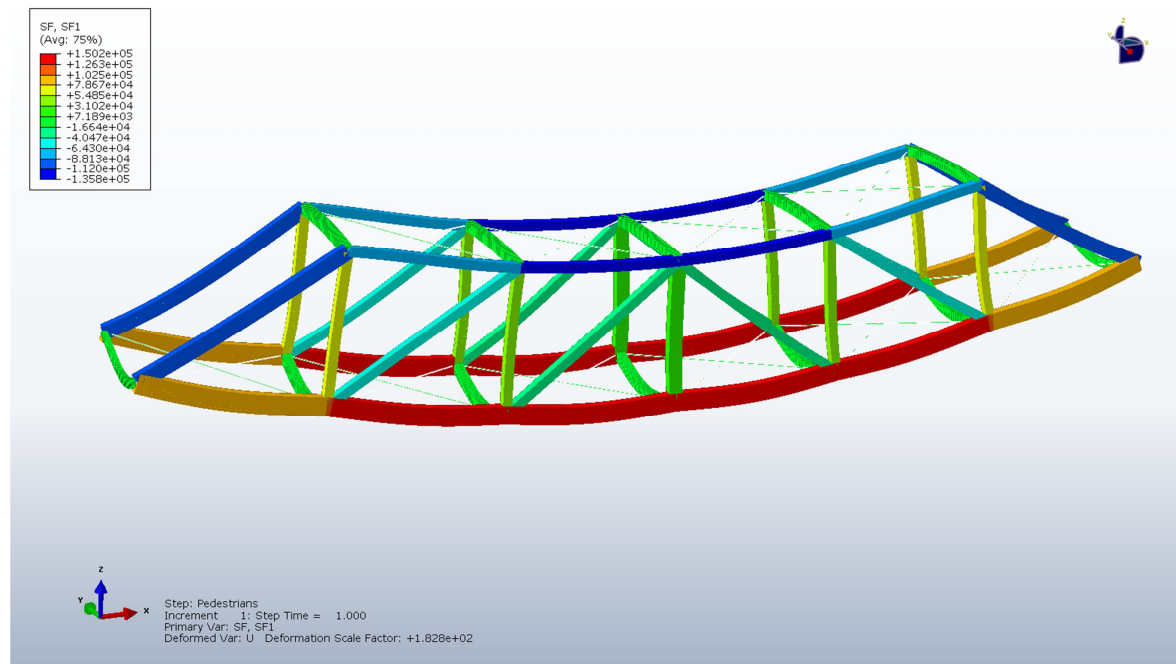
Wind

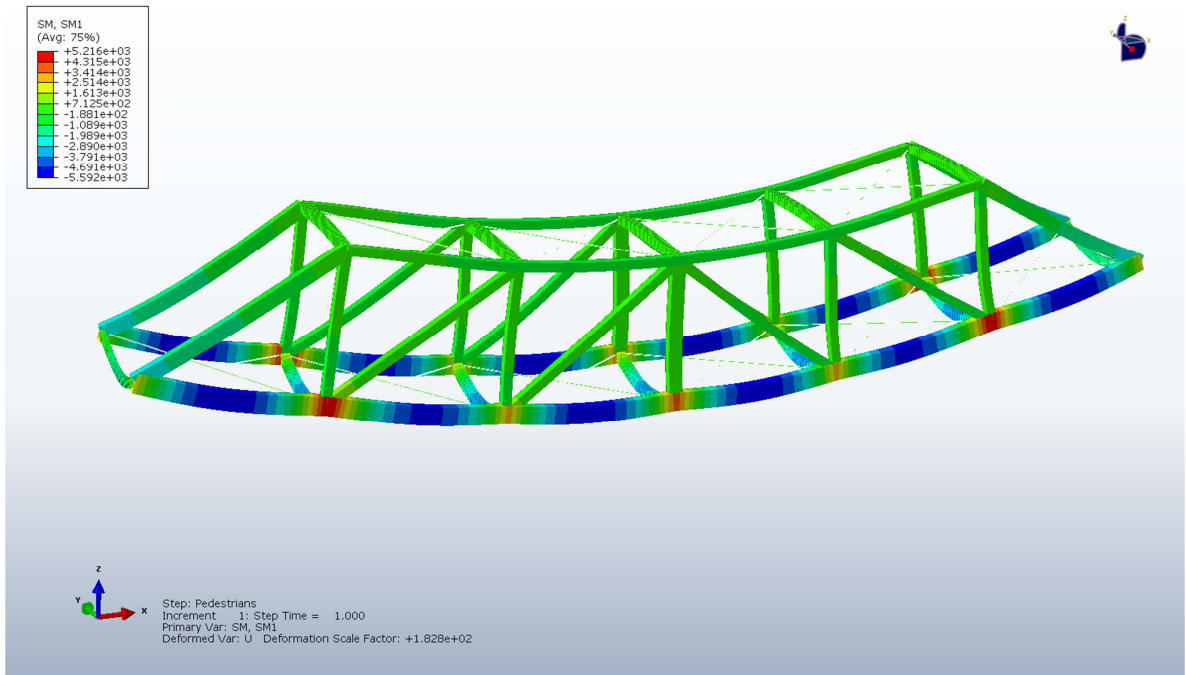
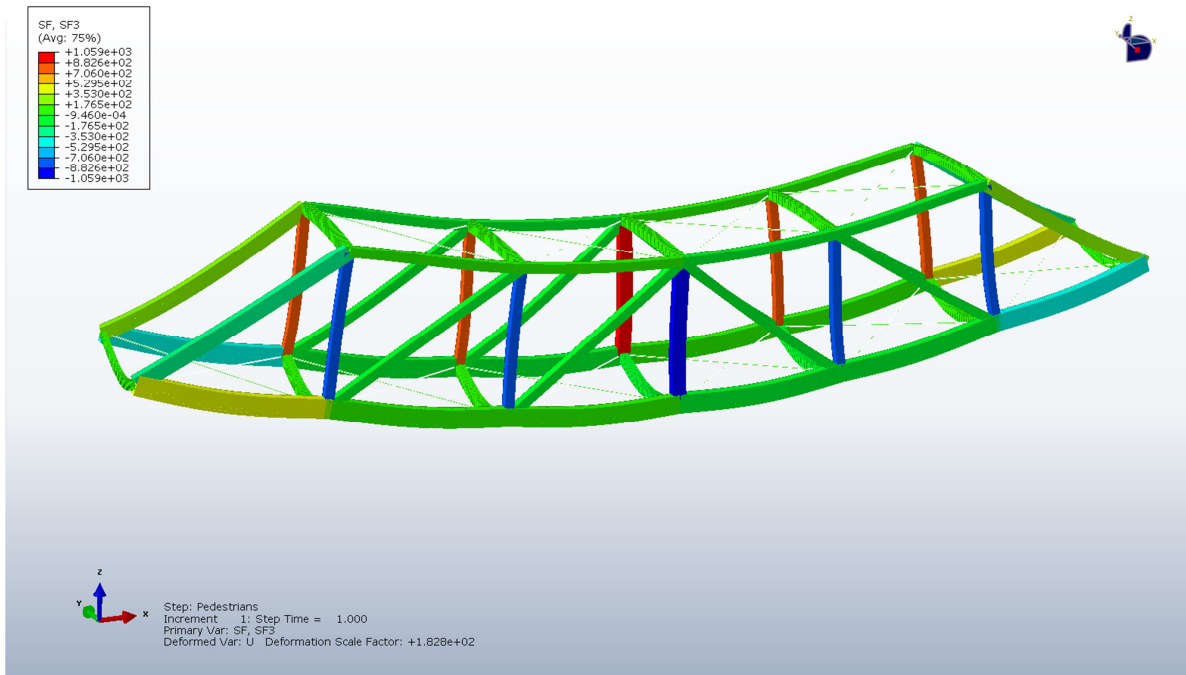


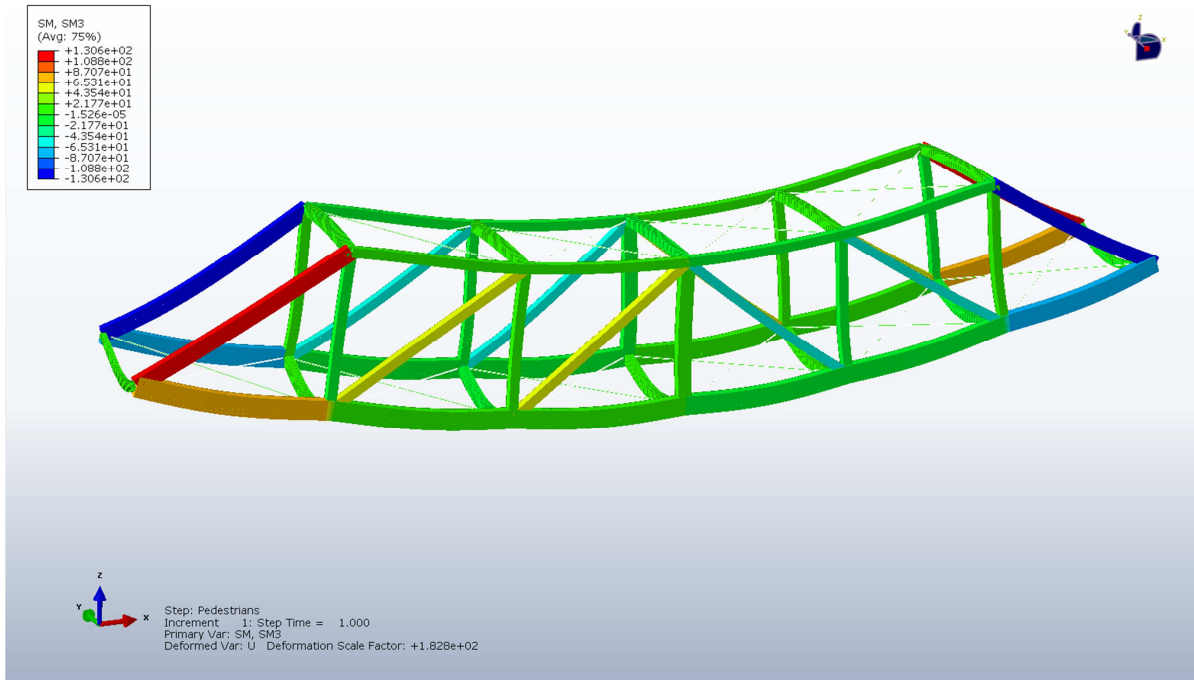
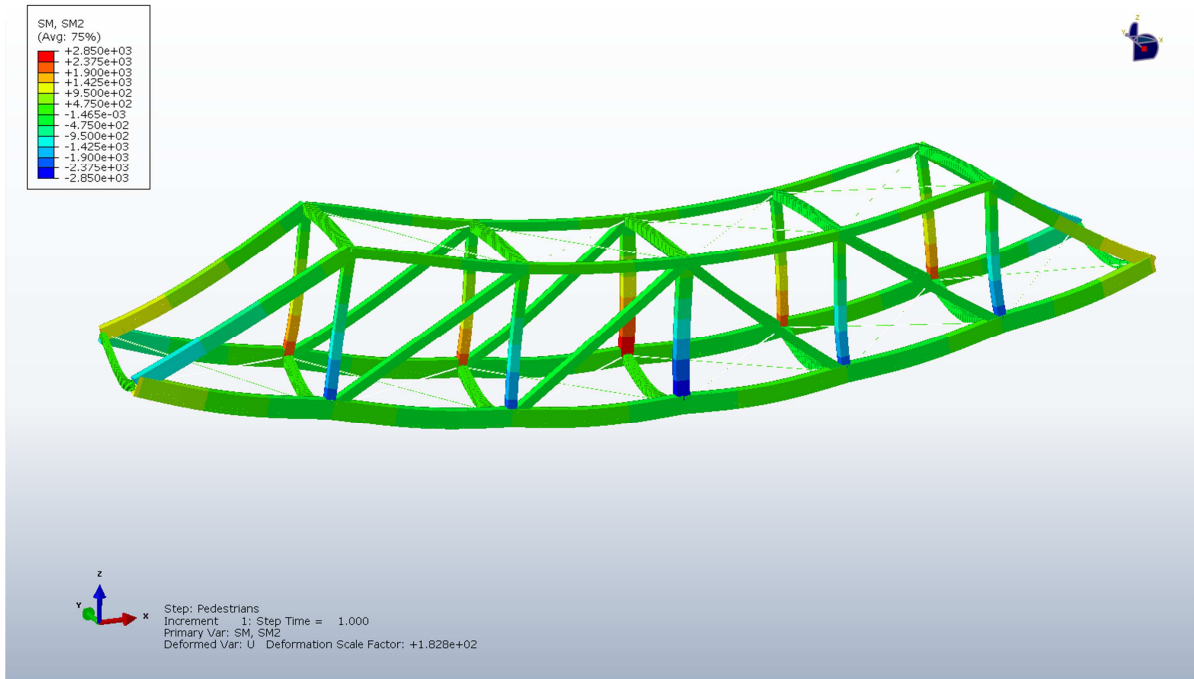




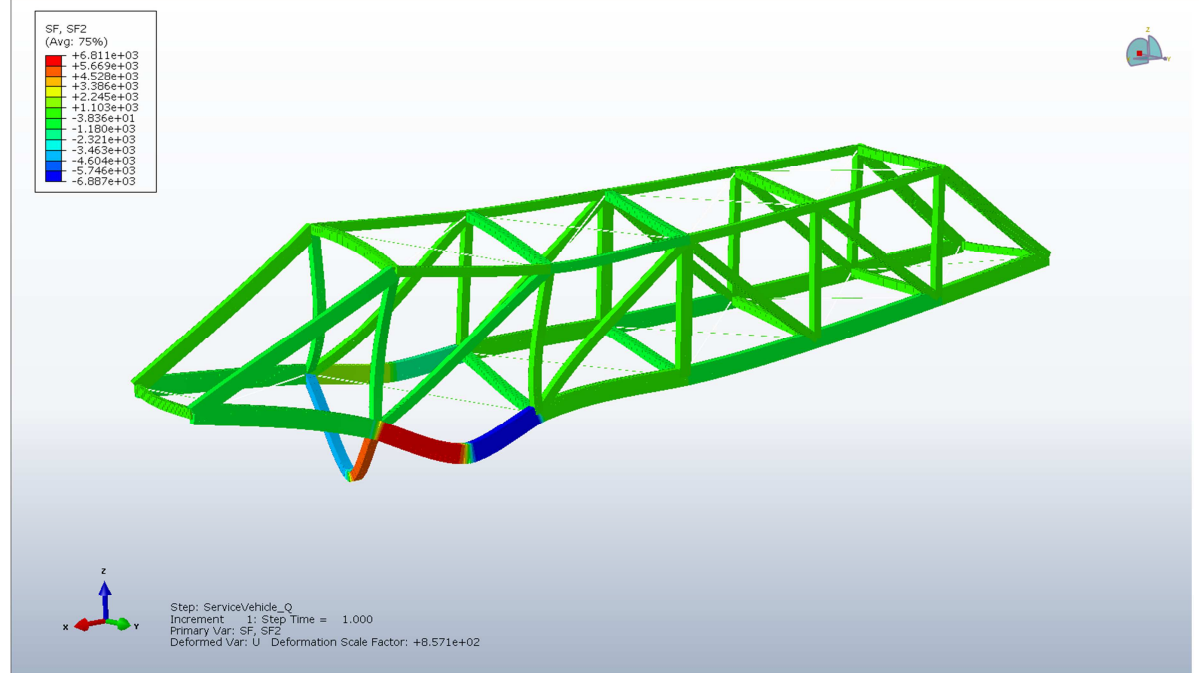
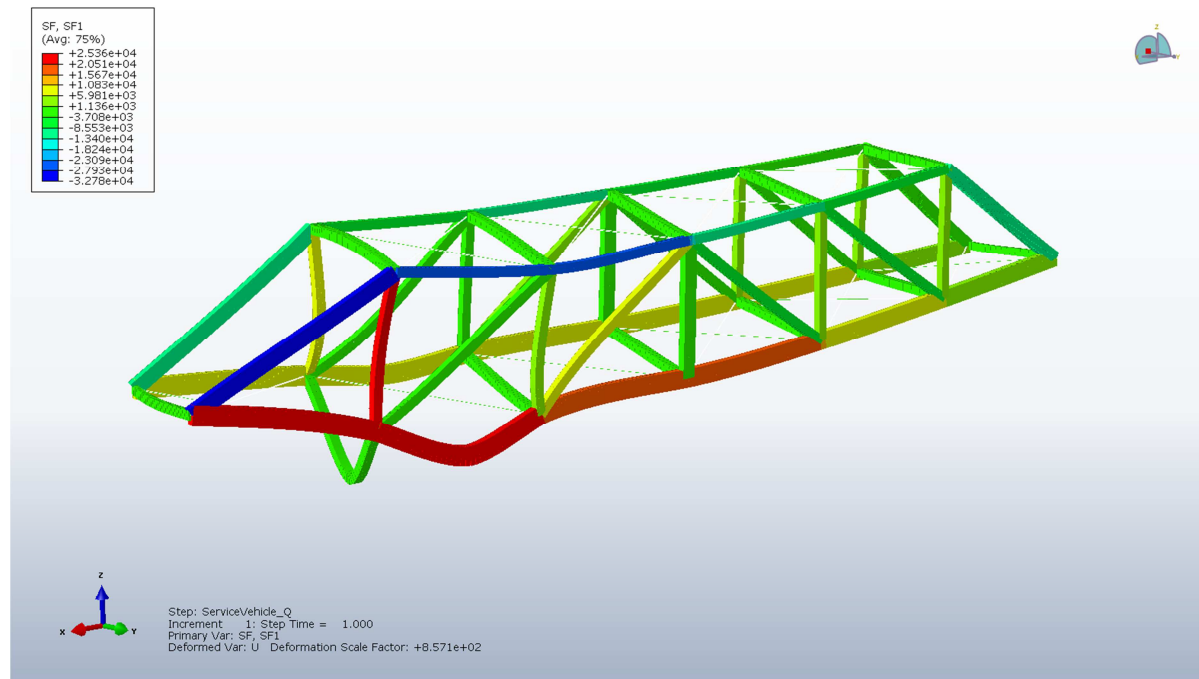
Pedestrian

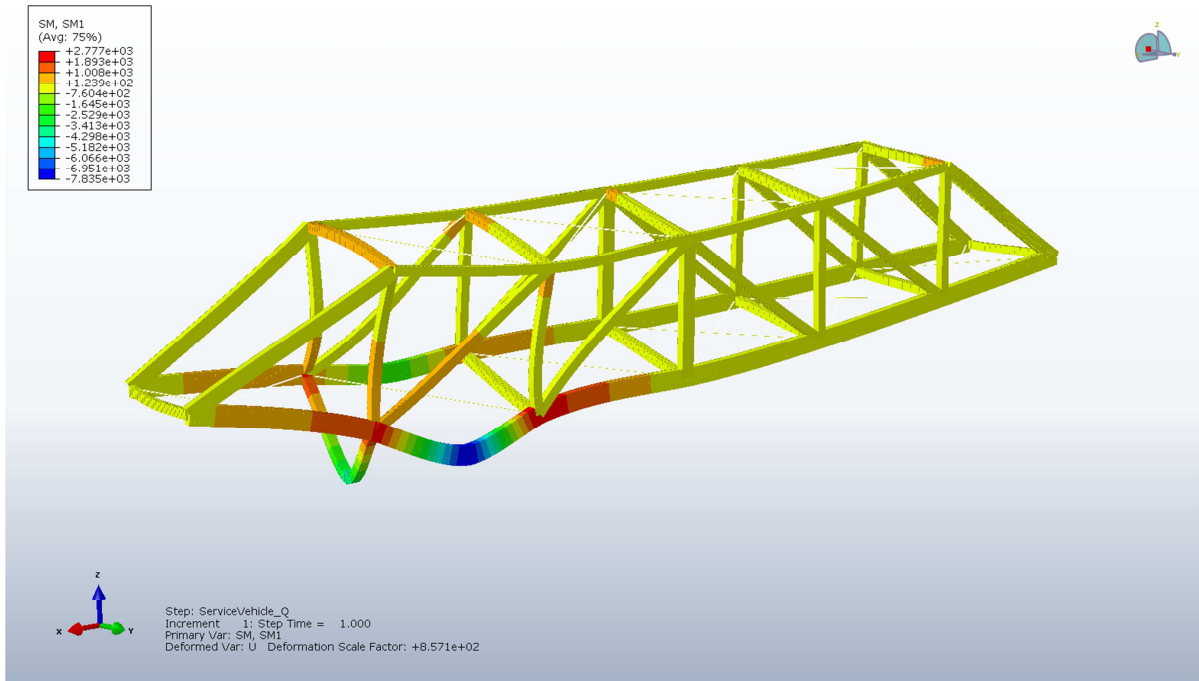
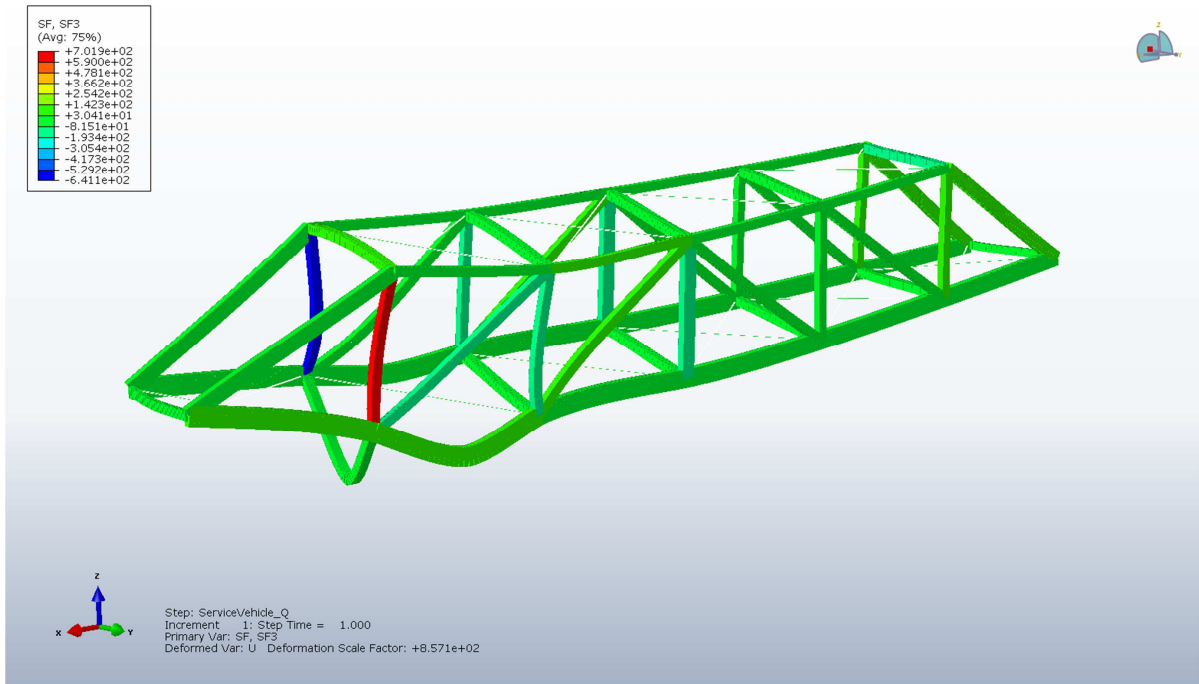


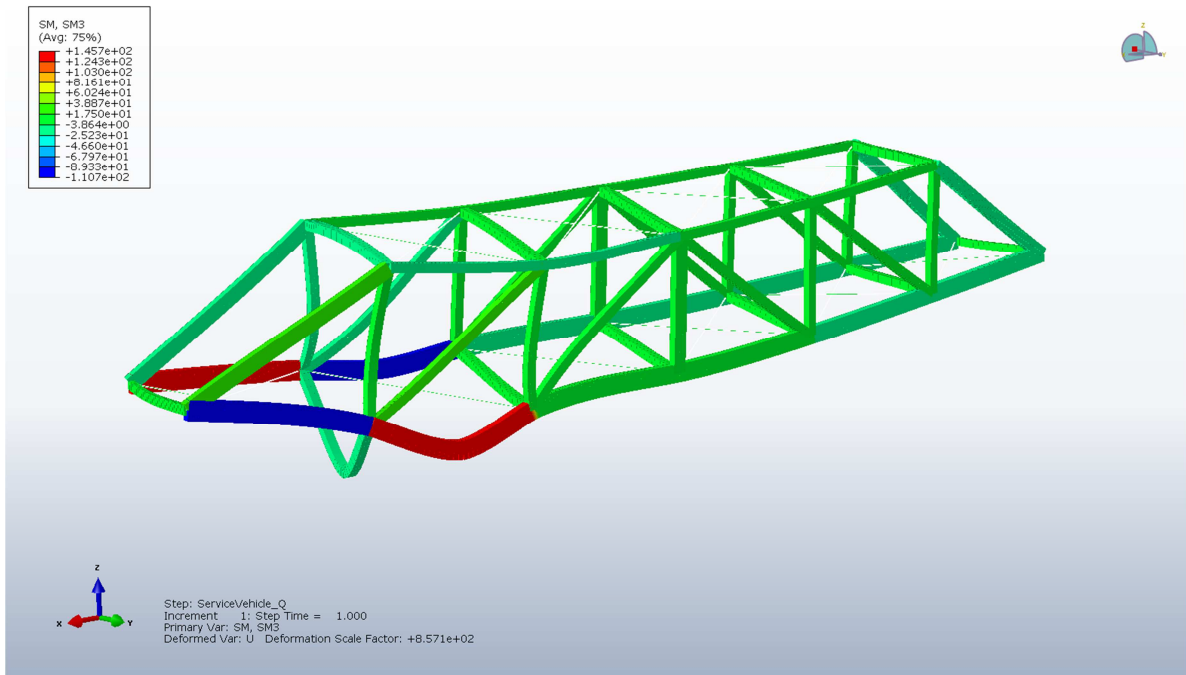
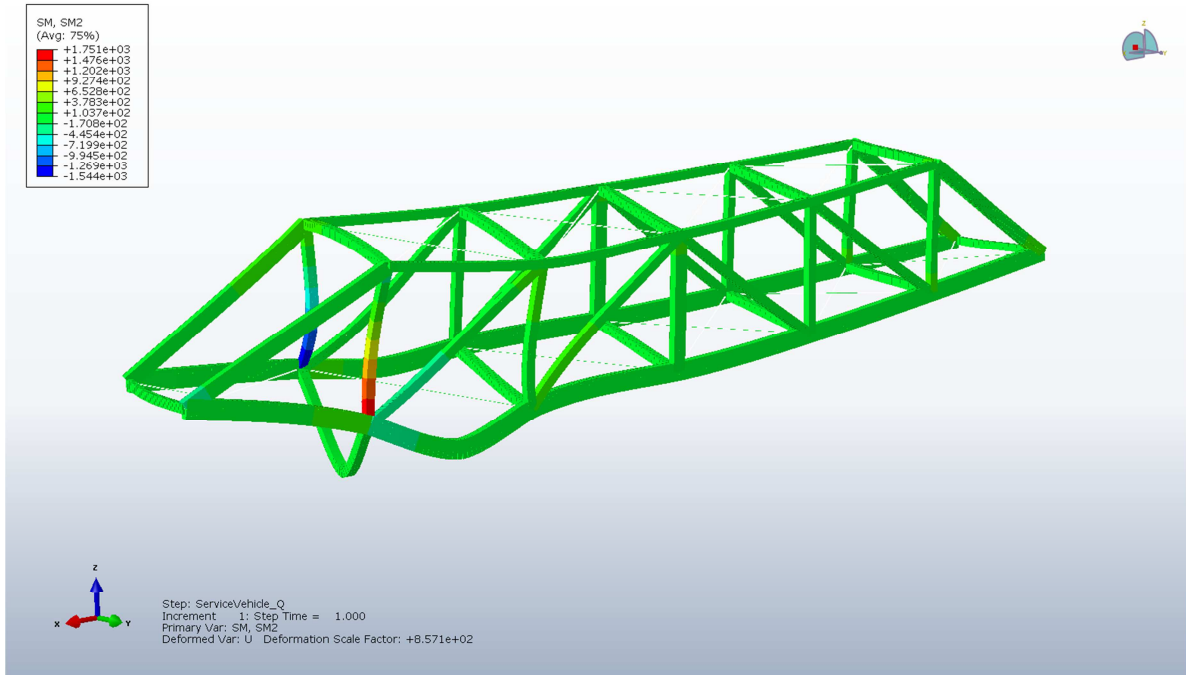




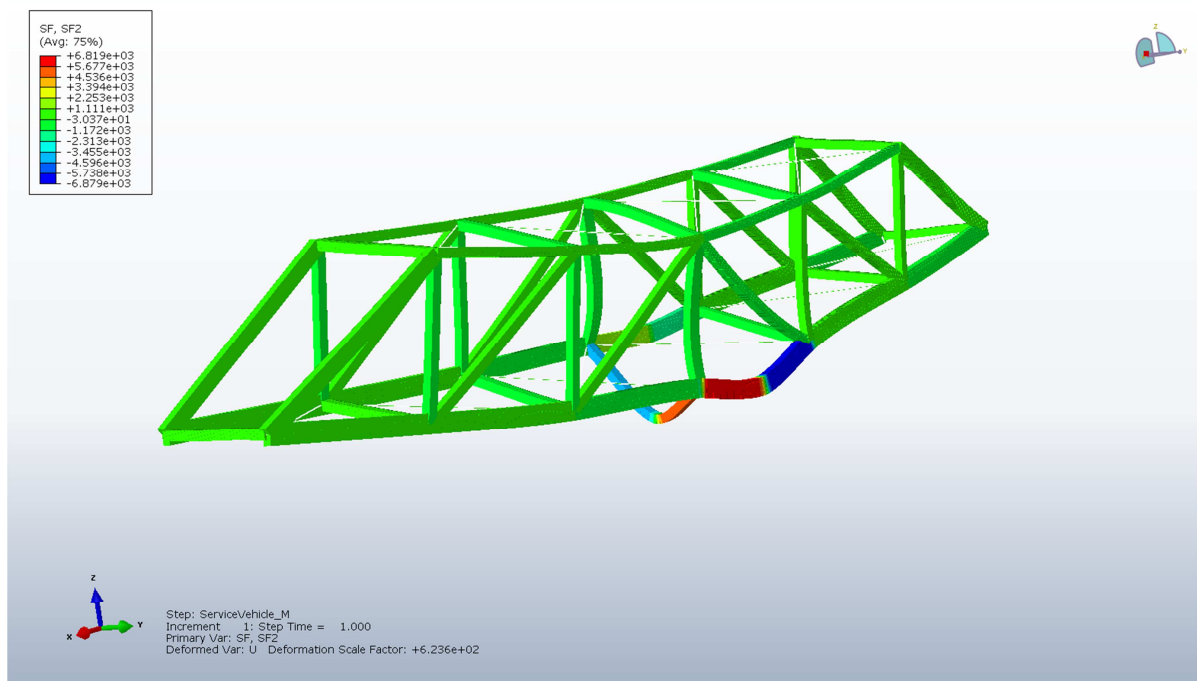
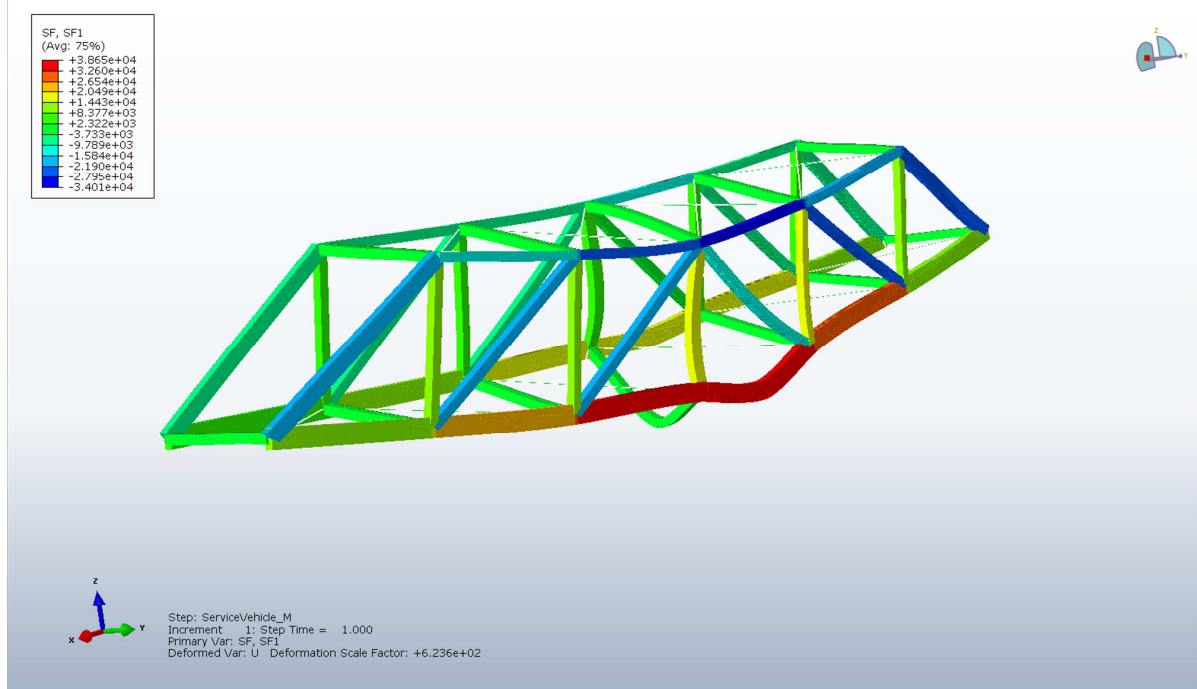
Service Vehicle near the support

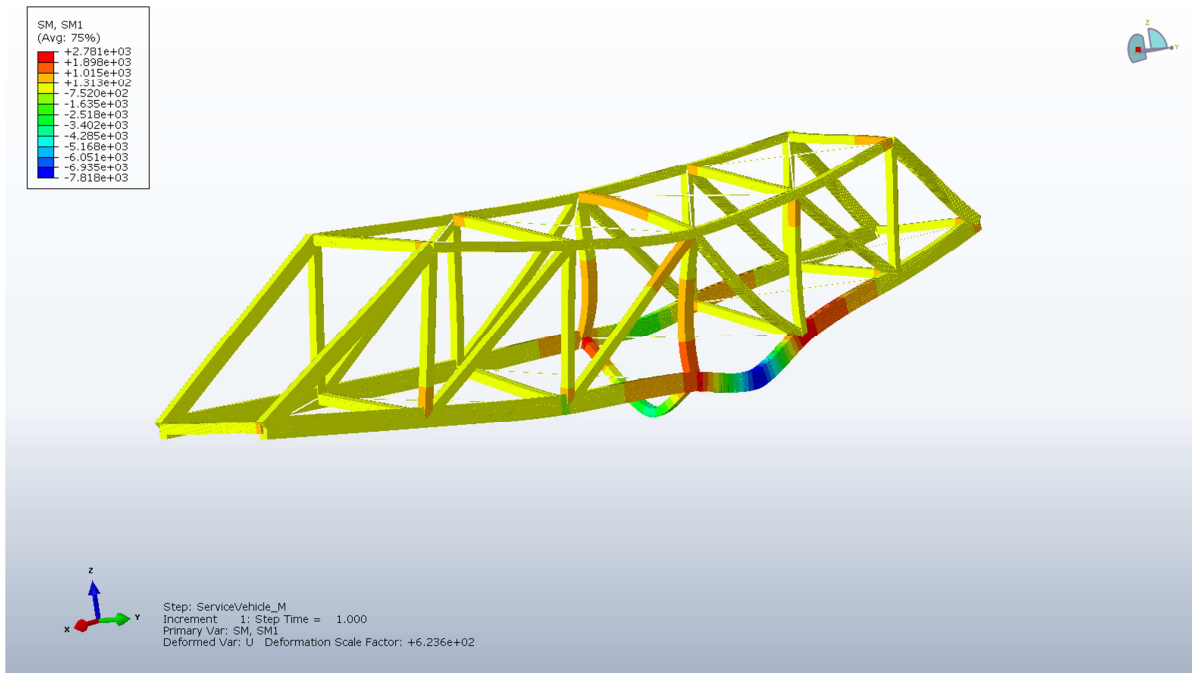
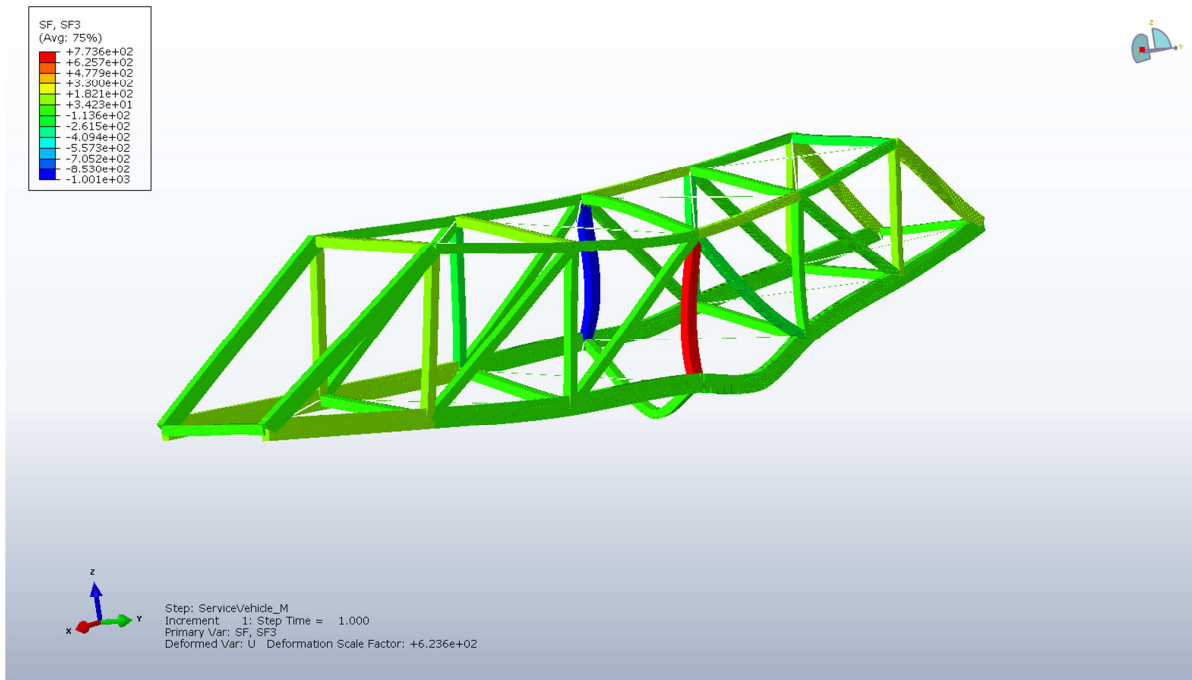


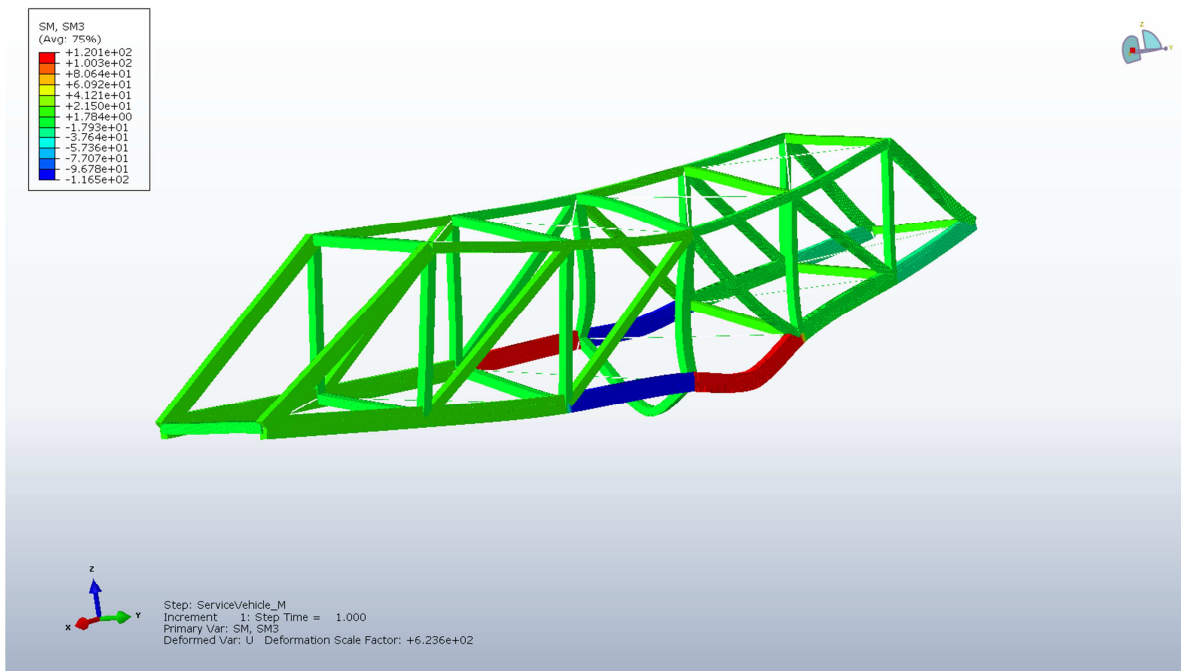
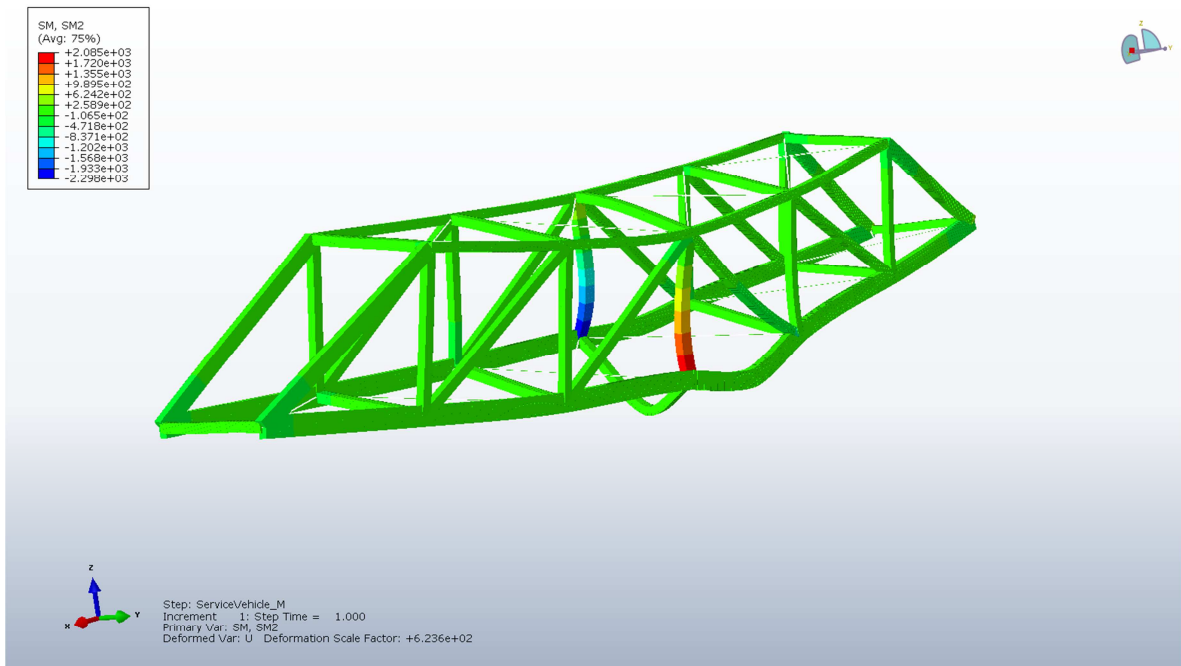




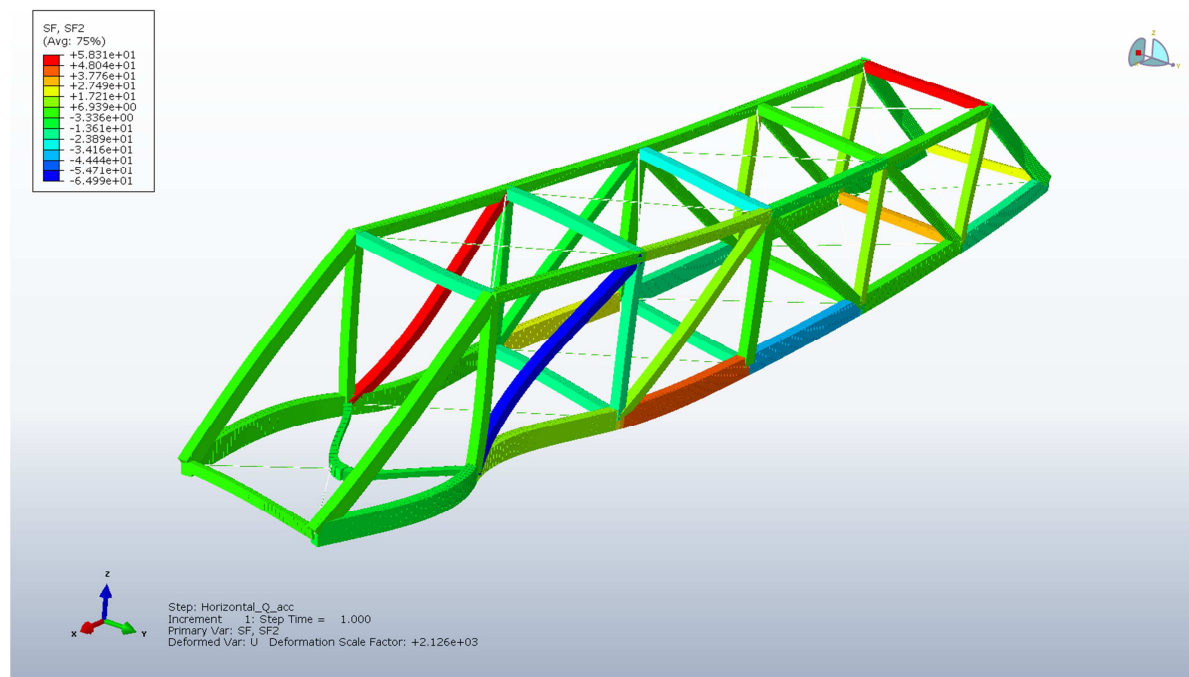
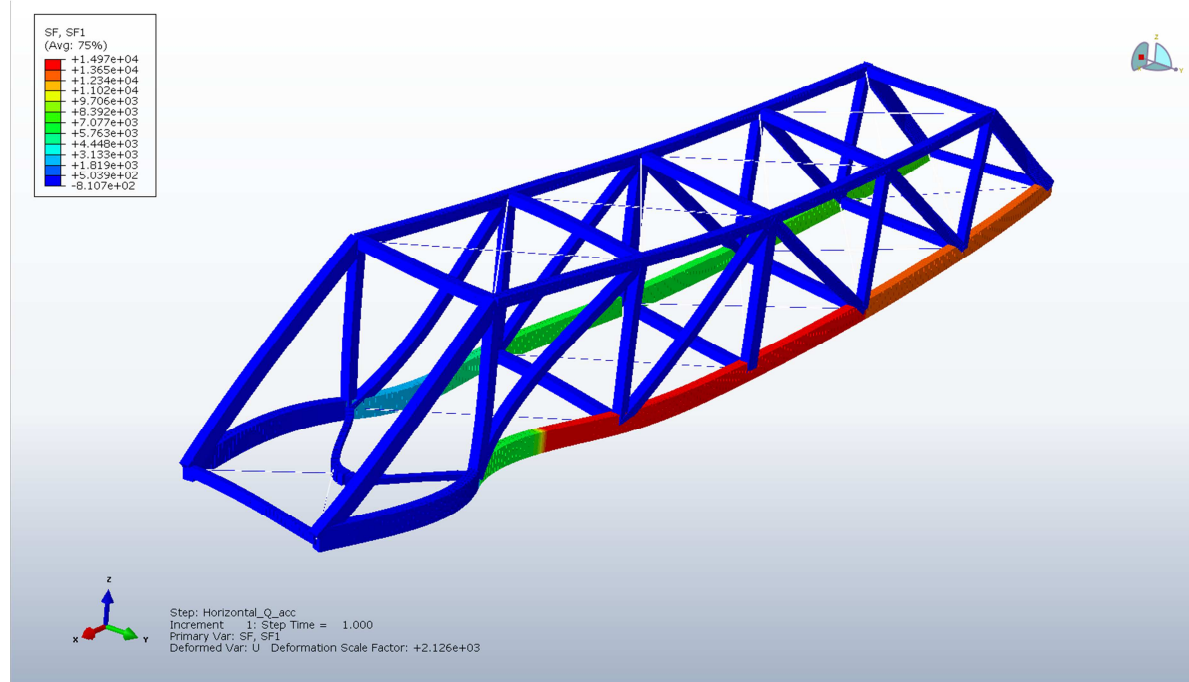
Service Vehicle in the middle of the bridge

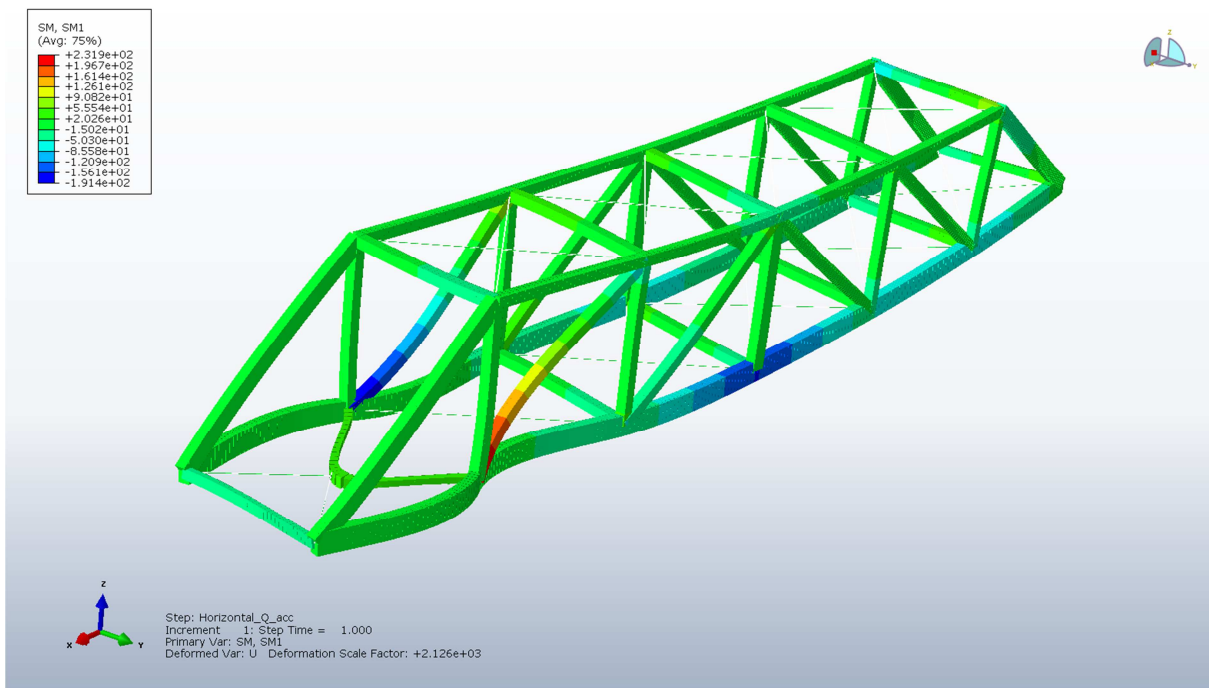
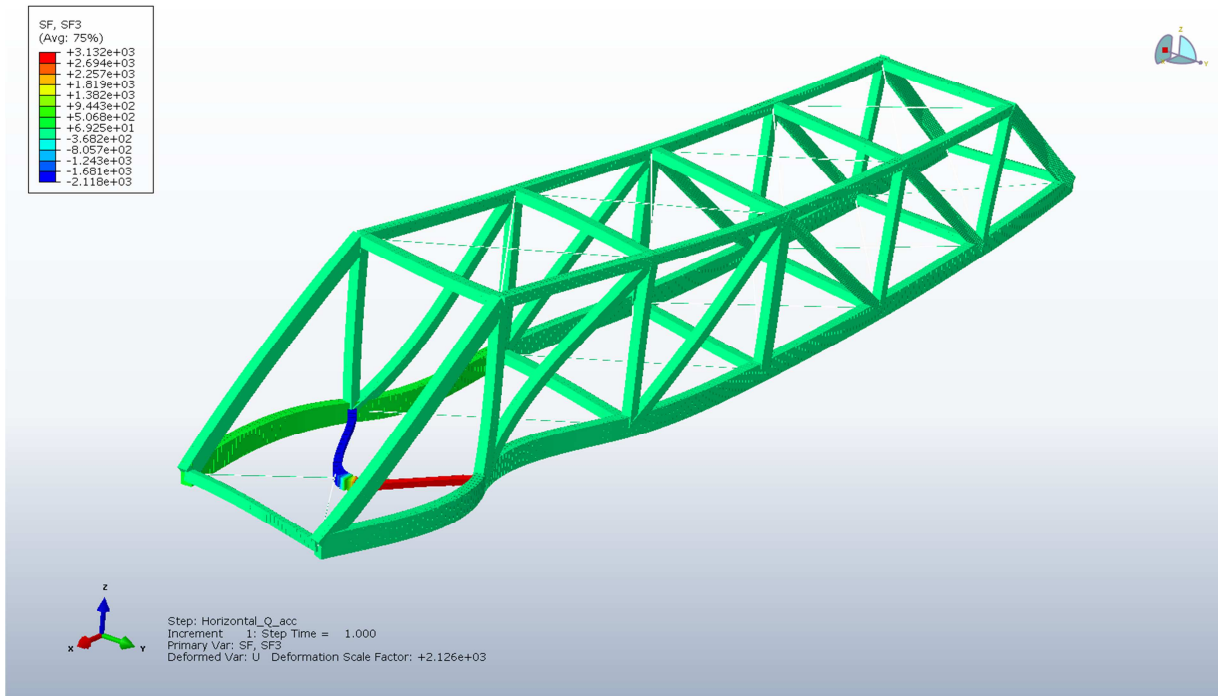


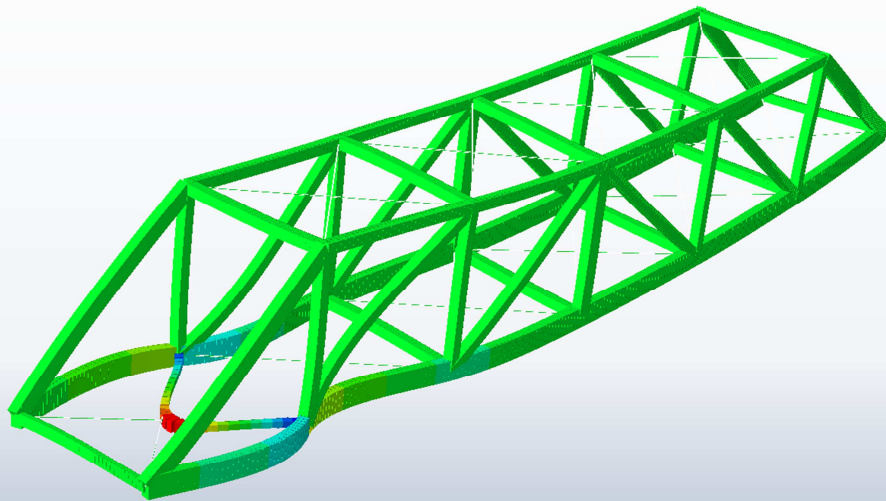
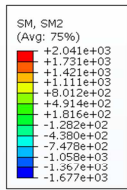




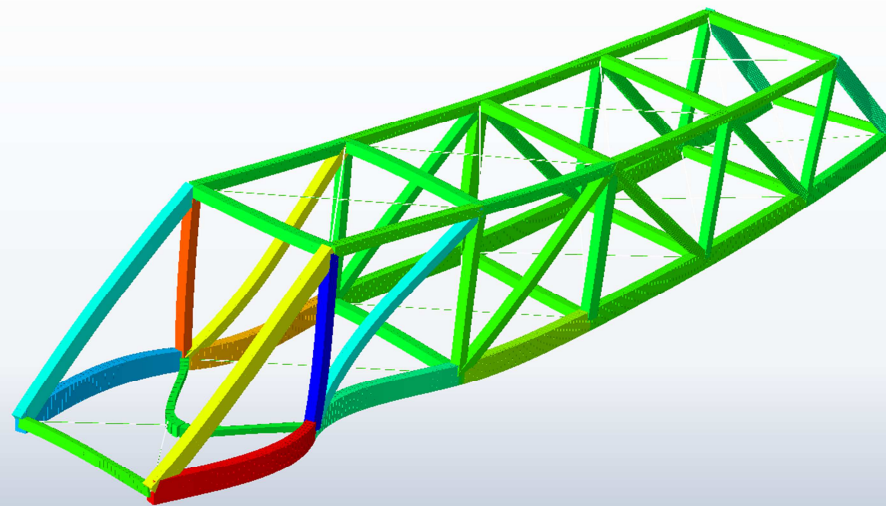
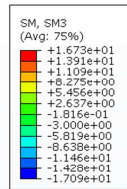
Horizontal load – acceleration







Step: Horizontal_Q_acc
Increment: 1; Step Time = 1.000
Primary Var: SM, SM2
Deformed Var: U Deformation Scale Factor: +2.126e+03



Step: Horizontal_Q_acc
Increment: 1; Step Time = 1.000
Primary Var: SM, SM3
Deformed Var: U Deformation Scale Factor: +2.126e+03

Horizontal load – retardation

